INVESTIGATING THE CONTRIBUTIONS OF TRPP2 AND α7 nAChR TO MOUSE AUDITORY FUNCTION UTILISING VARIOUS GENETIC APPROACHES

Inaugural-Dissertation to obtain the academic degree

Doctor rerum naturalium (Dr. rer. nat.)

Submitted to the Department of Biology, Chemistry and Pharmacy

of Freie Universität Berlin

by

Martin Laqua

from Pirna

2011

This work was carried out between March 2005 and December 2010 under the supervision of Dr. Inés Ibañez-Tallon at the Max-Delbrück Center for Molecular Medicine (MDC) in Berlin-Buch.

1st Reviewer: Prof. Dr. Constance Scharff

2nd Reviewer: Prof. Dr. Gary Lewin

Date of defence: 06.06.2011

Biologischer Walzer

Zwischen Kapstadt und Grönland liegt dieser Wald
Aus Begierden, Begierden die niemand kennt.
Wenn es stimmt, daß wir schwierige Tiere sind
Sind wir schwierige Tiere weil nichts mehr stimmt.

Steter Tropfen im Mund war das Wort der Beginn
Des Verzichts, einer langen Flucht in die Zeit.
Nichts erklärt, wie ein trockener Gaumen Vokale,
Wie ein Leck in der Kehle Konsonanten erbricht.

Offen bleibt, was ein Ohr im Laborglas sucht,
Eine fleischliche Brosche, gelb in Formaldehyd.
Wann es oben schwimmt, wann es untergeht,
Wie in toten Nerven das Gleichgewicht klingt.

Fraglich auch, ob die tausend Drähtchen im Pelz
Des gelehrigen Affen den Heißhunger stillen.
Was es heißt, wenn sich Trauer im Hirnstrom zeigt.
Jeden flüchtigen Blick ein Phantomschmerz lenkt.

Zwischen Kapstadt und Grönland liegt dieser Wald
... Ironie, die den Körper ins Dickicht schickt.
Wenn es stimmt, daß wir schwierige Tiere sind
Sind wir schwierige Tiere weil nichts mehr stimmt.

Durs Grünbein

ACKNOWLEDGEMENTS

Dass unsere Aufgabe genau so groß ist wie unser Leben,
gibt ihr einen Schein von Unendlichkeit.
Franz Kafka

I would like to thank my group leader Dr. Inés Ibañez-Tallon for giving me the opportunity to work on this project, for her advice and support throughout the years. I also would like to thank Prof. Dr. Constance Scharff for the official supervision of my PhD project.

I also thank the people I have been working with: Beatriz Antolin-Fontes, Sebastian Auer, Silke Frahm, Leiron Ferrarese, Sarah Foote, Mandë Holford, Branka Kampfrath, Daniela Kurzhals, Beate Liehl, Julio Santos-Torres, Marta Slimak, Annika Stürzebecher and Susanne Wojtke. It was a pleasure to have you as my colleagues. I will cherish the precious moments we had.

Heaps of props go to all my pals from the neighbouring labs. Ángel, Anne, Daniel, Katja, Kristina, Lena, Peter, Sebastian, Sven, Susann, Tamara - I think the MDC is a good place to make some good friends! I hope some friendships will stand the test of time. Ach was, I know they will!

Obwohl ich nun schon seit geraumer Zeit in Berlin lebe, weiß ich, dass auf die alten Freunde Verlass ist. Dani, Eric, Franzi, Jule, Katja, Steffen, Thomas, Uwe - vielen Dank für eure Unterstützung. Ich bin stolz auf euch.

Besonders danke ich meiner kleinen großen Familie. Ein streitbarer, chaotischer, zerrissener und herzlicher Haufen. Ein Rückhalt, den ich zu schätzen weiß. Ich hoffe, dass ich mit den Jahren immer mehr zurückgeben darf. Seid mehrfach umarmt!

Die letzten Zeilen den wichtigsten Personen: Marko. Mutti. Streitet euch um das letzte Wort. Mein Puls schlägt höher, wenn ich an euch denke. Danke.

TABLE OF CONTENTS

NOMENCLATURE

I. The TRP channel TRPP2 is also known as Polycystin-2, PC-2 or PKD2. Throughout this work the prevailing forms *TRPP2* and TRPP2 are used to designate the nucleic acids and the protein, respectively. However, some primers and probes may still contain historical name elements (*Pkd2*). The gene *PKD1* encodes the protein Polycystin-1 (PC-1). Here, the original names are still in use.

II. According to standard nomenclature (deoxy)ribonucleic acids are written in italics, proteins not. Capital letters are used when discussing human nucleic acids and proteins. With the exception of the first letter murine nucleic acids and proteins are written in lower case (*Trpp2*/Trpp2). If the host is not known or not important usually the human nomenclature is used.

III. Promoter and enhancer elements of a gene – but not the gene itself – are written in italic small capital letters and are separated from the protein whose expression they direct by a hyphen (*TRPP2*-GFP). Another convention in this work is the use of '_' to indicate fusion proteins (EGFP_L10a).

I. INTRODUCTION

The inner ear provides us with the abilities to hear and perceive linear and angular acceleration. Inner ear disorders thus affect our senses of hearing and balance. Genetic disposition, ageing, noise exposure, certain infections and ototoxic drugs reinforce hearing loss. The principal cause for this hearing loss is the degeneration and subsequent death of sensory hair cells (80%). This introduction gives an overview of the auditory system (1.1) and the two classes of ion channels that were in the centre of this study, viz. the nicotinic acetylcholine receptors (nAChRs, 1.2) and the transient receptor potential channels (TRPs, 1.3). The last chapters of the introduction describe the genetic approaches employed in this study (1.4, 1.5).

1.1 Gross structure of the auditory system

In mammals sound is first captured and directed by the outer ear. Then, in the middle ear, air pressure differences are translated into fluid pressure differences. The process of translating mechanical into electrochemical information is accomplished by the inner ear. Specialised structures of the central nervous system (Fig. 1) then integrate and process the information. This work focuses on the inner ear and on the first relay stations in the lower brainstem.

1.1.1 ORGAN OF CORTI AND SOUND DETECTION

([1-3]) The organ of Corti (o/C) is a stripe of cells harbouring the mechanosensory cells detecting sound (Fig. 2). These specialised inner (IHC) and outer (OHC) hair cells bear cilia with the mechano-electrical transducer (MET) apparatus on their apical side. They are arranged in more or less 1 (IHC, near the modiolus) plus 3 (OHC, near the periphery) rows which spiral around the axis of the cochlea from the base to the apex. The organ of Corti is lying on the basilar membrane. As it is part of the scala media it is surrounded by endolymph. Several supporting cells are sitting directly on the basilar membrane: Hensen's cells, Deiters' cells (also: outer phalangeal cells), outer rod (pillar) cells, inner rod (pillar) cells, inner phalangeal cells and inner sulcus (border) cells (near the vestibular lip of the spiral limbus). The outer and inner phalangeal cells carry the outer and inner hair cells, respectively. The stereocilia of the outer hair cells (and arguable also those of the inner hair cells) contact the tectorial membrane. Adjacent to the o/C on the peripheral side Böttcher's cells, Claudius' cells and external sulcus cells lie on the basilar membrane near the site where the o/C contacts the spiral ligament.

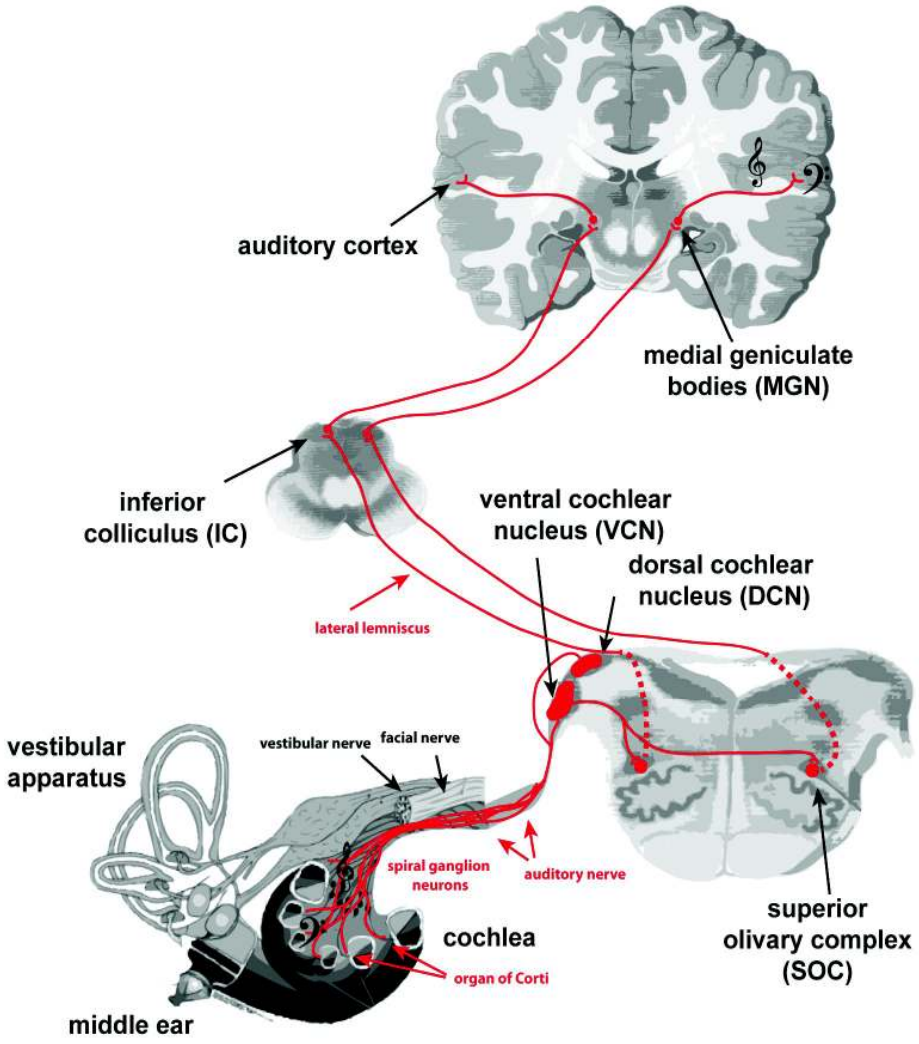

FIG. 1: THE AUDITORY PATHWAY
Adapted from Kahle & Frotscher (2002). Bass (treble) clef indicates processing of low (high) frequencies.

Hair bundles are the mechanosensitive organelles of hair cells. One bundle is composed of a few tens to hundreds of actin-rich stereocilia that are arranged in a staircase fashion. Immature and vestibular hair cells also possess an axonemal kinocilium. Individual stereocilia are linked along their longitudinal shafts, which allows the whole bundle to move as a unit. Additionally, shorter stereocilia are connected with their taller neighbours via so-called tip links (recently reviewed by Gillespie and Müller[3]).

Sound is converted from air pressure differences into liquid pressure waves in the middle ear. As the wave travels in the cochlea up (scala vestibuli) and down (scala tympani) it sets the basilar membrane into vibration. This leads to a deflection of the hair bundle on hair cells towards their tallest stereocilia. This mechanical deflection – or displacement – is converted into a chemical signal at the tips of the stereocilia, resulting in an influx of cations that depolarise the hair cell, thereby generating a receptor potential which is then propagated along the hair cell.

The stiffness of the basilar membrane is different from turn to turn, so that a given frequency sets a preferred section of the basilar membrane into vibration. As a rule high frequencies are coded near the windows (base) whereas low frequencies are coded near the helicotrema (apex). This defines the tonotopic map of frequencies. Tonotopy is maintained throughout almost all processing modules of the auditory system (Fig. 1).

1.1.2 SPIRAL GANGLION

([4-8]) The spiral ganglion (SG, Fig. 2) is a collection of neuronal cell bodies in the cochlea providing the afferent (sensory) innervation of hair cells. Its central processes form a major part of the acoustic nerve. The SG is situated in Rosenthal's canal, a bony channel that spirals around the axis of the cochlea (modiolus). The inner-ear ganglion formation is a phylogenetic novelty in vertebrates in the otherwise conserved developmental programme of mechanosensory cells[9]. For example in insects, one cell, the bristle mechanosensory neuron, contains the MET in its dendrites, and also transmits the afferent information to the brain. (For a detailed review see Fritzsch et al.[10].)

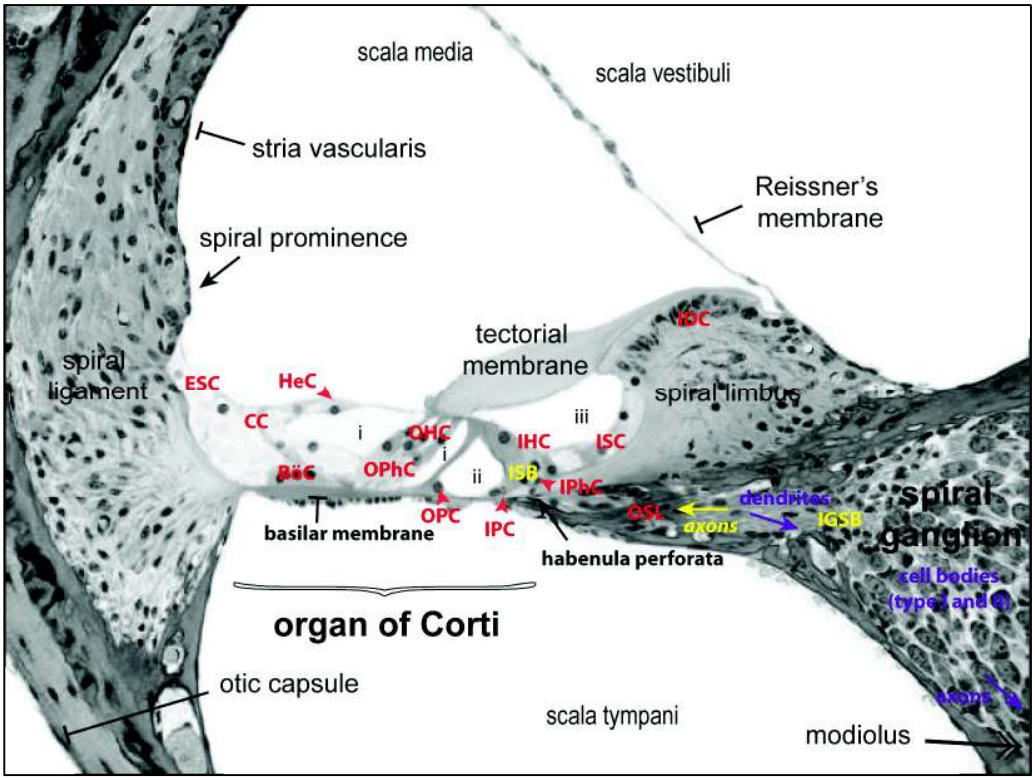

FIG. 2: CELL TYPES AND STRUCTURES IN THE MAMMALIAN INNER EAR

A middle turn of a midmodiolar section is shown. The organ of Corti (o/C) is encompassed by three fluid-filled cavities (narrow lettering), the endolymph-filled spaces of the o/C are parts of the scala media: (i) outer tunnel, (ii) inner tunnel and (iii) internal spiral tunnel. Purple colouring indicates afferent, yellow colouring efferent projections. Afferents enter and efferents leave the bony modiolus through the habenulae perforatae (nervous foramina) and move within the osseous spiral lamina (OSL) to the cell bodies in the spiral ganglion or within the OSL and the IGSB to the brainstem, respectively. *BöC* Böttcher's cells, *CC* cells of Claudius, *ESC* external sulcus cells, *HeC* Hensen's cell, *IDC* interdental cells, *IGSB* intraganglionic spiral bundle, *IHC* inner hair cell, *IPC* inner pillar cell (rod), *IPhC* inner phalangeal cells, *ISB* inner spiral bundle, *ISC* internal sulcus cells, *OHC* outer hair cells, *OPC* outer pillar cell (rod), *OPhC* outer phalangeal cells (Deiters' cells), *OSL* outer spiral lamina

The two types of hair cells are innervated by at least two distinct types of spiral ganglion neurons (SGNs, Fig. 3). Type I spiral SGNs innervate inner hair cells and transmit acoustic information to the brainstem. Type II SGNs contact outer hair cells. As a part of an olivocochlear feedback loop OHCs modulate the level of IHC activation. In most scrutinised organisms the majority of SGNs are myelinated (from cat 95% to rhesus monkey 85%), humans being the exception with only 5% of all SGNs myelinated[11]. In most model organisms one can distinguish large, evenly distributed, myelinated neurons (type I) from fewer in number, small, peripherally located, unmyelinated neurons (type II). The membrane properties of type I SGNs are determined (1) by hyperpolarisation-activated nonspecific cation currents and (2) by various depolarisation-activated K^+ currents (dendrotoxin-sensitive, transient, delayed rectifier). Most type I cells are rapidly adapting but some apical neurons seem to produce slowly adapting currents. This suggests that firing properties also depend on the influence of neurotrophic factors like BDNF and NT-3 (that show an apical-to-basal gradient in gene expression)[8].

(I) SPIRAL GANGLION NEURONS OF TYPE I

Flask-shaped IHCs make glutamatergic synapses with type I SGNs (mainly AMPA receptors, Fig. 3). Every SGN innervates one to at most five IHCs but one IHC is in contact with 15 to 20 type I SGNs. Thus up to 20 fibres transmit the same information in parallel to the brainstem. About three times more type I afferents per IHC are found in the basal turn than in the apex. In most species type I cells are myelinated. An interesting feature of guinea pig, cat and mouse SGNs is the complete myelination of not only neurites but also the cell body. However, myelination is far more loose and heterogeneous around the cell body than around neurites. Thus it cannot be concluded whether the cell bodies behave as true internodes or more like axon initial segments.

(II) SPIRAL GANGLION NEURONS OF TYPE II

Type II SGNs comprise 5 to 10% of the auditory nerve. One SGN type II contacts about 30 to 60 rod-shaped OHCs (Fig. 3) and therefore is the first integrator of OHC information. Synapses are glutamatergic but contrary to afferent type I synapses at IHCs here AMPA-type glutamate receptors are probably not involved in transmission[12]. Compared to type I, type II innervation is less topographic. Also, opposite to the situation for type I SGNs, two times more type II synapses are present in the apex than in the base. Their central and peripheral axons are small and unmyelinated. Single-fibre recordings are thus difficult to obtain and little is known about transmission at the OHC – type II SGN synapse. Prominent ribbon synapses are usually absent in adult OHC which suggests together with other morphological findings that OHC – SGN (type II) synapses are less active than IHC – SGN (type I) synapses. In mammals some type II terminals seem to be reciprocal synapses as they have both standard afferent (vesicle cluster in OHC) and unusual efferent synapses (vesicle cluster in the terminal, subsynaptic cistern in the OHC). The

efferent synapses at those terminals are morphologically similar to the classic efferent synapses of the medial olivocochlear fibres onto OHCs. Reciprocal synapses could facilitate bidirectional signalling so that OHCs can communicate via this local network with each other over the whole spiral bundle – without CNS involvement[13]. Like type I cells type II cells bifurcate in the cochlear nucleus (CN) and contact a wide area of the VCN in a topographic fashion.

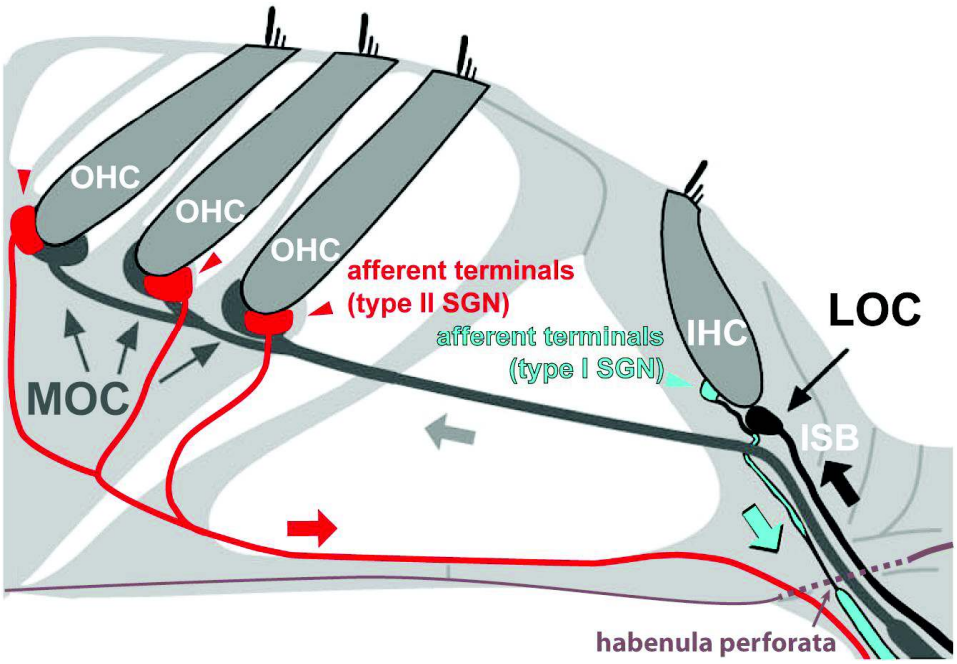

FIG. 3: AFFERENT AND EFFERENT FIBRES IN THE ORGAN OF CORTI
Schematic illustration of the peripheral origins of afferent SGN dendrites and the peripheral projections of the medial and lateral components of the olivocochlear (OC) efferent system. Type I afferent synapses are directly on IHCs (turquoise arrowhead); type II afferents have synaptic contacts with OHCs and MOC efferents (red arrowheads). Efferents to the OHC coming from the brainstem (MOC fibres, grey) cross directly through the inner tunnel. LOC efferent fibres (thin black arrow) take the same direct pathway through the habenula perforata as the type I afferents they are contacting. Bold arrows indicate direction of action potential transmission.
LOC lateral and *MOC* medial olivocochlear; *ISB* inner spiral bundle

(III) SYNAPSES IN THE SPIRAL GANGLION

Axo-somatic, axo-dendritic and axo-axonic contacts upon the soma and neurites of small neurons (presumably type II SGNs) have been described in man and monkey, but are only rarely found in lower vertebrates. Presynapses originate from efferent fibres coming from the superior olivary complex (SOC). They pass through the modiolus within the spiral ganglion as the so-called intraganglionic spiral bundle (IGSB, Fig. 2). Humans also display synapses on large SGNs[14] (presumably type I SGNs) so that here both, the IHC and the OHC afferent systems can be modulated by olivocochlear fibres. This possible neuronal processing in man is facilitated by the missing myelination of human SGNs.

(IV) DISTINCTION OF SGN CELL TYPES

In mice adult SGNs do not show evident size differences in fixed and gelatine-embedded specimen. Additionally few type II cells (OHC synapses determined by tracers) were distinctively larger than the majority of other type II cells which makes the categorisation of SGNs even more complex[15]. The distinction between type I and II SGNs is difficult in development (e.g. until P8 in rat) as they are morphologically indistinguishable. But even in older animals (P7 to P10) the categorisation into two pools does not apply. Jagger and Housley describe three SGN cell types in rat: type I (130 μm^2), small type II (101 μm^2) and large type II (148 μm^2) cells[16]. Also the position of the SGNs along the axis has a certain influence. In cats more elongated cells are found near the apex, spherical cells are found predominantly near the base. Cell size also varies with the smallest cell being present in the middle turn. Another morphologic parameter, neurite diameter, can also be a useful tool to distinguish type I from type II SGNs[8]. The bulk of physiological data has been obtained from SGN cell cultures of various species. Although most studies find two distinctly differing firing behaviours it is until now not clear if they correlate with the different SGN cell morphologies or if they represent apex-to-base differences (reviewed by Rusznák and Szucs[8]).

1.1.3 COCHLEAR NUCLEI

([5,17-19]) The cochlear nucleus (CN) is the first relay station in the auditory sensory system. It can be found between pons and medulla at the dorsolateral side of the brainstem. Cochlear nucleus neurons receive their main input from the o/C via the SGNs of the 8th cranial nerve (vestibulocochlear nerve). The incoming auditory nerve fibres divide the ventral part of the cochlear nucleus (VCN) into an anterior (AVCN) and a posterior (PVCN) portion. The third main structure of the CN is the dorsal cochlear nucleus (DCN). Type I SGN axons are branching in the CN to connect each of those three parts. The majority of inputs come from the ipsilateral ear, some also from the contralateral one. Additional inputs (mainly to the DCN; and not to the VCN) come from the auditory cortex, pontine nuclei, the trigeminal ganglion, the inferior colliculus (IC) or the second dorsal root ganglion. Because of its many inputs and the more complex architecture the DCN resembles the cerebellum in many aspects. Thus it is thought to do complex auditory processing (e.g. localisation of a sound stimulus on the vertical axis). Common to all three CN parts is their tonotopic make-up. SGNs of the lower frequency range innervate lateral-ventral portions of the DCN and ventrolateral portions of the AVCN. In contrast, SGNs of the higher frequency range project to dorsal-medial portions of the DCN and the dorsal portion of the AVCN. The mid frequency projections end up in between these two extremes.

The different branches of a type I SGN axon innervate cells in all CN parts. In the PVCN the targeted cells are the so-called octopus cells located in a small subregion of the PVCN. Octopus

cells are among those neurons in the brain that fire with very high temporal precision. Spherical (SBC) and globular bushy cells (GBC) reside in the ventral portion of the AVCN. Their physiological characteristics are similar to those of SGNs. The synapses made by SGNs and bushy cells are also called 'Endbulbs of Held'. The DCN mainly consists of fusiform (pyramidal) and giant cells that are both innervated by SGNs. The axons of fusiform cells constitute the output of the DCN. They do not project to anything at the level of the pons, so that the vertical axis sound localisation information is processed only at the level of the IC. The input of higher order nuclei is relayed through another subset of DCN cells called granule cells.

1.1.4 SUPERIOR OLIVARY COMPLEX

([20-24]) The main projections of all cells of the cochlear nuclei ultimately terminate at the inferior colliculi. Some project there directly (stellate neurons of the VCN, fusiform cells of the DCN), others via the superior olivary complex (SOC) and trapezoid body, and some via the pons and the nuclei of the lateral lemniscus (NLL).

The SOC is situated on the dorsal surface of the lateral part of the trapezoid body. Its main input comes from the AVCN, some minor input from the PVCN. The complex is comprised of three main subnuclei related to the localisation of sound in space (the ascending azimuthal localisation pathway): The medial nucleus of the trapezoid body (MNTB) is the smallest part of the three. It converts the well-timed excitatory input from the contralateral AVCN to an inhibitory projection to the ipsilateral lateral superior olive (LSO). The conspicuous synapses in the MNTB are called 'Calyces of Held'. In the LSO the inhibitory input from the opposite side (contralateral AVCN globular bushy cells via the ipsilateral MNTB) is compared to an excitatory input from the same side (ipsilateral AVCN spherical bushy cells). This profile provides a powerful way of comparing intensities from both sides of the head (interaural level difference, ILD) that helps determining the source of (mainly high-frequency) sounds on the left-right axis. ILDs arise because the head produces an asymmetrical attenuation of sounds off the centre axis. Mice can resolve azimuthal differences of ~15° at 15 kHz which corresponds to an ILD < 1 dB. In addition, inhibitory inputs damp low-frequency time-locked excitatory signals from both sides of the head as they project onto the dendrites of linearly arrayed cells in the medial superior olivary complex (MSO). The MSO is primarily concerned with comparing arrival time of the sound from both sides of the head (interaural time difference, ITD). It is thus important for localising low-frequency sounds (left – right axis). When binaural stimuli are presented, ITD seems to be preferred over the ILD because of a better response of the MSO (when compared with the LSO response).

The outputs of the SOC mainly constitute the lateral lemniscus (LL, Fig. 1). Other axons being present in the LL come from the different (primarily inhibitory) nuclei of the LL (NLL) that are interspersed within the fibres of the LL. The LSO not only projects contralaterally excitatory but

also ipsilaterally inhibitory (glycinergic) to the IC. Another fibre tract from the LSO forms part of the olivocochlear (OC) efferent system: Lateral (L) OC fibres innervate IHCs and are thought to normalise sound levels detected by each ear (see 1.2.4). The MSO mainly projects to the ipsilateral IC. Several periolivary nuclei are counted as part of the SOC as well. Depending on species and describing scientist there are between 6 and 8 of these periolivary nuclei. The cells of the other part of the olivocochlear efferent system reside here: Medial (M) OC fibres are projecting from the ventral NTB to OHCs (see 1.2.3). Whilst the functions of different neuronal types in the CN and the SOC are quite well understood, the nature of the code at the level of higher auditory relay stations like the inferior colliculus (IC), medial geniculate body (MGB) and primary auditory cortex (A1) are apprehended less well.

1.2 Nicotinic signalling in the cochlea and in the auditory brainstem

([25,26]) Cholinergic neurotransmission is introduced by discussing both the source of acetylcholine (ACh, cholinergic cells) and the cells expressing the corresponding receptors (nAChRs, cholinoceptive cells). The first implication of nicotinic signalling in the auditory system dates back to 1994 when a new nAChR subunit with an unusual mixed nicotinic- and muscarinic-sensitive pharmacology was discovered in hair cells: α9 nAChR (Chrna9)[27]. Later on yet another subunit, α10, was shown to be co-expressed with α9[28]. But not only hair cells are cholinoceptive (see 1.2.3); also SGNs have been shown to respond to ACh[29]. Evidence for nicotinic receptors in SGNs, including α7 homomeric nAChRs, is discussed in 1.2.5. Cholinergic efferents project from the superior olivary complex (SOC) to the organ of Corti (o/C) as medial (1.2.3) and lateral (1.2.4) olivocochlear fibres (OC). In section 1.2.6 the cholinergic nature of SGNs is discussed.

1.2.1 CHOLINERGIC NEUROTRANSMISSION

In classical or synaptic cholinergic neurotransmission – as first described at the neuromuscular junction – ACh is brought into presynaptic vesicles of cholinergic cells by the vesicular acetylcholine transporter (VAChT). Sequestered ACh binds to post- (and pre-)synaptic nAChRs. The kinetics of ACh is dependent on the quality of the receptor, and the amounts of released transmitter, synaptic cleft acetylcholine esterase (AChE) and presynaptic membrane hemicholinium-sensitive choline transporters (CHT1). AChE hydrolyses acetylcholine and CHT1 returns the resulting choline to the cell. There the enzyme choline acetyltransferase (ChAT) converts choline back to acetylcholine and the cycle may begin anew.

All key proteins of this cycle, including the receptors, are often abundantly found in many non-innervated tissues, suggesting that ACh may also be involved in paracrine or autocrine

signalling[30,31]. Studies of non-neuronal expression of neuronal nAChRs find β4 in astrocytes[32], α7 and α9α10 in lymphocytes[33-35], α3, 5, β2 and 4 in endothelial cells[36] as well as α7 and α9 in keratinocytes[37,38]. This concept of non-synaptic transmission is also discussed in the brain because there are only few nicotinic cholinergic synapses that are characterised by fast excitatory postsynaptic potentials. Instead, most cholinergic terminals appear to be randomly distributed with respect to neighbouring tissue[39,40]. This way of transmission has been dubbed 'volume' or 'wireless' transmission because ACh diffuses to its receptors – wherever they are localised.

1.2.2 NICOTINIC ACETYLCHOLINE RECEPTORS

In mammals, 16 subunits of nicotinic acetylcholine receptors (nAChRs) assemble in hetero- and homopentameric receptors with distinct structural and pharmacological properties[41,42]. The muscle nicotinic receptor (α1, β1, γ, δ/ε) mediates synaptic transmission at the neuromuscular junction whilst the neuronal forms of the receptor (α2 – 7, α9 – 10, β2 – 4) are mainly found both postsynaptically and presynaptically in the central and peripheral nervous system. They are involved in important functions like sleep and arousal patterning, fatigue, hunger, and anxiety[43]. There is much current interest in the study of various neuronal nAChR subtypes because they are also implicated in diverse neurological disorders such as Alzheimer‘s disease, tobacco addiction, schizophrenia, epilepsy, and pain[44,45]. Nicotinic AChRs are ligand-gated ion channels that belong to the Cys-loop receptor superfamily (like $GABA_A$, glycine and $5HT_3$ neurotransmitter receptors). Each of the five subunits of an assembled receptor has four transmembrane- (TM-) domains. The second TM-domains contribute to the formation of the hydrophilic pore of the assembled channel. Among the 11 neuronal subunits α7 to α10 subunits represent a subclass that can form functional homopentamers upon heterologous expression. The neuronal subunits α2 to α6 require co-expression of at least one beta subunit to form functional channels. Pairwise combinations do not always result in functional channels so that three or even four different subunits form functional receptors. The proposed stoichiometry in heterologous systems (oocytes) is $(\alpha)_2(\beta)_3$ but the situation in native nAChRs is still not entirely clear. nAChRs pass positively charged ions (Ca^{2+} inward, K^+ outward) upon opening. The net flow is inward. In general these ion channels are considered non-selective but some neuronal subunit combinations allow calcium to pass more effectively. This can affect the release of other neurotransmitters, synaptic plasticity and cell motility (see Fucile[46]).

1.2.3 THE MEDIAL OLIVOCOCHLEAR PATHWAY

Within the efferent cholinergic pathway, one can distinguish cells of the lateral olivocochlear (LOC) pathway (cell somata in the lateral superior olive, LSO, axons terminating on the dendrites

of type I spiral ganglion neurons, SGN) from the cells of the medial olivocochlear pathway (MOC, cell bodies in the VNTB, axons terminating on OHC). Both are known to be primarily cholinergic[47]. While MOC cells exclusively project to the OHC area and never send branches to - or make en passant swellings in - the IHC area, LOC cells might also send few projections to OHC.

(I) THE MEDIAL OLIVOCOCHLEAR PATHWAY (MOC) – ORIGIN AND TRANSMITTERS

The main targets of MOC fibres are the three rows of OHCs. MOC terminal numbers seem to be similar between the three rows in mice, but in cat and guinea pig a dramatic radial gradient has been observed with four times more terminals beneath the first than the third row. Studies on different model organisms are concordant when describing the origins of MOC fibres. About 25% of all MOC fibres come from the ipsilateral ventral nucleus of the trapezoid body (VNTB), the remaining 75% from the contralateral VNTB. The terminals beneath the OHC are positive for cholinergic (VAChT) and GABAergic (glutamic acid decarboxylase, GAD) markers, as well as calcitonin related-gene product (CGRP). The three proteins are either co-expressed in the same neurons[48] or expressed by different MOC fibre types[49]. The idea that GABA and ACh are co-localised within the same terminal, although not commonly reported in the nervous system, is not without precedent. The coexistence of GAD and choline acetyltransferase in some cell types of the retina, cerebral cortex, basal forebrain, and spinal cord has been reported as well as GABA co-localising with AChE in neurons of the mouse adrenal gland[48]. Functionally, GABA / CGRP may modulate the strength of cholinergic effects, as has been suggested for CGRP at the neuromuscular junction[50] and in isolated chicken hair cells[51]. These functional aspects can also be applied to the LOC terminals that might even have more different transmitters per cell.

(II) CHOLINERGIC MOC FIBRES TARGET α9 AND α10 nACh RECEPTORS

Unlike afferent activity of other major sensory systems, sound transmission is directly controlled by a sound-evoked feedback loop, the olivocochlear efferent (OC) system. The released transmitters acetylcholine and GABA likely mediate an inhibitory effect[43]. In fact, current models describe a biphasic response: Upon receptor binding by ACh Ca^{2+} enters the cell and binds to small-conductance Ca^{2+}-activated potassium channels. Channel opening hyperpolarises OHCs, thus reducing their responsiveness to basilar membrane movements. This is how the OHC amplifier function tightly controls the afferent output (of IHCs)[52]. OHCs express α9 and α10 nicotinic acetylcholine receptor (nAChR) subunits. α9 homomeric channels are functional, whereas α10 channels are not. The functional hair cell nAChR consists of both subunits as (1) in *Xenopus* oocytes heteromeric α9α10 receptors generate 100-fold larger currents than homomeric α9 receptors and (2) α9α10 receptors have some biophysical characteristics that resemble the native hair cell nAChR. Both subunits are considered as distant members of the nicotinic receptor family; heteromeric channels display a pharmacological

profile different from that of other nAChRs with sensitivity to glycinergic, gabaergic, serotonergic as well as nicotinic and muscarinic antagonists[27,28]. Strikingly, nicotine and most nicotinic agonists, with ACh and carbachol being the exceptions, act as antagonists of this receptor.

OHCs maintain their nAChR subunit composition (α9α10) into adulthood. In $\alpha9^{-/-}$ mice abnormal synaptic morphology including hypertrophy of OC efferent synaptic terminals at the base of OHC is observed (ultimately leading to missing classic OC responses in adult mice)[53]. However, no cell type loss or a reduction in cell number has been described. The afferent system is likely also not affected in those KO mice. A growing body of evidence, including data from mice overexpressing α9, implies a protective function against noise-induced cochlear injury for the MOC system[54,55].

(III) TRANSIENT INNERVATION OF INNER HAIR CELLS

In the developing o/C MOC fibres not only make intact synapses on OHCs but also on IHCs where they exert an inhibitory effect (mediated via nAChRs, Ca^{2+} influx and potassium channel activation)[56]. This results in synaptic transmission before the onset of hearing. At hearing onset IHC stop expressing *α10* (*Chrna10*) mRNA[28,57] and *SK2 calcium-sensitive potassium channel* mRNA[25] while maintaining the expression of *α9* (*Chrna9*) into adulthood[27,58]. Also the direct efferent synapses on IHCs are retracted[59]. Katz et al. show that IHC become increasingly responsive to acetylcholine (ACh) from postnatal day 3 (P3) to P10. Then, by P16, cholinergic sensitivity is again markedly reduced so that native hair cell nAChRs, like those expressed in *Xenopus* oocytes, seem to require α10 subunits for optimal function[25]. As α10 is only present when intact synapses are formed at hair cells, the current hypothesis is that α10, but not α9, is regulated by synaptic activity. At P8 $\alpha10^{-/-}$ IHCs do not have any ACh-gated currents – unlike wildtype mice[60]. Interestingly, this does not have an effect on the correct establishment of the intrinsic electrical properties of IHCs during development[61]. Contrasting this, deleting the other key player of this inhibiting transient synapse (K^+ channel) changes cholinergic innervation[62] and the spiking activity of pre-hearing IHCs[63]. In $SK2^{-/-}$ mice both IHCs and OHCs do not respond to ACh – even though α9 and α10 mRNA levels are unaltered[64]. SK2 channels seem to be necessary for the functional localisation of α9α10 nAChRs at the hair cell plasma membrane whereas α10 is not necessary for the functional expression of the SK2 channel in IHCs.

1.2.4 THE LATERAL OLIVOCOCHLEAR PATHWAY

Cells in the lateral superior olive (LSO) make synapses on dendrites of type I SGNs – directly beneath IHCs. These efferent fibres constitute the lateral olivocochlear (LOC) pathway. LOC fibre terminals are present in the inner spiral bundle (ISB) of mainly the ipsilateral o/C. Only about 1% of these LOC fibres come from the contralateral LSO. LOC projections are in general smaller than MOC projections; and have smaller synaptic terminals (~2 $\mu m^2/\mu m$ vs. ~5 $\mu m^2/\mu m$).

(I) THE LATERAL OLIVOCOCHLEAR PATHWAY (LOC) – ORIGIN AND TRANSMITTERS

The contacts between LOC fibres and SGNs in the ISB are often called swellings. On average four LOC fibre swellings are present on a single afferent dendrite. Projections of a single LOC neuron in the ISB consist of (1) an initial spiral portion with small en passant swellings and no branching and (2) a terminal portion with several collaterals that each show numerous large en passant swellings as well as terminal branchlets with large terminal swellings[65].

The existence of different fibre types within the LOC bundle is still unclear. Whilst some authors suggest chemically distinct LOC subpopulations[49], others believe most LOC efferents of rats and guinea pigs contain all putative LOC neurotransmitters[66]. In mice the clear and complete co-localisation of GABAergic and cholinergic markers suggests that these two fibre subgroups do not exist[48]. In hamsters the ACh-expressing subtype expresses CRGP and enkephalins. Other studies also found that neurotransmitters dopamine and dynorphin are expressed by LOC neurons. A morphologic study on guinea pig and cat could not find evidence for different LOC fibre subtypes based on swelling sizes, numbers and densities[65]. Studies in mice find that ACh and CGRP expression patterns are not 100% correlated as CGRP is also expressed by MOC cells[48]. Furthermore, their co-localisation studies show that not only ACh and CGRP but also GABA is present in LOC terminals. Darrow et al. found that dopaminergic markers stain a new LOC neuron subtype[67]. No overlap between cholinergic and dopaminergic (10-20%) terminals in the ISB as well as cell somata in the brainstem was seen. The authors point out that these dopaminergic cells might correspond to the so-called LSO 'shell' neurons[68] that surround the small cells within the LSO proper.

(II) LOC FIBRES MODULATE SGN ACTIVITY

Modulation of SGN activity by LOC fibres is detected when the LSO is either lesioned or stimulated[69,70]. Dopamine is the only transmitter described in LOC – but not in MOC – neurons. Therefore a neurotoxin targeting the dopamine receptor of LOC terminals was applied to the perilymph to selectively destroy LOC neurons[71]. Synaptophysin labelling revealed a reduction in LOC innervation in the ISB. The loss of LOC efferents leads to a depressed amplitude of the sound-evoked whole-nerve compound action potential (CAP) over all frequencies tested, and a hearing threshold elevation at the highest frequencies tested (16 and 18 kHz) – whilst not altering the outcome of MOC-related auditory tests. The current model of LOC efferent function proposes that delivering putative LOC transmitter substances such as ACh and/or dynorphin (excitatory transmitters?) selectively lowers the cochlear set point, thereby enhancing neural activity. In contrast, release of substances such as dopamine, GABA and enkephalin (inhibitory transmitters?) selectively raises the set point of the cochlea, thereby decreasing cochlear activity. This tonic input from the LOC neurons maintains the distribution of spontaneous

activity and sensitivity of the SGN in conditions of quiet and noise. The finding that disrupted LOC signalling depresses the CAP amplitude in guinea pigs is consistent with an excitatory net effect of LOC innervation in the cochlea[72].

Interestingly, work done in the same lab found that lesioning the LSO in mice leads to an increase in the CAP in the ipsilateral ear[73]. This hints on a net inhibitory input of LOC efferents to the SGNs beneath the IHC. They also found that the CAP of the contralateral ear is depressed when compared to ears of mice with intact LSO. Integrating the results they could show that the LOC system is interdigitating the excitabilities of both ears: Even though sending 99% of all efferents to the ipsilateral ear the lesion also affected – probably via the contralateral MNTB – the contralateral LSO and ear. In a lesioned mouse the excitabilities of both ears are thus not coupled anymore. The authors reasoned that this may have implications on the computation of interaural level differences (ILDs, see 1.1.4), which is a major cue for the localisation of sounds in the azimuthal plane.

To reconcile the opposing findings from guinea pig and mouse it is thought that species differences in LOC transmitter co-localisation and release account for the depression or, respectively, increase in the CAP after ablation of LSO neurons[74]. Although the direction of LOC modulation of auditory nerve activity is opposite in the guinea pig and the mouse, it appears that the LOC system may act to reduce noise-induced trauma in both animals[71,75]: Without LOC efferents a greater loss of SGNs and increased excitotoxic trauma is observed. Current data support the idea that dopaminergic and cholinergic components of the LOC efferents are responsible for the neuroprotective and antiexcitotoxic effects[76,77]. Mechanistically this could result from postsynaptic modulation of the Ca^{2+} entry (e.g. gene expression changes of Ca^{2+}-buffering proteins in the SGN-terminals). However, as LOC fibres may also make synapses directly on IHCs[75] (based on initial findings in the cat[78]) a LOC fibre-induced protection from noise trauma could also be mediated presynaptically (e.g. by reducing glutamate release from the IHC).

1.2.5 EXPRESSION OF NICOTINIC RECEPTORS IN THE SPIRAL GANGLION

(I) EXPRESSION OF nAChR SUBUNITS

Recently the specificities of a large panel of anti nAChR antibodies have been tested utilising α3-, α4-, α7-, β2- and β4-subunit knockout mouse brain tissues[79,80]. Surprisingly, each of the antibodies tested and believed to be subunit-specific gives a significant signal in the corresponding null mutant mouse. Consequently, the authors conclude that the results of nAChR expression pattern analyses based on antibody stainings are not reliable per se. In contrast, the presence of transcripts is regarded as a credible indicator of nicotinic receptor subunit (protein) presence. In a detailed study the subunit composition of SGNs in adult rats was identified by *in situ* hybridisations: α6, α7 and β2 were found in type I cells; β2 also in type II SGNs (SGNs are

considered as neither cholinergic nor cholinoceptive)[58]. RT-PCR data from that study also suggest that α5 and β3 transcripts are present in the ganglion, whereas RT-PCRs on isolated SGN populations of adult mice detected in addition to the previous subunits also α2 nAChR mRNAs[81]. Interestingly both studies (and an RT-PCR experiment on RNA isolated from whole cochleae: Drescher et al.[82]) did not detect α3 and β4 transcripts which are the predominant nAChR subunits in other sensory or autonomic ganglia[83-85]. Only for the subunit β2 a role in cochlea physiology has been discovered. Its downregulation in old mice leads to an age-related loss of SGNs und subsequent hearing loss (presbycusis)[81]. Null mutant mice of both α5 and β2 do not show any signs of hearing deficiencies in (young) mice. So the role of α5 and β2, as well as the function of α2, α6, α7 and β3 in SGNs remain unclear.

(II) RECEPTOR ASSEMBLY

The subunits α6 and β2 give the strongest ISH signal in rat SGNs but a receptor composed of these subunits (possibly also involving α7) has not been identified previously[86]. α6 subunits are only found in limited areas of the brain and the properties of α6-containing receptors are not yet fully understood. In most systems studied α6 and β2 subunits require a third subunit to establish a functional receptor (mostly β3[87]). However, the presence of α6β2β3 receptors is doubtful because β3 levels are very low. In addition, β3 assembles with α4, β2, and β4 subunits to a functional channel when expressed in COS cells. There is also some evidence for the presence of α5 in SGNs. α5 is a subunit of an α5α4β2 receptor but it does not form a functional receptor when it is – without any supporting α subunit – co-injected into *Xenopus* oocytes with any β subunit. Since neither α4 nor β4 were found in the cochlea, α4β2β3β4 and α5α4β2 are not putative cochlear receptors. Therefore most existing subunits might be part of an orphan nAChR receptor that is likely composed also of one or more yet undiscovered nAChR subunits.

The subunit α7 has been described in a native nAChR together with β2[88] but the relevance of this finding remains controversial. Therefore, α7 homopentameric receptors are the most likely candidate nicotinic receptors in the SG. α7 subunits are widely expressed in the central nervous system and in peripheral tissues. As α7 nAChRs are the best Ca^{2+}-permeable ionotrophic receptors known[46], a role in the regulation of intracellular calcium $[Ca^{2+}]_i$ levels has been suggested. α7 nAChR is permeable to Ca^{2+} in the absence of depolarisation[89]. Already low levels of local ACh can produce Ca^{2+} influx and a significant elevation of $[Ca^{2+}]_i$. Activation of α7 channels, for example, could promote cell survival or induce neuronal apoptosis[90,91]. This apparent paradoxical function may depend on the expression level of the α7 subunit and subsequently on functional interactions among various signal pathways triggered by α7 activation. As α7-containing receptors have very fast inactivation kinetics and long lasting desensitisation,

they often act in concert with one (or more) nAChR channels of different composition that desensitise much slower[92]. α6 and β2 may possibly be subunits of this elusive channel.

1.2.6 THE AFFERENT CHOLINERGIC PATHWAY

At the level of the brainstem all SGN synapses are glutamatergic. In addition afferent type I spiral ganglion cells (SGNs) connecting inner hair cells (IHCs) with the cochlear nucleus (CN) are also considered cholinoceptive (see previous chapter). However, in many species they have been shown to express also a marker for cholinergic neurons: acetylcholine esterase (AChE). In addition to its classical enzymatic function (see 1.2.1) also some non-catalytic functions like gene expression induction, receptor clustering, neuron guiding and nAChR activation are discussed for AChE[26]. It has been discovered that a 14-amino-acid peptide of the C-terminal domain can bind to the same site of the α7 receptor as the known allosteric modulator ivermectin[93]. Also, at least two AChE-derived peptides affect cholinergic responses on postsynaptic sites, with or without on hand ACh. In a peptide-treated rat-derived cell line, for example, α7 mRNA and protein levels were increased, and the trafficking of this subunit to the plasma membrane was improved[94,95]. SGNs branching extensively in the cochlear nuclei form excitatory synapses with neurons in nearly all subregions. It is conceivable that sequestered AChE – and not ACh – modulates the target cells in the cochlear nuclei.

Several different nACh receptors are expressed in the lower auditory brainstem. The predominant nAChR is the α7 homomeric nAChR but also α3β4 nAChRs are transiently expressed. The decrease of α3β4 expression in the rat coincides with an increase in α7 expression – indicating a switch in nAChR subtypes just before the onset of synaptogenesis[96,97]. In most nuclei α7 expression increases from birth to the second postnatal week. Peak expression before hearing onset suggests a non-conventional role for α7 nAChRs. There are two possible explanations for the transient expression of α7. First, α7 is an excitatory receptor that is necessary to stabilise developing synapses. Synaptic-like structures can already be found on the somatic spines of PVCN octopus cells at the age of P5 – well before canonical synapses are formed. It is well known that the auditory brainstem is organised by network-intrinsic rhythmic bursting or oscillatory activity also in the absence of sensory information input. (However, some final maturation steps occur after P12.) The source of this excitatory activity in the brainstem is not known but glutamatergic synapses can be ruled out as they mature later in development[98]. So it is likely that the other identified excitatory pathway in the auditory brainstem, the cholinergic pathway, drives neuronal activity – especially as a similar phenomenon is seen in the visual system[99]. Second, α7 regulates other neurotransmitter systems via activity-dependent gene expression as has been shown for glutamatergic synapses in the hippocampus[100]. The tightly controlled intracellular Ca^{2+} concentration may be the missing mechanistic lever. $[Ca^{2+}]_i$ is

critical for the proper regulation of gene expression, as well as for the survival and maturation of SGNs[101].

1.3 TRPP2 – A polycystin-type TRP channel

TRP ion channels (TRPs) emerge as candidate transduction channels in a wide variety of sensory systems. They are involved in the detection of chemical and thermal stimuli, and particularly in sensing mechanical stimuli: TRP channels are essential for mechanosensation in various systems like hearing in fruit flies, touch in nematodes and mechanical pain in mice[102-104]. After a general account on the TRP channel family (1.3.1) TRPP2, a member of the polycystin family of TRP channels, is introduced in more detail (1.3.2). The state of knowledge about expression and function of TRPs in the inner ear is summarised thereafter (1.3.3).

1.3.1 THE TRP CHANNEL FAMILY

TRP channels are expressed in almost every tissue and cell type and play an important role in the regulation of various cell functions. The first TRP channel was identified in 1969[105] as the gene product defective in a blind *Drosophila* mutant. In response to light the photoreceptors displayed a transient current instead of the sustained current seen in the wildtype, hence the name of the mutant: transient receptor potential (*trp*). The cloning of the channel was accomplished 20 years later and marked the beginning of the discovery of a whole new group of ion channels[106]. Homologues have now been found in many animals, both vertebrate and invertebrate (Fig. 4). Animal genomes carry between 13 (*Drosophila*) and 50 (zebrafish) homologues, which have been divided into seven subfamilies: TRPC (canonical or classical), TRPM (melastatin), TRPV (vanilloid), TRPN (NOMPC), TRPA (ankyrin), TRPP (polycystin) and TRPML (mucolipin)[102]. Not all subfamilies occur in all animals (e.g. TRPN not in mammals), and some subfamilies (TRPV, TRPP) contain distinct subgroups. Mice and humans have a similar number of TRP channels (27-28 with known function, ±33 in total), and also the phenotypes caused by TRP mutations resemble each other.

(I) COMMON STRUCTURAL FEATURES

TRPs have a molecular architecture similar to that of voltage-gated ion channels, with each subunit containing (usually) six TM-domains, and the subunits being arranged to form a tetrameric channel. An exciting property of TRP channels is their ability to heteromultimerise; resulting in the formation of channels with new biophysical properties, modes of activation, or simply more efficient trafficking of the ion-conducting subunit. The pore is formed between TM-domains 5 and 6 (Fig. 5). TRPs are generally non-selective cation channels found in plasma or lysosomal membranes. A conserved sequence of 25 amino acids, the TRP-domain, is found in

many TRP channels C-terminally of the last TM-domain. Within it lies a highly conserved, 6 amino acids long, proline-rich segment – the so-called TRP-box. Both termini are located intracellularly. Other common structural motifs are the coiled-coil-domain, the calmodulin-binding-domain and ankyrin repeats of varying length. Almost all functionally characterised TRP channels are permeable to Ca^{2+}, but most of them not selectively (P_{Ca}/P_{Na}=0.3 to 10). Although TRP channels have many roles in neuronal and non-neuronal cells, they are conspicuously involved in sensory function, being essential (in one species or another) for vision, hearing, taste, olfaction, pheromone sensation, mechanosensation and thermosensation. Some are activated directly by sensory stimuli, others by a variety of second-messengers. Detailed reviews deal with all members of the TRP family[102,107].

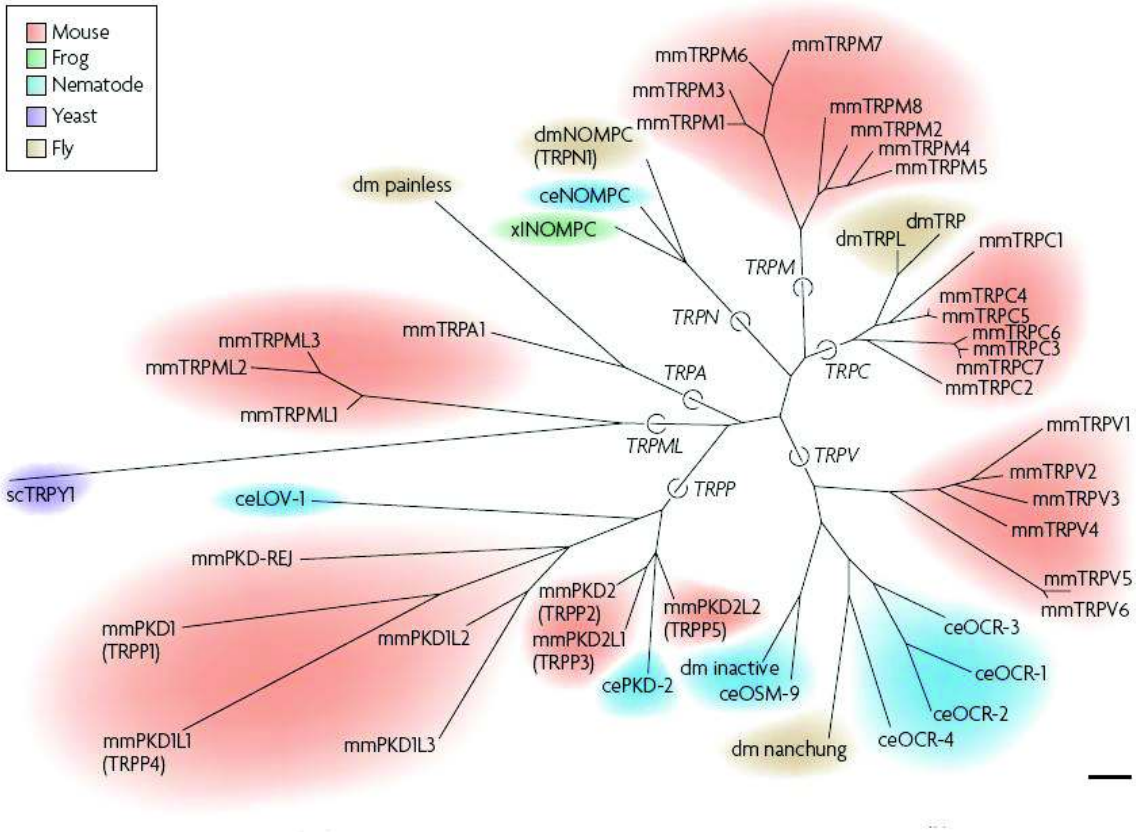

FIG. 4: PHYLOGENY OF REPRESENTATIVE TRP CHANNELS.
A phylogenic tree done in ClustalX by aligning the TM-domains of all 33 TRP channels from mouse and other species. The seven main branches are denoted by circles at the branch roots. Species are indicated by different colours and prefixes. ce, *Caenorhabditis elegans*; dm, *Drosophila melanogaster*; mm, *Mus musculus*; sc, *Saccharomyces cerevisiae*; xl, *Xenopus laevis*. Scale bar represents 0.2 nucleotide substitutions per site. Illustration taken from Christensen and Corey (2007).

(II) GATING AND FUNCTION

As TRP channels are permeable to cations, they can regulate intracellular ion concentrations and affect the membrane potential in excitable and non-excitable cells. They can directly depolarise the cell and drive the action potential in neuronal cells or, more indirectly, regulate other

voltage-gated ion channels in different cell types. The influx of Ca^{2+} can also affect cellular signalling. As the activation is mainly polymodal the cellular context is decisive of the final response to a given stimulus. TRP channels can also be activated by endogenous and exogenous ligands, by stimulation of interacting receptors (like GPCR, RTK, lipid signalling) as well as by physical changes of the environment (temperature, ionic strength, pH and mechanical stimuli; also see Ramsey et al.[108]). Some TRP channels seem to be constitutively open whereas others appear to become activated upon depletion of intracellular Ca^{2+} stores. Although most of the TRP family members lack the full complement of charged amino acids in the S4 TM-domain characteristic for voltage-dependent channels, a number of them do indeed exhibit voltage-dependent behaviour.

(III) MEMBRANE LOCALISATION

Initially thought to be solely plasma membrane (PM) channels, almost all mammalian TRPs studied so far have also been found in intracellular vesicular membranes. Several TRPs are constitutively localised in the ER and Golgi and, more importantly, can be activated in these compartments by their agonists. As multiple transport steps in the ER and the Golgi apparatus are regulated by intraluminal Ca^{2+} release, this points to active roles of TRPs in ER- or Golgi-mediated signal transduction or membrane trafficking[109]. Those TRPs are therefore not simply passive cargo, but instead play active roles in membrane fusion and fission, signal transduction, and vesicular homeostasis. For some TRP channels (TRPP2, TRPV1, TRPM8) evidence accumulated that they are present and active in intracellular membranes. Therefore they are held responsible for Ca^{2+} release from intracellular stores[110].

(IV) THE TRPP FAMILY OF ION CHANNELS

The TRPP family is very inhomogeneous and can be divided, on structural criteria, into PKD1-like and TRPP2-like proteins. A common feature of both is that they do not possess TRP-domains at the C-terminus. PKD1-like proteins are PKD1, PKDREJ, PKD1L1, PKD1L2 and PKD1L3. PKD1 consists of 11 TM-domains and a very long (~3,000 aa) and complex extracellular domain (Fig. 5). The inclusion of PKD1-like proteins within the TRP superfamily is somewhat tentative and is based upon a degree of structural similarity between TRP channels and the six distal TM-domains of at least some PKD1-like members[111]. On the other hand the TRPP2-like members structurally better resemble other TRP channels because they have intracellular termini, six TM-domains and a pore region. So far three members have been identified: The name-giving TRPP2 (also: PKD2), TRPP3 (PKD2L1) and TRPP5 (PKD2L2). All have a coiled-coil structure in their C-terminus and can form multiprotein complexes. TRPP2 and TRPP3 additionally possess a Ca^{2+}-binding EF-hand motif in the C-terminus. In heterologous expression systems TRPP2 and TRPP3 form constitutively active cation-selective channels of relatively large conductance[112]. TRPP3 is a

widely expressed, non-selective, Ca^{2+}-modulated ion channel. *Trpp3* KO mice show retinal and renal defects[113,114]. Trpp3 is sensitive to pH, voltage and cell-swelling, additionally it is inhibited by large monovalent cations and multivalent cations (Mg^{2+}, Gd^{3+} and La^{3+})[115]. Also, TRPP3 together with a PKD1-like protein, PKD1L3, has been identified in sour taste sensory cells and spinal cord sensory neurons in mammals[116-118]. However, most likely it is not part of the transducer channel[119]. No channel activity or functionality has been proposed for TRPP5 so far[108]. PKDREJ is a human homologue of the sea urchin receptor for egg jelly. In mammalians it has been found only in testis tissue where it is restricted to the spermatogenic lineage (including mature sperm). It can modulate G protein signalling and associates with several members of the TRPP2 family. However, its role in sperm biology is not fully understood[120,121].

1.3.2 TRPP2 – LOCALISATION, INTERACTION AND ACTIVATION

(I) POLYCYSTIN-1 / PC-1

PC-1 (polycystin-1, also PKD1) is the protein product of one of two genes that can be mutated in polycystic kidney disease (PKD). It is a very large protein (~4,300 aa) with 10 – 12 transmembrane- (TM-) domains and a long extracellular N-terminal extension (~2,500 aa). The extracellular portion of PC-1 contains several domains present in known cell adhesion molecules (see Fig. 5). Among them – just ahead of the first TM segment – is a G protein-coupled receptor (GPCR) proteolytic site (GPS) that is responsible for the proteolytic cleavage of full-length PC-1 into two pieces. The N-terminal fragment encompasses almost the entire extracellular domain whilst the C-terminal fragment contains the remaining molecule. PC-1 is localised to the ciliary membranes of kidney epithelial cells where it mediates flow-induced Ca^{2+} influx. However, both heterologously-expressed and endogenous proteins are also localised to the ER[122]. By reconstitution into a lipid bilayer, PC-1 was shown to be activated by Ca^{2+} on the cytoplasmic side. PC-1 may therefore function as a calcium-induced calcium release (CICR) channel like IP_3- and Ry-receptors[123]. In *Pkd1*-deficient cells, the basal $[Ca^{2+}]_{cyt}$ is significantly lower than in control cells[124]. In contrast, overexpression of PC-1 leads to an increase of $[Ca^{2+}]_{cyt}$ and a concurrent decrease of $[Ca^{2+}]_{ER}$. These results suggest that PC-1 may function as an ER leak channel.

(II) POLYCYSTIN-2 / TRPP2

([111,125-129]) TRPP2, or polycystin-2, is encoded by the gene *TRPP2*. The C-terminus of TRPP2 contains an ER-retention signal, an EF-hand motif, and a coiled-coil-domain (Fig. 5). Electrophysiological studies indicate that TRPP2 is a Ca^{2+}-activated, non-selective cation channel with multiple subconductance states and a high permeability for Ca^{2+}. TRPP2 shows its highest expression in the kidney. In embryogenesis it is also expressed in embryonic node monocilia. There it senses fluid flow from nearby motile cilia and is involved in determining the left-right

body axis[130]. Lack of TRPP2 can cause *situs inversus*[131]. TRPP2 can interact with itself which suggests that this channel may function as a dimer, trimer or tetramer. Interactions with channels of other TRP subgroups are also known (TRPC1[132] and TRPV4, Fig. 6D). TRPP2/TRPC1 mediates G protein-coupled receptor activation and shows different properties than TRPP2 or TRPC1 alone. Overall conductance of a particular tetrameric TRPP2/TRPC1 channel depends on the composition of the complex[133]. Native TRPP2/TRPC1 activity is shown in two different kidney cell lines. Its existence under physiological conditions is supported by co-localisation at the primary cilium and by co-immunoprecipitation from kidney membranes[134]. TRPP2 and TRPV4 form a mechano- and thermosensitive molecular sensor in the cilium. TRPV4-depletion in renal epithelial cells abolishes flow-induced Ca^{2+} transients; demonstrating that TRPV4, like TRPP2, is an essential component of the ciliary mechanosensor[135].

(III) ALTERNATIVE SPLICING OF *Trpp2*

The National Institute of Ageing lists 6 different *Trpp2* splice isoforms in mice, five of them are supposed to code proteins ranging from 966 aa to 311 aa*. The two full-length transcripts *Trpp2_1* and *Trpp2_2* – only differing in the splicing of their 3' UTR (3896 vs. 5127 bp) – are differently expressed in the cochlea. Ensembl proposes 3 different transcripts; two of them are non-coding†. In humans Ensembl suggests 7 *TRPP2* transcripts with 3 of them coding for proteins (968 aa and 386 aa)‡. The Alternative Splicing Database (ASD) Project lists 4 possible human isoforms§ from 73 aa to 859 aa. Interestingly, there is no overlap between these sources except for the full-length transcript. ASD data for most splice variants are derived from only one EST of single (but different) cDNA libraries whereas the existence of the full-length transcript is based on data from 24 ESTs of 20 different libraries. This means that evidence for protein-coding alternative splice variants is sparse – both in humans and mice. An experimental study discovered another 4 novel, naturally occurring isoforms in human cell lines or murine tissues (Δ6, Δ7, Δ9, Δ12-13). *Trpp2Δ7* transcript is predominantly expressed in the brain (although only at low levels: 3 – 6.4% of all brain *Trpp2* transcripts)[136]. Trpp2Δ7 is stable when expressed heterologously. As its C-terminus is expected to be located on the extracellular side of the membrane this finding could have far-reaching consequences for the interaction and trafficking of neuronal Trpp2, and the detection by available antibodies. However, so far the existence of this proposed protein isoforms lacks additional proof.

* http://lgsun.grc.nia.nih.gov/geneindex4/bin/giU.cgi?genename=U042663

† http://www.ensembl.org/Mus_musculus/Gene/Splice?db=core;g=ENSMUSG00000034462;r=5%3A10 4887489-104934838;t=ENSMUST00000133540

‡ http://www.ensembl.org/Homo_sapiens/Gene/Splice?g=ENSG00000118762;r=4:88928820-88998929

§ http://www.ebi.ac.uk/asd-srv/Index.cgi?ensembl_id=ENSG00000118762&method=ENSEMBL&specie=H&product=SINGLE&release=

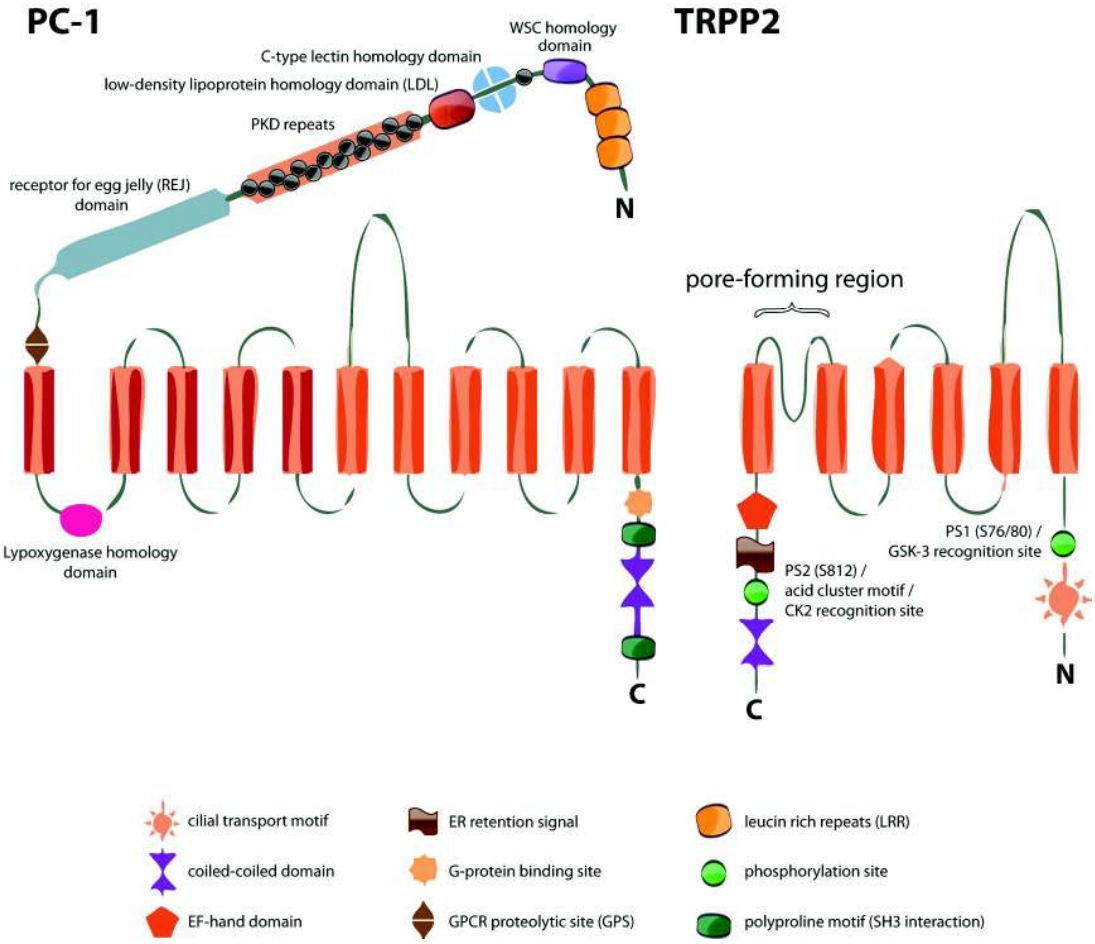

FIG. 5: MEMBRANE TOPOLOGY OF PC-1 AND TRPP2

CK2 casein kinase 2, *ER* endoplasmic reticulum, *GPRC* G protein-coupled receptor, *GSK-3* glycogen synthase kinase 3, *SH3* src homology domain, *WSC* cell wall integrity and stress response component. Structures are not drawn to scale. Illustration adapted from Giamarchi et al. (2006)

(IV) COMPLEXES OF PC-1-LIKE AND TRPP2-LIKE PROTEINS

The concerted action of a PC-1-like and a TRPP2-like protein as in the already mentioned sour taste detection first has been discovered between PC-1 proper and TRPP2 proper[137,138]. TRPP2 is found on the basolateral side of kidney epithelial cells whilst PC-1 staining is more pronounced on the lateral sides of the cell[139]. This would hint on TRPP2 and PC-1 not being in the same signal transduction complex but instead having different functions in non-overlapping regions of the cell. However, more recent work detected TRPP2 together with PC-1 in the short primary cilia on the apical side of kidney epithelial cells where they act together as mechanosensors[140,141] (Fig. 6A, E). PC-1 and TRPP2 form functional ion channels when they are co-expressed in cultured cells[140]. They physically couple to act as a signalling complex at the plasma membrane (PM). TRPP2 is recruited to the PM by PC-1[140,142]. Cells from mutant mice lacking *Pkd1* do not show flow-activated Ca^{2+} influx, nor do cells treated with antibodies that bind extracellular epitopes of either PC-1 or TRPP2[141]. The association of the two proteins suppresses (1) the ability of PC-1 to activate G proteins[143] (Fig. 6A) and (2) the constitutive channel activity of TRPP2[142]. Antibodies

directed against an extracellular domain of PC-1 diminish such mutual inhibition, thus enhancing channel activity of TRPP2 and G protein activation by PC-1. Such a mode of activation might mimic the physiological stimulus that activates the complex.

(V) POLYCYSTIC KIDNEY DISEASE (PKD)

Polycystic kidney disease (PKD) is an inheritable disease leading to fluid-filled cysts in kidney, pancreas and liver[144]. The autosomal recessive form (ARPKD) is a rare hereditary disease that is not related to defects in TRPP subfamily members. Instead ARPKD is caused by mutations in the gene coding for fibrocystin/polyductin (FPC). Interestingly, FPC colocalises with TRPP2 at the basal bodies of primary cilia suggesting an underlying common mechanism in the disease aetiology of ARPKD and ADPKD[145,146]. The disruption of cilium formation in renal epithelia induces cystogenesis. Missing or downregulated FPC or TRPP2 thus decreases cilia formation and ultimately leads to cyst formation[147,148].

The symptoms of the more common (90%) autosomal dominant form (ADPKD) usually develop between the ages of 30 and 40. This disease is characterised by a progressive development of numerous, fluid-filled, spherical cysts of different size in all nephron segments. They can grow so massive that the cystic tissue compresses and destroys the remaining normal renal tissue, ultimately leading to kidney failure or end-stage renal disease. ADPKD patients also suffer from cardiovascular complications, including intracranial aneurysms and thoracic aortic dissections. ADPKD arises from mutations in *PKD1* (85% of all cases, 56 disease-causing mutations and 384 single nucleotide polymorphisms known) or *TRPP2* (15%, 45 disease causing mutations and 186 SNPs known)[149,150]. About 3 – 5% of all ADPKD cases can be related to atypical splicing events. So far 18 of these mutations affecting splicing have been found in *PKD1* and *TRPP2* genes[151]. Patients with *PKD1* defects show a more severe aetiopathology and have a shorter survival time than those with *TRPP2* defects. It is assumed that cystic tissue lacks the functional PC-1/TRPP2 complex[112,152]. ADPKD is the result of a two-hit mechanism whereby the inherited, mutated *PKD1* or *TRPP2* allele is counted as the first hit and the somatic inactivation of the other, wildtype allele in individual polarised epithelial cells is the second. This loss of heterozygosity initiates cyst formation[152]. The PC-1/TRPP2 complex has an indispensable role in kidney development but its activation mechanisms, its precise cellular functions, and its specific roles in ADPKD pathophysiology are still unclear.

So far several competing theories seek to explain ADPKD pathophysiology. Among them are hyperproliferation after interference with the AP-1/β-catenin/Wnt pathway[148] (Fig. 6B), the JAK-STAT pathway[153] or mislead regulation by a basal helix-loop-helix protein (Id2)[154] (Fig. 6C). Also abnormal phosphorylation of TRPP2[155] and de-regulated apoptosis[156] are discussed as causes. However, opposing most of the these findings a detailed gene expression profiling in a

rat disease model (affecting *Trpp2*) suggests that all proliferation-dependent pathways are deregulated after cysts have already been established. Instead, their data suggest that the RAS system is the first signalling system that shows aberrant regulation[157].

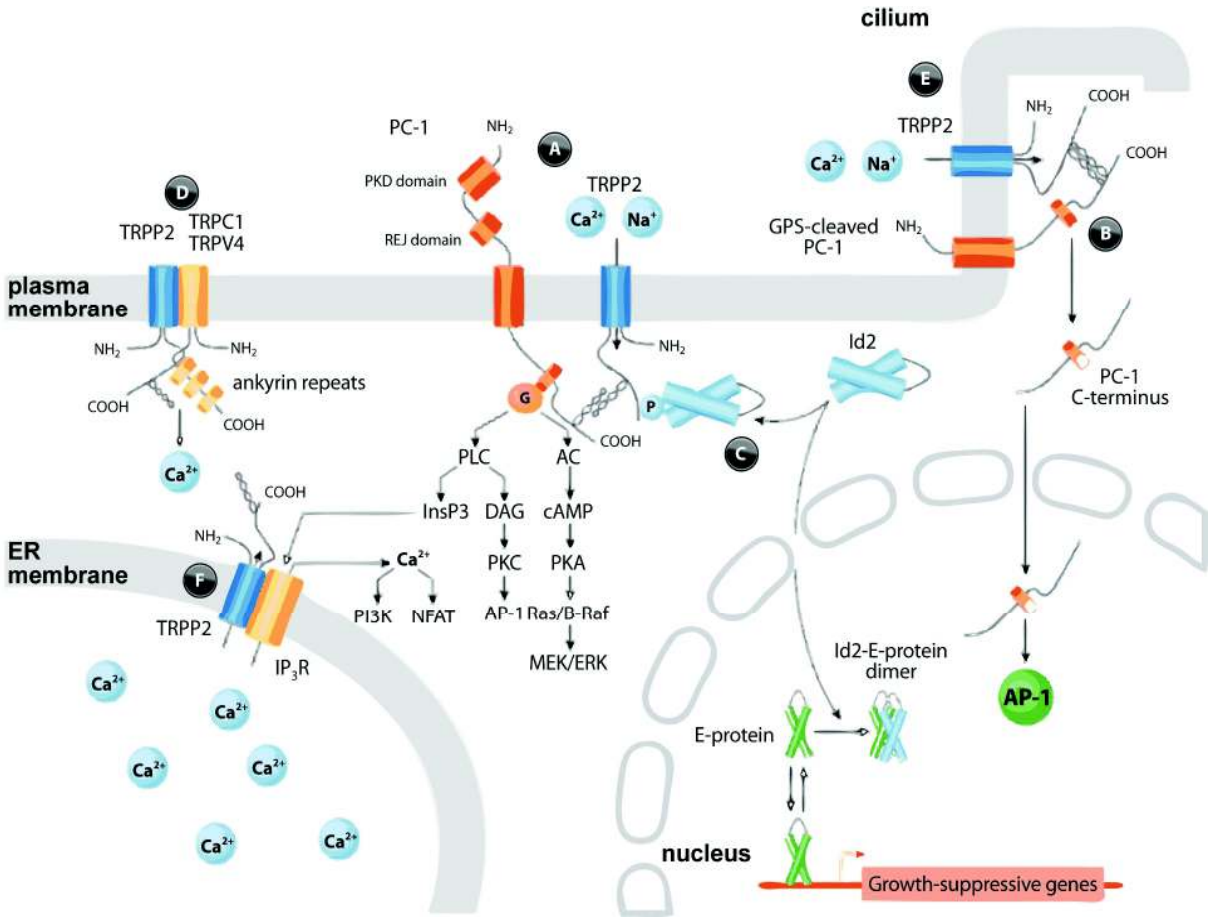

FIG. 6: COMPARTMENT-SPECIFIC FUNCTIONS OF TRPP2
ERK extracellular signal-regulated kinase; *GPCR* G protein-coupled receptor; *Id2* inhibitor of DNA binding 2; *MEK* mitogen-activated protein kinase/ERK kinase; *NFAT* nuclear factor of activated T-cells; *PI3K* phosphatidyl-inositol 3-kinase; *PKA* cAMP-dependent protein kinase; *PKC* protein kinase C; *REJ* receptor for egg jelly. Illustration adapted from Giamarchi et al. (2006)

(VI) TRPP2 AT THE PRIMARY CILIUM

TRPP2 interacts with a variety of partners at the plasma membrane (PM, Fig. 6A, D), at the primary cilium (Fig. 6E) and at intracellular membranes (Fig. 6F). The primary cilium has evolved as a multifunctional cellular compartment that decorates most vertebrate cells. TRPP2 is required for cilia-mediated Ca^{2+} transients but if it itself is a bona fide mechanosensitive channel is doubtful[158]. Cilia are assembled from basal bodies by a process called intraflagellar transport (IFT). The centrosome protein pericentrin (Pcnt) co-localises with IFT proteins at the base of primary and motile cilia. After depletion of its mRNA in human epithelial cells cilia do not assemble. A complex of Pcnt, IFT proteins and TRPP2 is needed for the correct assembly of primary cilia[159]. TRPP2 and PC-1 are expressed in cilia[160]. As cilium bending is associated with

increased Ca^{2+} entry into the cell[161] a connection was drawn between those findings: Fluid shear stress applied to ciliated cells results in a TRPP2- or PC-1-dependent Ca^{2+} entry into the cell body[141]. The authors propose that TRPP2 and PC-1 play a mechanosensitive role in kidney cells and that the loss of fluid-flow-induced PC-1/TRPP2-mediated Ca^{2+}-entry through the cilium may be the primary defect in ADPKD. Primary cilia are organelles with a microtubule skeleton (axoneme). Stabilising microtubules (taxol) leads to an increase in TRPP2 activity whilst destabilising them (colchicine) decreases TRPP2 activity[162]. This modulation seems to be indirect and kinesin motors, KIF3A and KIF3B, have been suggested to be the missing link. They physically interact with TRPP2, α-tubulin[163] (both) and FPC[164] (only KIF3B), thus also connecting ARPKD with ADPKD. Data suggest that KIF3A/B have a non-traditional role (not as motor proteins) in the cilia complex. The TRPP2-KIF3B-fibrocystin complex possibly is a part of the sensor in the cilium. Furthermore it is unclear if this complex is different from the PC-1/TRPP2 complex – or if they constitute a large, singular complex.

(VII) TRPP2 AT THE PLASMA MEMBRANE

As mentioned before TRPP2 interacts with TRPC1 and TRPV4 probably at the cilium (1.3.2.II). However, some authors also suggest an interaction at the PM (Fig. 6D). TRPP2 at the PM is intertwined with the cytoskeleton network as the actin cytoskeleton can directly modulate TRPP2 and *vice versa* (e.g. α-actinin-2, tropomyosin-1, troponin I, Hax-1/Cortactin)[165-171]. Also, PC-1 associates with components of the filament network, such as α-actinin, vimentin, cytokeratin and desmin[172]. The direct coupling of TRPP2 to the actin cytoskeleton suggests that TRPP2 activity could be modulated by mechanical changes transferred to the channel through the actin network. Whether these results stand on their own or can be reconciled with processes at the microtubule-based cilium remains controversial. mDia1-mediated blocking of TRPP2 at negative – but not positive potentials – is postulated for the primary cilium, mitotic spindles[173] and also for the PM. Membrane depolarisation activates TRPP2 by releasing the mDia1-dependent block[174]. This might be a general molecular basis for a voltage-dependent gating of TRP channels. How the unblocking effects TRPP2 function at the different compartments remains largely unclear. In fact, membrane depolarisation seems to be more important for TRPP2 activation at the PM whereas EGF-activation (via EGFR, RhoA, mDia1) might be prevailing at the cilium. TRPP2 is only active at the base of the cilium where prepro-EGF concentration is high. Hence, there highly sensitised TRPP2 mediates efficient mechanotransduction secondary to fluid flow changes[125]. At the cilium TRPP2 is also kept insensitive to flow stimulation by PIP_2-mediated inhibition. This inhibition is switched off by breaking down PIP_2 into DAG and IP_3 by PLCγ2 (activation possibly also via EGF/EGFR)[175].

(VIII) TRPP2 AT THE ENDOPLASMIC RETICULUM

Overexpressed TRPP2 likely stays in the endoplasmic reticulum (ER)[122,140]. When co-expressed with PC-1 in Chinese hamster ovary (CHO) cells TRPP2 traffics to the PM where the complex is associated with increased cell conductance (likely due to TRPP2 channel function)[140]. The adaptor proteins PACS-1 and PACS-2 bind to an (phosphorylated) acidic motif in the C-terminus of TRPP2. This prevents the transport of the channel from the ER to the Golgi and so reduces surface expression of the channel[176]. Other reported interaction partners at the ER membrane are the ER-resident kinase PERK and the eukaryotic translation initiation factor eIF2α[177]. TRPP2 represses protein synthesis and cell growth through promoting PERK-dependent phosphorylation of eIF2α. Other interacting ER-associated proteins are Herp, P97[178] and PIGEA-14[179]. Trafficking of TRPP2 to the PM – but not to cilia – is also regulated by phosphorylation at a unique GSK3 site in its N-terminal domain (Fig. 5) *in vivo* and *in vitro*. This site is functionally significant for the maintenance of normal glomerular and tubular morphology as shown by antisense morpholino injection in zebrafish. The cystic phenotype can be rescued by co-injecting wildtype but not site-directed mutated mRNA[180].

TRPP2 also has an antiapoptotic function in renal epithelial cells where it functions as a Ca^{2+} release channel in the ER. Knocking down *Trpp2* leads to increased Ca^{2+} levels inside the ER. Apoptotic stimuli induce Ca^{2+} release from the ER. In *Trpp2*$^{-/-}$ cells this efflux is so potent that also mitochondria answer with high Ca^{2+} release. The magnitude of the mitochondrial Ca^{2+} signal and additional proapoptotic stimuli determine whether cytochrome C is released to ultimately trigger apoptosis. These findings provide a molecular mechanism for the increased apoptosis rate in ADPKD upon loss of TRPP2 channel function[181]. The functional interaction of TRPP2 and type I IP_3R (C-terminal, possibly via the coiled-coil-domain) also modulates intracellular Ca^{2+} signalling[182] (Fig. 6F). Hereby, IP_3R is in competition with PC-1 for binding to TRPP2. A new twist was introduced when it became clear that PC-1 not only traffics TRPP2 to the plasma membrane but that the complex also has a functional role in the ER membrane itself. When being overexpressed it prevents Ca^{2+} leakage from the ER into the cytoplasm[183]. Thus the formation of PC-1/TRPP2 complexes in ER membranes might prevent Ca^{2+} leakage through TRPP2 channels (reviewed by Sutters[184]). In general, healthy cells maintain a tightly controlled balance of PC-1, TRPP2 and IP_3R at the ER membrane. When either IP_3- or TRPP2-mediated Ca^{2+} signalling is disturbed (also by overexpression or deficiency of PC-1) kidney cystogenesis is facilitated.

(IX) NATURAL LIGANDS AND DRUGS TARGETING POLYCYSTINS

The paucity of selective modulators is a general hallmark of all TRP channels. Because of its high incidence (1 in 400 to 1000 individuals[185]) a specific treatment for PKD is long sought after. Among several drugs currently under investigation[186] only one targets TRPP2 directly:

triptolide. This compound is derived from *Tripterygium wilfordii* – an herb that has been used in natural medicine in China for hundreds of years. Triptolide is a small hydrophobic molecule (diterpenoid triepoxide) that can pass cell membranes. PM-located TRPP2 is a major target of triptolide. There it facilitates Ca^{2+} release through a TRPP2-dependent pathway[187]. Triptolide can still induce a Ca^{2+} response in cells without PC-1 but in *TRPP2*$^{-/-}$ cells this response is highly reduced (though not completely abolished). Via increased intracellular Ca^{2+} levels, inhibited adenylyl cyclases and therefore decreased cAMP levels cyst growth is reportedly reduced in different mouse models of ADPKD caused by mutated *Pkd1*[188,189]. Triptolide also has been shown to (1) induce rapid apoptosis in a myriad of cancer cell lines and (2) inhibit NFκB transactivation (via at least two distinct cellular pathways). This activation of TRPP2 marks one more functionality among the plenitude of modes of action for growth arrest or cell death of TRPP2.

1.3.3 TRP CHANNELS IN THE MAMMALIAN INNER EAR

([107,158]) So far 43 syndromic and 57 non-syndromic* deafness genes have been found and their corresponding mouse models scrutinised† – none of them is a TRP channel. However, several of the null mutant mice that have been done of most of the known 30 TRP channels show an auditory phenotype. Because TRP channels assemble as heterotetramers it is thought that in a knockout of a single TRP channel other, functionally redundant TRP channels substitute for the loss. The observation that the conductance of the still unknown mechanotransduction channel (MET) in hair cells increases along the longitudinal axis of the cochlea might also be explained by a multimeric layout. The channel is more sensitive at the base (high frequencies) than at the apex. The substitution of subunits within this multimer could easily explain the growth of conductance (single channel pore size) towards the apex where low frequencies are coded. Some members of the TRP ion channel family have properties similar to the elusive MET channel in hair cells. The mechanotransducer channel opens exceptionally rapidly (latencies between 20 and 40 μs) which disqualifies enzymatic conversion and diffusion to be involved in mechanotransduction. The single channel conductance of this channel is estimated to be around 100 pS[190] (TRP channels: up to 300 pS). Also the pharmacology suggests that the MET could be a TRP channel. However, no known family of TRP channels combines all the necessary properties in conjunction[191], so that this channel either belongs to a yet unknown TRP channel family or – more probable – to an entirely new ion channel family (possibly: the Piezos[192]).

Data about TRP channel transcripts in the inner ear come from samples that consist of o/C alone[193] or o/C together with Reissner's membrane and stria vascularis[194]. Another study compares 3 different mouse tissues with each other: o/C, stria vascularis and vestibular organs[195].

* Hearing impairment is the one and only clinical symptom present.
† http://hearingimpairment.jax.org/models.html

(I) TRPA CHANNELS

TRP channels TRPA1 was discussed as a candidate for the elusive mechanically gated transduction channel necessary for the auditory response[196] but two independently generated *Trpa1*$^{-/-}$ mouse strains do not show hearing deficits[197,198]. However, the high incidence of its transcripts in the inner ear suggests a relevant function[194]. The authors speculate that a functional redundant protein takes over Trpa1 function in the knockout mouse.

(II) TRPV CHANNELS

TRPV1, like TRPA1, is expressed in the o/C. Agonists of TRPV1 can reduce cochlear microphonic potentials and elevate the threshold for the auditory nerve compound action potential. TRPV1 channels located on OHCs may play a role in cochlear homeostasis, rather than in mechanotransduction[199]. TRPA1 and TRPV1 channels can interact and regulate the expression of each other. Therefore they may compensate for each other in the respective knockout mice[200]. The locus for the progressive non-syndromic hearing loss DFNA25 in humans corresponds to another vanilloid TRP channel, *TRPV4*[201]. In the cochlea TRPV4 is expressed by sensory cells (low level, particularly in older mammals), large cell bodies of SGNs, and marginal cells of the stria vascularis[202]. TRPV4 is gated by hypotonicity that is regarded as a form of mechanosensation. The hypothetical role of mammalian TRPV4 in mechanotransduction is also strengthened by its homology with the invertebrate osmo- and mechanoreceptor OSM-9 and with the *Drosophila* TRP genes *Inactive* and *Nanchung* (reviewed by Cuajungco[104,193]). Nevertheless the gating is more probably mediated by an indirect mechanism[203,204]. Knockout mice display a delayed-onset hearing loss and a higher vulnerability of the cochlea to acoustic injury that are both not consistent with a seminal role in mechanotransduction[205].

Expression analyses of murine o/C tissue suggest the presence of another TRPV channel: TRPV2[193]. *TRPV2* (and *TRPV6*) expression in a mouse inner ear sample was confirmed later on[195]. In an investigation of inner ear tissue of various ages in development the presence of above mentioned transcripts could be confirmed. Additionally *TRPV3* was detected so that only *TRPV5* seemed to be absent[194]. Interestingly, also *TRPV5* (as well as *TRPV6*) knockout mice are deaf (Pendred syndrome[206]). Immunohistochemistry suggests that TRPV1 proteins are not located at the PM but rather in perinuclear compartments[207]. TRPV1 might promote cell survival because its expression is upregulated upon kanamycin and noise exposure[208,209]. Later on stainings showed rather equivocally also TRPV2/3/4-ir in hair cells, SGNs and VGNs[210]. The presence of TRPV4 in the soma of murine SGNs was also confirmed elsewhere[211]. Stainings against TRPV5 and 6 show – opposite to the observed transcript incidences – that TRPV5 is more prevalent. TRPV6 is mainly found in the supporting cells of the o/C[212].

(III) TRPML CHANNELS

TRPML3 is expressed in the stereocilia of cochlear hair cells. Structural defects in cilia in gain-of-function mutants also hint on a role in stereocilia function. *Trpml3*$^{-/-}$ mice (varitint-waddler) are profoundly deaf and display vestibular defects[213]. RT-PCR data indicate that *TRPML1* (but not *TRPML2*)[193] or all three *TRPMLs*[194] are expressed in the organ of Corti. Antibody stainings show similar expression profiles for all three proteins in the inner ear of mice[214].

(IV) TRPM CHANNELS

The transcripts of the melastatins *TRPM3* to *7* (but not *TRPM1*, *2* and *8*) are present in the organ of Corti[214]. For *TRPM3* (and its various splice forms), *4*, *5* and *7* additional evidence comes from a screen of EST libraries of human and murine inner ear samples[215]. Possibly also *TRPM1*[195] or even all *TRPMs* except *TRPM8*[194] might be expressed. *TRPM1* stands out because of its manifold increase at P2 in the basal turn. *TRPM5* and *7* decrease sharply at P6 whereas *TRPM6* transcript numbers constantly increase from E17 to P8[194].

(V) TRPC CHANNELS

TRPC3 contributes to Ca^{2+} entry supporting Ca^{2+} homeostasis in cochlear hair cells. It is expressed differently strong in apical and basal turns[216]. In SGNs TRPC3 is activated by G protein-coupled receptor (GPCR) signalling. Antibody staining against TRPC3 shows increased ir from birth to adulthood in SGNs; the opposite applies for hair cells[217]. Another study found that staining in IHCs is stronger than in OHCs. Additionally, basal hair cells are stained stronger than apical ones[218]. In the o/C the transcripts of canonical (classical) TRP channels *TRPC1*, *2*, *3*, *5* and *6* (and not *TRPC4* and *7*) are present[193]. The most extensive immunohistochemical characterisation has been done in adult mice[219]: All TRPCs are expressed in the mouse inner ear, e.g. lateral wall of the cochlea, o/C, and SG. Moreover, the strength and pattern of the stainings differed among the TRPCs, especially in the spiral and vestibular ganglia. The aTRPC6 ab, for instance, predominantly stains cell nuclei whereas other abs stain cell somata. The significance of the different subcellular distributions is not known but it is suggested that individual TRPC channels fulfil different functions.

1.4 Cell-autonomous inactivation of ion channels

1.4.1 CONOTOXINS: PEPTIDE TOXINS DERIVED FROM CONE SNAILS

Conopeptides are components of the venom of marine snails belonging to the genus *Conus*. They act on diverse ion channels; ultimately, to help to capture prey or deter predators. Their tantalising therapeutic potential is reviewed by Twede et al.[220]. Each of the 500 known *Conus*

species produces dozens of different toxins per venom, resulting in more than 50,000 pharmacologically active conopeptides[221]. Among them the group of conotoxins is characterised by their small size and their richness in disulfide bonds. After secretion into the cone snail duct, conotoxin precursors are cleaved by proteases generating active toxins that are often subject to posttranslational modifications. Conotoxins target different voltage- or ligand-gated ion channels like noradrenaline transporters (κ-conotoxins), sodium channels (μ-, μO- and δ-conotoxins), calcium channels (ω-conotoxins), the N-methyl-D-aspartate (NMDA) receptor (conantokins) and neurotensin receptors (contulakins)[222].

(I) CONOTOXINS TARGETING NICOTINIC ACETYLCHOLINE RECEPTORS

([223,224]) αA-conotoxins and ψ-conotoxins comprise only few conotoxins – all targeting muscular nAChRs and thus will not be introduced further. α-conotoxins represent the largest family. They consist of 12 to 19 amino acids, and are characterised by a specific cysteine pattern (C_1C_2-C_3-C_4). Disulfide bonds are made between C_1 and C_3 – and C_2 and C_4, respectively. Based on the number of other amino acids between the cysteins C_2 and C_3 (first loop) and C_3 and C_4 (second loop) a further classification into α3/5 (which also target muscular nAChRs) and α4/7, α4/6, α4/4 and α4/3 (which all target neuronal nAChRs) is made. The toxins infer either competitively or non-competitively with channel function. It seems that toxin binding on only one subunit interface is sufficient to block receptor function. This is in contrast to the necessity of agonist-binding on two interfaces for channel opening.

(II) α -CONOTOXINS TARGETING α7 HOMOMERIC nAChRs

Toxins targeting α7 homomeric receptors are fairly abundant (see McIntosh et al.[225]). The snake peptide α-bungarotoxin (αBgtx) is one of the most powerful tools for nAChR purification and subtype specification. It induces seizures when injected into the brain and additionally blocks α1-containing (muscle) receptors. Its blocking of neuronal α7- and α9-, as well as muscle α1-containing nAChRs is quite unspecific when compared to conotoxins. ImI, isolated from the worm-eating species *Conus imperialis*, is the first characterised, neuronal nAChR-targeted α-conotoxin. It selectively blocks α7 nAChRs expressed in *Xenopus* oocytes and induces seizures when injected into mammalian cerebra[226]. Other α7-prefering toxins are PnIB and [A10L]PnIA from *Conus pennaceus*[227,228], a 2nd toxin from *Conus imperialis* (ImII)[229] and AnIB from *Conus anemone*[230]. MII of *Conus magnus* blocks α7 with an IC_{50} of roughly 100 nM. It works best on α3β2 receptors – with or without co-expressed α6 subunits (IC_{50} between 0.4 and 8.0 nM). MII also potently and selectively blocks nAChR currents in native preparations[231,232]. The majority of α-conotoxins antagonising α7 also block closely related α9 and α10 receptors.

(III) MAMMALIAN EXPRESSION OF THE SNAIL TOXIN GID

The α-conotoxin GID from *Conus geographus* also blocks α7 nAChRs. It has a 4/7 inter-cysteine loop spacing. A couple of modifications are outstanding for this toxin among other neuronal nAChR-targeted α-conotoxins. First, it has additional N-terminal residues. Second, it also consists of amino acids with posttranslational modifications (γ-carboxyglutamic acid and hydroxylproline). Furthermore its 12th amino acid is positively charged (Arg) – and not hydrophobic (Ala, Phe) or uncharged (Asn) as usual. Lastly, GID lacks the amidated C-terminus typical for α-conotoxins:

$$IRD\gamma C_1C_2SNPAC_3RVNNOHVC_4$$

When the channels are expressed in oocytes GID has a high affinity for α4β2 nAChRs (IC_{50}= 152nM) but it blocks α3β2 (3.1nM) and also α7 (4.5nM) nAChRs even more potently[233,234]. Its effect on α1β1γδ, α3β4 and α4β4 combinations is at least 1000-fold less potent.

So far GID has not been expressed transgenically in mammals – or in other species. As in this study transgenic mice will express the toxin by themselves ('tethered-toxin' approach, see 1.4.2) the posttranslational amino acid modifications made in cone snails will be missing. It is therefore important to note that the substitution of γ-carboxyglutamic acid by glutamic acid does not change the IC_{50} values of GID on all three nAChR rat subunit combinations[234]. The truncation of the N-terminal tail leads to a profound loss of activity on α4β2 and a smaller, but nevertheless significant loss of activity on α7 and α3β2 receptors[233] which should not have a major influence on the activity of our tethered GID. The substitution of hydroxyproline with proline also only mildly changes the IC_{50} on α7 homomeric nAChRs (from 5.1 to 8.4 nM). The tethered version of GID thus has the following amino acid composition:

$$IRDEC_1C_2SNPAC_3RVNNPHVC_4$$

1.4.2 GENETIC APPROACHES TO STUDY ION CHANNEL FUNCTION IN MICE

Ion channels and receptors constitute the fundamental framework for neuronal circuit function. Detailed knowledge of these elements is essential to understand how the nervous system works under physiological and pathophysiological conditions. Conventional methods to study ion channel function include pharmacological manipulations and the generation of knockout (KO) mice (specific gene deletions). KO mice are a powerful tool to study the function of a wide array of proteins. However, due to the promiscuous nature of many ion channels constitutive global gene deletions hinder the investigation of some of the channel functions: Because of major, essential functions of the missing protein in development many KO mice die before they reach adulthood. This makes behavioural or physiological experiments cumbersome or even

obnoxious. To circumvent this problem more elaborate methods take advantage of promoters to restrict gene deletion to specific (brain) tissues[235].

Large-scale screening projects have been initiated to determine the brain expression patterns of a tremendous number of specific promoters. This allows researchers to choose a promoter that targets a particular class of neurons, e.g. neurons that produce a specific neurotransmitter or express a specific receptor. Examples of these screening projects are GENSAT* and the Allen Brain Atlas†. Such promoters are useful tools to direct the expression of transgenes, e.g. transgenes that can interfere with native cell function by expressing toxins (1.4.2 II) or enzymes (1.4.2 III). With this approach ion channel blocking (1.4.2 II) or gene deletion (1.4.2 III) can be restricted temporally and spatially.

Another caveat when dealing with (conditional) knockouts of ion channel genes is their functional promiscuity. Most ion channels are coded by a variety of genes for all of their subunits. In KO mice related ion channels or related subunits of ion channels may compensate for the loss[236,237]. To overcome this problem silencing methods have to affect all contributing subunits of an ion channel. Overexpression of a dysfunctional form of a crucial (part of a) subunit has been shown to be a feasible option[238], the aforementioned tethered toxin strategy is another[239,240]. Other methods have been developed to silence neuronal circuits *in vivo* by delivering exogenous ion channels that shift the membrane potential to more hyperpolarised states upon activation by specific signals. However, these approaches are often hampered by the inaccessibility of certain tissues for the signal (chemicals or light). In addition they may display hyperpolarisation-caused modifications of normal neuron physiology[241,242].

(I) TETHERED TOXINS

Conotoxins are potent modulators of ion channels that are able to discriminate between closely related subtypes. Most toxins retain their activity and specificity when tethered to the plasma membrane (PM) via a glycosylphosphatidylinositol (GPI) anchor[243]. This idea was prompted by studies on the protoxin lynx1 that shares structural similarities with the snake peptide α-bungarotoxin. Lynx1 is a GPI-tethered molecule that is highly expressed in the mammalian CNS. Lynx1 physically interacts with nAChRs[243,244]. Similarly, naturally occurring peptide neurotoxins can be genetically expressed on the cell surface where they remain anchored because of the GPI-anchor[243]. The general efficiency of this strategy has been shown in zebrafish and chicken by blocking nAChRs[243,245], in Drosophila[246] and mouse[240] by modulating VGSCs. The attained effect is long-lasting because tethered toxins (t-toxins) – unlike soluble toxins – underlie a constant cell-intrinsic replenishment. In the second generation of t-toxins the GPI-anchor has been

* http://www.gensat.org
† http://www.brain-map.org

substituted by a transmembrane- (TM-) domain of the PDGF receptor. This modification enhances the stability of t-toxins[240] because 1st-generation toxins are prone to be clipped off of GPI-anchors by endogenous phosphatidylinositol-specific phospholipases C (PI-PLC)[247]. Additionally, 2nd generation t-toxins harbour fluorescent markers that increase the ability to monitor expression levels and subcellular localisation of the recombinant molecules upon genetic delivery into neurons[239]. The t-toxin approach is an extremely useful tool to block or modify ion channel function *in vivo* because of (1) its flexibility to combine it with other genetic methodologies like BAC-transgenesis, (2) the ability to restrict the toxins' action by membrane tethering (enhanced working concentration close to their points of activity) and (3) the high affinity of the peptide toxins (also see Holford et al.[248]).

An example of a tethered toxin used in this study is given in Fig. 7. Possible modifications of t-toxin constructs used in this study include varying linker length (short, long, 2x long, 3x long), different methods of tethering the toxin to the membrane (GPI-anchor or PDGF membrane-domain) and – where applicable – the addition of fluorescent molecules to the N- or C-terminus (Venus, EGFP). The optimal linker length is different for each toxin-channel-combination. In general ligand-gated channels are better inhibited by short-linker constructs; voltage-gated ion channels require the use of longer linkers[248].

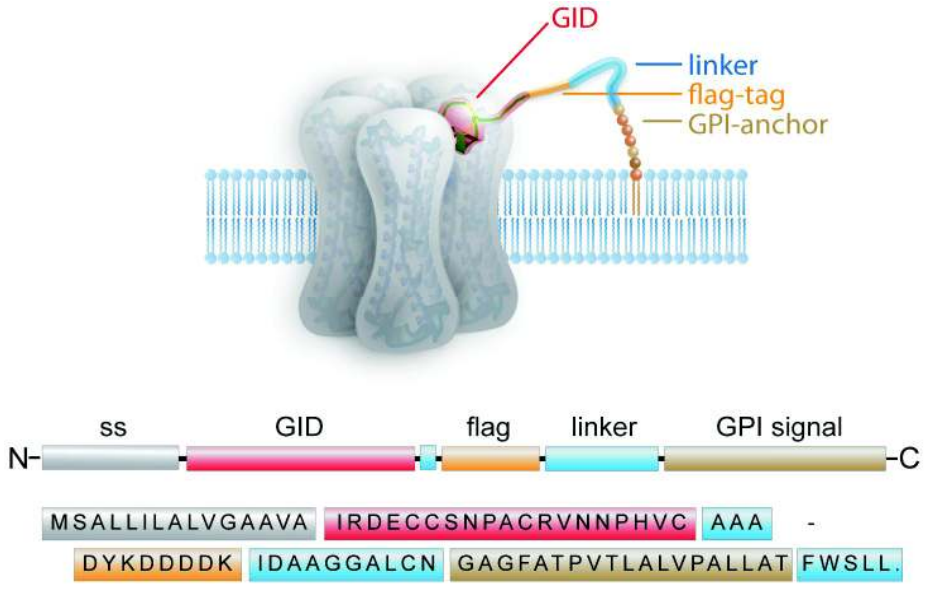

FIG. 7: A MEMBRANE-TETHERED FORM OF THE CONOTOXIN GID

Upper panel: Model of a pentameric nAChR and a tethered toxin molecule attached to its ACh-binding site at the interface of two channel subunits. Bottom panel: Linearised scheme and amino acid sequence of the transgenically expressed t-toxin used in this study. The selected toxin is GID, the chosen linker is of short length and membrane tethering is done via a GPI-anchor (1st generation of tethered toxins). *ss* secretion signal, *GPI* glycosylphosphatidylinositol. Illustration adapted from Auer et al., 2010.

(II) BACs AS CARRIERS OF t-TOXIN CASSETTES IN TRANSGENIC MICE

The delivery of the t-toxins in *in vivo* models has been accomplished so far in two ways. First, gene delivery based on viral vectors such as lentivirus, retrovirus or adeno-associated virus (AAV) was shown to work in chicken[245] and mice[239]. Viruses are naturally evolved vehicles that efficiently transfer their genes into host cells. This desirable ability has been shown to be useful for engineering vector systems delivering therapeutic genes. However, viruses feature disadvantages such as small packaging capacities, toxicities, and immunoresponses towards viral antigens. Bacterial Artificial Chromosome (BAC) transgenesis is an alternative approach to deliver t-toxins and has been shown to work in mice[240]. BACs are large genomic DNA fragments able to carry inserts up to 350 kb. A comprehensive array of BAC-transgenic mice with cell-specific expression of a fluorescent marker in different neuronal populations demonstrates the utility of this approach for mapping genes in the CNS[249]. Furthermore the use of homologous recombination enables the expression of large transgenes avoiding the introduction of point mutations by PCR. This precise and efficient engineering of BACs facilitates a variety of studies that could not be accomplished by conventional approaches. The large genomic inserts of BACs contain whole transcription units. They include promoter and regulatory elements that foster cell-specific gene expression of the introduced transgene. Besides, the homologous recombination method developed by Gong et al.[250] enables precise targeting of the expression cassette into the BAC together with the complete removal of any unwanted bacterial vector sequences[251,252]. The delivery of t-toxins on viral vectors is done via stereotactic injection. This approach is difficult to apply in the developing cochlea and has not been tried so far. Hence, BAC transgenesis is employed for this study. Here modified BACs are injected in mouse blastocysts ultimately leading to transgenic mice carrying multiple BAC copies constitutively in all cells – thus circumventing the need to bring the transgene into SGNs via stereotactic injection. The expression of the transgene depends on the chosen promoter and follows the expression of the native gene controlled by the very same promoter[251]. In this study BAC transgenesis is combined with the t-toxin approach to block α7 nAChRs cell-autonomously in spiral ganglion neurons.

(III) CREATING CONDITIONAL KNOCKOUT MICE USING THE CRE-loxP-TECHNOLOGY

The Cre-lox mechanism was discovered in P1 bacteriophage as part of its normal life cycle[253,254]. Since being discovered, this recombination strategy has been developed as a technology for genome manipulation[235]. It is based on the ability of Cre recombinase to induce recombination between two recognition sequences (loxP, 34 bp). Depending on the orientation of the loxP sites Cre recombinase can induce inversion, deletion or chromosomal translocation of the enclosed sequences. The loxP sites become an integral part of the genome of genetically altered mice flanking one or more exons of the target gene (referred to as a 'floxed' gene). Most floxed genes

are designed to produce deletions. Mice homozygous for a floxed gene (flox/flox) are then crossed to a transgenic mouse line that expresses Cre recombinase under control of a promoter that restricts the expression temporally and spatially. In Cre^+ flox offsprings the floxed gene is excised only in those cells where the chosen promoter is active.

1.5 The use of translating ribosome affinity purification (TRAP) in inner ear cells

The ability to monitor the identity and quantity of proteins that a cell produces would explain nearly all aspects of its biology. Classical proteome analysis in the inner ear so far generated only a modest amount of data[255] – with the most interesting identified proteins present in inner ear connective tissue and inner ear liquids[256]. Technologies measuring mRNA abundance have revolutionised the study of gene expression. However, mRNA levels are an imperfect proxy for protein production because mRNA translation is subject to extensive regulation[257]. Also, predicting the exact protein product from the transcript sequence is not possible because of internal ribosome entry sites, initiation at non-AUG codons, and nonsense read-through[258,259]. Finally, programmed ribosomal pausing during protein synthesis is thought to aid the co-translational folding and secretion of some proteins. However, polysome profiling, where mRNAs are recovered from actively translating ribosomes for subsequent analysis, can provide a useful estimate of protein synthesis[260]. This fraction of the entire mRNA pool (transcriptome) is commonly termed 'translatome'. There are currently substantial limits in quantitative proteomics to independently determine protein sequences and measure low-abundance proteins. Deciphering the complete functional protein content of (e.g.) inner and outer hair cells is therefore not yet feasible[261]. Other methods have been used successfully to constitute functional interactions of inner ear proteins. In a co-immunoprecipitation / 2D-PAGE / mass spectrometry approach a protein network around a cochlear BKα channel was established[262]. Potential interaction partners of Cadherin 23 (a tip link protein of IHC) and Prestin (a motor protein of OHC) have been revealed by a membrane-based yeast two-hybrid assay[263]. However, these results are only as meaningful as the underlying cDNA library used. Therefore the analysis of the translatome currently often remains the method of choice when studying protein expression in certain cells or tissues.

1.5.1 CHARACTERISING THE TRANSCRIPTOME OF THE ORGAN OF CORTI

In the last decade several attempts have been made to elucidate fundamental characteristics of sound transduction in the inner ear by analysing the RNA composition of involved tissues. Special consideration was given to unveil the identity of the mechanoelectrical transducer

(MET) channel at the stereocilia (see Fettiplace[264] for an excellent review on the nature of this channel).

(I) CONSTRUCTION AND ANALYSIS OF INNER EAR cDNA LIBRARIES

Although the inner ear features a characteristic anatomy the analysis of single cell types remains an arduous task. Several inner ear cDNA libraries exist but RNA is obtained at best from micro-dissected tissues which include the whole organ of Corti (o/C)[265], whole vestibular end organs[266], or the complete cochlea[267-270]. Some libraries are even constructed from whole inner ear tissue[271,272].

Based on the above mentioned available cDNA libraries Gabashvili et al. searched for expressed ion channels with a bioinformatics approach[215]. Another group constructed a custom mouse inner ear microarray based on these cDNA libraries and subsequently validated the functionality of their custom chip by analysing total RNA preparations of the whole o/C, the lateral wall (stria vascularis and spiral ligament) and – as one of very few studies – also the spiral ganglion[270]. Other expression studies rely on commercially available chips to study either adult rat[273] or P2 and P32 mouse[274] cochlear tissues. The most extensive analysis of the developmental changes in inner ear gene expression (E9 to E15) was done with standard Affymetrix arrays[275]. Interestingly, only very little overlap between the results of these studies is observed[270]. Also, the number of genes preferentially expressed in the inner ear is as low as 6%[276]. Even when a relatively small fraction of the murine inner ear, the o/C, is processed, the transcript of one of the most abundant OHC proteins, the motor protein Prestin, could not be detected[265]. Taken together this alludes to three limitations: (1) RNA preparation (microdissection), (2) RNA amplification (PCR) and (3) transcript detection (hybridisation).

Detection methods based on sequencing – rather than hybridisation – feature a much lower false-positive error rate. All first-generation sequencing methods (SAGE, CAGE, PMAGE, differential display) were successfully applied to detect mRNAs in numerous cell lines and tissues. As these techniques still rely on the selective (biased) amplification of isolated RNA molecules with PCR methods, they lack the sensitivity to reveal low-abundance mRNAs (<10 copies per cell). Innovative methods like microarray-based genomic selection (MGS) tackle this problem but as the sensitivity of high-throughput / deep sequencing methods is getting better in rapid strides, the RNA amplification step might soon become dispensable. In the field of auditory research the age of high-throughput sequencing began with a publication by Peters et al. who performed the first MPSS (massively parallel signature sequencing) experiment. The isolation of RNA from various different cell types (o/C, striae vasculares and vestibular receptor organs) impeded the identification of low-abundance transcripts[195] because they are usually masked by assay noise. This is a serious problem as the majority of transcripts (~86%) are present with

only 5 copies per cell[277]. Additionally, – due to the composite nature of these tissue samples – a verification of attained differently expressed transcripts (or proteins) by *in situ* hybridisation (or immunohistochemistry) is necessary to allocate them to a single cell type.

(II) MECHANICAL ISOLATION OF INNER EAR CELL TYPES

Important rare-frequency inner-ear-pertinent transcripts are consequently diluted out in the sample because of the large number of different cell types and the resulting low percentage of single target cell types within the cochlea. Isolating transcripts from a single cell type is therefore a desired approach. The isolation of hair cells from the receptor organ of zebrafish ears is easily accomplishable so that a thoroughly done study could increase the percentage of hair-cell-specific genes to 16%[278]. Although new deafness genes could be discovered, the use of RNA amplification and microarray hybridisation probably prevented the discovery of more (low-abundance) transcripts. In mammalians the isolation of fresh hair cells is more elaborate and therefore lacks wide circulation[279,280]. Isolating inner ear tissues of formalin-fixed specimen (with laser capture microdissection, LCM) severely reduces RNA quality so that the range of application of this technique will be restricted to already preserved and non-retrievable specimen (biodiversity and evolution research)[281]. LCM is considered a suboptimal method to isolate sufficient numbers of fresh cells as it is very time-consuming (RNA degradation)[280]. Therefore the main technical challenge, obtaining a pristine cell population of at least 500 cells for downstream transcriptome, translatome or proteome analysis, still remains[282].

1.5.2 THE TRAP METHODOLOGY – AN INNOVATIVE WAY TO ISOLATE THE TRANSLATOME

In the last few years several methods have been developed to isolate specifically the fraction of mRNAs that is being actively translated (ribosome or polysome profiling). Some methods are tag-dependent[283,284], others not[285]. The former ones are superior when the identification of the translatome of a single cell type cells is desired. The latter one is quicker as it is purely based on deep sequencing (without the need for transient or stable genetic modifications); however, although working fine in yeast its usefulness in eukaryotic cells has not been proven yet.

(I) INTRODUCTION TO THE BASIC PRINCIPLES

For this study the seminal method called TRAP (translating ribosome affinity purification) is chosen[286,283]. This auspicious methodology for the analysis of single cell types is based on BAC-transgenic mouse lines that express an EGFP-tagged ribosomal subunit (L10a) specifically in the desired cell type. The specific expression of modified L10a is controlled by enhancers and promoters of a suitable driver gene. In BAC-transgenic mice the polysomes of the targeted cells therefore not only consist of endogenously coded (non-fluorescent) ribosomes but also of EGFP-

labelled ones coded for on the BAC. Heiman et al. confirm the existence of green polysomes in the desired cell type by immunoprecipitation and Western blot experiments[286,283]. The extraction of polysome-bound mRNAs is done via immunoprecipitation with magnetic-bead-coupled antibodies directed against EGFP. After mRNA amplification the cRNA is labelled with Biotin and brought on a chip for hybridisation.

Only transcripts that are translated at the time of tissue harvest in the targeted cell type get enriched: The immunoprecipitation step separates the (partly) green polysomes of the targeted cell type from the non-green polysomes of neighbouring cells. In a dissected and processed organ-of-Corti-sample where only the outer hair cells express green ribosomal subunits, the enriched RNA fraction will not contain polysomes (and hence mRNA) from non-green (e.g.) Deiter's cells or inner hair cells. All kinds of non-coding RNA forms (tRNA, siRNA, miRNA, nasRNA, lncRNA, snoRNA etc.) largely remain in the fraction that is not immunoprecipitated. rRNAs, being ribosome-intrinsic, stay within the purified RNA pool while other ribozymes – which are probably only present in little amounts – will not.

(II) TRANSCRIPT DETECTION – A MATTER OF DEBATE

The obtained mRNA fraction can be analysed using high-throughput sequencing techniques (RNA-seq[287]) or somewhat more classical biochip microarrays. In terms of sensitivity (with the ultimate aim to detect low-abundance transcripts) one should prefer RNA-seq over hybridisation for three reasons: (1) Sequencing techniques do not require a biasing RNA amplification step, (2) microarrays have a higher false-positive rate and (3) are not feasible for the detection of *ex novo* products (SNPs, splice isoforms et al.). Unknown splice variants are probably more common than previously thought[288]. In the initial publications the TRAP technique is combined with microarray analyses[286,283]. Therefore the general feasibility of the deep sequencing approach has yet to be demonstrated. Microarray analysis is comparatively cheap and a by now established technique in many labs. However, with the combination of high-throughput and low-cost sequencing techniques – like the ones offered by Roche (454), Illumina (Solexa), Applied Biosystems (SOLiD) et al. – RNA analysis on full-genome biochips seems to founder (summarised by Hardiman[289]).

(III) SIMILAR METHODS

Also other tagged ribosomal proteins are used as tools to isolate actively translated mRNA: The Amieux laboratory modified the endogenous *Rpl22* gene ('RiboTag mice'). Therefore the expression of the ribosomal protein is high and proportional to the ribosomal content of the cell. On the contrary the TRAP technique depends on expression levels from cell-type-specific promoters that are (1) quite variable in transcriptional activity and (2) generally much lower than rivalling ribosomal protein promoters. Crossing RiboTag mice with any existing mouse line

expressing Cre recombinase results in offspring with cell-specifically tagged ribosomes (depending on the Cre recombinase expression pattern)[284]. As a plethora of existing Cre recombinase-expressing mouse lines can be used, it remains open which strategy will prevail over time.

The TRAP method has been initially developed to assess the mRNA content of mammalian brain cell types[286,283]. Similar techniques were then successfully used (1) in plants to compare expressed transcripts under hypoxia and normal conditions[290], and (2) in yeast to differentiate changes in both transcriptome and translatome quality (as well as quantity) under different stress conditions[285,291]. To our knowledge neither the TRAP nor the RiboTag methodology have been utilised by other than their native laboratories. Additionally, the applicability of the TRAP approach in non-neuronal tissues is still in question. (The RiboTag system has been shown to work in testis cells.)

In this study the TRAP method will be adopted to study the translatome of several cell types in the inner ear. This is the first time the TRAP methodology is employed outside the central nervous system.

II. AIMS

2.1 Aim I: Silencing cholinergic LOC signalling with tethered toxins

The first aim of this work is the application of the tethered toxin strategy *in vivo*. Tethered toxins retain their blocking capability *in vitro* in different model systems[243,245,246]. Parallel to this work the usefulness of this approach in mice has been demonstrated[239,240]. However, instead of modulating voltage-gated sodium or high-voltage-gated calcium channels this work focuses on nicotinic acetylcholine receptors. This work aims to block nAChRs in murine spiral ganglion neurons (SGNs) to prove that also this ion channel family is a profitable target for tethered toxins. Physiologically, interrupting transmission between efferent lateral olivocochlear fibres (LOC fibres, cholinergic) and afferent SGNs (cholinoceptive) will clarify the importance of acetylcholine in comparison to other LOC fibre neurotransmitters. In particular this work aims to determine the nature of acetylcholine at this synapse. Applying acetylcholine to the dendritic region beneath IHCs by microiontophoresis leads to increased SGN activity[29]. On the other hand also an inhibitory role – as described for the medial olivocochlear (MOC) system at outer hair cells – is discussed. Therefore there is so far no conclusion whether ACh is an excitatory or inhibitory transmitter in the ISB.

In this study the α7 homomeric nAChR is the actual target receptor. It is the only functionally described receptor that can be composed by the different subunits expressed in SGNs. Although α7 subunits can also be found at presynapses[292] the most accepted view is that the majority of SGN nAChRs are present in the postsynaptic membrane in the inner spiral bundle (ISB). This view is affirmed by the finding that *Chrna7* transcripts are detected also in the organ of Corti (o/C) of guinea pig and rat[293,58]. ISH data suggest that o/C cells do not express *Chrna7*. This indicates that the detected *Chrna7* transcripts are present in the dendrites of SGNs (that are located in the o/C). Additionally, α7 is the most likely nAChR subunit expressed in SGNs to link ACh-binding with changes in gene expression[91,77]. After removal of the L/MOC system the afferent spontaneous discharge rate in the mammalian ear changes not directly after acute sectioning but only about 12 h later[294]. This suggests a mechanism involving changes in gene expression that leads e.g. to a change in the number of glutamate receptors at the inner hair cell.

Chrna7 knockout mice are viable but phenotypic analysis of these mice is cumbersome as α7 is expressed throughout the brain. With the tethered toxin strategy this problem can be addressed in a temporally and spatially controlled manner (see 1.4.2). To achieve a strong and specific effect first different tethered toxins are tested for their blocking specificities on α7 nAChRs. Following that, a BAC-transgenic mouse expressing the most promising toxin specifically in SGNs

is generated and characterised for its transgene expression. The analysis of the auditory brainstem response of mice with altered cholinergic neurotransmission in the ISB will help establishing a role for acetylcholine in LOC signalling.

2.2 Aim II: Characterising the expression pattern of Trpp2 in the mouse inner ear

TRP channels play important roles in mechanosensation in various animal models. Initial data from *TRPP2*-GFP and *PKD1*-GFP reporter mice suggest that these two members of the polycystin family of TRP channels might have a function in hearing. Scrutinising the inner ears of these reporter mice in detail will help identifying the cell types – and therefore also the physiological system(s) – these proteins are involved in. In particular, polycystins are considered to have an indispensable role in auditory hair cells that had not been assessed at the time the study was designed.

2.3 Aim III: Studying the function of Trpp2 in the auditory system

After unfolding the intriguing expression pattern of Trpp2 the functional relevance of this ion channel in the mouse cochlea is assessed. *Trpp2* knockout mice die *in utero* between E13.5 and birth[295,131] – probably due to abnormalities in placental development[296]. They also exhibit structural defects in the cardiac septum as well as cyst formation in maturing nephrons and pancreatic ducts. They also display embryonic whole body oedemas, renal failure and bone deformation. For the study of Trpp2 function several genetically altered mouse strains have been created (hypomorphic alleles, substitution of amino acids)[295,297,298]. Although they all survive into adulthood they are not applicable for our purpose: The possible functions of Trpp2 in the auditory system can only be investigated when the gene is silenced (1) completely and (2) specifically in neurons. The Somlo laboratory kindly provided a mouse strain with two intronic loxP sites inserted into the *Trpp2* locus (Pkd2^{Tm3Som}, herein after referred to as *Trpp2*flox). In this study the *Trpp2*flox strain is characterised for the first time. Then the Cre-loxP-system for conditional mutagenesis (see 1.4.2III) is employed: Different, commonly available Cre-expressing mouse strains are crossed with *Trpp2*flox mice to produce dysfunctional transcripts of *Trpp2* specifically in neurons. The transient expression of Trpp2 in spiral ganglion neurons suggests that the channel could be involved in neurite outgrowth, target innervation or synaptic pruning. Therefore the connectivity beneath inner and outer hair cells of mice with conditionally inactivated *Trpp2* alleles is investigated immunohistologically. Resulting offsprings are also tested for proper hearing.

2.4 Aim IV: Generating transgenic mice for ribosome profiling of inner ear cell types

The understanding of sound transmission processes in the cochlea has advanced tremendously over the last two decades. Nevertheless, the most intriguing puzzle remains unsolved: So far the proteins and mechanisms involved in the transduction of mechanical movements into electrochemical signals are not known. Proteome analysis in the inner ear produced only a modest amount of data[255] – because of substantial limits in measuring low-abundance proteins. Therefore deciphering the complete functional protein content of (e.g.) inner and outer hair cells is not yet feasible[261]. Technologies measuring mRNA abundance have revolutionised the study of gene expression but mRNA levels are an imperfect proxy for protein production[257]. However, ribosome or polysome profiling, where mRNAs are recovered for subsequent analysis from actively translating ribosomes, can provide a useful estimate of protein synthesis[260]. The actively translated fraction of the mRNA pool is commonly referred to as the translatome. Ribosome profiling employing BAC-transgenic mice (that express an EGFP-tagged ribosomal protein) has been shown to work for various cell types in the mouse brain. One aim of this work is to generate and characterise transgenic mouse lines that will be useful for ribosome profiling of hair cells. Ultimately, these mice could help to identify rare transcripts of proteins that are part of the mechano-electrical transducer (MET) apparatus.

III. MATERIAL AND METHODS

3.1 Preface

3.1.1 ANIMALS

All mice were housed with *ad libitum* access to food and water in air conditioned rooms at 22-23 °C at a standard 12 h light/dark cycle. African clawed frogs (*Xenopus laevis*) were kept in water tanks filled with tap water at a standard 12 h light/dark cycle. Room temperature was kept between 16 and 22 °C. Water was constantly cleaned using an EHEIM professional II external filter (Deizisau, Germany). Additionally, water was changed twice a week one day after feeding to clean the tanks. All procedures were in accordance with ethical guidelines laid down by the local governing body and approved by Landesamt für Gesundheit und Soziales, Berlin.

Table 1: Mouse strains generated and used in this work

Strain name as used throughout this work // according to the ICSGNM*	**Aliases**	**Source**
(I) BAC-TRANSGENIC REPORTER MICE		
***Pkd1*-GFP** (see Fig. 8) // (FVB/N x C56Bl/6)$^{Tg(Pkd1\text{-}EGFP)CG10Gsat}$	gene: *FLJ00285, MGC118471, PC1, mFLJ00285*	provided by: The GENSAT† Project, Rockefeller University, New York, USA
	mice: MMRRC 010321-UCD	also available at: MMRRC‡, NCRR-NIH§, Bethesda, USA
	BAC: GENSAT1-BX492	BAC available at: CHORI (BACPAC Resources), Oakland, CA, USA
***Trpp2*-GFP** (see Fig. 8) // (FVB/NTac x C56Bl/6)$^{Tg(Pkd2\text{-}EGFP)CG??Gsat}$	gene: *C030034P18Rik, Pkd2*	provided by: The GENSAT Project, Rockefeller University, New York, USA
	BAC: GENSAT1-BX489	BAC available at: CHORI (BACPAC Resources), Oakland, CA, USA
(II) BAC-TRANSGENIC MICE FOR GENE PROFILING		
***Chrna9*-EGFP_L10a** // (C57Bl/6xBDF)x C56Bl/6$^{Tg(Chrna9\text{-}EGFPL10a)}$	gene: *Chrna9, nAChR α9*	created in this study (MDC** Transgenic Core Facility, Berlin) founder lines: 2757, 2761, 2765
***Dlx1*-EGFP_L10a** C57Bl/6J$^{Tg(Dlx1\text{-}EGFPL10a)}$		provided by: N. Heintz, Rockefeller University, New York, NY, USA

* International Committee on Standardized Genetic Nomenclature for Mice
† Gene Expression Nervous System Atlas
‡ Mutant Mouse Regional Resource Centers
§ National Center for Research Resources – National Institute of Health
** Max-Delbrück-Center for Molecular Medicine

***NEUROD1*-EGFP_L10a** C57Bl/6J$^{Tg(Neurod1\text{-}EGFPL10a)}$	gene: *bHLHa3, Mody6, Bhf-1*	provided by: N. Heintz, Rockefeller University, New York, NY, USA
***PRESTIN*-EGFP_L10a //** (C57Bl/6xBDF)x C56Bl/6$^{Tg(Slc26a5\text{-}EGFPL10a)}$	gene: *Slc26a5, Dfnb61, Pres*	created in this study (MDC Transgenic Core Facility, Berlin, Germany) founder lines: 2744 / 2747 / 2751 / 2772 / 6826
***SNAP25*-EGFP_L10a //** C57Bl/6J$^{Tg(Snap25\text{-}EGFPL10aJd362)}$	gene: *Ric4, Sup, Sec9*	provided by: N. Heintz, Rockefeller University, New York, NY, USA
***VGLUT3*-EGFP_L10a //** C57Bl/6J$^{Tg(Slc17a8\text{-}EGFPL10aJx1887)}$	gene: *Slc17a8, Dfna25*	provided by: N. Heintz, Rockefeller University, New York, NY, USA

(III) BAC-TRANSGENIC TOXIN MOUSE

***TRPP2*-tGID$_s$ //** [(C57Bl/6xBDF)xC56Bl/6]$^{Tg(Pkd2\text{-}tG1Ds)}$	gene: *C030034P18Rik, Pkd2*	created in this study MDC Transgenic Core Facility, Berlin, Germany founder lines: 49 / 51 / 58 / 72

(IV) KNOCK-IN MICE

***ISL1*-Cre //** 129X1/SvJ-*Isl1*$^{tm1(IRES\text{-}Cre\text{-}SV40pA)Cos}$	gene: *Islet1*	provided by T. Jessell, Columbia University, New York, NY, USA
***Trpp2*flox // [(129-*Pkd2*^{tm3Som} x** C57Bl/6)F1xC57Bl/6]N2	gene: *Pkd2, C030034P18Rik,*	provided by S. Somlo, Yale University, New Haven, CT, USA

(V) OTHER TRANSGENIC MICE

Cre-del // BALB/cJ $^{Tg(CMV\text{-}NLS\text{-}cre)1Cgn}$	mice: *CMV-Cre; Cre deleter*	provided by K. Rajewsky, Institute for Genetics, University of Cologne
***NES*-Cre //** B6.Cg$^{Tg(Nes\text{-}cre)1Kln/J}$	gene: *Nestin, FLJ21841, Nbla00170*	provided by: R. Klein, MPI für Neurobiologie, Martinsried, Germany

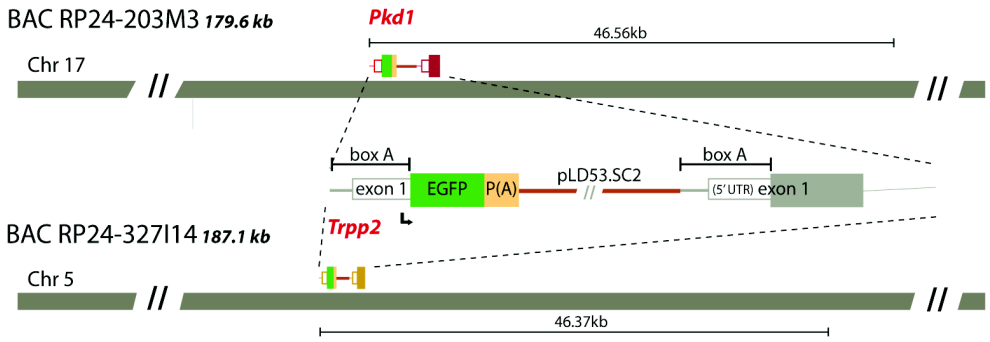

FIG. 8: MAKEUP OF REPORTER MOUSE BACs
Chr chromosome, *EGFP* enhanced green fluorescent protein, *UTR* untranslated region

3.1.2 CHEMICALS

Table 2: Chemicals

Name	Name (continued)
Acridin ointment[1]	Lipofectamine™ 2000[2]
Agarose, ultra-pure[2]	ß-mercaptoethanol[4]

Antibiotic-Antimycotic[2]	Methanol[3]
Ammonium chloride[3]	$MgCl_2$ (50 mM)[2]
Ampicillin sodium salt[4]	Mineral oil[3]
B27-Supplement[2]	Neurobasal medium[2]
BES[4]	O.C.T.™ TissueTek[7]
Bovine serum albumin (BSA)[4]	Opti-MEM®[2]
Bromphenolblue[3]	Paraformaldehyde[4]
Calcium chloride dihydrate[5]	P1 resuspension buffer, P2 lysis buffer, P3 neutralisation buffer[8]
Chloroform[3]	PBS (10x)[2]
Collagenase Type I[4]	PCR Rxn buffer (10x)[2]
Cytosine-β-D-arabinofuranoside[4]	Penicillin/streptomycin[2]
Dimethyl sulfoxide (DMSO)[5]	Peptone[3]
dNTP-Mix[4]	Poly-D/L-ornithine hydrobromide[4]
Doxycycline hyclate[4]	Poly-L-lysine 0.01%[4]
EDTA disodium-dihydrate[3]	Protease inhibitor (complete mini)[9]
Ethanol[3]	RNAlater®[8]
Ethidium bromide[3]	Rompun® (2% Xylazin)[10]
FBS (fetal bovine serum)[2]	Sodium chloride[3]
D-(+)-glucose[4]	Sodium hydrogen sulfate[4]
D-MEM[2]	Sodium hydroxide[4]
DNAse I[4]	Sucrose[4]
Glacial acetic acid[3]	TEA[4]
GlutaMAX™[2]	Tricaine[4]
Glycine[3]	TRIS[3]
Glycerol[3]	Triton X-100[4]
HBSS (10x)[2]	Trypsin-EDTA (0.25%)[2]
HEPES[3]	Trypsin inhibitor Type I-S (soybean)[4]
Horse serum[2]	Tween 20[11]
Immu-Mount™ [6]	Xylene cyanol[3]
IPTG[4]	X-Gal[3]
Isopropanol[3]	Yeast extract[3]
Ketamin 10%[1]	

[1] WDT eG, Garbsen, Germany; [2] Invitrogen GmbH, Karlsruhe, Germany; [3] Carl Roth GmbH & Co. KG, Karlsruhe, Germany; [4] Sigma-Aldrich Chemie GmbH, Schnelldorf, Germany; [5] Merck KgaA, Darmstadt, Germany; [6] Thermo Scientific, Pittsburgh, PA, USA; [7] Sakura Finetek, Zoeterwoude, Netherlands; [8] Qiagen GmbH, Hilden, Germany; [9] Roche Pharma AG, Grenzach-Wyhlen, Germany; [10] Bayer Vital GmbH, Leverkusen, Germany; [11] Serva Electrophoresis GmbH, Heidelberg, Germany

3.1.3 COMPOSITION OF PREPARED BUFFERS AND SOLUTIONS

All buffers and solutions were prepared using Type I water (MQ) with a resistivity of 18 MΩcm produced with a Barnstead E-pure water purification system.

Table 3: Composition of buffers and solutions

Name	Composition
1 kb DNA ladder	1 kb plus DNA ladder (Invitrogen), 10 mM Tris-HCl, 50 mM NaCl, 1x DNA loading buffer
aCSF (artificial cerebrospinal fluid)	130 mM NaCl, 3 mM KCl, 2 mM $CaCl_2$, 1.3 mM NaH_2PO_4, 2 mM $MgSO_4$, 20 mM glucose, 20 mM $NaHCO_3$, 0.4 mM ascorbic acid, pH7.4
Anaesthesia mix	174 µl ketamine (50 ng/ml), 50 µl xylazine (Rompun 2%), 776 µl 0,9% sodium chloride
Acetylation buffer	1,8 ml triethanolamine (RT), 160 µl conc. HCl (37%), add H_2O to 100 ml, 250 µl acetic anhydride (add before use)
Alkaline lysis solution	0.2 N NaOH, 1% SDS

Blocking solution (IHC) 1	1x PBS, 100 mM glycine
Blocking solution (IHC) 2	1x PBS, 10% normal goat serum, 0.3% Triton X-100
Chamber buffer (*in situ*)	50% formamide, 25% 20x SSC, 25% water
Cryosection buffer	50% 0.1 M phosphate buffer, 25% glycerol, 25% ethylene glycol, pH 7.4
Denaturation buffer	0.5 M NaOH, 1.5 M NaCl
Denhardt's solution	1% Ficoll, 1% polyvinylpyrolidone, 1% BSA V
High salt buffer (Southern blot)	2x SSC, 0.2% SDS
Hybridisation buffer (*in situ*)	12,5 ml 20x SSC, 25 ml formamide (100%), 5 ml of 50x Denhardt's solution, 75 µl Tween-20, 40 µl of 100 mg/ml heparin, 50 µl of 50 mg/ml yeast t-RNA, 100 µg/ml ssDNA (denatured at 95 °C, 5 min), pH 4,5 – 5,0 (with 1 M citric acid)
Hybridisation buffer (Southern blot)	6x SSC, 0.5% SDS, 10% Denhardt's solution, 100µg salmon sperm (denaturated)
Injection buffer	10 mM Tris-HCl, pH 7.5, 0.1 mM EDTA, 100 mM NaCl
L15/OR2	50% OR2, 50% L15 media, 1x penicillin/streptomycin
LB agar	LB-medium + 15% (w/v) agarose (BactoAgar)
LB medium (Luria-Bertoni medium)	10% (w/v) tryptone, 5% (w/v) yeast extract, 10% (w/v) NaCl, adjusted to pH 7.0
Loading dye (6x)	0.2% xylene cyanol, 0.2% bromphenolblue, 30% glycerol
Low salt buffer (Southern blot)	0.1x SSC, 0.1% SDS
Lysis buffer (*in vitro* transcription)	20 mM Tris-HCl pH 7.5, 1% SDS, 100 mM NaCl, 10 mM EDTA, 5µl of 20µg/µl proteinase K
Lysis buffer (Western blot)	150 mM NaCl, 50 mM HEPES, 10% glycerol, 1%Triton X-100
MAST	100 mM maleic acid, 150 mM NaCl, 0.3% Tween-20, adjusted to pH 7.5
MAST++	MAST +10% normal goat serum
NaCl-saturated butanol	add 20 ml 3 M NaCl to 100 ml butanol
NTMT (2x)	100 mM NaCl, 100 mM Tris-HCl (pH 9.5), 50 mM $MgCl_2$, 0.1% Tween-20
OR-2 buffer (*Xenopus* oocytes)	82.5 mM NaCl, 2,5 mM KCl, 1 mM $MgCl_2$, 1 mM $CaCl_2$, 1 mM $NaHPO_4$ and 5 mM HEPES at pH 7.8
PBS (10x)	80 g/l NaCl, 2 g/l KH_2PO_4, 2 g/l KCl, 21.6 g/l $Na_2HPO_4 \cdot 7H_2O$
PFA (4%)	dissolving 4% paraformaldehyde in boiling 1x PBS (add stir bar) with 0.2 M $Na_2H_2PO_4$, cooling on ice for 1 h, pH 7.4
Polyamine mix (1000x)	30 mM spermine, 70 mM spermidine
Prehybridisation buffer (*in situ*)	50 ml Formamide, 25 ml 20 x SSC, 40 µl heparin (100 mg/ml), 1 ml salmon sperm DNA (10 mg/ml), 100 µl t-RNA (50 mg/ml), 150 µl Tween-20, 6 ml 1M citric acid, H_20
Prehybridisation buffer (Southern blot)	for 20 ml: 6 ml 20x SSC, 2 ml Denhardt's solution, 1 ml SDS (1%), 10,8 ml MilliQ water (all prewarmed to 65 °C), 200 µl salmon sperm DNA (denaturated)
Ringer buffer, calcium-free (*Xenopus* oocytes)	82,5 mM NaCl, 2 mM KCl, 1 mM $MgCl_2$ and 10 mM HEPES at pH 7.4
$Na_2H_2PO_4$ (0.2M)	15.5% 1 M Na_2HPO_4, 4.5% 1 M NaH_2PO_4 in MQ, pH 7.4
SOC medium	2% tryptone, 0.5% yeast extract, 10 mM NaCl, 10 mM $MgCl_2$, 10 mM $MgSO_4$, 20 mM glucose
Solution I	125 ml formamide, 62.5 ml 20x SSC, 375 µl Tween-20, ad 250 ml H_20
Solution I (BAC DNA preparation)	50 mM glucose, 20 mM Tris-HCl (pH 8.0), 10 mM EDTA (pH 8.0)
Solution II	2.5 ml 1M Tris-HCl, pH 7.5, 25 ml 5M NaCl, 375 µl Tween-20, ad 250 ml H_20
Solution II (BAC DNA preparation)	0.2 N NaOH, 1% SDS
SSC (20x)	3 M NaCl, 300 mM sodium citrate, adjusted to pH 7.0
TAE (50x)	242 g/l Tris base, 5.71% (v/v) glacial acetic acid, 0.05 M

	EDTA, pH 8.0
Tail buffer 1	200 mM NaCl, 100 mM Tris-HCl pH 8.5, 5 mM EDTA, 0.2% SDS
Tail buffer 2	50 mM Tris (pH 8.0), 100 mM EDTA, 0.5% SDS, 50 µg/ml Proteinase K
TBS (10x)	0.5 M Tris/HCl pH 7.9, 1.5 M NaCl, 0.2 g/l KCl
TBS-T	TBS + 0.05% Tween-20
TE buffer	10 mM Tris pH 8.0, 1 mM EDTA
TE (10:50)	1 ml of 1 M Tris, 10 ml of 0.5 M EDTA, 89 ml H_2O

3.1.4 BACTERIA STRAINS, PLASMIDS AND BACS

All bacteria strains have been purchased from Invitrogen (Darmstadt, Germany) unless stated otherwise.

Table 4: Bacteria strains

Name	Genotype
E. coli TOP10	F-*mcr*A Δ(*mrr-hsd*RMS-*mcr*BC) φ80*lac*ZΔM15 Δ*lac*X74 *rec*A1 *ara*D139 Δ(*ara*leu) 7697 *gal*U *gal*K *rps*L (Str^R) *end*A1 *nup*G
E. coli DH5α	F-φ80*lac*Z ΔM15 Δ(*lac*ZYA-*arg*F) U169 *rec*A1 *end*A1 *hsd*R17(rk^-, mk^+) *pho*A *sup*E44*thi*-1 *gyr*A96 *rel*A1 *ton*A
E. coli DH10B	F- mcrA Δ(mrr-hsdRMS-mcrBC) φ80lacZΔM15 ΔlacX74 recA1 endA1 araΔ139 Δ(ara, leu)7697 galU galK λ- rpsL (Str^R) nupG deoR
E. coli PIR1*	F- Δlac169 rpoS(Am) robA1 creC510 hsdR514 endA recA1 uidA(ΔMluI)::pir-116
E. coli PIR2	F- Δlac169 rpoS(Am) robA1 creC510 hsdR514 endA recA1 uidA(ΔMluI)::pir
E. coli INV110	F´ {traΔ36 proAB $lacI_q$ lacZΔM15} rpsL (Str^R) thr leu endA thi-1 lacY galK galT ara tonA tsx dam dcm supE44 Δ(lac-proAB) Δ(mcrC-mrr)102::Tn10 (Tet^R)

* kindly provided by Y. Wang (Ivics Lab, MDC, Berlin)

Table 5: Plasmids

amp – ampicillin, cam – chloramphenicol, tet – tetracycline

Name (resistance gene)	Source	Affiliation/Address
pcDNA3 (AmpR)	Invitrogen GmbH	Karlsruhe, Germany
pCR®2.1-TOPO (AmpR)	Invitrogen GmbH	Karlsruhe, Germany
pCR®II-TOPO (AmpR)	Invitrogen GmbH	Karlsruhe, Germany
pCS2+ (AmpR)	Addgene Inc.	Cambridge, MA, USA
pLD53.SCA-E-B† (AmpR)	N. Heintz	Rockefeller University, NY, USA
pBACe3.6‡ (CamR) backbone of RP23 BAC clones	BACPAC Resources (CHORI*)	Oakland, CA, USA
pBlueScript SK- (AmpR)	Stratagene/Agilent Tech. Inc.	Santa Clara, CA, USA
pSV296† (AmpR)	N. Heintz	Rockefeller University, NY, USA
pSV1.RecA** (TetR)	N. Heintz	Rockefeller University, NY, USA
pTARBAC1‡ (CamR) backbone of RP24 BAC clones	BACPAC Resources (CHORI)	Oakland, CA, USA

E. coli ‡DH10B / †PIR2 / **PIR1 needed for replication

Table 6: BACs

Name	Source	Affiliation/Address
RP23-231J19 (Slc26a5)	Invitrogen GmbH	Darmstadt, Germany
RP23-255O16 (Slc26a5)*	Invitrogen GmbH	Darmstadt, Germany

* Children's Hospital Oakland Research Institute

RP23-222I9 (Calretinin)	Invitrogen GmbH	Darmstadt, Germany
RP23-276D5 (Calretinin)*	Invitrogen GmbH	Darmstadt, Germany
RP23-256I10 (α9 nAChR)*	Invitrogen GmbH	Darmstadt, Germany
RP23-141C13 (α9 nAChR)	Invitrogen GmbH	Darmstadt, Germany
RP24-327I14 (Pkd2)	BACPAC Resources (CHORI)	Oakland, CA, USA

*successful recombination between BAC DNA and shuttle vector, used for subsequent experiments

3.1.5 OLIGONUCLEOTIDES

A list of the utilised QuikChange® and sequencing primers can be given upon request.

Table 7: Short oligonucleotides

GT – genotyping, RT-PCR – reverse transcriptase polymerase chain reaction, ISH – *in situ* hybridisation

Name	Sequence 5‘ – 3‘	Usage
α9_exon2_F	CGTAGAGACAGCAAATGGAAAG	RT-PCR
α9_exon3_R	GAGTCCAGCCCGTCATACTG	RT-PCR
αTubulin_F	CCGCCTCATTGCGTTACTTA	RT-PCR
αTubulin_R	GCATCCTCCTTGCCTGTGAT	RT-PCR
after_PI-Sce_F	ATCCGGCGCGCCAATAGT	GT
after_PI-Sce_R	CGCGGATCCTCTCCCTAT	GT
before_PI-Sce_F	GCCAATATGGACAACTTCTTCGCC	GT
before_PI-Sce_R	CGCTTACGCAGGGCATCCATTTAT	GT
BoxA_F (ApaI-StuI-AscI_BoxA)	(CGGGGGCCCAGGCCTGGCGCGCC) GGATGAGGACATCCTATGAGAAG	BAC transgenesis
BoxA_R (ApaI_BoxA)	(CCTCCCGGG) CCCTGGCCTCGCCTGGACTGGACTTAGG	BAC transgenesis
BoxB_F(_EcoRI)	(CGAATT) CTTTCGTCCTGCTCCAGGCAAGCGTGGAGC	BAC transgenesis
BoxB_R(EcoRI-PacI_BoxB)	(CGAATTTTAATT)AACCTCTCTCTCAACCAAACCT TCAGACAATGACC	BAC transgenesis
BoxQ_F(_AscI)	(GTTGGCGCGCC) GAAAAGGAGATGCATTGTGG	BAC transgenesis
BoxQ_R(_NotI)	(GTAAGAATGCGGCCGC) CTGCCACAGTCACAAAACAG	BAC transgenesis
BoxR_F(_AscI)	(GTTGGCGCGCC) CTCCGAGCTACCTCAACCTG	BAC transgenesis
BoxR_R(_NotI)	(GTAAGAATGCGGCCGC) TCTTCTCTGCCAGGGTTCCT	BAC transgenesis
BoxS_F(_AscI)	(GTTGGCGCGCC) CCCAGGTCCTGAAACCTTTT	BAC transgenesis
BoxS_R(_NotI)	(GTAAGAATGCGGCCGC) GAACTGCAGAACACATCCCA	BAC transgenesis
CreN_F	ACGACCAAGTGACAGCAATG	GT
CreMath1ER_R	ACCAGCGTTTTCGTTCTGCC	GT
Dnahc5_18F	GTGTTAGAGGAAGCCCGTGA	GT
Dnahc5_18R	GCCGTCAATCGCTTATCATT	GT
EGFP_BAC_F	TGACCCTGAAGTTCATCTGCACCA	GT, RT-PCR
EGFP_BAC_R	TGTGGCGGATCTTGAAGTTCACCT	GT, RT-PCR
EGFPL10_BAC_F	ACGACGGCAACTACAAGACC	GT
EGFPL10_BAC_R	CCACCGTCTCCAGAAACTTG	GT
GAPDH_F	AACTTTGGCATTGTGGAAGG	RT-PCR
GAPDH_R	ACACATTGGGGGTAGGAACA	RT-PCR
GID_2F	TCCTAGCTCTTGTTGGAGCTG	GT
GID_2R	GCTCCAATCCTTCCATTCAA	GT
Isl1-Cre_3_F	GTTCCTATTCCGAAGTTCCTATTCTC	GT
Isl1-Cre_3_R	CGACGAGTGTATGGAAATTTGCTAGA	GT
Isl1_wt-PCR_F	CAGCAAGAACGACTTCGTGA	GT
Isl1_wt-PCR_R	TCTGGGTGGAGGAGTACCTG	GT

Pkd1(2)_F2	GCACCCTGTTCTCAGTGTTG	RT-PCR, ISH
Pkd1(2)_R2	ACTCGTCGTATGGAGGCTTG	RT-PCR, ISH
Pkd2(1.5)_pan_F	GAGTTTCTGGAATTGTCTGGATG	RT-PCR, ISH
Pkd2(1.5)_pan_R	GTAAAATAAAGTGGCCCCAAAAC	RT-PCR, ISH
Pkd2Δallele-cDNA_F	CTTTGAGGCAGAGGAGGATG	RT-PCR
Pkd2Δallele-cDNA_R	CAGGTAGTAACCCGCTCCAC	RT-PCR
Pkd2Δallele-gDNA_F	GAATCCATGCCAGATCCTTC	GT
Pkd2Δallele-gDNA_R	GGTCACAGTTTGGGAACAAG	GT
Pkd2_Coint_5'	ATCCAGTCCTATCCCCAAGG	BAC transgenesis
Pkd2_Coint_GID_S	CCCTGCAAGCTGGATTAGAG	BAC transgenesis
Pkd2_Coint_polyA	GCCTGAAGAACGAGATCAGC	BAC transgenesis
Pkd2_Coint_3'	TTGTTGGAATGGCAAAGGAC	BAC transgenesis
Pkd2_D2loxP_F	GGGTGCTGAAGAGATGGTTC	GT
Pkd2_D2loxP_R	TCCACAAAAGCTGCAATGAA	GT
Pkd2_flox_F4	GACCTACGGCATGATGAGC	ISH
Pkd2_flox_R4	GTCCAAATGGAGCTCTGTCC	ISH
SV_EGFP_R	TTCAGGGTCAGCTTGCCGTAGGTG	BAC transgenesis
SV_R6kγ-ori_F	AACAGGTTGAACTGCTGATCTTC	BAC transgenesis

Table 8: Oligonucleotides for toxin sequence generation

(Primers for the generation of α-bungarotoxin, κ-bungarotoxin & PnIB kindly provided by I. Ibañez-Tallon.)

Toxin name	Sequence 5' – 3'
BulA_F	ctgcagttgctggctgctgtagcacccccccctgcgccgtgctgtactgcggcatcgata
BulA_R	atcgatgccgcagtacagcacggcgcaggggggggtgctacagcagccagcaactgcaga
GID_F	atacgcgacgaatgttgctctaatccagcttgcagggtcaacaatcctcacgtatgta
GID_R	tacatacgtgaggattgttgaccctgcaagctggattagagcaacattcgtcgcgtat

3.1.6 ANTIBODIES AND MARKERS

Table 9: Primary and secondary antibodies, dyes and length standards

IHC – immunohistochemistry, WB – Western blot, AG – agarose gels

Name	Usage (dilution)	Supplier
1 kb Plus DNA Ladder	AG	Invitrogen GmbH[1]
4´,6-diamidino-2-phenylindole, dilactate (DAPI)	IHC (1:3000)	Invitrogen GmbH[1]
anti-B-FABP, polyclonal, rabbit	IHC (1:800)	Abcam plc, Cambridge, UK
anti-GFP, monoclonal, mouse 11E5	WB	Invitrogen GmbH[1]
anti-GFP, polyclonal, rabbit	IHC	Invitrogen GmbH[1]
anti-GFP, polyclonal, rabbit 6556	IHC (1:1500)	Abcam plc, Cambridge, UK
anti-GFP, polyclonal, rat	IHC (1:100)	kindly provided by C. Birchmeier, MDC, Berlin, Germany
anti-mouse IgG (Alexa Fluor® 594, goat)	IHC	Invitrogen GmbH[1]
anti-mouse IgG (Alexa Fluor® 633, goat)	IHC	Invitrogen GmbH[1]
anti-mouse IgG (Cy3, goat)	IHC (1:250)	Jackson ImmunoResearch Europe[2]
anti-mouse IgG (HRP, goat)	WB	Jackson ImmunoResearch Europe[2]
anti-NeuN, monoclonal, mouse	IHC (1:100)	Millipore GmbH (Chemicon)[3]
anti-Neurofilament, monoclonal, mouse	IHC (1:100)	Millipore GmbH (Chemicon)[3]
anti-NF200, monoclonal mouse	IHC (1:2000)	kindly provided by C. Birchmeier, MDC, Berlin, Germany
anti-Peripherin, polyclonal, rabbit	IHC (1:500)	Millipore GmbH (Chemicon)[3]
anti-PGP9.5, polyclonal, rabbit	IHC (1:800)	kindly provided by G. Lewin, MDC, Berlin, Germany
anti-PKD2 (G-20) sc-10376, polyclonal, goat	WB, IHC	Santa Cruz Biotechnology, Inc.[4]
anti-PKD2 (YCC2), polyclonal, rabbit	WB, IHC	kindly provided by S. Somlo, Yale University, New Haven, CT, USA

anti-Pkd2 AB9088, polyclonal, mouse	WB, IHC	Millipore GmbH (Chemicon)[3]
anti-rabbit IgG (Alexa Fluor® 488, goat)	IHC (1:250)	Invitrogen GmbH[1]
anti-rabbit IgG (Alexa Fluor® 594, goat)	IHC (1:250)	Invitrogen GmbH[1]
anti-rabbit IgG (Cy2, goat)	IHC (1:250)	Jackson ImmunoResearch Europe[2]
anti-rabbit IgG (Cy5, goat)	IHC (1:500)	Jackson ImmunoResearch Europe[2]
anti-rat IgG (Cy3, goat)	IHC (1:250)	Jackson ImmunoResearch Europe[2]
anti-TuJ1, monoclonal, mouse	IHC	kindly provided by C. Birchmeier, MDC, Berlin, Germany
PageRuler™ prestained protein ladder	SDS-PAGE	Fermentas GmbH[5]
RiboRuler™ high/low range RNA ladder	AG	Fermentas GmbH[5]

[1] Invitrogen GmbH (Molecular Probes), Karlsruhe, Germany; [2] Jackson ImmunoResearch Europe Ltd., Suffolk, UK; [3] Millipore GmbH (Chemicon), Schwalbach, Germany; [4] Santa Cruz Biotechnology, Inc., Santa Cruz, CA, USA; [5] Fermentas GmbH, St. Leon-Rot, Germany

The favoured aGFP ab is raised in rabbit (6556) which bars a side by side use in double stainings with aPeripherin-, aB-FABP- and aPGP9.5-antibodies (all rabbit). The alternatively used aGFP ab raised in rat gives less pronounced but still consistent and clear stainings.

3.1.7 ENZYMES

Table 10: Enzymes

Name	Source
Restriction enzymes	New England Biolabs GmbH, Frankfurt, Germany
DNase (TypeI)	Sigma-Aldrich Chemie GmbH, Schnelldorf, Germany
M-MLV RTase, RNase H-, point mutant	Promega GmbH, Mannheim, Germany
T4 DNA Ligase	New England Biolabs GmbH, Frankfurt, Germany
RNasin®	Promega GmbH, Mannheim, Germany
Shrimp alkaline phosphatase	USB Europe GmBH, Staufen, Germany
Trypsin from bovine pancreas	Sigma-Aldrich Chemie GmbH, Schnelldorf, Germany

3.1.8 KITS, LABORATORY EQUIPMENT AND SOFTWARE

Table 11: Kits

Name	Supplier
Amersham™ ECL plus WB detection Kit	GE Healthcare, Munich, Germany
DIG RNA labeling mix	Roche Pharma AG, Grenzach-Wyhlen, Germany
mMessage mMachine® SP6/T7 Kit	Applied Biosystems (Ambion), Austin, TX, USA
NuPAGE® 4-12% Bis-Tris gels	Invitrogen GmbH (Gibco), Karlsruhe, Germany
Prime-It®RmT Random Primer Labelling Kit	Stratagene/Agilent Tech., Inc., Santa Clara, USA
QIAfilter™ plasmid maxi kit	Qiagen GmbH, Hilden, Germany
QIAquick® gel extraction kit	Qiagen GmbH, Hilden, Germany
QIAprep® spin miniprep kit	Qiagen GmbH, Hilden, Germany
QuikChange® Site-Directed Mutagenesis Kit	Stratagene/Agilent Tech., Inc., Santa Clara, CA
RNeasy mini/micro kit	Qiagen GmbH, Hilden, Germany
SuperScript™ One-Step RT-PCR Kit	Invitrogen GmbH (Gibco), Karlsruhe, Germany
TOPO TA cloning® kit	Invitrogen GmbH (Gibco), Karlsruhe, Germany

Table 12: Equipment and software

Molecular-/Microbiology	
Beckmann J2-MC centrifuge	Beckman Coulter, Krefeld, Germany
Beckmann L70 ultracentrifuge	Beckman Coulter, Krefeld, Germany
BioPhotometer	Eppendorf AG, Hamburg, Germany

Chroma Spin-400 column	TakaraBioEurope/Clontech, Saint-Germain-en-Laye
CL-X Posure™ film	Thermo Fisher Scientific Inc., Karlsruhe, Germany
Cooling Incubator KB23	Binder GmbH, Tuttlingen, Germany
Cover Slips	Menzel-Gläser GmbH & Co. KG, Braunschweig
Cryostat Cryo-Star HM 560	Microm International, ThermoScientific, Walldorf
Dako wax pen	Dako A/S, Glostrup, Denmark
Filter 'V' series (mesh size 0.025 µm, diameter 25 mm)	Millipore GmbH, Schwalbach, Germany
FlexCycler	Analytik Jena AG, Jena, Germany
Gene Pulser II apparatus	BioRad
Gel Jet Imager	Intas Science Imaging Instruments GmbH, Göttingen, Germany
Heraeus Megafuge 1.0R	Heraeus Sepatech, Hanau, Germany
Immobilon polyvinylidene fluoride membranes (PVDF)	Millipore GmbH, Schwalbach, Germany
Incubator HT Infors	Infors HT, Bottmingen, Switzerland
Incubator Function Line B6	Heraeus Sepatech, Hanau, Germany
Microcentrifuges 5415D and 5415R	Eppendorf AG, Hamburg, Germany
Mikro-Dismembranator U	B. Braun Biotech International / Sartorius AG, Göttingen, Germany
PCR cycler PT200	MJ Research, San Francisco, USA
PerfectBlue™ gelsystem	Peqlab Biotechnologie GmbH, Erlangen, Germany
shaker Orbital Unimax 1010	Heidolph Instruments GmbH & Co. KG, Schwabach, Germany
shaker UniEquip Control	UniEquip GmbH, Planegg, Germany
sliding microtome SM 2000R	Leica Microsystems GmbH, Wetzlar, Germany
Vortex-Genie® 2	Scientific Industries, Inc., Bohemia, NY, USA
X-Ray Film Processor RG II	Fujifilm Corporation, Tokyo, Japan

Microscopy

Fluorescence microscope 1: Zeiss Axiovert 200, objectives: EC Plan-NEOFLUAR (10x, 20x, 40x, 63x, 100x); illuminating system: Zeiss HBO100	Carl Zeiss AG, Oberkochen, Germany
Microscope camera: Cascade 650	Photometrics, Tucson, AZ, USA
Imaging software: MetaMorph 6.3r6	Molecular Devices, Downingtown, PA, USA
Fluorescence microscope 2: Keyence Biozero BZ8100E	Keyence, Neu-Isenburg, Germany
Confocal microscope: Leica TCS SP5	Leica Microsystems GmbH, Wetzlar, Germany
Imaging software: Leica application suite (LAS)	Leica Microsystems GmbH, Wetzlar, Germany
Stereomicroscope MZ9.5	Leica Microsystems GmbH, Wetzlar, Germany
KL2500 LCD microscope illumination	Schott Inc., Southbridge, MA, USA

Electrophysiology

¼″ Brüel and Kjaer microphone (model 4939)	ABR	Brüel & Kjaer GmbH, Bremen, Germany
JHM NeuroAmp 401	ABR	Helbig Messtechnik, Mainaschaff, Germany
Bath Perfusion System valve controller (ALA-VM8)	oocyte recordings	Ala Scientific Instruments, Farmingdale, NY, USA
ED1/EC1 speaker system	DPOAE	Tucker-Davis-Technologies, Ft Lauderdale, FL, USA
GeneClamp 500B amplifier	oocyte recordings	Axon Instruments Inc., Foster City, CA, USA
heat blanket	ABR, DPOAE	Hugo Sachs Elektronik, Harvard Apparatus GmbH, March-Hugstetten, Germany
JBL 2402 speaker	ABR	JBL GmbH & Co., Neuhofen, Germany
MATLAB	ABR, DPOAE	The Mathworks, Natick, MA, USA
MKE-2 microphone	DPOAE	Sennheiser, Hannover, Germany
pCLAMP9 software	oocyte recordings	Axon Instruments Inc., Foster City, CA, USA

PLI-100 pico injector	oocyte recordings	Harvard Apparatus, Holliston, MA, USA
Tucker-Davis-Technologies (TDT) II or III System	ABR, DPOAE	Tucker-Davis-Technologies, Ft Lauderdale, FL, USA

3.1.9 STATISTICAL ANALYSES

Numerical data in this work is analysed with Microsoft Excel 2007 and GraphPad Prism (The Software MacKiev Company, Boston, MA, USA). Quantified results are presented as means ± s.e.m. Differences between means are determined by applying two-sided Student's t-tests (two unpaired samples of equal variance / homoskedastic variables) with $P < 0.05$ considered as statistically significant (* ≤ 0.05, ** ≤ 0.005). Two-way ANOVA (analysis of variance) is performed on data from ABR (sources of variation: interaction, volume, and genotype).

3.2 Molecular biology

3.2.1 VECTOR CONSTRUCTION

All vectors were made using standard cloning procedures and standard vector backbones (see Table 5). Subcloning to generate t-toxins was carried out in pCS2+ plasmids. The basic pCS2 vector contained the *lynx1* secretory pathway signal sequence (secretion signal), a flag epitope, a linker region 8x[Gly-Asn] and the *lynx1* GPI signal at the 3' end. Toxin sequences were generated earlier after back-translation of known amino acid codes by annealing overlapping oligonucleotides and subsequent TOPO-TA cloning (see 3.1.5). Boxes for ISH probes as well as for homologous recombination were amplified from the template (cDNA and gDNA, respectively) with specific primers via PCR and subsequently cloned into pCR2.1 or pCRII (TOPO-TA cloning) before being processed further. Primers for the generation of ISH probes were chosen to lie in adjacent but different exons to avoid probe hybridisation with genomic DNA. Introduction of restriction sites was done via adding the according sequences to the 5' side of newly synthesised oligos and subsequent PCR and TOPO-TA cloning.

To achieve high expression of the tethered toxins in the mouse the amino acid code was translated back into DNA following a mouse specific codon frequency map for the standard genetic code*. The same was done for constructs to be expressed in *Xenopus laevis* oocytes†. Sequences and vector maps of the generated constructs were created with Lasergene's SeqBuilder (DNASTAR, Madison, WI, USA).

* http://www.kazusa.or.jp/codon/cgi-bin/showcodon.cgi?species=10090&aa=1&style=N
† http://www.kazusa.or.jp/codon/cgi-bin/showcodon.cgi?species=8355

3.2.2 PRIMER DESIGN

In general, the melting temperatures of a pair of PCR primers were chosen in a way to have similar values (~57-63 °C). The GC content was preferably between 40 and 60%, maximum self complementarity was set to 6 and maximum 3' self complementarity was set to 2 using Primer3*. Primer sequences were checked for secondary structures like hairpins, self-dimers and cross-dimers, as well as palindromic sequences. A maximum of 4 identical bases in series was allowed and primers with a GC clamp were preferred. The primer sequences were checked with NetPrimer† for suitability. Extended primers carrying overhanging ends were used to insert restriction enzyme sites into PCR-amplified DNA fragments. Sizes of the cloning boxes varied between 729 bp (box A), 785 bp (box S), 809 bp (box B), 810 bp (box Q) and 850 bp (box R). Primers for the genotyping of mice and the detection of transcripts in RT-PCR experiments were chosen to yield amplicons of a size between 150 and 600 bp. The primers used in this work were ordered from BioTeZ GmbH (Berlin-Buch, Germany), sequences are found in Table 7.

3.2.3 RESTRICTION DIGESTION AND LIGATION

DNA was digested using specific endonucleases. 0.5 µl (10 U) of the restriction enzyme and 1x final dilution of the required restriction buffer were added to an appropriate amount of DNA (~0.5 µg). Some enzymes do not recognise methylated sequences. To efficiently cut the DNA it was therefore transformed into the dam and dcm methylase-deficient *E. coli* strain INV110. The final volume of the restriction reaction was adjusted to 20 µl with DNase-free water and the samples were then incubated for 1.5 – 2 h at the temperature required for the respective enzyme. Preparative digestions were set up in 50 µl to cut constructs which were further used for molecular cloning. Depending on the expected fragment sizes 5-15 µg of DNA were digested. Vector dephosphorylation with shrimp alkaline phosphatase (1 U added at the end of digestion for 1 h at 37 °C) was used to decrease the amount of re-ligated vectors lacking the insert of interest after transformation. All ligations were carried out as sticky end ligations with 3-6 fold molar ratios of inserts to vectors. Ligations were performed in a total volume of 10 µl containing 2 µl of T4 DNA ligase (NEB, Germany) and 1x ligation buffer at 16 °C o/n or at RT for >4 h.

3.2.4 TRANSFORMATION

Transformation was done using the heat shock method. For this purpose the self-made chemically competent *E. coli* cells were thawed on ice. An aliquot of 100 µl was mixed with 5 µl of either the ligation preparation or 1 µl of a purchased ready-to-use plasmid dilution. After 20 min incubation on ice the suspension was transferred to 42 °C for 45 s, followed by a short

* http://frodo.wi.mit.edu/primer3/
† http://www.premierbiosoft.com/netprimer/index.html

incubation on ice (2 min). Then 500 ml SOC medium was added and the cells were incubated at 37 °C for 1-2 h with shaking at 200 rpm. Finally, several dilutions were spread on agar plates containing the appropriate antibiotic (ampicillin: 100 µg/ml or kanamycin: 50 µg/ml). Colony analysis was performed after o/n incubation at 37 °C.

3.2.5 EXTRACTION OF GENOMIC DNA FROM MOUSE TAILS

For standard genotyping the tissue was digested in tail buffer 1 at 55 °C for 2 h. Following a heat inactivation for 10 min at 90 °C 300 µl of MQ water were added to the sample. 1 µl of this sample was used in a PCR reaction (3.10.10). For Southern blot analysis the tails were digested in tail buffer 2 and the genomic DNA was extracted with phenol/chloroform. After precipitation and two washing steps with 70% ethanol the DNA was dissolved in 100 µl of TE.

3.2.6 PLASMID DNA EXTRACTION

Plasmid DNA extraction was carried out using the QIAprep® spin miniprep kit with 1.2 ml bacterial culture or the QIAfilter™ plasmid maxi kit with 400 ml culture. All steps were performed according to the manual. For maxipreparations DNA concentration was adjusted to 1 µg/µl with TE buffer resulting in a total volume of 0.7-1.2 ml. All DNA was stored at -20 °C.

3.2.7 NUCLEIC ACID EXTRACTION FROM AGAROSE GELS

The QIAquick® gel extraction kit was used to isolate and purify digested or PCR-amplified DNA after separation of DNA fragments according to their size by agarose gel electrophoresis. The bands of interest were cut out of the gel under UV light with a sterile scalpel. The extraction was performed according to the manual. Elution was done using 30 µl of EB elution buffer.

3.2.8 DETERMINATION OF NUCLEIC ACID CONCENTRATION

Quantification of DNA and RNA was performed using either a spectrophotometer or the Nanodrop 1000 system (Thermo Fisher Scientific, Inc., Karlsruhe, Germany). Nucleic acid concentrations (µM/ml) were calculated by multiplying the OD_{260} by 50 (DNA) and by 40 (RNA).

3.2.9 SEQUENCING

DNA sequencing was carried out by InViTek, Gesellschaft für Biotechnik & Biodesign mbH, Berlin, Germany. For double-stranded plasmid DNA typically 10 µl of DNA (0.1 µg/µl) and 10 µl of sequencing primers (10 µM) were deployed. Sequencing results were sent as text file (.seq) and chromatogram files (.ab1), which were analysed with Lasergene 7 Suite (DNASTAR,

Madison, WI, USA) and Chromas 1.45 (Griffith University, Australia). If necessary single discovered point mutations were repaired using the QuikChange® Site-Directed Mutagenesis Kit.

3.2.10 GLYCEROL STOCK PREPARATION

For long-term storage of bacteria, glycerol stocks were prepared by mixing 0.7 ml fresh bacteria o/n culture (ideally grown to stationary phase: OD_{600}=1-2) with 0.7 ml of 40% glycerol. Filled cryovials were shortly mixed, frozen in liquid nitrogen and stored at -80 °C. One master stock was used to create working stocks for regular use. For revitalising bacteria, a heat-sterilised inoculating loop was lowered into the slightly thawed working stock and then shortly placed into 5 ml LB medium with appropriate antibiotics. The cells in medium were cultured at 37 °C o/n and then subjected to plasmid extraction.

3.2.11 AMPLIFICATION OF DNA FRAGMENTS

PCRs (polymerase chain reactions) were carried out to determine DNA sequences of plasmid DNA and genomic DNA samples (analytical PCRs) and to prepare DNA fragments for cloning (preparative PCR). For analytical PCRs of genomic DNA ('genotyping') DNA was extracted from mouse tails as described. The PCR reaction was prepared on ice. It contained 1 µl of heat-inactivated lysate (or 50 ng DNA, respectively), 2.5 µl 10x PCR buffer, 0.75 µl $MgCl_2$ (50 mM), 1 µl of dNTPs (20 mM), 1 µl forward primer (10 µM), 1 µl reverse primer (10 µM) and 0.2 µl of Taq DNA polymerase – which was added last – in a total volume of 25 µl (MQ as the remaining volume). For colony PCR, an analytical PCR of bacteria colonies after transformation, the DNA template was substituted by a bacteria colony picked with a sterile tooth stick and brayed in the prepared PCR reaction. All PCRs were carried out either in the PCR cycler PT200 or the FlexCycler. The standard cycler programme was as follows: 2 min denaturation and Taq activation at 94 °C, 35 cycles of 30 s at 94 °C (denaturation), 30 s at 55 – 60 °C* (primer annealing), 1 min† at 72 °C (elongation), followed by a final elongation step of 10 min at 72 °C. PCR products were analysed on a 1% agarose gel.

3.2.12 TOPO CLONING

The TOPO TA cloning® kit was used to directly subclone PCR fragments without prior enzymatic digestion into the TOPO plasmids pCR2.1 (or pCRII). The system utilises the enzyme DNA topoisomerase I which is covalently bound to each 3´ phosphate on the linearised TOPO vectors. Topoisomerase I enables the vectors to ligate with DNA sequences with single adenosine overhangs at both ends (PCR products). Overhangs are generated automatically by the non-

* depending on the primer meldting temperatures
† depending on length of the final, expected amplicon (roughly: 1 min for 1 kb)

template-dependent terminal transferase activity of Taq polymerase that adds a single deoxyadenosine (A) to the 3´ ends of PCR products. The TOPO cloning was performed according to the manual and colonies were grown on ampicillin (100 µg/ml) containing agar plates which had been pre-treated with 40 µl of 40 mg/ml X-gal and 40 µl of 100 mM IPTG. For selection of positive colonies blue/white screening was used. The mechanism is based on the disruption of the lacZ gene (β-galactosidase) in pCR2.1 by the integration of PCR fragments. Positive colonies appear white whereas cells containing empty pCR2.1 remain able to express β-galactosidase. This enzyme converts X-gal to galactose and 5,5'-dibromo-4,4'-dichloro-indigo, an insoluble blue molecule. 5-8 white colonies were inoculated in 5 ml LB medium with 100 µg/ml ampicillin (o/n at 37 °C). After plasmid extraction with the QIAprep® spin miniprep kit plasmids were further analysed by PCR and restriction digestion; and then used for subcloning procedures.

3.2.13 AGAROSE GEL ELECTROPHORESIS

DNA, cDNA and RNA samples were run on 0.7-1.5% agarose gels in the PerfectBlue™ system. Mid-size gels with 110 ml volume or small-size gels with 55 ml volume were prepared by heating the appropriate amount of agarose in 1x TAE buffer. 0.001% ethidium bromide was added to the chilled agarose solution, the gel was poured into the gel slides and allowed to cool down to polymerise. Samples were mixed with 6x DNA loading dye and finally ~200-500 ng of DNA (analytical gels) or 1-4 µg of DNA (preparative gels) were added per gel pocket. The 1 kb plus DNA ladder was used as DNA size marker, the RiboRuler™ high/low range ladders as RNA size markers. Electrophoresis was carried out at 80-100 volts for 80 min and gels were subsequently analysed under UV light in a Gel Jet Imager.

3.2.14 PREPARATION OF COMPETENT *E. COLI* CELLS

For the preparation of chemically competent *E. coli*, 100 ml LB medium containing the appropriate antibiotics were inoculated with 100 µl to 1 ml o/n culture of *E. coli* cells. Incubation with shaking at the appropriate temperature was done until an optic density (OD_{600}) of 0.35 (DH5α) or 0.7 (DH10B) was achieved. The following steps were carried out at 4 °C: Cells were harvested in 50 ml tubes by centrifugation (all 2700 g; 10 min) and the resulting pellet was resuspended in the same volume of ice-cold 0.1 M $MgCl_2$ (DH5α), 50 mM $CaCl_2$ (DH10B†) or 10% glycerol (DH10B+pSV1.RecA, DH10B‡). This step was repeated only for DH5α and DH10B+ pSV1RecA cells: They were pelleted again by centrifugation (same parameters as above), resuspended in 20 ml of 50 mM $CaCl_2$ (DH5α) or again 10% glycerol (DH10B+pSV1.RecA) and incubated on ice for 30 min. For all preparations a last centrifugation step was conducted, then the pellet was resuspended in 2 ml of 50 mM $CaCl_2$ with 15% (v/v) glycerol (DH5α), 500 µl of 50 mM $CaCl_2$ with 20% (v/v) glycerol (DH10B†) or 200 µl cold 10% glycerol only (DH10B+

pSV1.RecA, DH10B‡). A final incubation step on ice for 1 h was followed by the aliquoting of the cell solution into partial volumes of 200 (DH5α) / 100 (DH10B†) / 40 µl (DH10B+pSV1.RecA, DH10B‡) per 1.5 ml tube and immediate freezing of the tubes in liquid nitrogen. Competent cells were stored at -80 °C until use. Competent DH10B† cells for BAC transgenesis were processed further without intermediary freezing. *E. coli* INV110, TOP10, PIR1 and PIR2 cells were competent upon purchase.

following protocol of ‡3.4.1 or †3.4.2

3.2.15 SOUTHERN HYBRIDISATION

Southern hybridisation was used to screen for modified BAC clones and to determine the copy number of each transgenic founder line. First 5 µl of BAC DNA or 5-12 µg of genomic DNA were digested in restriction enzyme buffer (20 µl and 500 µl, respectively). For genomic DNA the extraction via phenol/chloroform solution was preferred. The samples were precipitated two times with ethanol to achieve clean and salt-free genomic DNA. In genomic DNA digestions also spermidine and spermin were added. For larger volumes the digestions were precipitated. The digestions were then run on a 1% agarose gel either for 20 V o/n or 40 V, 65 V, 90 V (each for 1.5 h). Gels were stained (30 min in ethidium bromide solution, 0.5 mg/ml) and distained (30 min wash in 0.5% TAE buffer) to take a picture of both the DNA and the marker together with a fluorescent size standard. Then the gel was washed in 0.2 M HCl for 15 min to depurinate the DNA. Afterwards the gel was washed twice in denaturation buffer for 25 min each followed by a quick wash in 10x SSC. The gel was placed upside-down on top of a glass plate and moistened with 10x SSC. The nylon membrane Hybond N(+) (Amersham) was placed on top of the gel avoiding the inclusion of air bubbles. Three thick blotting papers (Whatman) were soaked in 10x SSC and placed on top. A 10 cm pile of recycling paper was placed on top of the blotting sandwich that was ultimately weighted with two heavy glass plates. A sufficient amount of 10x SSC was put at the bottom of the blotting sandwich which was left standing o/n to ensure DNA transfer from the gel to the membrane. The next day the blotting sandwich was disassembled, the membrane quickly neutralised in 2x SSC, then dried for 2 h and optionally (depending on the membrane) cross-linked with UV light (Hoefer). In the meantime radioactively labelled probes were generated. DNA probes (25 to 50 ng) for Southern blotting were digested as required, gel-purified and radioactively labelled with [$^{\alpha\text{-}32}$P]dCTP (NEN) using the Prime-It®RmT Random Primer Labelling kit. The samples were purified via Probe-Quant G50 micro columns (Amersham) and denatured at 95 °C for 5 min directly before hybridisation. In parallel, the cross-linked membrane had been transferred to a preheated (65 °C) glass tube and 20 ml of hybridisation buffer had been added to equilibrate the membrane for 30 min at 65 °C. Now the freshly denatured probe was added to the hybridisation buffer. Incubation took place at 65 °C o/n. On the next day the solution was disposed and substituted by 10 ml of high salt

solution. This wash was repeated three times for 15 min before radioactivity was measured. If the radioactivity had been close to background levels an autoradiography was processed, otherwise the membrane was washed in low salt buffer until radioactivity fainted. Finally, the washed membrane was covered in cling foil and exposed to a film for at least 2 h (or up to one week) at -80 °C (light-protected). Films were developed automatically in a processor.

3.3 Synthesis of cDNA and RT-PCR

Mouse tissues were rapidly dissected in cold PBS on ice. Due to the presence of bone material tissue disruption was a critical step. Cochleae were either frozen in liquid nitrogen, homogenised using a metal pestle and taken up in Trizol, or disrupted by shaking at 3,000 rpm in a Mikro-Dismembranator in the presence of metal bowls (diameter: 2 mm) and Trizol for 1 min. When RNA contents of different ages were compared tissue was cut into pieces and stored in RNAlater according to the manufacturer's recommendations. Tissues of whole brain and kidney were subjected to an extra cleaning step (centrifugation at 12,000 g for 10 min, 4 °C). Volumes of this protocol refer to experiments with 50 to 100 mg starting material taken up in 1 ml Trizol. Protocol was scaled up and down according to the actual tissue weight. Supernatants were taken off the ice and incubated at RT for 5 min to allow the dissociation of nucleic acids. The following steps were carried out again at 4 °C. 200 µl chloroform were added to the sample that was mixed for 15 s and centrifuged for 5 min at 13,200 rpm. The upper, RNA-containing layer was transferred to a new tube where 500 µl isopropanol were added. The sample was incubated at RT for 10 min to allow precipitation of nucleic acids. After a 10 min centrifugation at 13,200 rpm the pellet was washed with 75% ethanol and was finally resuspended in 20 µl of RNase-free water. The following DNaseI reaction contained 2.5 µl 10x DNase buffer, 1.25 µl 20 mM DTT, 0.5 µl RNasin (RNase Out), 0.2 µl RNase-free DNaseI and 10 µg RNA in a total volume of 25 µl. After 1.5 h incubation at 37 °C another 0.5 µl of DNaseI were added to the sample which was then incubated for another hour. 75 µl of RNase-free water were then added, followed by a phenol/chloroform (24:1, 100 µl) extraction and precipitation (50 µl 7.5 M ammonium acetate, 400 µl pure ethanol). After two washes in 75% ethanol (all centrifugations at again 4 °C and 13,200 rpm for 10 min) the RNA was finally dissolved in 22 µl of RNase-free water and the concentration was determined spectro-photometrically. RNA was either stored at -80 °C or directly subjected to reverse transcription and PCR.

When primers that only produce a reasonably sized product with cDNA (and not gDNA) as a template could be designed, the SuperScript™ One-Step RT-PCR kit was used. For a 25 µl RT-reaction, 12.5 µl 2x reaction mix, 0.5 µl 10 µM F-primer, 0.5 µl 10 µM R-primer, 0.5 µl RT/Platinum® *Taq* Mix and 20 ng RNA template were mixed. Unspecific amplification of cDNA was done by reverse transcription with random hexamer primers: First 0.2 µg hexamer primers,

5 µg RNA and RNase-free water to 35 µl total volume were incubated at 65 °C for 5 min. 10 µl were then frozen as RT(-) samples to determine gDNA contamination. To the remaining volume of 25 µl the RT mix was added (10 µl 5x M-MLV RTase buffer, 2.5 µl 20 mM DTT, 1.25 µl RNasin (RNase Out), 2.5 µl 10 mM dNTP.mix, 8.25 µl water, 0.63 µl M-MLV reverse transcriptase). After 1 h at 42 °C the mix was diluted 1:1 with RNase-free water. For a standard analytical PCR (3.2.11) 0.5 µl of this RT(+) sample and the afore stored RT(-) sample were used with the same gene-specific primers. PCR products were brought on an agarose gel and compared. If gDNA is purged successfully no amplicon in the RT(-) sample is detected.

3.4 Generation of BAC-transgenic mice

3.4.1 CREATION OF MODIFIED BACs USING THE SHUTTLE VECTOR PLD53 AND HOMOLOGOUS RECOMBINATION VIA TWO GENE-SPECIFIC BOXES

A mouse BAC clone (RP24-327I14) encompassing the *Trpp2* gene was modified by two steps of homologous recombination in *E. coli* DH10B bacteria as described[299]. In short, the *E. coli* strain DH10B is devoid of RecA so that it cannot accomplish recombination on its own. RecA is therefore delivered in the shuttle vector (SV) pLD53.SCA-E-B together with the recombination cassette. This shuttle vector cannot replicate in DH10B cells as these cells do not possess the *pir2* gene necessary for replication of vectors with an R6kγ origin of replication. Therefore this system does not produce unnecessary shuttle vector copies in BAC-containing cells. This is why recombination is much more efficient with a low false-positive rate. BAC cells harbouring this shuttle vector therefore produce the amount of RecA necessary to drive recombination between the homology boxes on the SV and the corresponding sequences in the BAC.

The toxin expression cassette (containing the secretion signal, the mature GID toxin sequence, the flag sequence, a short hydrophobic linker sequence, the GPI sequence and a polyA tail) was cloned between the two recombination boxes upstream (box A) and downstream (box B) of the ATG of the *Trpp2* gene. The whole cassette was assembled in pGKpA by combining sequences from previous constructs. Together with the newly cloned homology boxes (in pCR2.1) the cassette was brought into the SV pLD53.SCA-E-B using restriction sites for AscI and NotI. Correct insertion of the boxes was monitored by PCR.

All steps were performed as indicated in the GENSAT protocol*. The method of choice for purifying BAC DNA is shortly summarised in 3.4.3; how the shuttle vectors were grown and purified is outlined in 3.4.3. Cells containing the chosen BAC were made competent (3.2.14), by subsequent electroporation (V = 1.8 kV, R = 200 Ω, C = 25 µF) the modified pLD53.SCA-E-B plasmid (1 µg shuttle vector DNA on 40 µl cells for 1 min on ice) was introduced to those cells. In

* http://www.gensat.org/BACProtocol.pdf

a series of incubation steps at 37 °C with increasing concentrations of chloramphenicol and ampicillin cells were stimulated to express RecA – thus accomplishing recombination. Clones with successful recombination via at least one homology box were screened for by PCR with 'Pkd2_Coint'-primers (3.1.5). Incubation of such 'co-integrates' in selective LB-chloramphenicol media without ampicillin removed the selective pressure of the SV leading to the resolved modified BAC clone and the free SV via a second homologous recombination event. Two more methods were used to help discovering resolved clones: First 100 µl of the chosen 'co-integrate' clones were spread on agar plates containing 4.5% sucrose (inducing the toxic activity of levansucrase). The gene for this enzyme, SacB, is present on the SV. Thus, resolved clones are not susceptible to this toxicity. The second way to test for resolution was exposing a copy of the master plate to UV light (6x15 W, 312 nm, 20 s). After growing the copy and the untreated master o/n at 37 °C size differences were detected. Clones that did not grow after UV-irradiation were devoid of the gene *RecA*. RecA is involved in *E. coli* DNA repair via the so-called SOS response[300]. It is only present on the SV and thus clones sensitive to UV light are likely the ones which have lost pLD53 by a second homologous recombination event. Such clones were then picked from the untreated control (master) plate and screened again by PCR and Southern blotting as described in 3.10.10 and 3.15 for the presence of cassette and boxes. One modified clone positive for all tests was finally purified by ultracentrifugation as described in 3.4.5.

3.4.2 CREATION OF MODIFIED BACs USING THE SHUTTLE VECTOR SV296 AND HOMOLOGOUS RECOMBINATION VIA ONLY ONE GENE-SPECIFIC BOX

The shuttle vector S296 utilised here contains an ampicillin resistance and has an R6kγ origin of replication similar to pLD53.SCE-A-B which calls for *E. coli* PIR2 cells as hosts for this vector. The cassette contains sequences for EGFP and the ribosomal protein L10a – forming a fusion protein when translated. To increase recombination efficiency we additionally transformed pSV1.RecA into the BAC cells because the amount of RecA transcribed and translated from pSV296 is sometimes not sufficient to drive successful recombination between shuttle vector and BAC homology boxes (Joe Doc, personal communication). The vector pSV1.RecA also has an R6kγ origin of replication and is maintained in *E. coli* PIR1 cells. It has a tetracycline resistance and is grown in LB medium with tetracycline (10 µg/ml) for at least 14 hours at 30 °C. The purification was not done via the standard shuttle vector DNA preparation with Chromas columns (3.4.3) which dramatically reduces yield (S. Gong, personal communication) but instead with a classical phenol/chloroform extraction. In a first transformation pSV1.RecA was brought into competent DH10B cells (see 3.2.14) harbouring the corresponding BAC (heat shock: 40 – 200 ng pSV1.RecA on 100 µl cells for 20 min; then 45 s at 42 °C, add 1 ml pre-warmed SOC medium, shake for 1 h at 30 °C and 225 rpm). Successful transformants could grow o/n in LB containing tetracycline (10 µg/ml) and chloramphenicol (20 mg/ml) at 30 °C at 300 rpm. The next day a fresh culture was

started with the same parameters and bacteria were grown to an OD_{600} of 0.7 and again made competent (see 3.2.14).

In this protocol recombination is happening only once and the vector sequences remain inside the BAC without being resolved. Therefore in the cloning process only one box per construct is needed. The boxes for the genes *Prestin* / *Slc26a5* (box S), *Calbindin* / *Calb2* (box R) and *α9 nAChR* / *Chrna9* (box Q) are designed as such that the shuttle vector will integrate after homologous recombination behind the TATAAA-box and directly in front of the ATG translation start. The 5'-UTR of exon 1 is thus disrupted in the final *Chrna9* construct (box Q). As the ATG of Slc26a5 is situated in exon 3 the box S lies directly in front of it in intron 2-3. In the final Calb2 construct the shuttle vector is integrated right in front of the complete exon 1, not disrupting the 5'-UTR. After introduction of the boxes in pSVS296 (as described in the previous chapter, using restriction enzymes AscI and NotI) the modified shuttle vectors were transformed into BAC-containing cells (see 3.1.4). Electroporation of the shuttle vectors into competent DH10B cells with the corresponding BAC as well as the plasmid pSV1.RecA was done as described before (3.4.1). Successful integrates were selected by growing the cells at now 30 °C in and on media containing chloramphenicol (20, resistance coded on BACs), ampicillin (50, resistance coded on pSVS296) and tetracycline (10 µg/ml, resistance coded on pSV1.RecA). The o/n culture was then spread out on plates without tetracycline and grown o/n at 43 °C. Both measures favour the loss of pSV1.RecA that – after the likely recombination – is not needed anymore. Picked clones were screened after purification for 'co-integrates' by PCR and Southern hybridisation using the according box-probes obtained from the original TOPO vectors (digested with AscI and NotI).

3.4.3 STANDARD SHUTTLE VECTOR DNA PREPARATION

Bacteria with pSV296 and pLD53.SCA-E-B were grown o/n at 37 °C in 15 ml LB supplemented with ampicillin (100 µg/ml). Harvest was done with a centrifuge (4000 rpm, 20 min, 4 °C). The pellet was then resuspended in 500 µl P1 buffer (all ready-to-use) and mixed on a vortex machine; 500 µl P2 buffer (mixed well, 5 min incubation at RT) and 500 µl ice-cold P3 buffer (mixed well) were subsequently added. Debris was removed by centrifuging at 14,000 rpm for 30 min. RNase (1.5 µl) was added to the supernatant (10 min incubation at 37 °C) and the total volume split in two. The content of both phase lock gel tubes (±750 µl) was treated with 750 µl phenol/chloroform (5 min mixing, centrifugation with 14,000 rpm for 10 min). The top layer was then taken off and treated with pure ethanol, mixed and centrifuged again (same parameters). After a washing step with 70% ethanol the pellet was dried and resolved in 200 µl TE buffer (total volume for both tubes). An additional purification was accomplished by applying the content to a Chroma Spin-400 column and a subsequent centrifugation step (1600 rpm, 5 min). Lastly the shuttle vector DNA was precipitated with 100 µl 7.5 M ammonium acetate and

750 µl 100% ethanol (gentle mixing, 10 min incubation at -80 °C, 30 min centrifugation at 14,000 rpm). After another washing step with 70% ethanol the pellet was resuspended in 10 to 15 µl TE buffer and checked for integrity and purity (agarose gel, Nanodrop analysis).

3.4.4 STANDARD BAC DNA PURIFICATION

E. coli DH10B cells carrying the desired BAC were grown in LB medium with 12.5 µg/ml chloramphenicol o/n with shaking (225 rpm). Bacteria of 1.5 ml culture medium were then pelleted by centrifugation for 30 s (all at 15,000 g and RT). The pellet was then resuspended in 100 µl Solution I supplemented with lysozyme (2.5 mg/ml). After 5 min incubation on ice 200 µl Solution II were added. After inverting the tube several times 150 µl 3 M potassium acetate were added. The reaction was then softly mixed and then centrifuged again (6 min). The supernatant was saved in a new tube and the DNA was then precipitated by adding 1 ml pure ethanol and subsequent centrifugation. Now the supernatant was discarded and the pellet air-dried. Another washing step was applied using 500 µl 70% ethanol. After air-drying the pellet completely the pellet was taken up in 20 µl EDTA (pH 8.0) supplemented with RNase (50 µg/ml). All BAC DNA was stored at 8 °C and clone verification was done using via either restriction enzyme analysis or sequencing with T7 and SP6 priming sites of pBACe3.6 – both flanking the insert.

3.4.5 BAC DNA PURIFICATION FOR TRANSGENESIS

All steps of BAC DNA isolation and ultracentrifugation were performed according to the GENSAT protocol*. In short, the ready-to-inject BAC clone was streaked out on a fresh LB plate, two single colonies were picked and grown first for 8 h at 37 °C and then o/n at 30 °C (0.4 to 1 ml of starter culture in 2x 500 ml LB each, resulting in 4 bottles). LB medium contained appropriate antibiotics (20 to 40 µg/ml chloramphenicol and – only in one-recombination-box BAC transgenesis – 50 µg/ml ampicillin). Bacteria were spun down 2x at 4,000 rpm for 30 min thus merging the content of the two 500 ml bottles each. All following steps were done in parallel for both picked colonies. First the pellet was resuspended in 80 ml 10 mM EDTA (pH 8.0) and incubated 5 min on ice. 160 ml of alkaline lysis solution were added; the mix gently swirled and then incubated for 5 min (RT). Then 120 ml of cold 2 M potassium acetate were added, incubation was carried out on ice for 5 min after repeated gentle mixing. Centrifugation of the reaction was then carried out at 11,650 rpm for 30 min. The saved supernatant was mixed with 360 ml isopropanol and spun down again (4,000 rpm, 30 min). The pelleted DNA was taken up in 36 ml of 10:50 TE buffer. Potassium acetate was added (9 ml of 7.5 M solution) and the reaction incubated at -80 °C for 30 min. Remaining debris was pelleted again (6,000 rpm, 10 min, 4 °C) and the DNA in the supernatant precipitated by the addition of ethanol (2.5 times

* http://www.gensat.org/about.jsp

the reaction volume), incubation at -20 °C (o/n) and centrifugation (11650 rpm, 30 min, 4 °C). The still moist pellet was dissolved in 4.4 ml TE. An aliquot was checked on an agarose gel for BAC DNA integrity. Then 4.4 ml of a caesium chloride solution (10.2 g in TE, filtered with 0.2 µm sieve) were added and mixed. 0.2 ml ethidium bromide (10 mg/ml) were added immediately. Debris was spun down at 4,000 rpm for 10 min, and then the remaining solution was loaded into Beckman Quickseal tubes using syringes and needles (18 gauge). Equilibrated and sealed tubes were subjected to ultracentrifugation (rotor Ti90, 65,000 rpm, o/n, 18 °C, without brake). The following day the BAC DNA (preferably the lower band) was removed with syringe and needle (18 gauge). The obtained volume (around 200 µl) was filled up to 2 ml with TE buffer and washed five times with NaCl-saturated butanol until ethidium bromide was invisible. Water (1 ml) and 2.5 volumes of ethanol were added and the mix was left to sit down on ice for 30 min. The spun down DNA (8,000 rpm, 10 min) was resuspended in 0.5 ml sodium acetate (0.3 M). DNA was then washed 1st with pure ethanol and 2nd with 70% ethanol. The slightly dried pellet was finally taken up in 20 – 40 µl TE buffer and transferred to an incubator (37 °C, 30 min). DNA integrity and quantity were checked (agarose gel, Nanodrop 1000 system). BAC DNA was linearised with PI-SceI (100 ng BAC DNA, 3 µl enzyme, 1 µl BSA, 10 µl 10x buffer) at 37 °C for 3 to 4 hours. Dialysis was then carried out to set up the proper salt concentration (0.025 µm filter floating on 20 ml injection buffer in a Petri dish for at least 4 h at RT). After a last check on an agarose gel the decision for one of the two BAC DNA preparations was made. Its DNA concentration was set to 2 ng/µl and the desired amount of DNA was mixed 1:1 with 2x polyamine mix 48 h before the injection at the MDC transgenic core facility (200 pronuclei of fertilised BDF/Bl6 mouse oocytes).

3.5 Immunohistochemistry

Animals were anaesthetised with 50 µl anaesthesia-mix per 10 g body weight and perfused with 4% PFA in 0.1 M PBS, pH 7.4 (4 °C) when large tissues were collected. (Mice were generally not perfused when only cochleae were taken.) Immediately after perfusion the cochlea (brain, kidney) was removed and post-fixed in the perfusion fixative at 4 °C for 2 h. Morphologic differences can be diminished after prolonged formaldehyde fixation that therefore should be kept at a minimum. The tissue was then washed three times for 10 min at RT in PBS. Bone-containing tissues were subjected to decalcification in 10% EDTA for several days (depending on ossification stage). Cochleae younger than P5 were not decalcified. All tissues were then immersed in sucrose (PBS). Brain and kidney were immersed with 30% sucrose o/n at 4 °C, cochleae for 30 min at RT in solutions with gradually increasing sucrose percentages – starting from 10% up to 30% (5% increments).

3.5.1 CRYOSECTIONING

Sucrose-soaked tissues were left ON at 4 °C in 1:1 30% sucrose solution and O.C.T.™ TissueTek. All tissues were shortly washed in TissueTek, embedded therein correctly positioned (cochleae: midmodiolar sections, brains: coronal, sagittal sections) and frozen on a metal block cooled by dry ice. Samples were stored at -80 °C until sectioning. Sections were cut on a cryostat (10 µm).

3.5.2 FLOATING SECTIONS

Mice were treated as mentioned in the previous section. Floating sections were done of collected sucrose-soaked brains of well-perfused mice. Sections were cut on a sliding microtome (thickness: 40 µm) and gathered in cryosection buffer where they also were stored until staining (short term at 4 °C, long term at -20 °C). For staining selected sections were carefully transferred to a new well and washed three times in PBS (passing over via a small sifter). Blocking, staining and washing were all done as described in 3.5.3. If valuable primary antibodies were used, the sections were transferred to an object tray with a fine paint brush. The blocking solution containing the 1st antibody was then applied directly on the section and covered by a glass slip. Thus the expended volume could be reduced. Completely stained sections were brought onto object trays, drained, dried quickly at RT and mounted with Immu-Mount™ / cover slips.

3.5.3 STAINING

Thawing of selected sections was carried out in a sealed plastic bag at 37 °C for 1-2 h. Sections were encircled with wax and rehydrated by adding PBS (RT, 10 min). All tissues were blocked first for 20 min with blocking solution 1, then for 1 h in solution 2. The primary antibodies and markers were applied o/n in diluted blocking solution 2 (1:1 with PBS). The next day the cells were washed 3x with PBS and incubated with corresponding secondary antibodies for 1.5 h at RT. Samples were then washed 3x in PBS for 10 min each. DAPI as a nuclear marker was added in the first washing step (1:3000). Finally sections were dried shortly at RT and mounted. Antibodies and markers used in this study (including their preferred applied dilutions) are summarised in Table 9. Pictures were taken on different microscopes (see Table 12).

3.5.4 TMRD DYE APPLICATION

The medial surface of the auditory bulla of freshly sacrificed mice was exposed by sectioning the cranium in the sagittal plane and removing the brain. The neuronal tracer TMRD (3000 Da MW, MP, USA) was applied manually to the vestibulocochlear nerve bundle at the internal auditory meatus and incubated for 20 min at RT. Excess dye was washed out with artificial cerebrospinal

fluid (aCSF). Cochleae were then dissected, incubated at RT for 4 h in carbogen-treated (95% O_2, 5 % CO_2) aCSF and beyond that subjected to standard treatment.

3.6 In situ hybridisation

3.6.1 DIG LABELLING OF RNA PROBES

All solutions were prepared with nuclease-free water. 40 U of the required restriction enzyme (see Table 13) was used to linearise the plasmid (50 µg) at 37 °C for 2 h or o/n. The enzyme was then degraded by adding lysis buffer (300 µl) and proteinase K (20 µg/µl) to the reaction (incubation for 30 min at 37 °C). The plasmid was then purified via a phenol/chloroform extraction (2x with 600 µl, 2nd time chloroform only) and precipitation with ammonium acetate and ethanol (1st 100%, at least 2.5x the volume, incubation for 30 min at -80 °C; 2nd 2x with 70% ethanol). The dried pellet was resuspended in 20 µl water. 1 µg of the purified and linearised plasmid was then used for the labelling reaction which contained the following components: 2 µl DIG RNA labelling mix, 2 µl transcription buffer (10x), 20 U RNase inhibitor, 1 µl T7 or SP6 RNA polymerase in a final volume of 20 µl (incubation at 37 °C for 2 h). Then a column-purification using the RNeasy kit was done (elution with 50 µl H_2O, addition of 50 µl formamide). The probe was then analysed for integrity on an agarose gel (10 µl). Aliquots were stored at -80 °C.

Table 13: *In situ* probes

Name	**Supplier**	**Vector / linearising enzyme**	**Size box / size transcript**	**Promoter** (antisense probe)
Pkd1(2)	generated in this study	pCRII / XbaI	549 bp / 699 bp	SP6
Pkd2flox	generated in this study	pCRII / XbaI	368 bp / 518 bp (wt and flox allele) Ø / Ø (Δ allele)	SP6
Pkd2pan 1.5	generated in this study	pCR2.1 / HindIII	474 bp / 623 bp (all alleles)	T7
EGFP	generated by C. Hanack	pBluescript / SmaI	n.d. / ~700 bp	T3
$tGID_S$	generated by S. Frahm	pCS2 / HindIII	n.d. / ~300 bp	T7
Peripherin	provided by S. Britsch	n.d. / EcoRV	n.d.	T7

3.6.2 *IN SITU* HYBRIDISATION ON CRYOSECTIONS

To avoid contamination with RNases all devices and tools were cleaned with RNaseZap (Ambion) according to the manufacturer's protocol. Handling with gloves was obligatory. Cochleae from mice of different ages were collected in ice-cold PBS. Helicotrema, oval and round windows were opened mechanically to allow penetration of solutions. After short washing in

ice-cold sucrose (20%) cochleae were frozen in O.C.T.™ TissueTek. Cryosections of 12 to 14 µm thicknesses were cut in a thoroughly cleaned cryostat and quickly stored until further use in a -80 °C freezer. At the first day the cryosections were thawed for 30 min, then fixed in freshly prepared 4% paraformaldehyde (PFA) on ice for 20 min and washed 3x in PBS (5 min each). Afterwards the sections were bleached in 3% H_2O_2 in methanol for 15 min at RT and washed 3x in PBS. The endogenous alkaline phosphatase activity was quenched by incubation 1st with 0.2 M HCl for 8 min at RT and 2nd with acetylation buffer for 10 min at RT. Two washing steps (5 min, RT) followed. Then slides were dehydrated in a series of ethanol solutions (increasing ethanol content) for 1 min each. Sections were then dried for 30 to 60 min and surrounded with a wax pen (Dako). Prehybridisation was done with 700 µl hybridisation buffer per slide for at least 2 – 3 h. In the meantime the cover slips were silanised (Sigmacoat) and the DIG-RNA probes were diluted in hybridisation buffer (1:10 to 1:100), denatured for 5 min at 80 °C and immediately cooled on ice. The probe was applied to the sections (100 to 150 µl/slide) and covered by a silanised cover slip. Incubation in a humid chamber (chamber buffer) at 70 °C lasted o/n. The next day sections were washed in prewarmed 5x SSC at 70 °C for 5 min in a shaking water bath to remove cover slips and excess probe. The sections were then 1st washed stringently for 2x 15 min in 50% formamide/1x SSC (prewarmed) at 60 °C and 2nd washed for 2x 30 min in 50% formamide/0.2x SSC again at 60 °C. Following washing the slides were transferred to MAST buffer for 10 min at RT, then washed in PBS for 10 min and blocked in freshly prepared MAST++ to remove excess detergent (30 min, RT, shaking). After removal of this blocking solution the sections were incubated with the anti-DIG (digoxigenin) antibody that was bound to alkaline phosphatase (1:2000) in MAST++ at 4 °C o/n in an humidified chamber. At the third day the sections were washed 4 h in MAST (frequent change of solution). Sections were equilibrated in NTMT for 10 min and then stained with BCIP/NBT (Roche) in NTMT under light protection at RT until the staining showed the desired intensity (up to several days). The sections were finally washed in PBS 3x and mounted with Immuno-Mount™ (Thermo).

3.7 Electrophysiology

3.7.1 *IN VITRO* TRANSCRIPTION

50 µg of plasmid DNA was linearised in a total reaction volume of 300 µl with 100 U of the appropriate restriction enzyme (see Table 14) at 37 °C for 4 h. Afterwards, 300 µl lysis buffer were added (30 min incubation at 37 °C). Phenol/chloroform extraction was followed by ethanol precipitation at -20 °C for 2 h. Subsequently, the pellet was washed with 70% ethanol and dried. Pellet was resuspended in nuclease-free water (Ambion) and DNA concentration adjusted to 1 µg/µl. 3 µg of plasmid DNA was used as starting material for the transcription reaction that

was assembled quickly at RT. The following steps were carried out using the mMessage mMachine® SP6/T7 kit according to the manufacturer's instructions. After resuspension of the produced cRNA in 50 µl nuclease-free water its quality (single bands) and size was evaluated by agarose gel electrophoresis. RNA quantity was measured spectro-photometrically. Concentration was adjusted to 0.1 µg/µl. RNA was kept on ice and stored at -80 °C as soon as possible. Purified RNA was used for two-electrode voltage clamp recordings.

Table 14: Generation of different cRNAs from plasmid DNA by *in vitro* transcription

Name (origin)	**Vector**	**Linearising enzyme**	**Promoter for transcription**	**Transcript size**
α1 (mouse)		XbaI	SP6	1.7 kb
α3 (mouse)		AscI	SP6	2.0 kb
α4 nAChR (chicken)		NheI	T7	2.2 kb
α7 (chicken)	pcDNA	NheI	T7	
α9 nAChR (rat)	pGEMHE	NheI	T7	
α10 nAChR (rat)	pSGEM	NheI	T7	
$\alpha Bgtx_S$-GPI	pCS2	AscI	SP6	200 bp
$\alpha Bgtx_S$-TM	pCS2	AscI	SP6	
β1 (mouse)		XbaI	SP6	2.0 kb
β2 (chicken)		NheI	T7	1.7 kb
β4 (mouse)	pCS2	AscI	SP6	1.7 kb
γ (mouse)		XbaI	SP6	2.0 kb
δ (mouse)		BamHI	SP6	2.0 kb
$\kappa Bgtx_S$-GPI	pCS2	AscI	SP6	200 bp
$BulA_S$-TM	pCS2	AscI	SP6	
GID_S-GPI	pCS2	AscI	SP6	550 bp
GID_S-TM	pCS2	AscI	SP6	
GID_L-TM	pCS2	AscI	SP6	
GID_S-PC	pCS2	AscI	SP6	1.4 kb
GID_L-PC	pCS2	AscI	SP6	1.4 kb
GID_S-PE	pCS2	AscI	SP6	1.3 kb
GID_L-PE	pCS2	AscI	SP6	1.3 kb
GID_{2L}-PE	pCS2	AscI	SP6	1.4 kb
GID_{3L}-PE	pCS2	AscI	SP6	1.4 kb
MII_S-GPI	pCS2	AscI	SP6	200 bp
MII_S-TM	pCS2	AscI	SP6	
MII_L-TM	pCS2	AscI	SP6	
$PnlB_S$-GPI	pCS2	AscI	SP6	200 bp

3.7.2 TWO-ELECTRODE VOLTAGE CLAMP RECORDINGS

Female adult *Xenopus laevis* frogs were anesthetised in 0.35% ethyl-3-aminobenzoate methane sulphate salt (Tricain, Roth). Afterwards they were placed on ice for surgery. Skin and muscle directly above the ovaries were cut (1-2 cm) with a scalpel. The oocyte sack was taken out and the desired amount of oocytes removed. Muscle tissue and skin were then stitched together independently with a PVDF-yarn (Marilon blau, Catgut, Markneukirchen, Germany). The frog was allowed to recover under supervision in cold water before returning it to the tank. Removed oocytes were collected in OR2 medium and digested with 2 mg/ml collagenase I in Ca^{2+}-free Ringer solution for 3 h shaking at RT in a 50 ml Falcon tube to disintegrate the connective tissue.

Then oocytes were quickly washed 3x in OR2 without enzyme and transferred into L15/OR2 media for incubation at 18 °C o/n. The next day stage V and VI oocytes were assorted for injection. Transcripts were diluted in DNase-free water to a final concentration of 50 ng/µl (for ion channels) and 225 ng/µl (for t-toxins). 20 nl of each mix were injected per oocyte with calibrated capillaries and a micromanipulator. Incubation of injected eggs was carried out at 18 °C (Binder). Two to five days after injection (medium exchange every 2 d) the oocytes were placed in the recording chamber. Borosilicate glass capillaries (WPI) were pulled with a resistance of 0.7-1.5 MΩ and filled with 3 M KCl. The oocytes were clamped by two electrodes at -70 mV (gene clamp 500 amplifier). Data were digitised using the 1322A 18 bit data acquisition system. The protocol was applied as follows: Oocytes were regarded as healthy when the leak currents were between 30 and 250 nA. First they were bathed in Ringer solution, and then valves were switched for 20 s to apply 1 mM acetylcholine (in Ringer). Data were recorded and analysed using the Clampex and Clampfit software (Axon).

3.8 Behaviour experiments

Mice were backcrossed to C57BL6/J for at least five generations. For all behaviour experiments the genotypes of mice were not made known to the experimenter. As C57BL/6J mice develop a marked and progressive late-onset hearing loss characterized by cochlear degeneration, which is caused by a mutant age-related hearing loss (ahl) locus[301], the auditory tests were preferably performed on young mice. For analyses of older mice backcrossing into the B6.CAST-*ahl*$^{+}$ strain (>N10F13 in C57BL/6J) that carry wild-type *ahl* alleles is recommended. Resulting congenic C57BL/6J mice have normal hearing even at 18 months of age.

Animals were anesthetised intraperitoneally with a combination of ketamine (125 mg/kg) and xylazine (2.5 mg/kg). Heart rate was constantly monitored to control the depth of anaesthesia. Body core temperature was maintained constant at 37 °C using a rectal-temperature-controlled heat blanket. For stimulus generation, presentation and data acquisition the Tucker-Davis-Technologies II (DPOAE) or III (ABR) systems were used (run by BioSig32 RP software or MATLAB routines). Sound pressure levels (SPLs) are provided in decibel SPL root mean square (RMS, tonal stimuli) or decibel peak equivalent SPL (p.e., clicks) and were calibrated using a ¼″ Brüel and Kjaer microphone. All stimuli were presented ipsilaterally in the free field.

3.8.1 AUDITORY BRAINSTEM RESPONSE

Auditory evoked potentials (AEPs) represent neural activity related to auditory stimulation. They show summated neural energy at the various synaptic levels of the auditory pathway. AEPs are extracted from the ongoing EEG activity by specialised technical manipulation. They are

recorded from the scalp representing activity in cochlea, brainstem, thalamus, and cortical areas. AEPs are distinguished in early, middle and late evoked potentials, respectively. The auditory brainstem response (ABR) is an 'early' evoked response, as it reflects neural function along the ascending auditory pathway, from the cochlea to the inferior colliculus (IC). It consists of a series of positivities and negativities occurring within 10 ms of the stimulus. The five distinct waves of the normal ABR waveform are mainly generated by successive nuclei in the ascending auditory pathway: waves I and II originate from the distal and proximal portions of the auditory nerve, respectively, wave III originates from the cochlear nucleus (CN), wave IV originates from the superior olivary complex (SOC) and wave V originates from the lateral lemniscus/inferior colliculus. Each high level order wave also receives contributions from lower levels[302].

ABR is also called 'brainstem auditory evoked potential' (BAEP) or 'brainstem evoked response audiometry' (BERA). A briefly played sound (JBL 2402 speaker) elicits a short latency potential that can be recorded from the head. In the experimental setup used three electrodes were placed at the anaesthetised mouse (1) near the vertex, (2) behind the ear the sound is played to (near the mastoid process) and (3) at the tail (ground). Responses were recorded by registration of the potential difference between subdermal electrodes (1) and (2). The recorded ABR is dependent on the placement of the recording electrode pair. In our setup it is dubbed 'vx-ie' for 'vertex' and 'ipsilateral ear'. Interelectrode impedances were less than 1 kΩ.

The acoustic stimulus for the tone-evoked ABR was a 12-ms tone-burst ($\cos^2$ rise/fall with a gate time of 1 ms; 10 ms plateau) presented at a stimulation rate of 40 Hz and frequencies of 4, 8, 10, 12, 16, 32, 38 and/or 44 kHz. The difference potential was amplified 50,000 times by a custom amplifier (JHM NeuroAmp 401) or 20 times by the medusa amplifier (TDT), filtered (0.4 kHz high-pass, 4 kHz low-pass), sampled (50 kHz for 20 ms) and averaged (2×1,300 sweeps) to obtain two mean traces at each intensity. To determine the hearing threshold both traces were compared visually after tone-burst presentation of decreasing SPLs (10 dB steps). The SPL where the two traces could still be brought in compliance was defined as the threshold. Clicks (duration of 0.03 ms) were applied at a rate of 20 Hz. Sweeps with excessive noise were rejected using the artefact rejection feature of the BioSig32 software. Amplitudes were measured either from the wave peak to the following trough or from wave peaks (both, positive and negative) to baseline.

3.8.2 DISTORTION PRODUCT OTOACOUSTIC EMISSIONS

Otoacoustic emissions (OAEs) are low level sounds emitted by the cochlea in the process of receiving sound vibrations and transforming them to cellular and neural stimulation. Recording of OAEs implies a functioning cochlea and a healthy middle ear. Distortion product (DP) OAEs are produced when the ear is stimulated with a combination of pure tones that are close in

frequency (primary tones). DPOAEs reflect non-linear processes of hair cell motion that are generated by the active cochlear mechanisms responsible for enhancing basilar membrane vibration (known as the 'cochlear amplifier')[303].

A 24-bit sound card (Sony Sound Forge 7.0) and an ED1/EC1 speaker system generated the two primary tones (ratio: $f_2/f_1 = 1.2$; f_2 level at 10 dB < f_1 level). Primary tones were coupled into the ear canal by a custom-made probe containing an MKE-2 microphone and adjusted to an intensity of 60 dB SPL at the position of the ear drum as mimicked in a mouse ear coupler. The microphone signal was amplified (DMP3, MIDIMAN), computed by fast Fourier transformation, and averaged over 5 consecutive waveform traces. The surrounding noise floor was subtracted before measuring DPOAE SPL amplitude at $2f_1$-f_2 (6, 8, 12, 16 and 20 kHz).

IV. RESULTS

4.1 Targeting the tethered conotoxin GID to α7 nACh receptors in mouse SGNs

To elucidate the role of α7 nAChRs in mouse spiral ganglion neurons first a screen for a conotoxin potently blocking homomeric α7 nAChRs was conducted (next chapter). Then, transgenic mice expressing this conotoxin in murine SGNs were generated (4.1.2) and analysed on a molecular (4.1.3) as well as on a behavioural (4.1.4) level.

4.1.1 TOXIN SELECTION AND PRELIMINARY *IN VITRO* WORK

The *Xenopus laevis* oocyte expression system was employed to test several toxins for their blocking properties on α7 nAChRs. As described previously first-generation toxins are tethered to the membrane via a GPI-anchor to achieve a stable and long-lasting block of α7 nAChRs[243] (also see Fig. 7). Of the five (GPI-) tethered-toxin constructs generated (tαBgtx, tκBgtx, tPnIB, tMII, tGID) only tMII failed to block nicotine-induced currents (Fig. 9A). tκBgtx and tPnIB were excluded from further analysis because of their low blocking effect when compared with tαBgtx and tGID – the most potent inhibitors. Then, an alternative way of anchoring the toxins in the membrane was investigated (Fig. 9B): MII again is the only exception as its blocking properties improve when being tethered with a transmembrane- (TM-) domain in the place of a GPI-anchor. However, tαBgtx and tGID (TM-domain) lose some of their blocking effectiveness when compared with their GPI-counterparts. BuIA was included in the experiment as a negative control as it only blocks α6* nAChRs[304]. Unexpectedly, the TM-domain BuIA construct blocks about 50% of the α7 nAChR current. The snake toxin tαBgtx has wide range of target channels[225]. Therefore tGID became the toxin of choice. However, as also GID blocks reportedly a wide range of nAChRs[233,234] the specificity of its tethered form (GPI-anchor) was tested on various nAChR subunit combinations (Fig. 10). Expectedly, the conotoxin does not block the muscular channel (α1β1γδ) and the neuronal channel α3β4. The non-tethered toxin blocks α4β2 receptors but, surprisingly, the tethered form does not. Therefore α3β2 and α7 are the remaining two nAChRs blocked by tGID. tGID (GPI) can be considered the best membrane-tethered toxin for silencing the spiral ganglion response upon ACh release by LOC fibres because the α3 subunit has not been reported to be present in the SG. α9 and α10 are also not present in the SG but (1) because of their localisation in the nearby inner hair cells (IHCs) and (2) an occasionally reported possibility of SGN-IHC synapses tGID (GPI) was tested on them: Although the amplitude is not reduced, the shape of the graph is altered as such, that the desensitisation of α9α10 nAChRs is prolonged upon tGID expression (Fig. 10, lower panel).

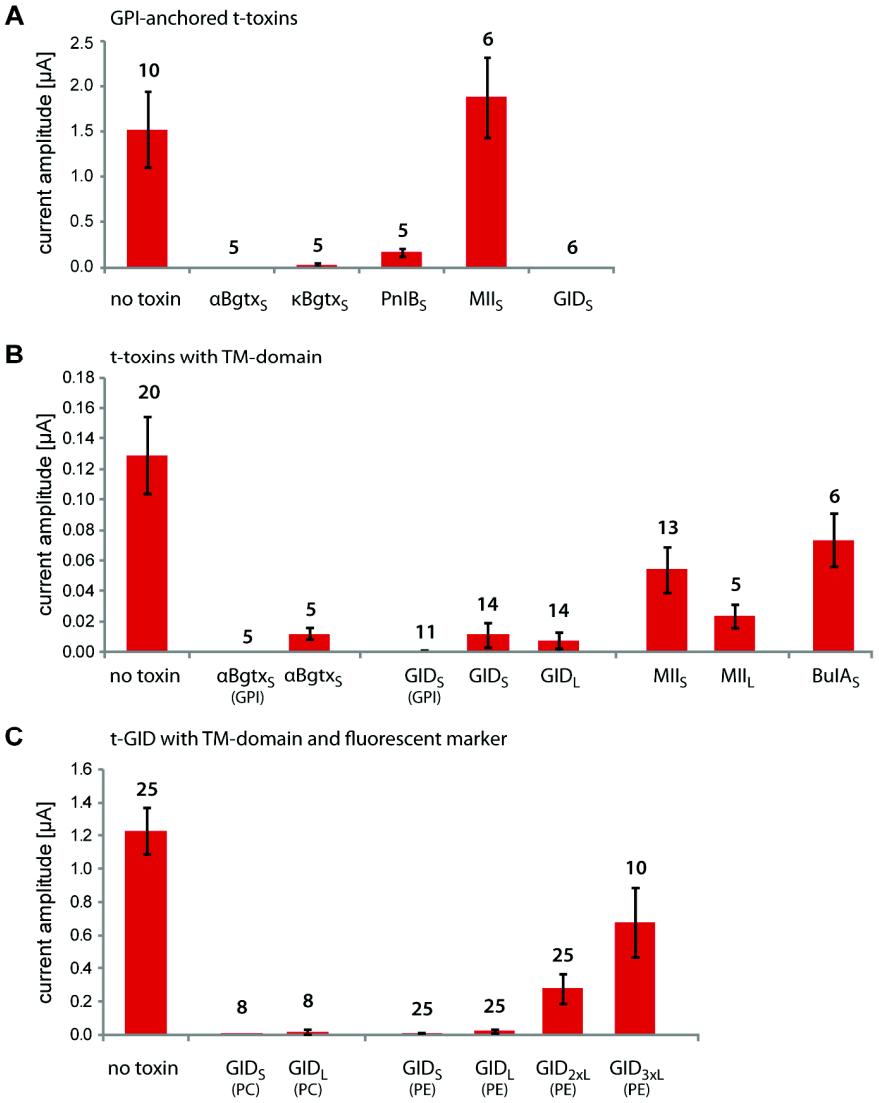

FIG. 9: BLOCKING ACTIVITY OF TETHERED TOXINS ON α7 nAChR CURRENTS IN *XENOPUS* OOCYTES

Electrophysiological whole cell, two-electrode voltage clamp recordings of *Xenopus* oocytes co-injected with cRNAs of t-toxins and α7 nAChR subunits. Quantification of peak current amplitudes recorded 3 to 6 days after injection upon channel activation by nicotine is shown. Data represent mean values ±s.e.m.; counts above bars indicate numbers of oocytes patched (minimum of two experiments). (A) Test of t-toxins from kraits and *Conus spp.* with short linkers and GPI-anchors. αBgtx and GID show complete block of currents. (B) Test of t-toxins from krait and *Conus spp.* with TM-domains. Two GPI-anchored t-toxins are included for comparison. Linker length varies for GID and MII between short (S) and long (L). TM-domain constructs do not block currents as reliably as GPI-anchored constructs. Long linker constructs of GID and MII block better than their short linker siblings. (C) Test of tGID with differing linker lengths (from S, 10 aa, to 3xL, 69 aa) and two different fluorescent markers (PC, PE) added to the intracellular end of the TM-domain. No difference between the differently tagged versions is visible, but increasing linker length markedly reduces tGID blocking ability. Disparate maximal amplitudes of ion channel currents due to varying quality of obtained oocytes. *GPI* glycosyl-phosphatidylinositol, *TM* PDGF transmembrane domain, *PC* TM with mCherry, *PE* TM with EGFP

The influence of the linker length on the blocking capability was also assessed: A long linker only slightly improves the ability of GID (TM-domain) to block α7 (Fig. 9B). However, for the TM-domain constructs fused to a fluorescent marker like EGFP (PE) or mCherry (PC) growing linker lengths decrease the blocking capabilities (Fig. 9C). Above all experiments the short version consistently performs best. Hence, short linker, GPI-tethered GID is considered as the most

potent α7-blocking toxin studied. Therefore BAC-transgenic mice carrying a cassette with the genetic information for $tGID_S$ will be generated.

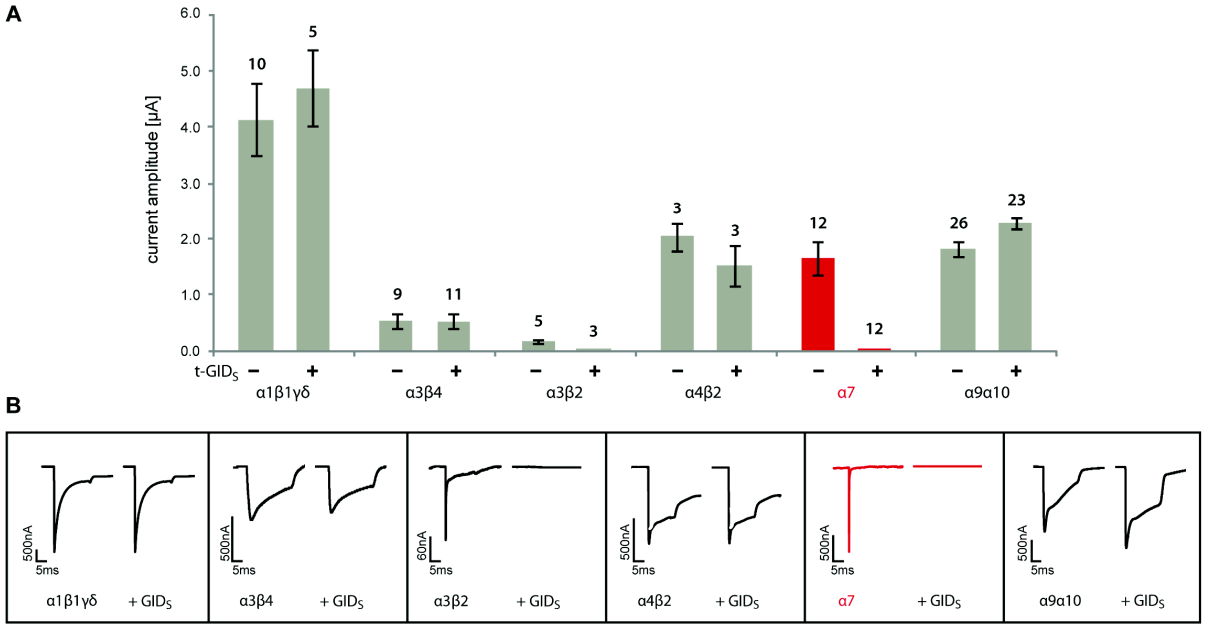

FIG. 10: BLOCKING ACTIVITY OF tGID ON nAChRs OF DIFFERING SUBUNIT COMPOSITION
Electrophysiological whole cell, two-electrode voltage clamp recordings of *Xenopus* oocytes co-injected with cRNA of GPI-anchored tGID and different nAChR subunit combinations. tGID construct has a short linker. (A): Quantification of peak nicotine-induced current amplitudes (axis of ordinates, measured in µA) is shown. Recordings done 2 to 6 days after injection at the time of best ion channel activity for each subunit combination. Data represent mean values ±s.e.m.; counts above bars indicate numbers of oocytes patched (minimum of two experiments). tGID blocks α7 and α3β2 nAChRs completely and is a mild inhibitor of α4β2. The amplitude of all other subunit combinations is not affected. (B): Representative traces of nicotine-induced ion channel currents. In addition to the complete block of α7 and α3β2 nAChR currents GID changes the desensitisation properties of α9α10 nAChRs.

4.1.2 CONSTRUCTION OF BAC-TRANSGENIC $tGID_S$ MICE

Protein expression analyses in mice producing tethered MrVIa show that GPI-anchored toxins get successfully trafficked to the plasma membrane (PM) where they correctly get integrated[240]. That study also showed that the stable expression of t-toxins at the PM can be transiently abolished by cleaving the toxin off of the GPI-anchor via the addition of phosphatidylinositol-specific phospholipase C (PI-PLC). In the present study this approach is carried forward to the auditory system where cells in the spiral ganglion of BAC-transgenic mice are prompted to produce tGID to block the activity of endogenous α7 nAChRs. The applied two-step modification system allows the precise targeting of the transgene to the genomic locus of the BAC via homologous recombination[299]. Fig. 11A shows a scheme of the utilised BAC. The *Trpp2* locus and the integration site of the tGID construct are indicated.

The tGID expression cassette flanked by homology boxes A and B was inserted into the shuttle vector pLD53. This construct then was transformed via electroporation into *E. coli* DH10B cells encompassing the *Trpp2*-containing BAC. After homologous recombination 'co-integrates' were

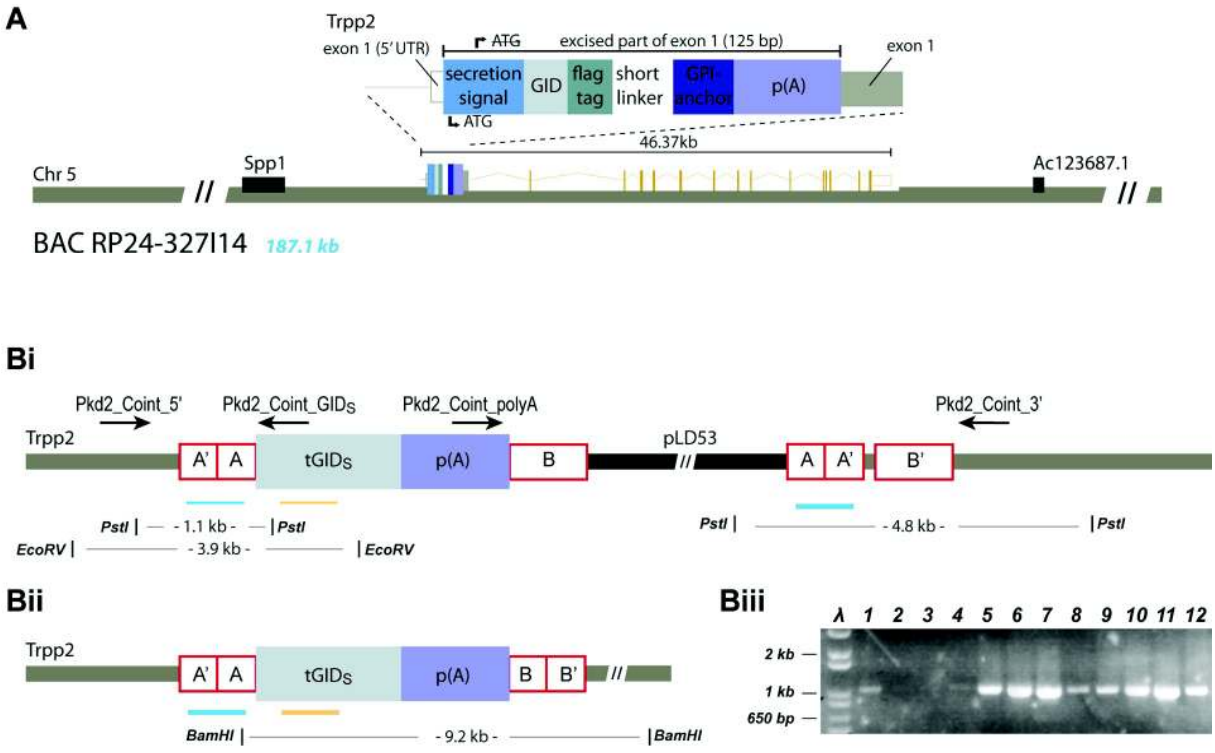

screened by PCR using two primers flanking the box A and B homology regions (Fig. 11Bi, result shown in Fig. 11Biii). A second homologous recombination was induced by selective incubation of 'co-integrate'-clones in chloramphenicol-containing media lacking ampicillin to obtain the modified BAC clone. After selection for sucrose tolerance and UV sensitivity the remaining positive clones were further analysed by Southern hybridisation (SH) using box A as a probe to ensure exclusion of unwanted bacterial vector sequence (Fig. 12Ai). Resolved clones show a 1.1 kb band, whereas a possible 2nd band of putative 'co-integrates' is not observed (Fig. 12Ai). SHs were carried out using the toxin sequence as a probe to ensure that the positive clones contain the tGID expression cassette: Almost all clones are positive (Fig. 12Aii, Aiii).

One positive clone was selected and its BAC DNA purified. After linearisation and dialysis it was injected into fertilised oocytes of BDF/BL6 mice. Following this, twelve transgenic founders were obtained. A preliminary characterisation was done by PCR screening for the presence of

FIG. 11: GENERATION OF THE MODIFIED BAC CONSTRUCT (I)
The utilised BAC clone is shown in (A). The toxin expression cassette will be inserted into the 1st exon of *Trpp2* thus excising the original translation start of the gene. The cassette also contains a polyadenylation signal p(A) ensuring cessation of transcription. The protein is targeted to the membrane with the help of a peptidic secretion signal. (Bi) Scheme of the BAC clone with fully integrated shuttle vector pLD53 ('co-integrate'). Shown is a first recombination event via box A. Another recombination between both boxes B is needed to resolve the shuttle vector so that only the expression cassette is maintained within the final modified BAC (Bii). Recombination via first box B and then box A is equally probable (corresponding scheme not shown). Arrows indicate primer pairs for the detection of successful integration of the shuttle vector. In the case of homologous recombination 1st via box A the left primer pair amplifies a band of 1019 bp (Bi). After resolution (successful 2nd recombination event) also the right primer pair yields an amplicon of 1215 bp (Bii). PCR analysis of 12 'co-integrate' clones with box A primers (Biii) shows amplicons in nearly all of them. The first recombination step is preferably carried out via box A as PCR with box B primers does not produce a specific signal in those 12 clones (not shown).
Restriction sites of endonucleases used for Southern blot experiments (next figure) are indicated together with the respective sizes of DNA fragments. Blue bar indicates situation of the Southern blot probe box A. Yellow bar indicates tGIDs probe.

BAC sequences (BAC primer pair before, BAC primer pair after) and toxin cassette sequences (primer pairs 2F/1R and 2F/2R, not shown). Following this, three lines were discarded due to incomplete presence of the modified BAC in the genome. Four more lines were discarded due to

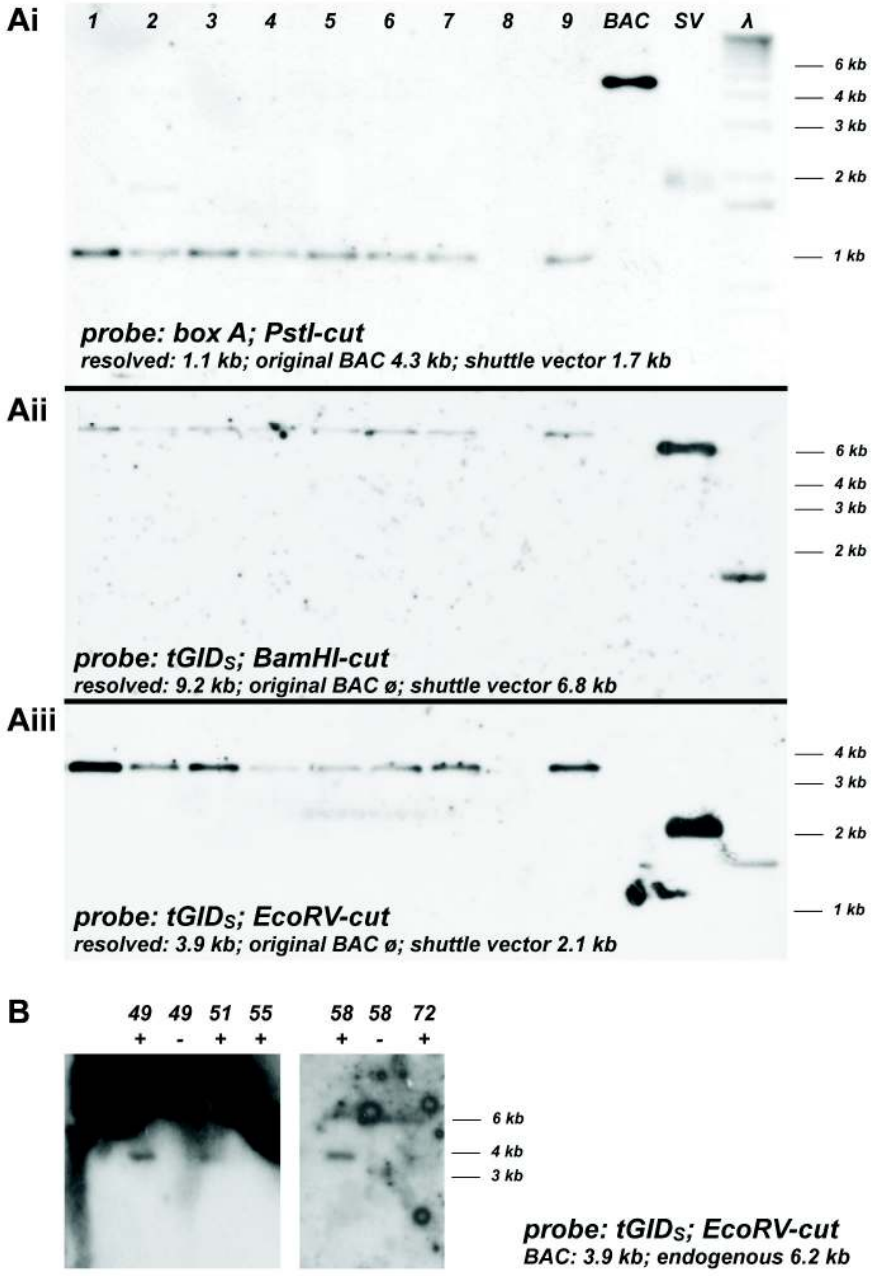

FIG. 12: GENERATION OF THE MODIFIED BAC CONSTRUCT (II) AND OF BAC-TRANSGENIC MICE

Southern blots of 9 different BAC clones after the induction of the 2nd recombination event (A) and of tissues of 5 different mouse founder lines (B). (A) BAC DNA was digested with PstI (Ai), BamHI (Aii) and EcoRV (Aiii). Southern probes were either hybridised with the box A (Ai) or the toxin cassette (Aii) sequence. Location of probe sequences and restriction sites are indicated in the previous figure. Expected sizes of the DNA fragments exhibiting a hybridisation signal are indicated for each enzyme/probe-combination in this figure. The unmodified BAC ('BAC') and the modified shuttle vector ('SV') served as controls. The size marker indicated by λ produces unspecific signals. Hybridisation with box A probe (Ai) only shows bands of resolved constructs (1.1 kb). No 2nd signal indicating remaining 'co-integrates' (4.8 kb) is visible. Thus resolution was successful in 8 of the 9 clones scrutinised. All of these 8 clones show a correctly sized signal when hybridised with the toxin probe (Aii, Aiii). Of the 12 founder lines obtained tissues of 5 were subjected to SH with the toxin probe (B). Of the founder lines 49 and 58 a BAC-negative littermate (determined by PCR analysis) was included. Endogenous signals with similar strength above all lines are faintly visible. Highest BAC signal and thus highest BAC copy number assumed is found in lines 49 and 58.

breeding problems and mosaic expression. The remaining founder lines (49, 51, 55, 58, 72) were analysed by SH using the toxin cassette sequence as a probe (Fig. 12B). The endogenous band (6.2 kb band) is detected in similar (weak) strength in every founder line. The signal strength of the transgenic band (3.9 kb) corresponds to the number of BAC copies integrated into the genome of the respective founder line. Line 55 shows no positive BAC signal whereas the others have a distinct band with increasing strength from line 72, 51, 58 to line 49. Taken together, these results show the successful generation of tGID$_S$-containing BAC-transgenic mice. The lines *TRPP2*-tGID$_S$/49 and /51 were used for further characterisation.

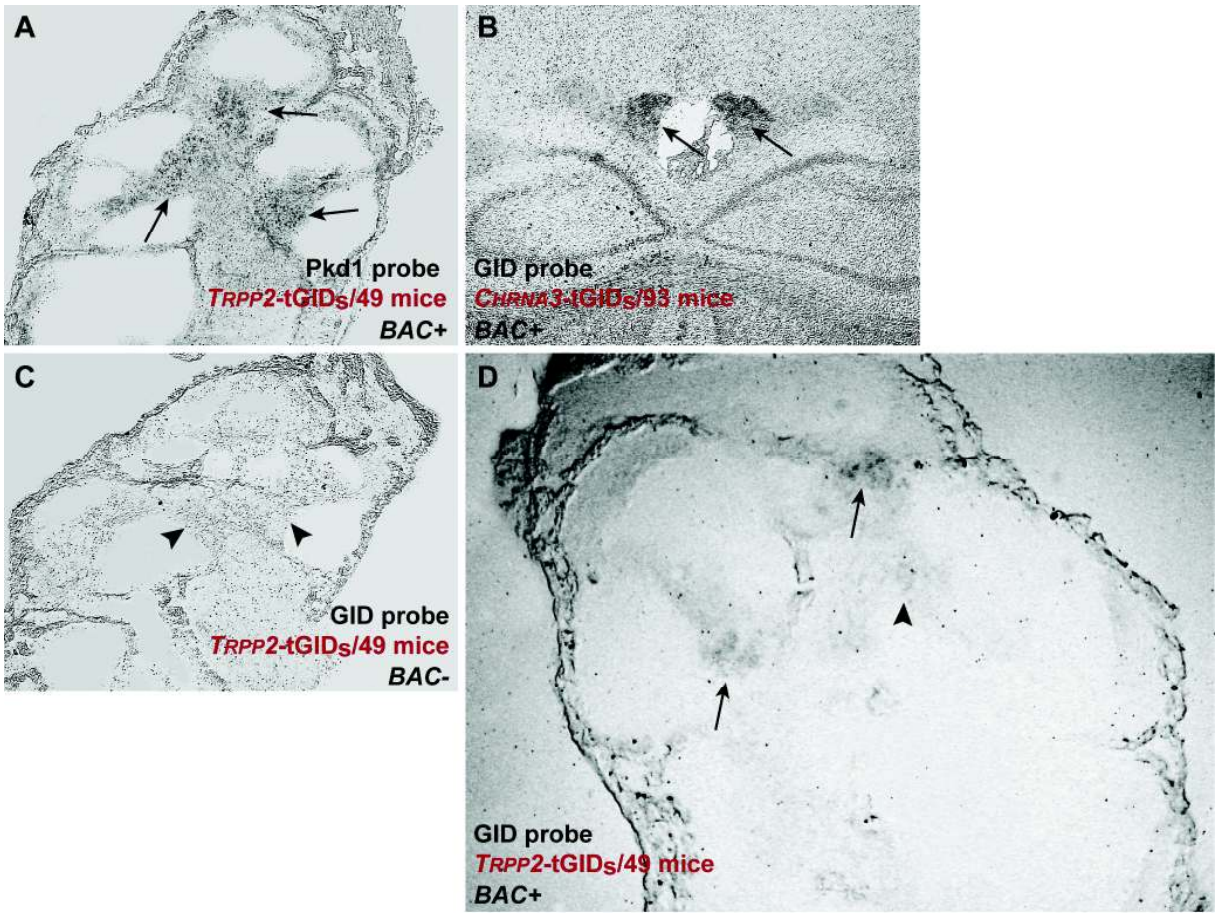

FIG. 13: tGID TRANSCRIPTS IN THE COCHLEA OF BAC-TRANSGENIC MICE

In situ hybridisation (ISH) on midmodiolar cochlea (A, C, D) or coronal brain (B) cryostat sections. Antisense probe, mouse strain and genotype designated in the upper right corner. Cochleae were isolated from P6 mice. Contrast increased in C and D compared to A and B. Habenulae of a different GID-expressing BAC-transgenic mouse strain exhibit a very strong signal (B, arrows) and serve as a positive control for the specificity of the probe. A positive control for the correct processing of mouse cochlear tissue shows a clear signal (A, arrows) whereas the toxin probe only labels SGNs very faintly (D, arrows). Littermates negative for the toxin-containing BAC were processed in parallel and show no labelling (C, arrowheads). Middle turn SGNs of GID-mice are not labelled (D, arrowhead) which is probably a technical artefact as middle turns of other sections are labelled (not shown). No signal detected in ISH with sense probes (not shown). *Chrna3* nicotinic acetylcholine receptor α3

4.1.3 *tGID$_S$* IS EXPRESSED IN SPIRAL GANGLION NEURONS

An ISH was performed to validate if the toxin is expressed by SGNs. In lines with weak signals in Southern hybridisation no transcript could be detected (not shown). Only line 49 shows a clear

signal when compared with a section of a BAC-negative littermate (Fig. 13). Relative to the signals of the positive controls the expression of the toxin is rather weak.

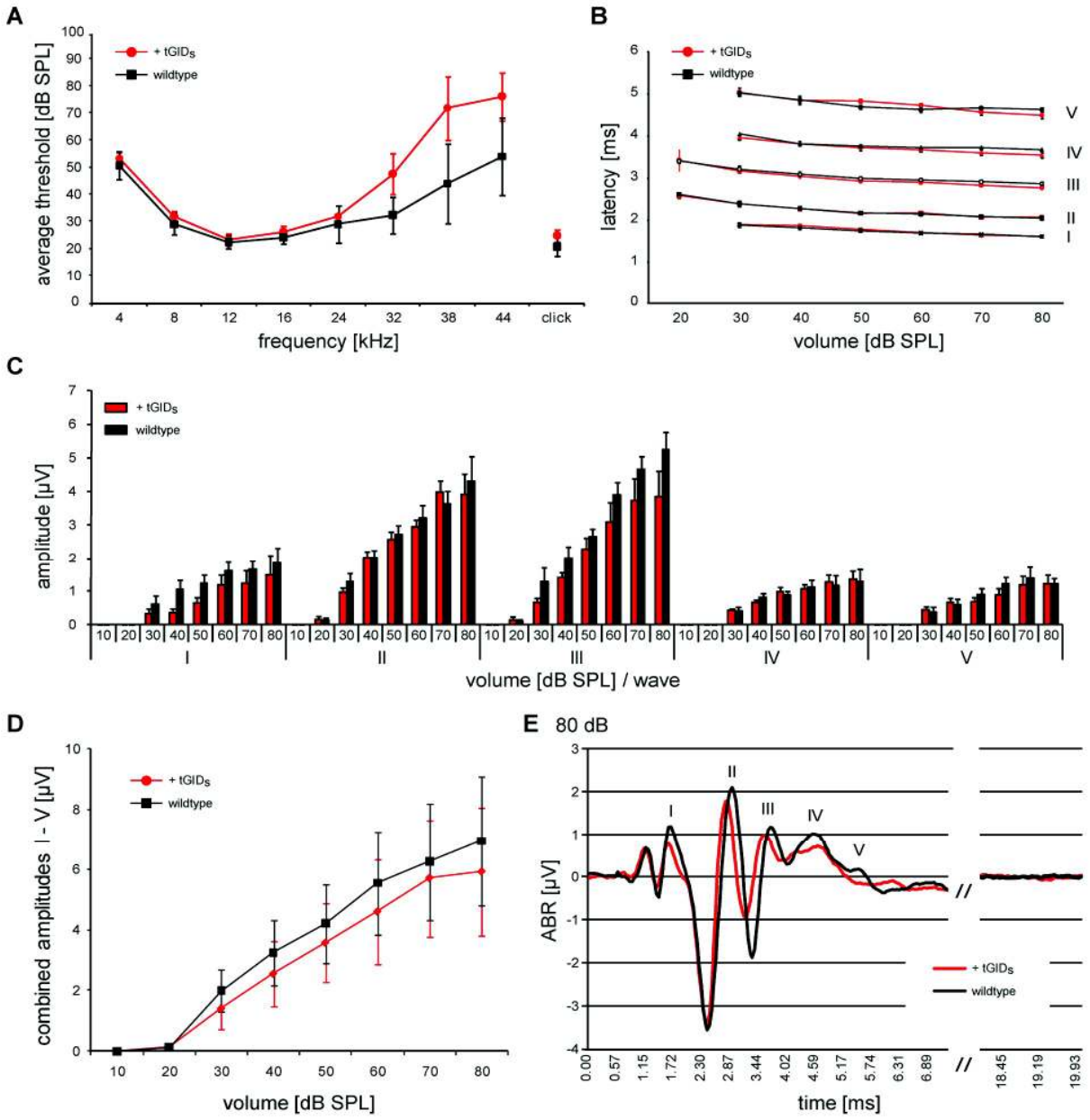

FIG. 14: AUDITORY BRAINSTEM RESPONSE OF *TRPP2*-tGID$_S$/49 MICE

Thresholds for pure frequencies and click sounds (A), peak wave latencies (B), single wave (C) and combined wave (D) ABR amplitudes do not differ between GID-expressing mice (n=7) and their littermates without toxin (n=6). ABR example traces after presenting clicks at 80 dB are depicted in (E). Click sound presentation at 20 kHz. Age of tested mice: 8 –10 weeks. *ABR* auditory brainstem response, *SPL* sound pressure level

4.1.4 AUDITORY TESTS

The founder lines *TRPP2*-tGID$_S$/49 and /51 were tested for proper auditory function. In both lines no difference between toxin-expressing mice and their transgene-free littermates is found. ABRs for the line with the highest Southern and *in situ* hybridisation signals are shown (line 49, Fig. 14), whereas ABR data for line 51 and DPOAEs for both lines are not.

4.2 The transient receptor potential channel Trpp2 is expressed in the inner ear

4.2.1 EXAMINATION OF *PKD1*-GFP AND *TRPP2*-GFP MOUSE ORGANS

Trpp2-driven GFP expression is detected in the adult kidney (Fig. 15, Fig. 16E, G). Interestingly, on whole organs GFP fluorescence is only seen in *TRPP2*-GFP and not *PKD1*-GFP kidneys. Although only little overlap of expression of TRPP2 and PC-1 in cortical tubules has been reported, PC-1 is expressed in far more tubules than TRPP2 so that *PKD1*-GFP kidneys were expected to fluoresce brighter than the ones of *TRPP2*-GFP mice. However, upon exposition of the medulla strong GFP expression is also seen in *PKD1*-GFP kidneys (not shown). In the medulla the two proteins follow a reciprocal pattern of expression with PC-1 being strongly expressed in the collecting ducts (CDs) and weakly in the thick ascending loops (TAL) of Henle – and TRPP2 having its highest expression in the TAL of Henle and much weaker staining for medullar CDs[305,139]. High expression of TRPP2 is also found in the distal convoluted tubules (DCT). In Fig. 15 an aGFP staining of adult kidney cross sections of *TRPP2*-GFP mice is compared with that of wildtype rats[306]. Expression strongly correlates in the tubular profiles in the cortex and in the outer medulla. Also in the rat, the authors identify the TAL, DCT and connecting tubule as TRPP2-positive structures. The connecting duct is again only faintly stained. The first (ureteric-bud-derived) TRPP2-positive structures in the kidney are seen at E14.5[139] which is also in line with the observations in *TRPP2*-GFP mice (Fig. 16Bii).

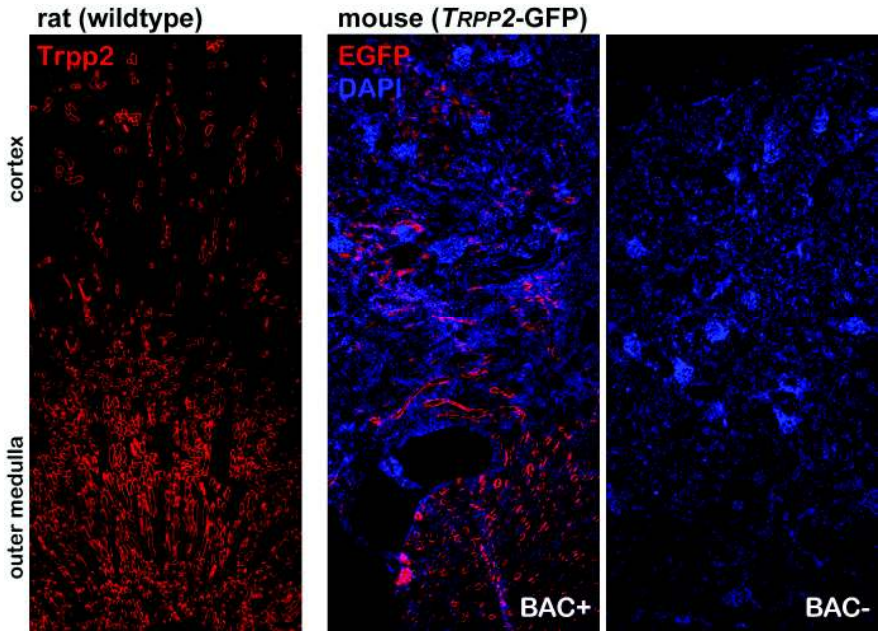

FIG. 15: DISTRIBUTION OF Trpp2-POSITIVE CELLS IN THE ADULT KIDNEY
Picture of rat is taken from Obermüller et al. (1999). Cross sections of rat (32x magnified) and mouse (40x) adult kidneys. Antibody staining of Trpp2 (rat) and EGFP (mouse) proteins, respectively. DAPI is a marker for nuclei. No staining of GFP is seen in BAC-negative mice (right panel).

On the other side the expression pattern of *PKD1*-GFP mice cannot be conciliated with already published data. In the developing human and murine kidney expression levels increase for both proteins during gestation with PC-1 being expressed stronger than TRPP2. In contrast to TRPP2, which has its height of expression in the adult organ, PC-1 expression declines postnatally to a lower level[307-309]. At P6 no bright fluorescence in the kidney and elsewhere is detected (not shown). At P20 Pc-1 expression is strong in lung, spleen and heart; and relatively low in the kidney[309]. Again, no GFP is detected in these tissues of *PKD1*-GFP mice. However, beginning GFP fluorescence is seen in the brains of newborn *PKD1*-GFP mice. This expression is maintained into adulthood (Fig. 17A). Extraneuronal tissues of *PKD1*-GFP mice were not analysed further because the expression of GFP does not follow the expected pattern in the kidney and in embryos.

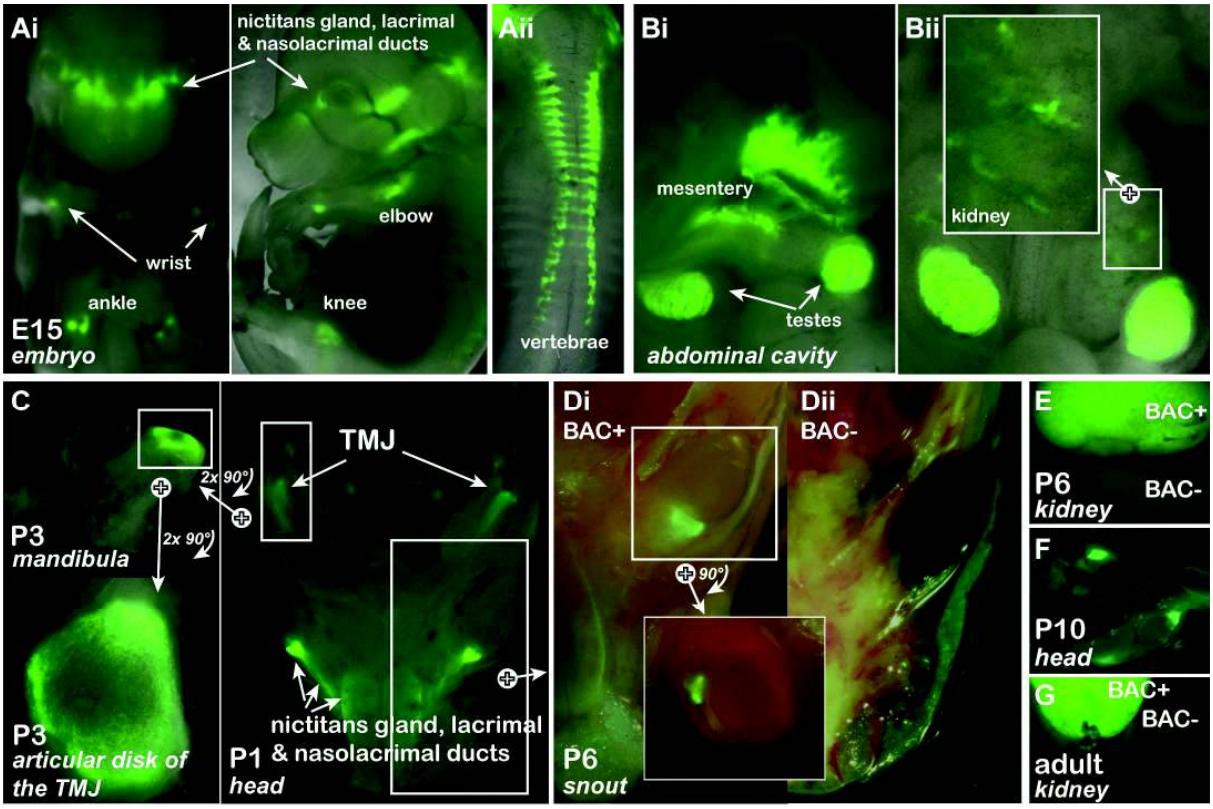

FIG. 16: GFP EXPRESSION IN *TRPP2*-GFP MICE

Direct GFP expression in embryonic (A, B), early (C) and late (D-F) postnatal as well as adult (G) BAC-transgenic (A-C, Di, F) and control (Dii) mouse tissues. P6 and adult kidneys (E, G) are from GFP-positive BAC-transgenic mice (BAC+) and GFP-negative littermates (BAC-). Expression of GFP increases during kidney development (Bii, E, G); in joints (Ai), spine (Aii), testes (B) and mesentery (Bi) GFP is seen only before birth. A constantly high GFP expression is seen in the nictitans glands, their ducts (nasolacrimal and lacrimal) as well as at the TMJ (A, C, D, F). GFP channel superimposed on greyscale (A-C, E-G) or RGB (D) brightfield images.

Among the various GFP-positive tissues in *TRPP2*-GFP mice are several bone-associated structures like spine/vertebrae, ribs and several joints (wrist, knee, temporomandibular joint). Mechanosensing osteoblasts and osteocytes possess ciliary structures as well as PC-1 and TRPP2[310-312]. Additionally, PC-1 is important for the mineralisation during bone development. In adult mice the loss of one functional *Pkd1* allele leads to a reduction in bone mineral density.

Primary cilia, but not polycystins, have been implicated in skeletogenesis. However, there is still no direct evidence that Trpp2 is part of a cilia/polycystin complex similar to the one in renal cells. Hence, the role of polycystins as bone mechanosensors is not yet established. This study indirectly confirms the presence of enhancer and promoter elements necessary for the transcription of *Trpp2* mRNA in bone structures. Interestingly, not all bones are GFP-positive. It remains to be clarified if also the other bones show GFP-ir at earlier stages in embryogenesis. Most of the GFP-positive bone structures lose their fluorescence in development: vertebrae, ribs, wrists, et al. until birth (Fig. 16A) and ossicles around P12 (Fig. 16B). The only notable exception is the temporomandibular joint (TMJ) which is strongly GFP-positive from E15 (Fig. 16A) over P1, P3 (Fig. 16C) and P10 (Fig. 16F) into adulthood (not shown). Timing and way of joint formation distinguishes this complex structure only found in mammals from other synovial joints (see Purcell[313]) and could point to a yet unknown function of Trpp2 there. TRPV1, expressed in synovial lining cells of the TMJ, is implicated in nociception and inflammation[314]. A similar role for TRPP2 is conceivable but TRPV1 has – in contrast to TRPV4 – not been shown to interact with TRPP2 so far.

The expression of Trpp2 in developing testes (Fig. 16B) has been described for Leydig cells in human foetuses by Ong et al.[315]. Functionally, a targeted mutation in *Trpp2* misleads germ cell differentiation in mice[316]. Also, a close homologue of Trpp2, Trpp5, is expressed in mouse testes where it is implicated in mid- to late-stage spermatogenesis[317]. The nematode PKD homologues lov-1 and pkd2 are located in male-specific sensory cilia and are needed for mating, in a role that is likely to be mechanosensory[318]. In *Drosophila* the targeted disruption of *pkd2* (found at the head and tail of the sperm) results in male infertility without an effect on spermatogenesis[319]. A TRPP2 homologue in sea urchins (suPC2) and another homologue in the fly ('almost there', amo)[320] also have been implicated in sperm function and fertilisation (see Kierszenbaum[321]). The transient expression of GFP in testes of *Trpp2*-GFP mice is therefore worth of further investigation. In the adult rat ovary Trpp2 has been detected in granulosa cells of the corpora lutea where it does not show the typical basal to basal-lateral distribution as in epithelial cells of kidney and salivary duct but instead is finely dispersed all over the cytoplasm[306]. Similar to Leydig cells in the testis and granulosa cells in the adrenal cortex these cells produce steroid hormones. Endocrine cells thus constitute a second class of cells next to epithelial cells that express TRPP2. Likely the function of the ion channel is different in these two classes.

Similar to the situation in testes in the mesentery GFP is transiently expressed before birth (Fig. 16B). The mesentery was not studied in more detail so that expression cannot be confined to a more specialised structure like blood or lymph vessel, peritoneum or nerve. In any case the bright fluorescence is intriguing and a possible role of Trpp2 here could be worth studying.

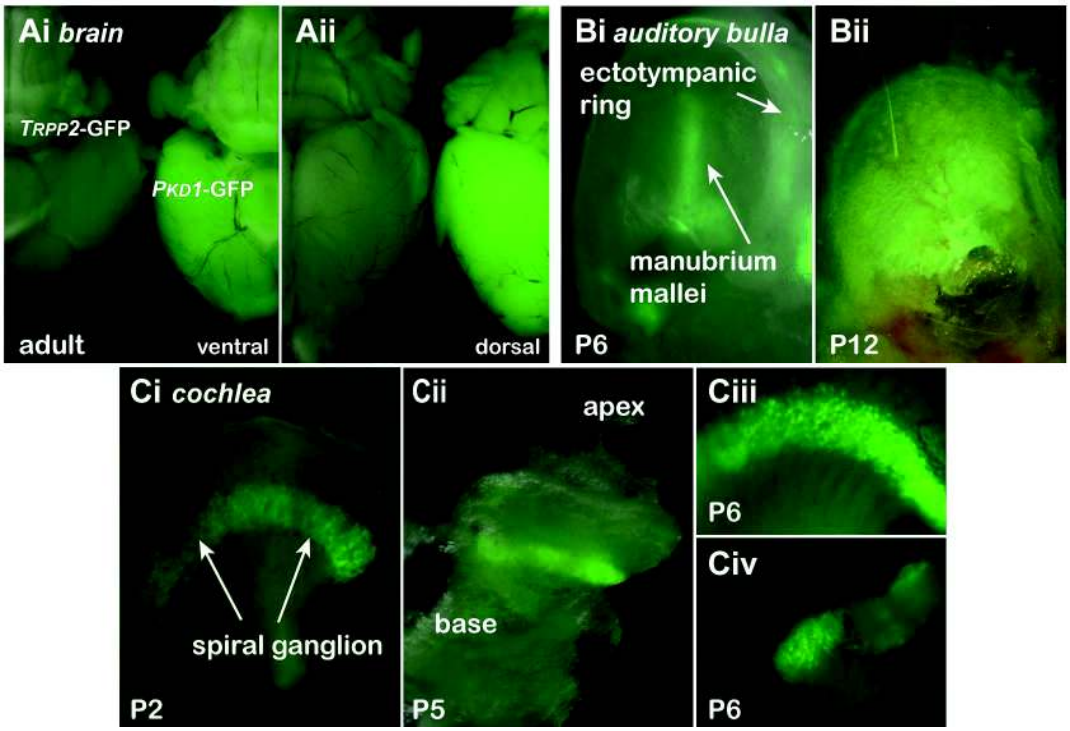

FIG. 17: GFP EXPRESSION IN BRAIN AND EAR OF BAC-REPORTER MICE

Direct GFP expression in whole mount preparations of adult brains (A), postnatal auditory bullae (B) and cochleae (C) of BAC-transgenic mice. In the brain GFP expression is visible in *PKD1*-GFP mice but not in *TRPP2*-GFP mice (A). Expression in some middle ear structures of *TRPP2*-GFP mice fades from P6 to P12 (B). Inside the cochlea no bony structures are green; instead, the spiral ganglion is heavily GFP-positive (C). GFP channel superimposed on greyscale (A, Bi, Cii) or RGB (Bii) brightfield images – or shown solo (Ci, Ciii, Civ).

Next to the temporomandibular joint and the kidney only the nictitans gland and its ducts show a strong expression of GFP/Trpp2 well into adulthood (Fig. 16A, C, D). This gland has a common ancestry with the (GFP-negative) Harderian gland situated on the medial and basal sides of the orbit (concealed by the nictitans gland). Salivary (or other) glands of *TRPP2*-GFP mice are also GFP-negative. It is therefore tempting to speculate that endocrine cells of the nictitans gland produce steroids similar to granulosa cells in adrenal cortex and ovary. Although no steroid production has been described in this gland, their neighbouring sister gland, the Harderian gland, produces steroids in rats, hamsters, birds and turtles[322]. However, also then it is not obvious why the nictitans gland shows such a prominent GFP expression in the adult *TRPP2*-GFP mouse – and adrenal cortex and ovary do not.

4.2.2 EXPRESSION OF TRPP2 AND PC-1 IN THE COCHLEA

By plain observation no fluorescence in the brain of *TRPP2*-GFP mice can be detected (Fig. 17A). In respect to GENSAT data fluorescence of SGN axons in cochlear nuclei (CN) was expected. By whole brain examination, however, no fluorescence was seen in CN. In contrast, the brain of *PKD1*-GFP mice displays a strong GFP signal, which is in line with the ubiquitous GFP expression

shown in the GENSAT database*. Also during development no GFP is detectable in the brainstem of *TRPP2*-GFP mice (not shown). Isolated spiral ganglia are GFP-positive (Fig. 17C), though. The presence of transcripts of *Pkd1* and *Trpp2* is verified by RT-PCR and *in situ* hybridisation to exclude that GFP expression in the SGN is an artefact. RT-PCR on brainstem, kidney, and whole

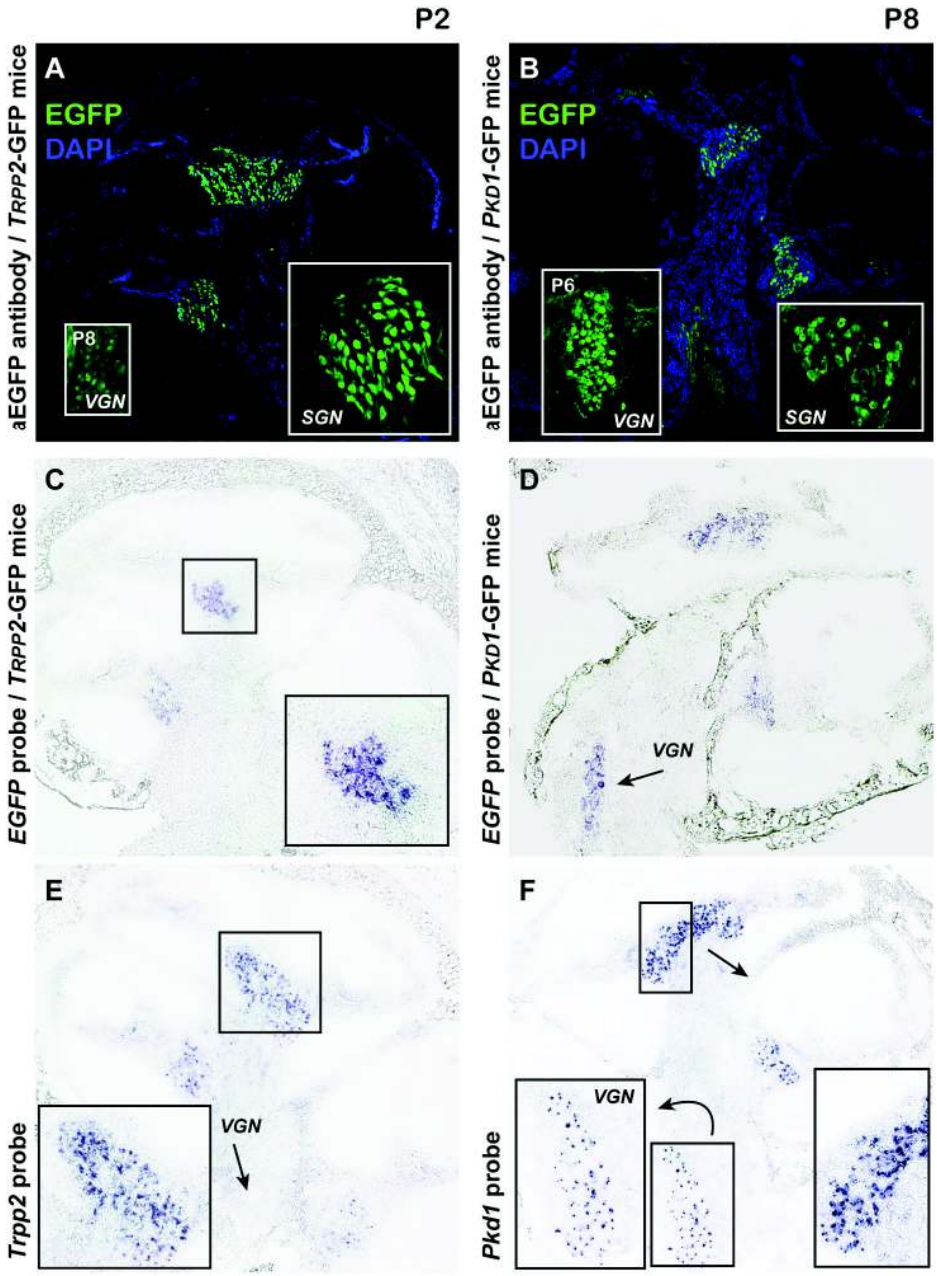

FIG. 18: CO-EXPRESSION OF GF PROTEIN, *PKD1* AND *TRPP2* TRANSCRIPTS IN THE MOUSE COCHLEA
Immunolabelling (A, B) and *in situ* hybridisation with antisense probes (C-F) on midmodiolar cochlea sections of *TRPP2*-GFP (A, C), *PKD1*-GFP (B, D) and control mice (E, F) is shown. Spiral ganglia of all turns show a similar signal pattern of GFP (A, B) and *GFP* (C, D) expression; probes directed against the transcripts of *Trpp2* (E) and *Pkd1* (F) confirm concordance of GFP and transcript presence. Differences in gene expression in VGNs are coherently detected by both methods: Trpp2 presumably is not present in VGNs (A inset, E arrow) whereas Pc-1 is (B, F insets, D arrow). No signals are found in modioli, organs of Corti and lateral walls. Also, no signal is detected in ISHs with sense probes and immunolabellings without aGFP antibody (not shown).

* http://www.gensat.org/imagenavigator.jsp?imageID=12312

cochlea tissue was done with *Trpp2*-specific primers (Pkd2(1.5)_pan_F/R). *Trpp2* transcripts are present in all three tissues. The PCR products of kidney and cochlea samples were cloned into pCR2.1 (TOPO-TA cloning) and sequenced. In all cases results match the mRNA sequences that were targeted by the primers thus confirming the presence of the transcript (not shown). *In situ* hybridisations show that *Trpp2* is expressed specifically in the spiral ganglion (Fig. 18): Endogenous *Trpp2* transcripts, BAC-coded *GFP* transcripts and proteins are unequivocally found only in the spiral ganglion (Fig. 18A, C, E). *Pkd1* signals are also detected in the SG and, additionally, in vestibular ganglion neurons (Fig. 18B, D, F). Detailed analyses were done primarily on *TRPP2*-GFP mice because the ubiquitous expression of Pc-1 in the brain is well-known. First, the developmental expression pattern was analysed (Fig. 19). GFP expression fades to background levels from around P12 onwards with apical turns lagging behind basal turns. At P24 only few positive neurons are found in the apical turn (Fig. 19 arrows) while in the basal turn fluorescence is gone. Peak expression is observed around P6.

The majority of SGNs show GFP-ir until hearing onset. Hence, either all SGNs or only prospective type I SGNs express GFP/Trpp2. In the first postnatal week SGNs find their proper targets in the organ of Corti (synaptic pruning) and either make afferent synapses with IHC (type I SGNs) or with OHC (type II SGNs). It is therefore tempting to speculate that Trpp2 is involved in pruning processes of SGNs. In addition, the paucity of GFP-positive neurons at P24 suggests that type II SGNs could express Trpp2 in the adult mouse. Double immunolabelling experiments were performed to clarify the SGN subtype of GFP-positive neurons in early development and at P24.

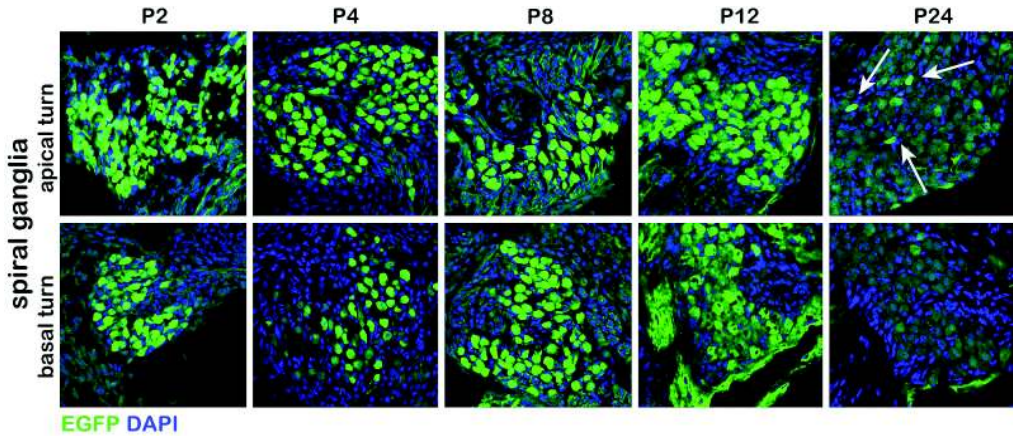

FIG. 19: DEVELOPMENTAL COURSE OF GFP EXPRESSION IN *TRPP2*-GFP MOUSE SPIRAL GANGLIA
Immunoreactivity after staining with rabbit aGFP primary antibody (ab) and corresponding Cy2-coupled secondary ab. Weak signal from intrinsic GFP fluorescence detectable when 1st ab is omitted (not shown). Expression is first reduced in the basal turn, later also in the apical one (compare P12 and P24). At P24 few cells retain strong GFP expression (arrows).

4.2.3 TRPP2 IS EXPRESSED IN A SUBSET OF SGNs

First, in this chapter several markers for SGN subtype specification are tested on adult spiral ganglia. Hereby known markers (TMRD, βIII tubulin and Peripherin, I) are employed and new

markers (B-FABP and PGP9.5, II) are introduced. Then the expression pattern of Peripherin during development is briefly shown (III). Finally, some of these markers are used to characterise GFP-positive cells in *TRPP2*-GFP mice (IV, V).

(I) KNOWN MARKERS FOR SGN SUBTYPE DISTINCTION

The dye tetramethylrhodamine-conjugated dextran (TMRD) and the antibody (ab) aTuJ1 were used as markers for type I SGNs[323]. The TMRD uptake mechanism is not fully understood. It is thought that the diameters of type I SGN axons (>1 µm) and efferent axons (0.8 µm) enable TMRD uptake. In contrast, type II SGN axons are probably too small (0.7 µm) to do so. aTuJ1 ab has been widely used as a reliable marker for type I SGNs. It labels βIII tubulin in cell somata and axons, but it does not stain glial tubulin[324-326]. TMRD labelling is not a reliable method to mark cells because several cells do not take up the dye (Fig. 20D, E, F asterisks). In contrast, staining with an aTuJ1 antibody marks all neurons (A, B, C). However, aTuJ1 does not stain the dendrites of neurons and therefore cannot be employed to study pruning processes in the organ of Corti. A second difference to TMRD is that aTuJ1 ab does not stain efferent fibres (compare IGSB in Fig. 20A and D). Hence, both type I markers are not ideally suited to fulfil all requirements. Surprisingly, a protein initially described as a marker for type II SGNs in rats[327] turned out to be good indicator for the majority of SGNs (Fig. 24A). NF-200 is the 200 kDa subunit of a neuron-specific intermediate filament protein. aNF-200 ab is preferred over aTuJ1 ab because it not only stains the majority of SGN somata but also most fibres of the auditory nerve, IGSB fibres and – most importantly for pruning studies – fibres reaching the organ of Corti (SGN dendrites). The discrepancy between the studies on rat and mouse is most likely due to varying specificities of the antibodies used. Different NF-200 phosphorylation states can also influence the specificity of the antibody[328]. Finally, Peripherin is a 57 kDa type III intermediate filament protein that is the most widely applied marker for type II SGNs[323,326,327,329]. It is implicated in the process of axonal extension and in the regeneration of nerve fibres[326]. Expectedly, it reliably stains type II SGNs in the adult mouse cochlea (Fig. 20C, F). Type II SGNs are unmyelinated cells that express Peripherin beyond the establishment of axonal projections. It is thought that Peripherin could give SGN fibres some stabilisation[330]. This structural support role is also discussed for Peripherin in small-sized DRG neurons that are also unmyelinated[331].

(II) ANTIBODIES AGAINST PGP9.5 AND B-FABP CAN BE USED TO IDENTIFY A SUBSET OF SGNS

The other employed antibodies have not yet been described as specific type II SGN markers. Protein gene product 9.5 (PGP9.5) is a member of a gene family whose products hydrolyse small C-terminal adducts of ubiquitin to generate the ubiquitin monomer. Expression of PGP9.5 is highly specific to neurons and to cells of the diffuse neuroendocrine system and their tumours. It

is present in all neurons. Fig. 20 shows that indeed all neurons are stained by aPGP9.5 ab (Fig. 20A), but to a different extent: A subpopulation of neurons displays immunoreactivities (ir) several times higher than the ir of the majority of neurons (A). The difference is so stalwart that gain adjustment can easily hide PGP9.5-ir of type I SGNs (D). The other novel marker introduced in this study is the ab against brain-specific fatty acid binding proteins (aB-FABP ab). B-FABP is required for the establishment of the radial glial fibre system in the developing brain, a system that is necessary for the migration of immature neurons to establish cortical layers[332]. Its presence in several cochlea cell types, including a subset of satellite cells within Rosenthal's channel, has recently been reported[333] but the authors fail to acknowledge the importance of the protein as a marker for SGN subtype specification. Fig. 20B reveals that B-FABP-positive satellite cells enclose only SGNs which show no TuJ1-ir. Number (2 to 5 per sectioned ganglion) and location (mainly near the IGSB) of cells strongly suggest that high-level PGP9.5-ir and B-FABP-positive satellite cells can be used as type II SGN markers.

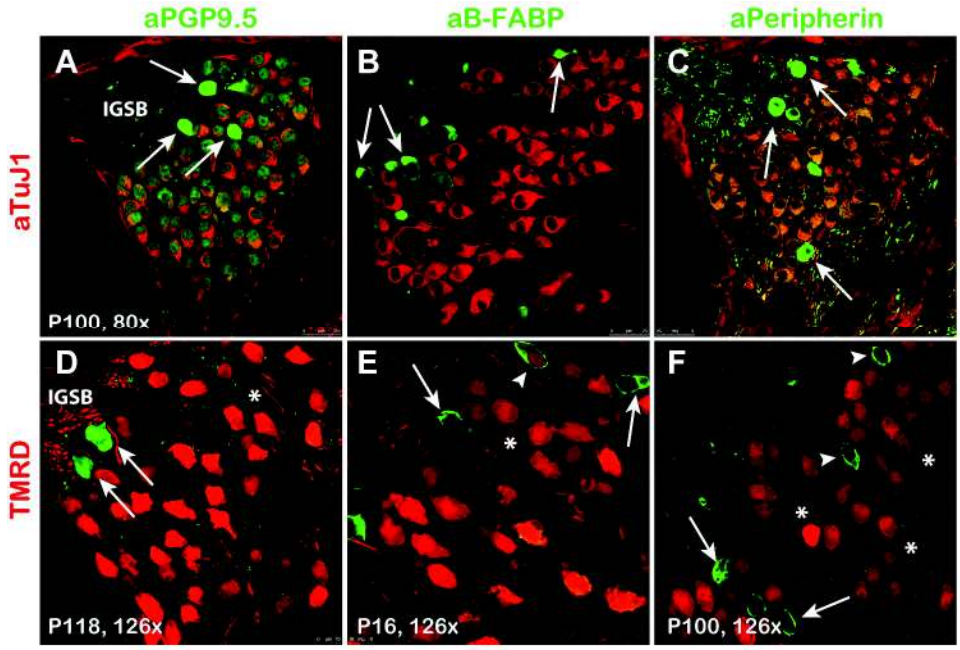

FIG. 20: MARKERS FOR TYPE I AND II NEURONS IN SPIRAL GANGLIA

Double immunolabelling of midbasal or basal turn SGNs. aB-FABP labels glial satellite cells whereas the other abs are neuronal markers. Red channel: anti Tubulin ab (TuJ1, upper row) stains a subpopulation of adult SGNs. Application of TMRD dye to the truncated 8th nerve fills presumably the same subpopulation (lower row). Green channel: aPGP9.5 is a pan-neuronal marker, however, with a strong preference for a subset of SGNs (A, D arrows). aB-FABP stains only satellite cells that wrap a small (TuJ1- and TMRD-negative) subset of SGNs (B, E arrows). aPeripherin labels presumably the same PGP9.5(strong)- and B-FABP-positive SGN fraction (C, F arrows). Non-uniform TMRD uptake leaves single neurons completely unstained (asterisks). Few co-labelled cells point to (SGN-)subtype-unspecific TMRD uptake (E, F, arrowheads). aPGP9.5 ab and TMRD label the nuclear region, aB-FABP, aPeripherin and aTuJ1 ab do not. Age of mice and magnification are indicated in the lower left corner of the pictures.

(III) PERIPHERIN EXPRESSION IN POSTNATAL SPIRAL GANGLIA

Not much is known about the usefulness of SGN subtype markers in the developing mouse cochlea. In the prenatal cochlea peripherin is expressed in all spiral ganglion neurons as it is

involved in the process of axonal extension. In this study its maximal expression is in the first postnatal week around P6 (Fig. 21Aii), then expression gets restricted so that at P10 the typical adult-like staining pattern becomes evident (Fig. 21Aiv, compare with Fig. 20C, F). Overlay with TMRD-labelling shows two distinct SGN populations in both, the ganglion with the cell somata (Fig. 21Bi), and the modiolus with SGN axons (Fig. 21Bii) at P10. However, in the rat Peripherin expression declines already shortly after birth[326]. This implicates that in the mouse cochlea this decline is delayed for 5 to 6 days. Other studies in mice contradict our observation as they report that Peripherin is a reliable marker of mouse SGN type II already from E18 (Huang), or P1 (Barclay) respectively, onwards[323,334]. This margin is too articulate (<6-10 days) that the use of different mouse strains could be held responsible. Possibly the specificities of employed antibodies vary so that epitopes of related intermediate filament proteins are recognised. Although Peripherin remains a valuable marker for a subset of SGNs (recently summarised by Liu et al.[335]) our employed antibody could only be reliably used on specimen of ≥P10 mice.

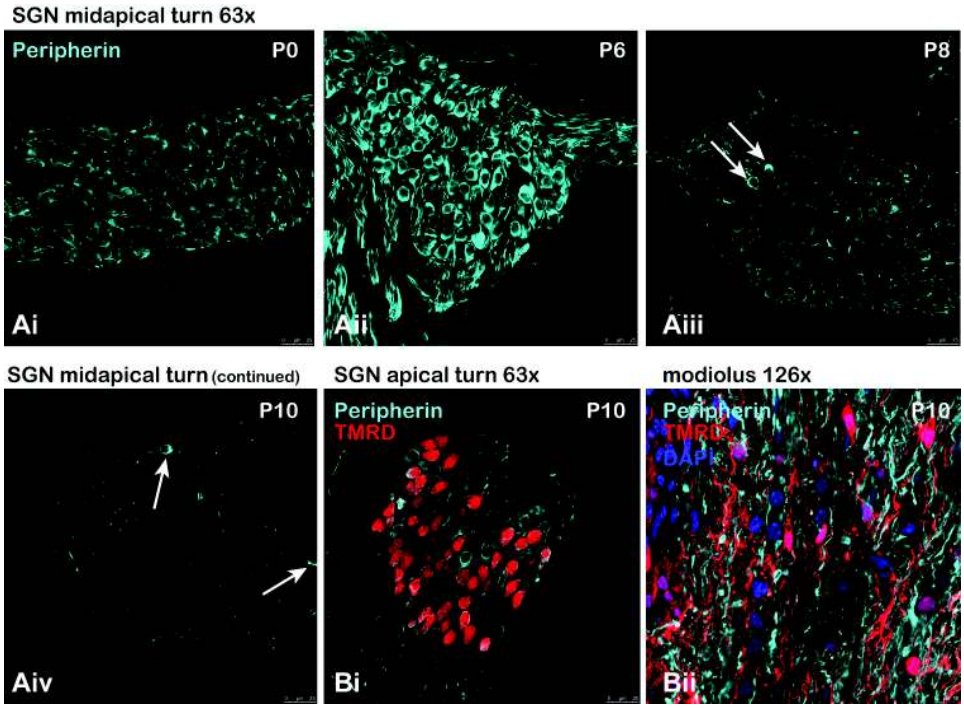

FIG. 21: EXPRESSION OF THE TYPE II SGN MARKER PERIPHERIN IN DEVELOPMENT
Immunolabelling on TMRD-infused P0 (Ai) to P10 (Aiv, B) *TRPP2*-GFP mouse cochleae. Ab staining reveals that around P6 (Aii) all neurons are Peripherin-positive and restriction to type II SGNs is not evident until P10 (Aiv, arrows). A clear distinction between type I and II SGNs is seen when also TMRD-labelling is shown (B): Only few co-stained cell somata (Bi) and axons (Bii) are present.

(IV) aGFP ANTIBODIES DO NOT STAIN TMRD-INFUSED NEURONS

After establishing several markers for SGN subtype distinction in mice they were employed in immunohistochemistry (ihc) experiments on *TRPP2*-GFP cochleae. First, TMRD-infused *TRPP2*-GFP mice were stained with aGFP abs (Fig. 22). Interestingly neurons that successfully have

taken up the dye lose their clear GFP-ir (compare with Fig. 19). This effect is dose-dependent as intermediate dye uptake leads to intermediate GFP fluorescence. This effect of mutual exclusion is also observed when TMRD-infused cochleae are stained with aTuJ1 ab. The TMRD dye and the aTuJ1 ab are both type I SGN markers and should show co-expression. However, TuJ1-ir is only seen in type I cells without dextran staining (not shown). Other antibodies (e.g. aPeripherin ab) stain TMRD-infused SGNs without difficulty (clear, undamped double labelling in P6 SGNs, not shown).

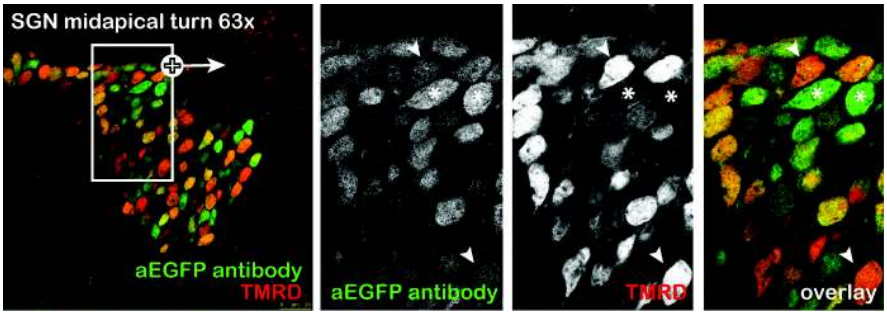

FIG. 22: TMRD IS NOT A SUITABLE MARKER FOR SGN SUBTYPE DIFFERENTIATION
Immunolabelling on TMRD-infused *TRPP2*-GFP P10 mouse cochleae. GFP-ir is severely restricted in TMRD-infused cells. Instead of widespread co-labelling the majority of neurons are either TMRD-positive and GFP-negative (red, arrowheads) or TMRD-negative (incomplete uptake) and GFP-positive (green, asterisks). SGNs with intermediate dye uptake display weak GFP-ir and appear yellow.

(V) GFP/Trpp2 EXPRESSION IN P10 AND P24 SPIRAL GANGLION NEURONS

Although immunolabelling with aGFP antibodies on TMRD-infused cochleae of *TRPP2*-GFP mice is not feasible, intrinsic GFP levels are sufficiently high for co-labelling experiments (also see Fig. 17). These stainings show that the majority of SGNs are TMRD- and GFP-positive – even though with varying strengths (Fig. 23B, arrowheads). Conversely, small, peripherally located Peripherin-positive cells are negative for TMRD and GFP (Fig. 23B, arrows). This result indicates that GFP/Trpp2 is expressed in type I SGNs. Interestingly, Peripherin-ir is also found in intermediate-sized, centrally located GFP-positive cells (Fig. 23C, arrows). These cells normally take up TMRD (white arrows) but due to the stochastic nature of the method occasionally fail to do so (yellow arrow). Additionally, they lack classical satellite cell company. Satellite cells are glial cells that do not display GFP-, TMRD- and Peripherin-ir but they are recognisable by their half-moon-shaped nuclei (Fig. 23C, arrowheads). Based on these stainings and the lack of satellite cells a new subclass of SGNs is hypothesised here: type III SGNs. However, as intrinsic GFP expression is only weakly above background levels further validation is needed.

Additional evidence for a new class of SGNs comes from stainings on older mice (after the onset of hearing). As mentioned before few SGN remain GFP-positive even after hearing onset (Fig. 19). Double immunostainings on P24 mice were performed to characterise these cells in more detail (Fig. 24). Double staining with an aNF-200 ab shows that at P24 GFP levels are low in most

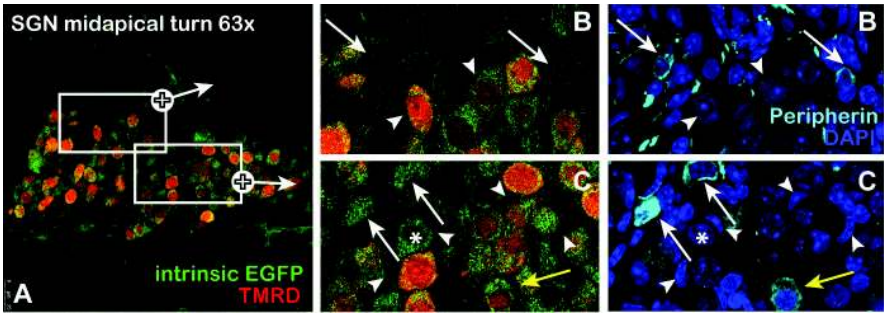

FIG. 23: A SUBSET OF GFP/Trpp2-POSITIVE SGNs ALSO DISPLAYS PERIPHERIN-ir
Immunolabelling on TMRD-infused *TRPP2*-GFP P10 mouse cochleae. Intrinsic GFP-fluorescence with Peripherin-ir on TMRD-infused SGNs is shown (A): The majority of cells contain GFP and has taken up TMRD but does not stain for Peripherin (B, SGN type I; arrowheads). At the peripheral rim of the ganglion small, TMRD- and GFP-negative but Peripherin-positive cells are located (B, SGN type II; arrows). Due to the incomplete uptake of TMRD few classical type I SGNs (GFP-positive but Peripherin-negative) are without red TMRD labelling (C, asterisks). Interestingly, some cells are GFP- and Peripherin-positive (C, arrows) – with (yellow) or without (white) dextran dye. This SGN cell type is not accompanied by satellite cells as classical type I SGNs are (Half-moon-shaped nuclei of satellite cells are indicated by arrowheads in C).

cells, so that the maintained green fluorescence of prospective type III cells becomes clearly visible (Fig. 24Aii, arrows). Also, the morphology of these cells does not resemble typical type II SGNs.

In addition to aPeripherin, also aPGP9.5 and aB-FABP antibodies were applied as type II SGN markers. Interestingly, at P24 few cells display a very strong PGP9.5-ir (Fig. 24B, white asterisk),

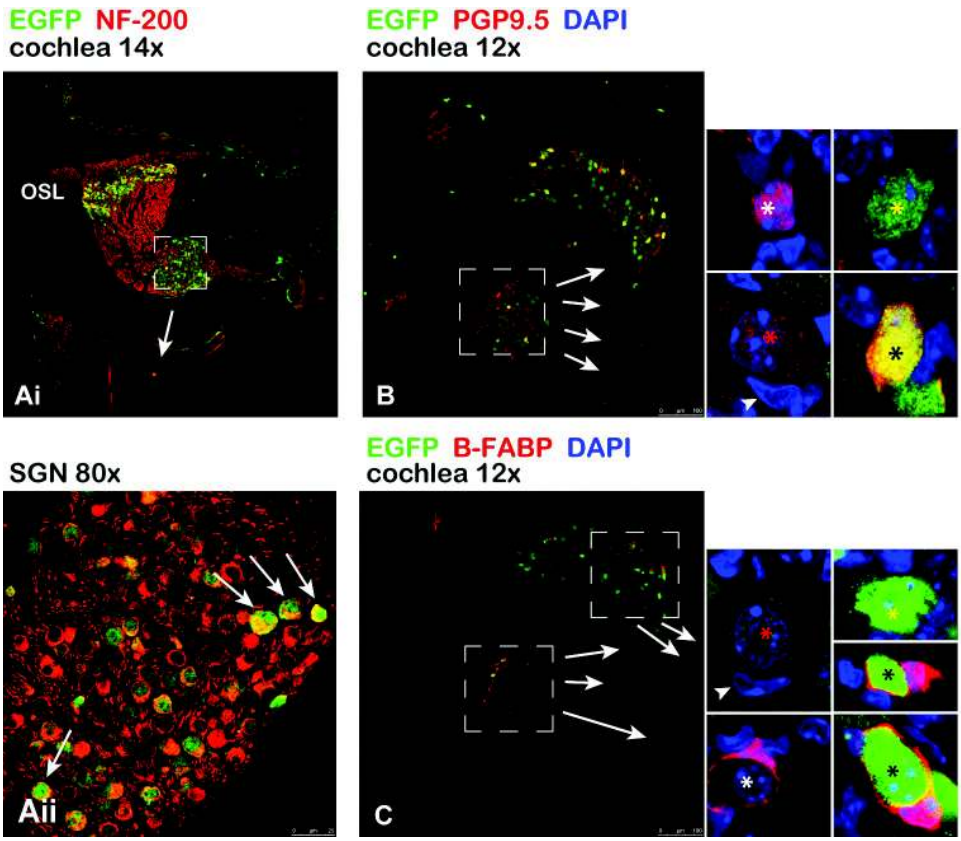

FIG. 24: GFP/Trpp2 EXPRESSION IN P24 SPIRAL GANGLION NEURONS
Immunolabelling on midmodiolar cochlea cryosections of P24 *TRPP2*-GFP mice. Green channel shows GFP-ir of an rabbit ab (A) or rat ab (B, C). Red channel shows NF-200-ir (A), PGP9.5-ir (B) and B-FABP-ir (C). Aii shows a magnification of the area in Ai indicated by a breached square outline. *OSL* outer spiral lamina

some cells have strong remaining GFP fluorescence (yellow asterisk) and others have both (black asterisk). For comparison an example of the majority of classical type I SGNs is shown as well (Fig. 24B, red asterisk): These neurons are Trpp2-negative, exhibit only basal PGP9.5-ir and are ensheathed by an accompanying satellite cell (arrowhead). Compared to NF-200 PGP9.5 is not the best pan-neuronal marker in adult SGNs as its expression is not uniformly distributed over the SG. It rather might stain a subpopulation of SG neurons, the prospective type III SGNs.

Staining of satellite cells with aB-FABP ab shows that the majority of cells at P24 are Trpp2-negative and are accompanied by B-FABP-negative satellite cells (Fig. 24C, red asterisk). These cells are typical type I SGNs. Cells that are not green but do have a B-FABP-stained coat (white asterisk) are considered as type II SGNs. However, few cells are ensheathed by B-FABP-positive satellite cells and still exhibit strong GFP-fluorescence (black asterisks). Again these cells are tentatively classified as type III neurons. Similar to the situation in the aPGP9.5 staining very few cells are GFP-positive but do not display any other immunoreactivity. They also lack satellite cell company (yellow asterisks in Fig. 24B, C). So far the nature of these neurons cannot be disclosed and further analysis is hampered because of their paucity.

Table 15: Suggested classification of SGN subtypes upon marker protein expression

P0	type I	type III	type II
GFP (Trpp2)	+	+	-
Peripherin	+	+	+
satellite cell: B-FABP	+	+	?
PGP9.5	+ (uniform)	+ (uniform)	+ (uniform)
NF-200	-	?	+
P10			
GFP (Trpp2)	+	+	-
Peripherin	-	+	+
satellite cell: B-FABP	-	+	?
PGP9.5	+ (uniform)	+ (uniform)	+ (uniform)
NF-200	+	+	n.d.
P24	**type I**	**type III**	**type II**
GFP (Trpp2)	-	+	-
Peripherin	-	+	+
satellite cell: B-FABP	-	+	+
PGP9.5	+ (weak)	+ (strong)	+ (strong)
NF-200	+	+	n.d.
TuJ1	+	-	-
half-moon-shaped satellite cell nucleus	+	+	-
size	big	big	small
location	whole ganglion	whole ganglion	near IGSB

change from P0 to P10 | change from P10 to P24 | type III SGNs display features of type I & II SGNs

In summary, the histological findings in this study suggest the presence of a new subclass of spiral ganglion neurons (Table 15). These neurons share features of type I neurons (cell morphology, satellite cell company) and type II neurons (cell number, Peripherin-ir, B-FABP-ir, PGP9.5-ir). Most importantly, they are characterised by GFP(Trpp2)-immunoreactivity which has not yet been described in the mammalian cochlea so far.

(VI) GFP/Trpp2 EXPRESSION IN POSTNATAL SPIRAL GANGLION NEURONS

As already shown before, the majority of SGNs are positive for GFP/Trpp2 one week before and one week after birth. For a detailed analysis of Trpp2 expression in development aPGP9.5 and aB-FABP antibodies as type II SGN markers, and an aNF-200 ab as a (presumably) pan-neuronal marker were used in double ihc (Fig. 25).

At **P0** NF-200-ir is only present in VGNs, but not (or only very weakly) in the majority of SGNs (Fig. 25Ai). However, in a small subset of SGNs (arrowheads) NF-200-ir is found. This is a clear indication that Trpp2 is not present in all SGNs (Fig. 25Aii). Conversely, NF-200-ir could mark type II SGNs as has already been described in rats[327]. NF-200-ir is the earliest manifestation of a subclass of SGNs observed in this study. However, NF-200 is not a general marker for type II SGN because most SGNs gain NF-200-ir over the next days. PGP9.5-ir and B-FABP-ir are not yet restricted to type II/III SGNs so that all Trpp2-positive neurons are co-labelled (Fig. 25B) and ensheathed (Fig. 25C). Some SGNs do not show Trpp2-ir which might be due to ineffective aGFP (rat) staining. Cell size, number, shape and their situation within the ganglion do not suggest that they are type II SGNs (arrowheads, Fig. 25B).

At **P6** aNF-200 staining is specific for all neurons in the cochlea including somata and neurites of SGNs and VGNs (Fig. 25Di). Now, NF-200-ir and Trpp2-ir overlap completely in SGNs, even though NF-200-ir in the cell somata is relatively weak when compared with dendrites or axons (Fig. 25Dii). GFP expression starts to fade in basalmost turns already at P6 which makes the ganglion look rather patchy in the aPGP9.5 staining (arrow, Fig. 25Ei), in the middle turn the majority of cells are – similar to the situation in P0 cochleae – still co-labelled for GFP and PGP9.5 (Fig. 25Eii); arrows indicate Trpp2-negative efferent fibres of the IGSB. B-FABP is a marker for glia cells which produce central myelin (mostly oligodendrocytes). Therefore the olivocochlear nerve is heavily B-FABP-positive until the neuronal fibres reach the glial limitans. There cells producing peripheral myelin take over fibre myelination (Fig. 25Fi). However, few peripheral glia (satellite) cells continue to express B-FABP. In the spiral ganglion B-FABP-ir is markedly reduced when compared to P0 but the number of B-FABP-positive satellite cells is still too high to clearly distinguish type I from type II SGNs (Fig. 25Fii). Most cells with classic type I features (big size, located inside the ganglion) are wrapped up by B-FABP-positive satellite cells (inset, Fig. 25Fii).

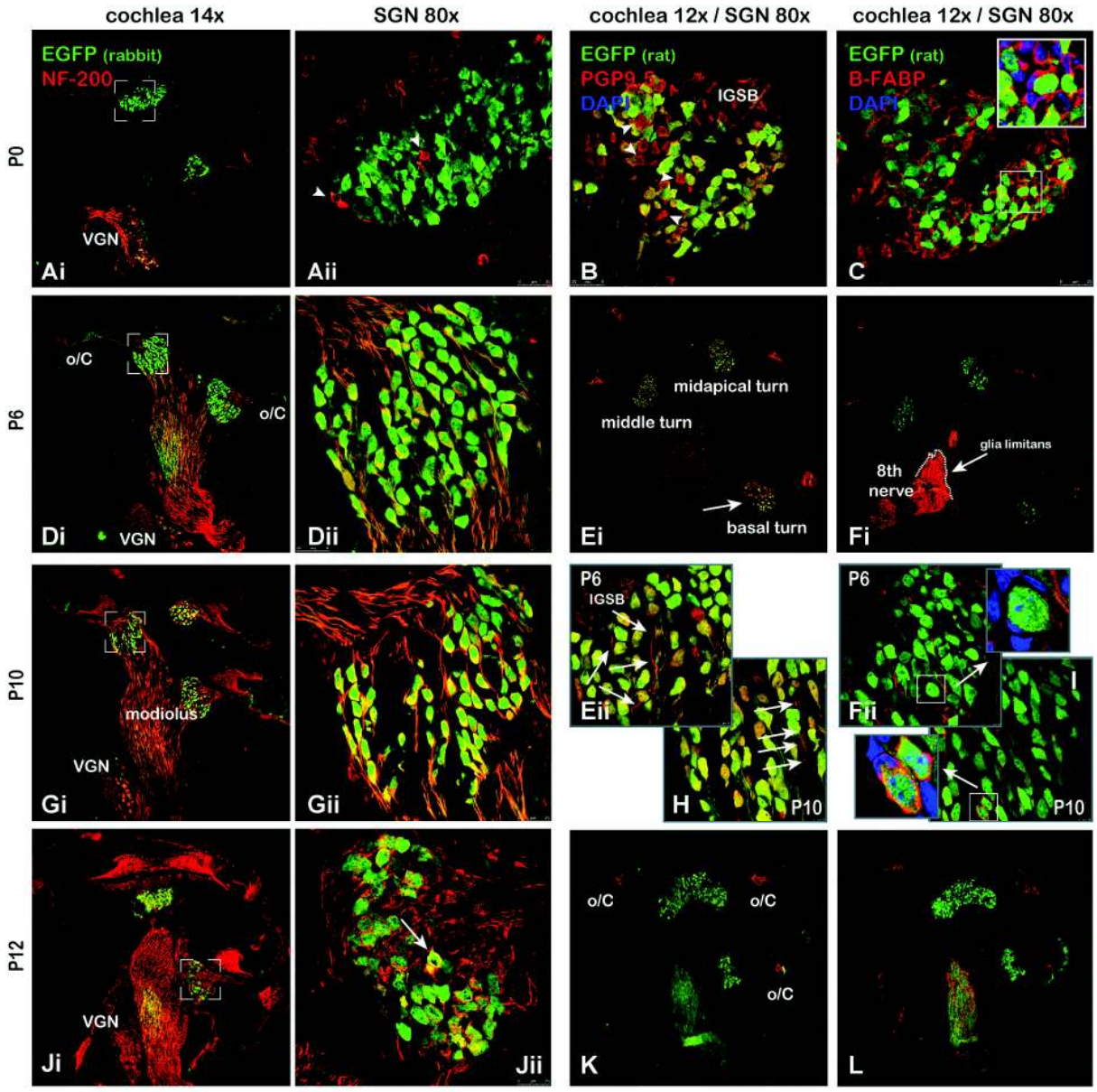

FIG. 25: TRANSIENT GFP/Trpp2 EXPRESSION IN THE MAJORITY OF SPIRAL GANGLION NEURONS
Immunolabelling on midmodiolar cochlea cryosections of P0 (1st), P6 (2nd), P10 (3rd), and P12 (4th row) *TRPP2*-GFP mice. Green channel shows GFP-ir of an rabbit ab (1st and 2nd column) or rat ab (3rd and 4th column). Red channel shows NF-200-ir (1st and 2nd), PGP9.5-ir (3rd) and B-FABP-ir (4th column). 2nd column shows magnifications of 1st column areas (indicated by breached square outlines). Other magnifications indicated by continuous rectangle outlines. For a detailed description see text.
IGSB intraganglionic spiral bundle, *o/C* organ of Corti, *VGN* vestibular ganglion neuron

At **P10** and **P12** NF-200 signals are additionally observed in the tectorial membrane, spiral limbus, stria vascularis and the spiral ligament. All signals seem to be transient as at P24 the signal is again delimited to neuronal structures (SGNs, MOC and LOC fibres, modiolus, osseous spiral lamina; Fig. 25Gi, Ji, Mi). In the P10 spiral ganglion a complete and clear overlap of Trpp2-ir and NF-200-ir is obvious (Fig. 25Gii). Also PGP9.5-ir is similar to ir at P6 (Fig. 25H; arrows indicate Trpp2-negative efferent fibres). B-FABP in satellite cells is the first marker that allows making a distinction between SGN subsets: In Fig. 25I two neurons are surrounded by B-FABP-positive cells (inset) while the majority of neurons are not. Size, shape and location suggest that

these neurons are not type I SGNs. At P12 Trpp2 levels decrease while NF-200-ir persists (Fig. 25J). Low magnification pictures show that now not only B-FABP expression got restricted in SGNs but also that of PGP9.5. The staining in the organ of Corti and in the inner modiolus (Fig. 25L) remains. Already at P12 single cells exhibit a GFP signal well above average (Fig. 25Jii, arrow). These cells might constitute a new class of SGNs as suggested in the previous chapter.

The vast majority of spiral ganglion neurons – but most likely not all – express Trpp2 during development. No expression is seen in auditory hair cells, other cells of the organ of Corti and axons of the efferent, olivocochlear system. Immunohistochemistry results propose that prospective type I and type III SGNs express Trpp2 at least well into the second postnatal week. If also prospective type II SGNs express Trpp2 in development could not be shown conclusively because of a lack of a meaningful type II marker that works before P10. Around hearing onset expression is reduced to background levels in most neurons. This suggests a function for Trpp2 in cochlea development. In particular, a function in synaptic pruning or synaptogenesis is hypothesised. Because of its early expression already before birth a role in neurite outgrowth and target innervation (hair cells) cannot be excluded. Investigation of morphogenesis and physiology in tissue-specific *Trpp2* knockouts might help to delimit the possible modes of action of this ion channel and therefore was pursued in this study (next chapter).

4.3 Tissue-specific knockouts of Trpp2 using the Cre-loxP-system

After elucidating the intriguing expression pattern in mouse spiral ganglion neurons the physiological relevance of Trpp2 in the afferent system is assessed using the Cre-loxP-system for conditional mutagenesis (see 1.4.2III): First, the yet undescribed *Trpp2*flox mouse strain is characterised (4.3.1). Then different, neuron-specific Cre-expressing mouse strains are crossed with *Trpp2*flox mice to produce dysfunctional *Trpp2* transcripts in SGNs of resulting offsprings. In this study mice expressing Cre recombinase under the control of promoter sequences of *Islet-1* (4.3.2) and *Nestin* (4.3.3) are used. The transient expression of Trpp2 in spiral ganglion neurons before the onset of hearing suggests that the channel could be involved in pruning processes. Therefore the connectivity beneath inner and outer hair cells of mice with conditionally inactivated *Trpp2* alleles is investigated immunohistologically. Additionally, mice are also tested for proper hearing.

4.3.1 CHARACTERISATION OF THE *Trpp2*flox MOUSE STRAIN

Targeted mutations in the murine genes *Pkd1* and *Trpp2* produce a cystic kidney phenotype[295,336]. By crossing the *Trpp2*flox strain with a mouse strain expressing Cre recombi-

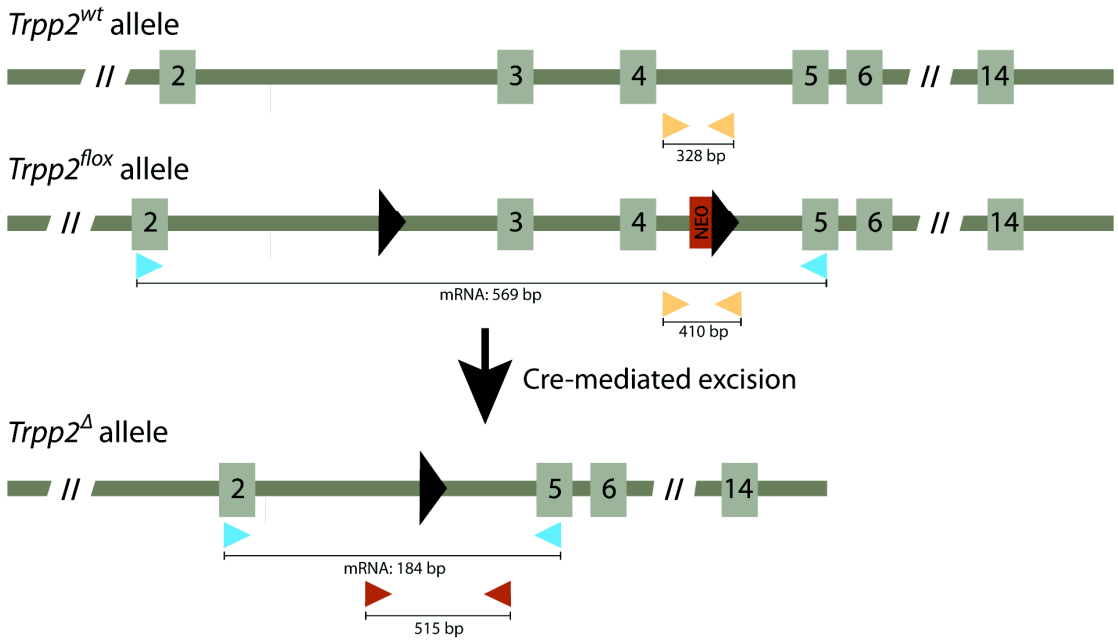

FIG. 26: SCHEMATIC REPRESENTATION OF DIFFERENT *Trpp2* ALLELES

Numerals in grey boxes indicate *Trpp2* exons. Black arrowheads represent loxP sites. Light orange arrowheads mark locations of PCR primers detecting wildtype and floxed alleles (Pkd2_D2loxP_F/R), dark orange arrowheads those of PCR primers detecting the delta allele (Pkd2Δallele-gDNA_F/R). Primers for RT-PCR experiments are depicted in blue (Pkd2Δallele-cDNA_F/R).
Cre Cre recombinase, *NEO* neomycin cassette

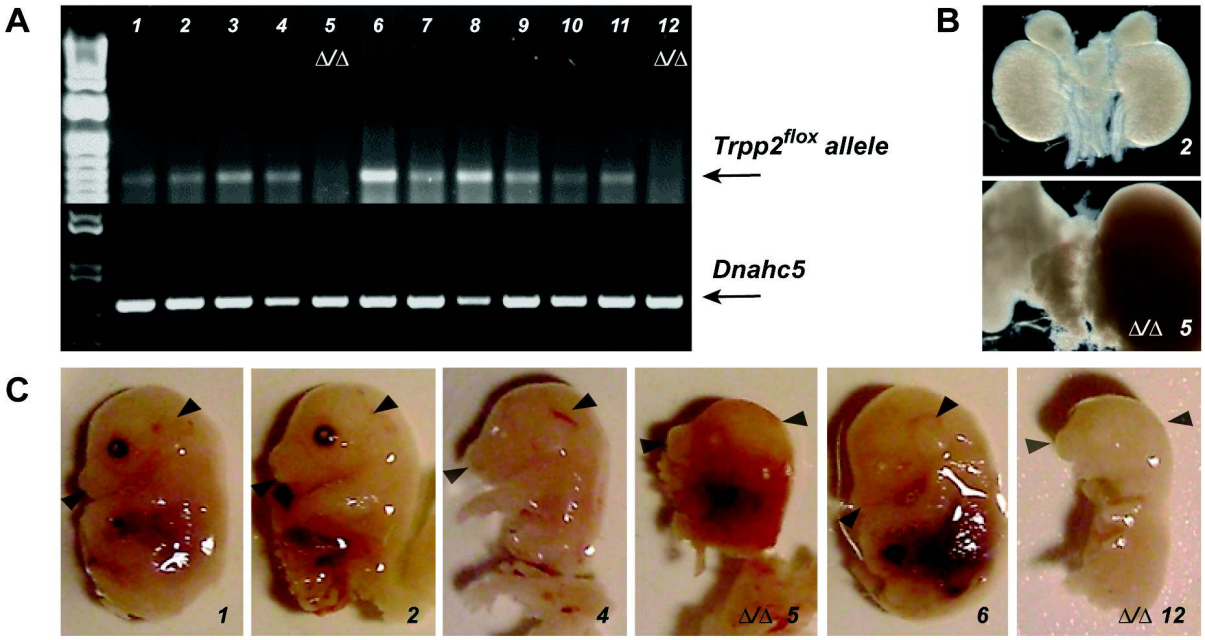

FIG. 27: THE *Trpp2*^{flox} ALLELE IS FUNCTIONAL

Breeding *Trpp2*$^{flox/\Delta}$ mice with each other yields roughly 25% *Trpp2*$^{\Delta/\Delta}$ pubs (A, #5 and #12) which exhibit enlarged kidneys (B) and reduced body size (C, arrows indicating head length of Δ/Δ mice) when compared with their *Trpp2*$^{flox/flox}$ or *Trpp2*$^{flox/\Delta}$ littermates (#1-4, 6-11). Sizes of PCR products are 410 bp (*Trpp2* flox allele) and 580 bp (positive control: axonemal dynein heavy chain 5 gene, *Dnahc5*).

nase ubiquitously (*CMV*-Cre, see 3.1.1) offspring with a phenotype similar to that of *Trpp2*$^{-/-}$ mice is expected: Crossing *Trpp2*$^{flox/\Delta}$ mice with each other reduces the number of viable pubs by roughly 25% which is already a good indication of effective recombination. At E15 two out of twelve embryos have two *Trpp2* delta alleles (Fig. 27A). *Trpp2*$^{\Delta/\Delta}$ embryos have enlarged kidneys (Fig. 27B) and smaller body sizes (Fig. 27C). As these observations are reminiscent of appearances of *Trpp2* null mutant mice it is reasoned that the loxP sites of the *Trpp2*flox allele are fully functional and the successful excision of exons 3 and 4 is sufficient to produce dysfunctional *Trpp2* transcripts (Fig. 26).

4.3.2 THE *Islet-1* PROMOTER AS A DRIVER FOR CRE EXPRESSION IN THE SG

To drive Cre-mediated DNA sequence deletion of two *Trpp2* exons specifically in spiral ganglion cells, *ISL1*-Cre mice were obtained from Tom Jessell. The LIM/homeodomain gene *islet-1* (*isl1*) is highly expressed during axogenesis in the developing nervous system[337]. In the developing avian auditory system Isl1 expression starts when postmitotic ganglion neurons begin to delaminate. The expression in the ventral otic placode is maintained at otic pit and otocyst stages (during invagination and cochlear elongation)[338]. Auditory and vestibular neurons originate from this Isl1-positive otocyst zone; and these neurons maintain Isl1 expression into adulthood[339]. Also in mouse spiral ganglia of various ages *Isl1* is detected by RT-PCR or ISH[340-342].

Offspring of *ISL1*-Cre::*Trpp2*flox breedings was analysed for abnormalities in synapse formation in the organ of Corti and changes in SGN subtype determination. In P16 mice a minor increase in Peripherin-positive SGNs (together with an increase of B-FABP-positive satellite cells) is seen in *ISL1*-Cre^{+} *Trpp2*$^{flox/flox}$ mice compared to their *ISL1*-Cre^{-} *Trpp2*$^{flox/flox}$ littermates (not shown). TuJ1-ir (type I SGNs) and Peripherin-ir (type II and III SGNs) fibres innervate their corresponding targets correctly in P16 mice of all investigated genotypes (not shown). Spiral ganglia and organs of Corti of P6 and P10 mice also do not show any differences in morphology and staining patterns between genotypes (not shown).

Kidneys sometimes are enlarged (not genotype-related) but never have cysts. *ISL1*-Cre-positive mice sometimes (3/10) have just one kidney (kidney agenesis). ABRs and DPOAEs of six F1 hybrids of an *ISL1*-Cre::*Trpp2*flox breeding show severely elevated hearing thresholds (increase of 20 – 60 dB SPL) in three mice (not shown). Hearing deficits are not genotype-related, though.

4.3.3 THE *Nestin* PROMOTER AS A DRIVER FOR CRE EXPRESSION IN THE SG

Like Peripherin, GFABP, neurofilaments and keratins Nestin is an intermediate filament protein. It is mostly expressed in nerve cells where it co-assembles with type IV intermediate filaments to form heteropolymers. Because of their reliability and strength *Nestin* promoter and enhancer elements are frequently used to prompt expression of transgenes. In this study the *NES*-Cre

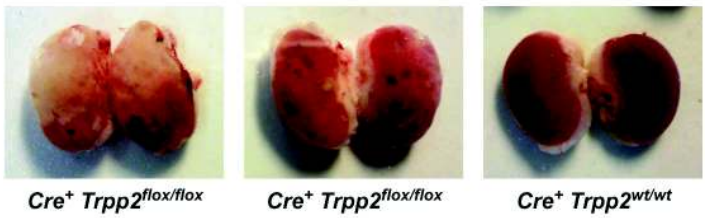

FIG. 28: *Nestin* PROMOTER ACTIVITY IN THE KIDNEY
Kidneys of 100-day-old male *NES*-Cre^{+} *Trpp2*$^{flox/flox}$ mice have cysts. Wildtype littermates have normal kidneys.

strain made by R. Klein is used (kindly provided by C. Birchmeier). First, the offspring of *NES*-Cre::*Trpp2*flox matings was screened for non-neuronal phenotypes. Cre recombinase has been shown to be active in kidney and heart. *NES*-Cre^{+} *Trpp2*$^{flox/flox}$ mice do not exhibit obvious heart defects but they have polycystic kidneys (Fig. 28). Cre recombinase does not exert a toxic effect on brain development as assessed by ventricle size comparison of *NES*-Cre^{+} and *NES*-Cre^{-} mice (not shown). Nevertheless – to avoid possible mild cytopathic effects due to high recombinase levels – the gene for Cre recombinase was kept hemizygous. Also *NES*-Cre^{+} *Trpp2*$^{flox/flox}$ mice do not develop hydrocephalus (not shown).

Analysis of isolated genomic DNA of different tissues showed that the truncated allele is present

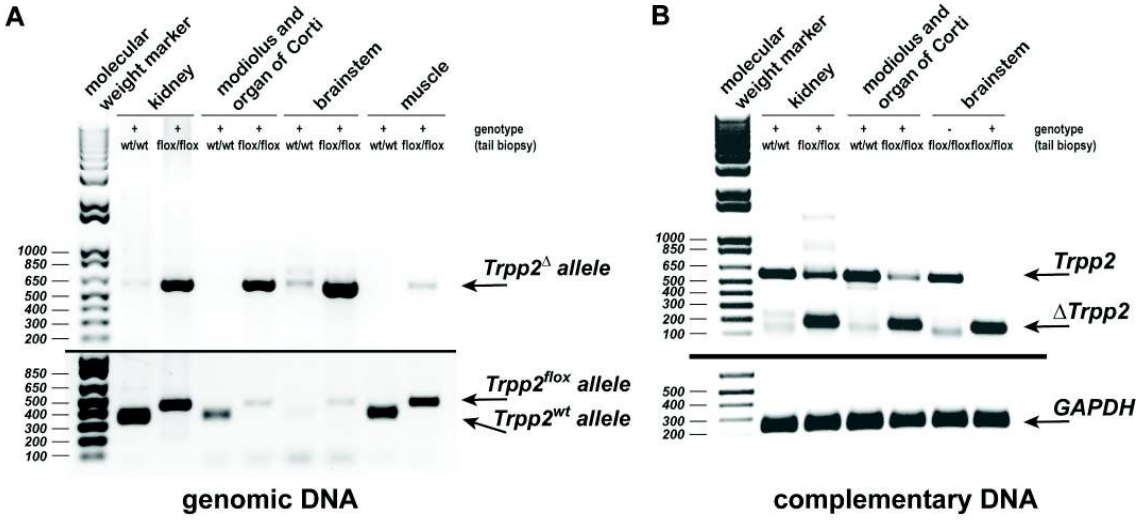

FIG. 29: SUCCESSFUL EXCISION OF *Trpp2* EXONS 3 AND 4 IN *Nes*-EXPRESSING CELLS
Genotyping of different mouse tissues with two different primer pairs (A, also see Fig. 26) reveals that delta alleles are only present in *Nes*-expressing cells (upper panel). All tissues are positive for *Cre* (+), littermates possess either flox alleles (flox/flox) or are wild type controls (wt/wt). Signal specificity is proven by testing presumably Cre-negative muscle tissue (faint signal in *Nes*-Cre^{+} *Trpp2*$^{flox/flox}$ mice could result from contamination by Cre-positive nerve tissue*). *Trpp2*$^{wt/wt}$ brainstem and kidney samples show double bands (unspecific PCR products). The presence of unaltered flox alleles also in *Cre*-positive *Trpp2*$^{flox/flox}$ mice suggests that *Nes* is not active in all cell types (lower panel). Cre recombinase seems to have been expressed ubiquitously in all brainstem cells as the delta allele signal is strong whereas the flox allele signal is very faint. RT-PCRs on extracted cDNAs of the same tissues (B, Fig. 26) show that the truncated transcript is present only in *Nes-Cre*$^{+}$ *Trpp2*$^{flox/flox}$, but not in *Cre*$^{+}$ *Trpp2*$^{wt/wt}$ or *Cre*$^{-}$ *Trpp2*$^{flox/flox}$ samples. Intact transcripts are detected in all tissues except *Nes-Cre*$^{+}$ *Trpp2*$^{flox/flox}$ brainstem. Genotyping of *Nes-Cre*$^{+}$ *Trpp2*$^{flox/flox}$ tail DNA suggests also low-level presence of *Trpp2*$^{\Delta}$ alleles there (not shown). Tail biopsies are taken from P1 mice, remaining tissues harvested at P6. (Situation of primer pairs and sizes of corresponding amplicons are indicated in Fig. 26.)

* http://cre.jax.org/Nes/Nes_Ad_muscle_Images.html

in kidney, cochlea and brainstem, but not in muscles of *NES*-Cre^{+} *Trpp2*$^{flox/flox}$ mice. As expected, in *NES-Cre*$^{+}$ *Trpp2*$^{wt/wt}$ mice no delta allele is present in any tissue (Fig. 29A). Accordingly, truncated *Trpp2* transcripts were detected by RT-PCR in kidney, cochlea and brainstem of the same mice (Fig. 29B). Intact transcripts additionally are present in most tissues because the *Nestin* promoter does not induce Cre expression in all cell types of the examined tissues during development. However, probably due to the common origin of neuron and glia cell types the exons are entirely excised in all brainstem cells so that here no full-length transcript was found.

Overall cochlear morphology as well as the histology of organs of Corti and spiral ganglia are indistinguishable between *NES-Cre*$^{+}$ *Trpp2*$^{flox/flox}$ mice and their *Cre*-negative littermates or *TRPP2*-GFP mice (not shown). Both, the pruning of type I dendrites (retraction from OHCs, abidance at IHC) and the specification of spiral ganglion neuron subtypes (type I, II, III) are unchanged in mice devoid of neuronal Trpp2.

In spite of no obvious morphological changes in the cochlea *NES-Cre*$^{+}$ *Trpp2*$^{flox/flox}$ mice show two noticeable aberrations in auditory function (Fig. 30B, C): First, the combined amplitudes of all waves are increased in flox/flox mice at all tested volumes. At 30, 40, 50 and 60 dB sound pressure level the differences are significant (Fig. 30B). The analysis of the amplitudes of single ABR components revealed a second, highly significant difference: The negative oscillation of wave III (N3) displays increased amplitudes in flox/flox mice. Robust increases are recorded not only when clicks are presented at 40 dB SPL (Fig. 30C) but also at 30, 50, and 80 dB SPL (not shown). The significant differences in the positive oscillations of wave I (P1) and wave II (P2) are only seen at 40 dB and partially at 50 dB. Hence, they are not yet considered robust. Hearing thresholds (Fig. 30A) and outer hair cell function as assessed by DPOAEs (not shown) are not different between genotypes. Interpeak latencies between wave extremes are not differing between flox/flox and wt/wt mice at all volumes tested (not shown). Wave I of the ABR graph represents the compound action potential of the vestibulocochlear nerve. Missing Trpp2 channels in SGNs does not likely account for the auditory phenotype observed in *NES-Cre*$^{+}$ *Trpp2*$^{flox/flox}$ mice because the amplitude of wave I is not changed significantly. However, these mice show robust differences of N3 amplitudes. ABR waves 2 to 4 correspond to different sound processing steps at the level of the brainstem. Hence, the brainstem of *TRPP2*-GFP mice was scrutinised in more detail to disclose a link between N3 amplitude increase and Trpp2 expression (Fig. 31). Interestingly, not only SGN axons but also several cell bodies in the cochlear nucleus exhibit GFP-fluorescence (Fig. 31A). These cells probably make synaptic contacts with cells in the medial nucleus of the trapezoid body (MNTB, Fig. 31B). Because of their eccentric nuclei, their innervation targets, and their situation within the cochlear nucleus the GFP(Trpp2)-positive cells might be globular bushy cells (GBC). Trpp2 expression in the brainstem is also transient as at P21 fluorescence is completely absent in both, the MNTB and the somata of CN

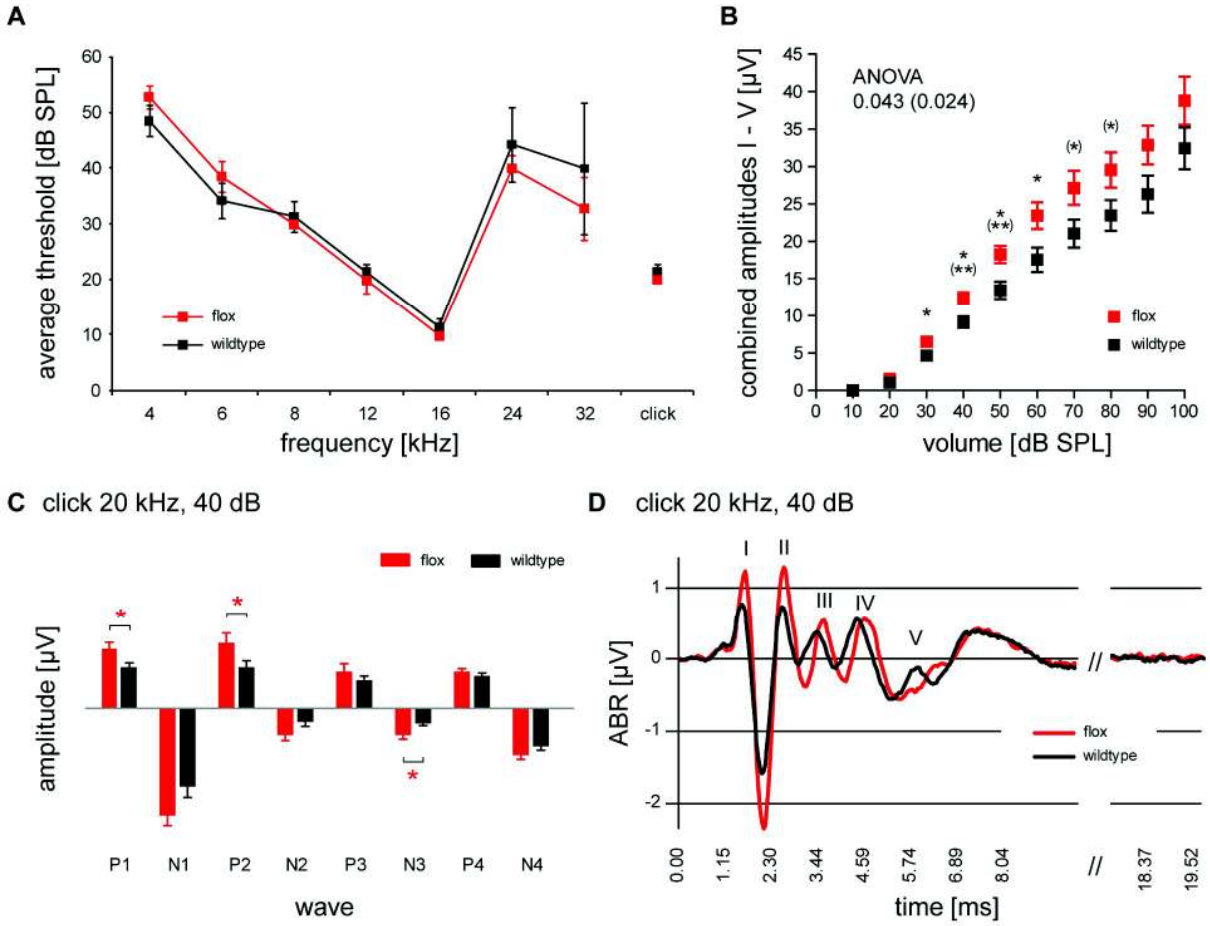

FIG. 30: AUDITORY BRAINSTEM RESPONSE OF *NES-CRE*+ *Trpp2*FLOX/FLOX MICE

Thresholds for pure frequencies and click sounds (A) do not differ between *NES-Cre*+ *Trpp2*flox/flox mice ('flox', n=7) and their *NES-Cre*+ *Trpp2*wt/wt littermates ('wildtype', n=7). Combined (B, all volumes tested) and single wave (C, 40 dB SPL) amplitudes are significantly increased in flox/flox mice. In C waves I to IV are separated into their positive and negative fractions, wave V is omitted. ABR example traces after presenting clicks at 40 dB are depicted in (D). Age of tested mice is ±3 weeks. Significance levels given in brackets refer to data analysed from 8 mice each, where both additional mice are not age-matched (8 weeks).
ABR auditory brainstem response, *SPL* sound pressure level

cells. Only in the posterior ventral cochlear nucleus (PVCN), which exhibits the strongest fluorescence signal at P6, a signal faintly above background was detected in SGN axons (not shown).

In summary, no obvious changes in cochlea development are seen in *NES*-Cre+ *Trpp2*flox/flox mice. Nevertheless these mice display significant increases in overall neuron activity in the lower auditory system. Whether this auditory phenotype is related to reduced *Trpp2* transcript levels in SGNs, complete deprivation of *Trpp2* transcripts in the brainstem, or both remains to be clarified. The robust increase in the amplitude of the negative oscillation of ABR wave III (N3) implies a more decisive role for Trpp2 in the connectivity of brainstem neurons.

FIG. 31: Trpp2 IS PRESUMABLY EXPRESSED IN A SUBSET OF COCHLEAR NUCLEUS CELLS

Sagittal floating sections (cochlear nuclei, A) and cryosections (pons, B) of brainstem tissue of P6 *TRPP2*-GFP mice. Single GFP-positive cells (arrows) are detected in the AVCN among the bulk of GFP-positive axons of SGNs (Ai – Aiii). The presence of such cells in the PVCN (Aiv) and DCN is doubtful. In the SOC GFP-positive fibres and presynapses (calyx-like, arrowheads), but no positive cell bodies are found (B). BAC-*TRPP2*-GFP-negative littermates do not exhibit fluorescence (not shown).
4V 4th ventricle, *A/PVCN* anterior/posterior ventral cochlear nucleus, *DCN* dorsal cochlear nucleus, *DN* dentate nucleus (cerebellum), *gl* granular layer of cochlear nuclei, *IPF* interpeduncular fossa, *mcp* middle cerebellar peduncle, *MNTB* medial nucleus of the trapezoid body, *MVeN* medial vestibular nucleus, *Pn* pontine nuclei, *PnC* caudal pontine reticular nucleus, *py* pyramidal tract, *tz* trapezoid body. orientation: left ≙ caudal, right ≙ cranial.

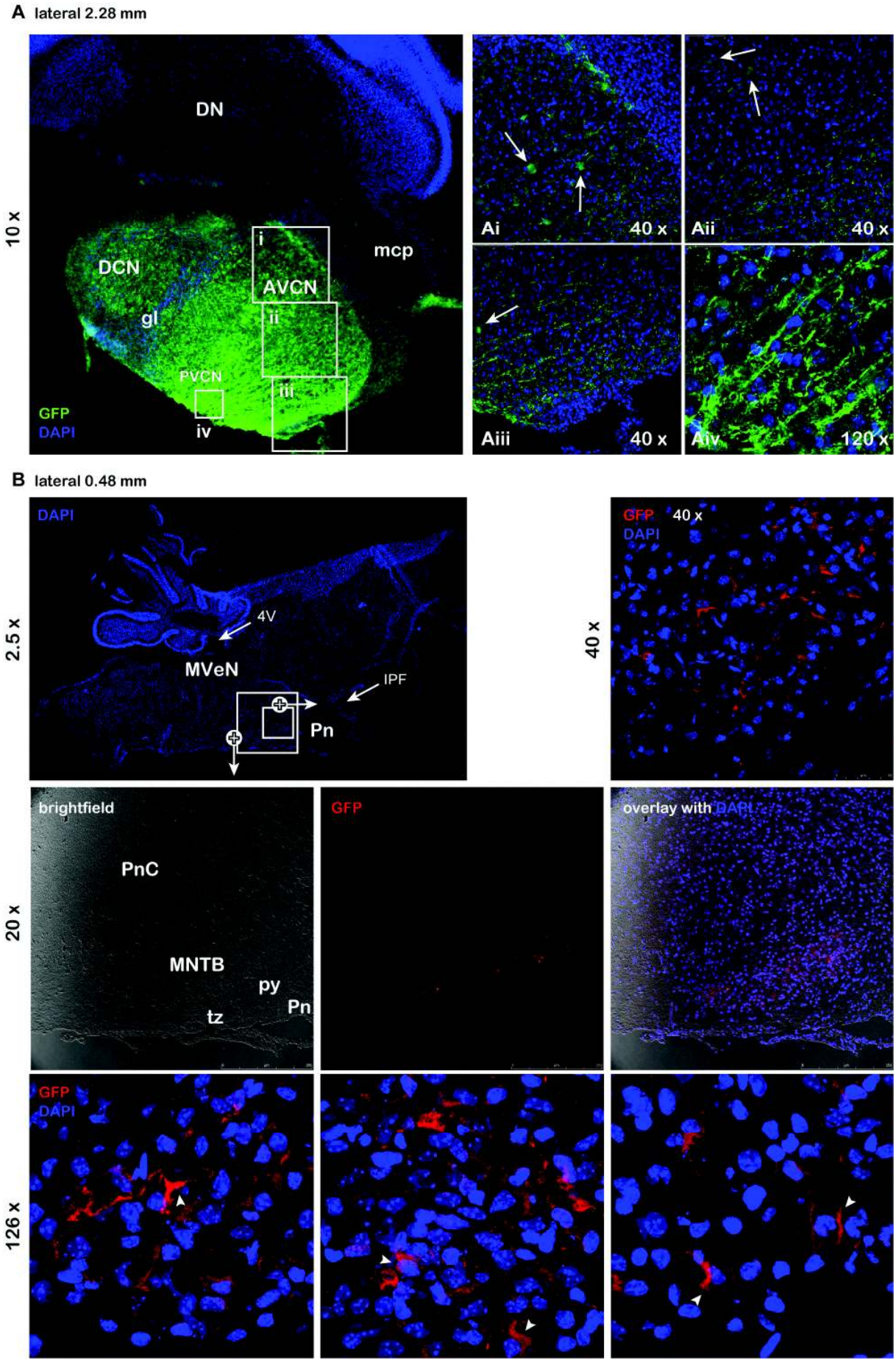
A lateral 2.28 mm
10 x
DN
DCN
gl
PVCN
i
ii
iii
iv
AVCN
mcp
GFP
DAPI
Ai
40 x
Aii
40 x
Aiii
40 x
Aiv
120 x
B lateral 0.48 mm
2.5 x
DAPI
4V
MVeN
IPF
Pn
40 x
GFP
40 x
DAPI
20 x
brightfield
PnC
MNTB
py
tz
Pn
GFP
overlay with DAPI
126 x
GFP
DAPI

4.4 A new method for selectively isolating mRNA of specific inner ear cell types

The TRAP (translating ribosome affinity purification) allows gene profiling of specific cell types. This method requires transgenic mice expressing an EGFP-tagged ribosomal subunit (L10a) specifically in the desired cell type(s) (1.5.2). In this study BAC transgenesis is used to generate transgenic mice (also see 1.4.2ii). Cell-type-specificity of EGFP_L10a expression is accomplished by selecting appropriate promoter and enhancer elements. Here, the promoters of *Calretinin* (*Calb2*), *Prestin* and *nicotinic acetylcholine receptor alpha 9* (*Chrna9*) were employed to direct expression to inner hair cells, outer hair cells and both, inner and outer hair cells, respectively. In addition, several other EGFP_L10a mouse strains obtained from the GENSAT venture were analysed for EGFP_L10a expression in hair cells and spiral ganglion neurons.

4.4.1 CONSTRUCTION OF BAC-TRANSGENIC TRAP MICE

BACs carrying the gene for EGFP_L10a under the control of different promoters were generated by recombination between homology regions on promoter-containing BACs and *EGFP_L10a*-containing shuttle vectors (SV, 3.4.2). First, the successful cloning of the homology boxes into pSV296 was confirmed by colony PCR with the primers SV_R6ky_ori_F and SV_EGFP_R (Fig. 29A), and subsequent sequencing of TOPO clones carrying the PCR product (not shown). Recombination between BACs and corresponding box-containing SVs was carried out in *E. coli* DH10B cells (see 3.4.2). Isolated BAC clones were screened for integrated SVs (Fig. 32B, C). Southern hybridisations (SHs) show the successful generation of *PRESTIN-EGFP_L10a* and *CHRNA9-EGFP_L10a* BACs. However, recombination did not occur via box R so that no *Calb2*-EGFP-L10a mice could be generated. BAC DNA of one positive clone for each remaining BAC construct was purified via ultracentrifugation in a CsCl gradient. After linearisation and dialysis both BACs were injected into fertilised oocytes of BDF/BL6 mice. In total 23 [13] tail biopsies of mice injected with the *PRESTIN*-BAC [*CHRNA9*-BAC] were received, 5 [4] of them having genome-integrated BACs. Genotyping with 4 primer pairs was performed to verify complete BAC integration: (1) box S[Q]_F(_AscI) and SV_EGFP_R, (2) EGFP_BAC_F/R, (3) before_PI-Sce_F/R and (4) after_PI-Sce_F/R. 4 [3] PCRs produce specific amplicons (not shown). In one *α9* line the BAC was not passed on to the next generation. Copy number determination by SH was not considered necessary because EGFP can be used to compare protein expression between founder lines.

4.4.2 IMMUNOHISTOLOGICAL DESCRIPTION OF GENERATED TRAP MICE

The remaining 6 lines, 3 for each construct, were directly analysed by RT-PCR and immunohistochemistry (Fig. 33). Transcripts of *EGFP* were detected in one line each (Fig. 33A),

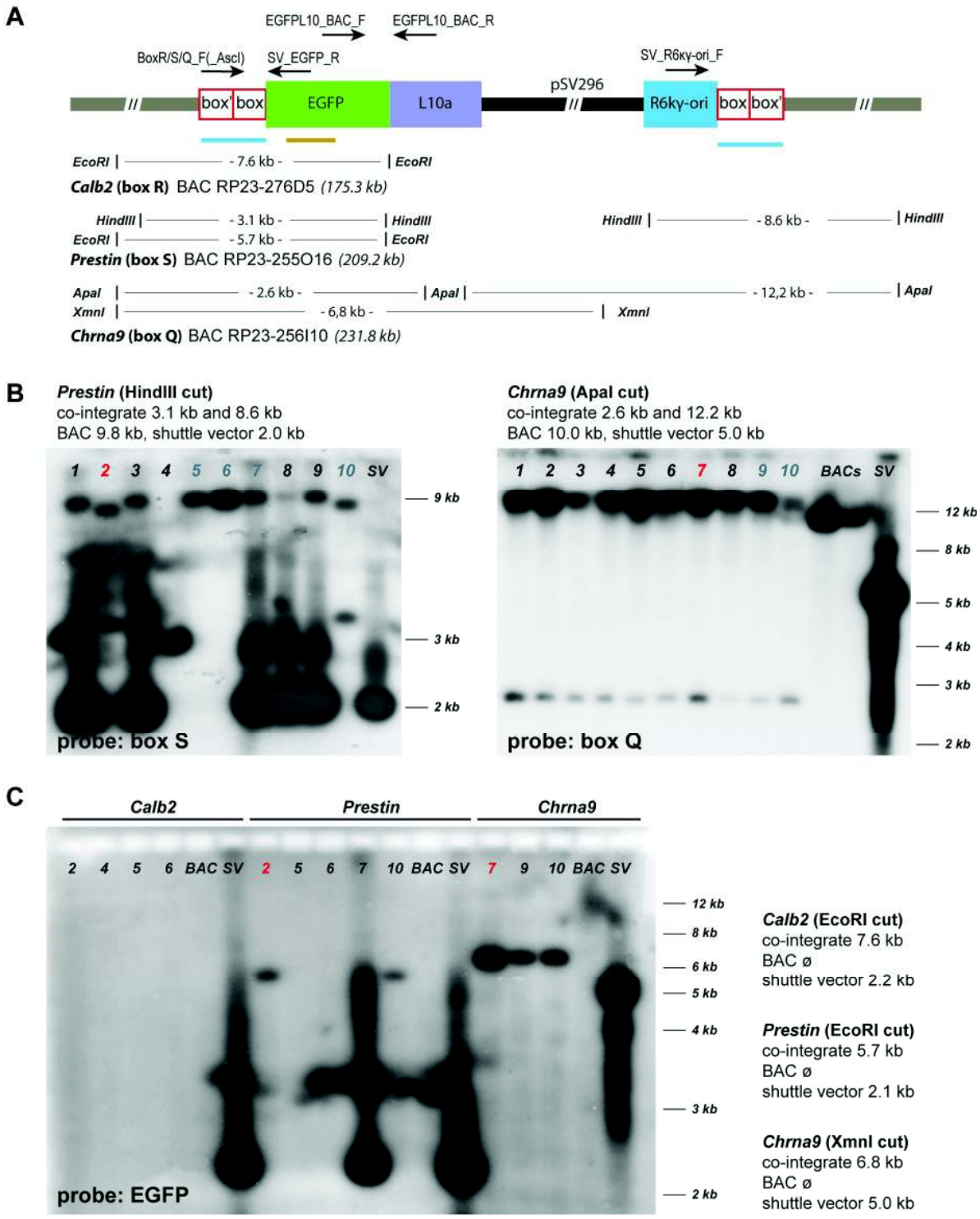

FIG. 32: GENERATION OF *EGFP_L10a*-CONTAINING BACs

Schematic illustration of the final BAC constructs (A). Names, situation of primers (arrows), restriction sites (vertical strokes) and hybridisation probes (coloured bars) are indicated for all three BAC constructs. Southern hybridisation (SH) with box-specific probes shows successful recombination in *Prestin* (2, 10) and *Chrna9* (all) clones (B). Clones indicated with coloured numbers were subsequently utilised for a SH with an EGFP-specific probe (C). Both *Prestin* and the three utilised *Chrna9* clones exhibit band sizes which indicate correct insertion of *EGFP_L10a*-containing SVs. Clones 2 and 7 (coloured red) were used to generate transgenic mice. The generation of *Calb2-EGFP_L10a* clones was not successful as no clone featured correctly sized double bands in SHs with the box-specific probe (not shown) and no band at all in the SH with an EGFP probe (C). Original BAC clones (BAC) and SVs with the corresponding boxes (SV) serve as positive controls for SHs. Fragment sizes after restriction enzyme digestion are shown on top of (B) or right to (C) the blots.

but immunohistochemistry revealed that none of the three *CHRNA9*-EGFP_L10a founder lines expresses GFP (not shown). Conversely, all three *PRESTIN*-EGFP_L10a lines show GFP-positive OHCs (Fig. 33B). GFP expression is specific for OHCs; neither IHCs nor any other cell type is stained positively for GFP. However, expression is restricted to a fraction of OHC (±5%). Also, no intrinsic GFP fluorescence is visible and GFP could only be detected by immunolabelling. Therefore expression levels are considered low. GFP-positive OHCs are found over all turns. Also, positive cells are found among all three rows of OHCs. Therefore expression of GFP in OHCs is stochastic in these mouse lines.

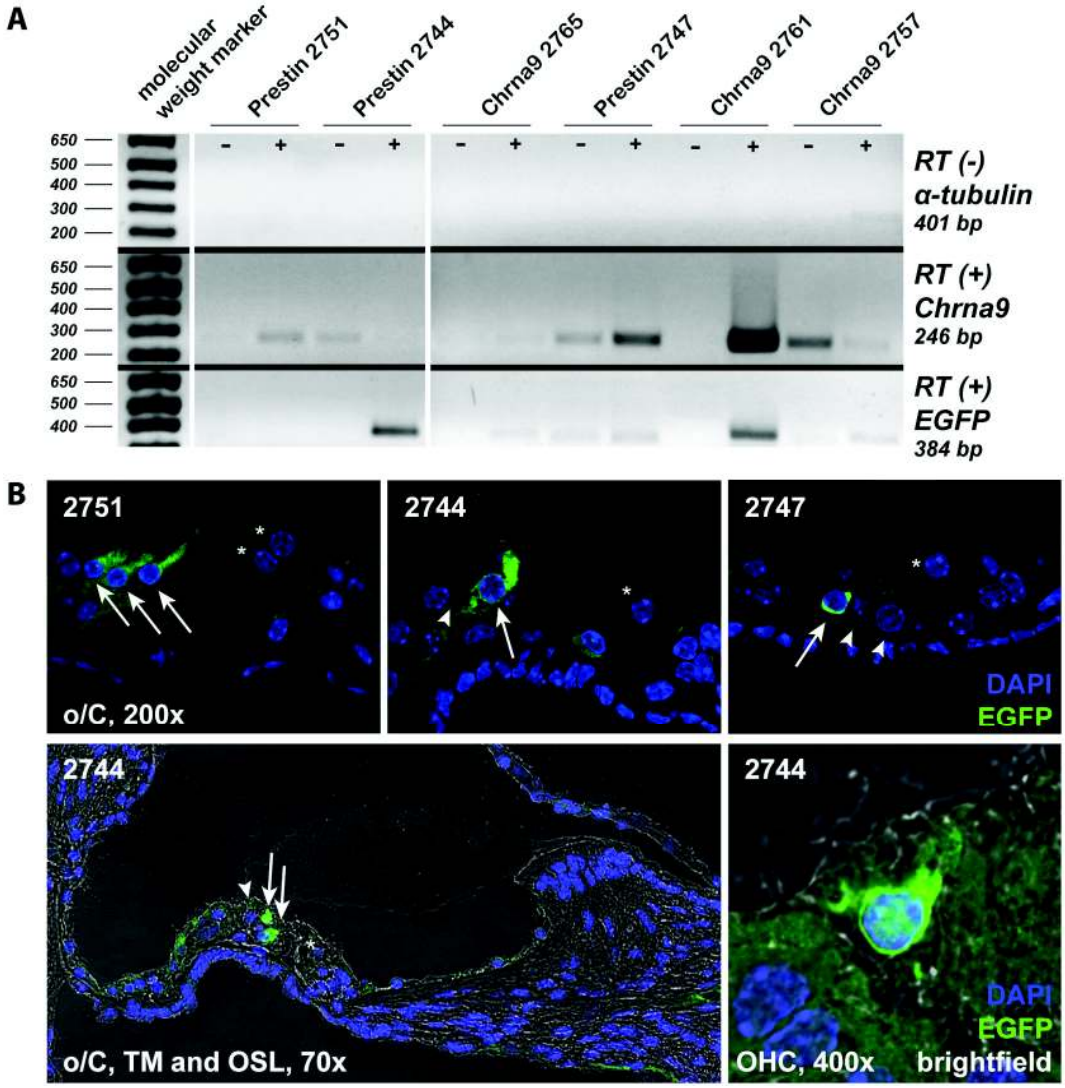

FIG. 33: ANALYSIS OF TRAP MICE GENERATED WITHIN THIS STUDY

A: Cochleae of six BAC-transgenic mouse lines were examined by RT-PCR (A). Of each line RNA samples isolated from BAC-positive (+) and BAC-negative (-) littermates were analysed. A high number of *EGFP* transcripts is detected in the lines *PRESTIN-EGFP_L10a*/2744 and *CHRNA9-EGFP_L10a*/2761 (last row). Samples are not contaminated with genomic DNA (first row) and exhibit comparable amounts of RNA (α-tubulin primers on RT(+) sample, not shown). However, the varying strength of the amplicon of the tissue-specific positive control (*Chrna9*) suggests that in the samples hair cell RNA is represented to different extents (middle row). B: Stainings with aGFP antibodies on midmodiolar cryosections of cochleae of the three *PRESTIN-EGFP_L10a* lines (2751, 2744, 2747) show that only a small fraction of OHCs is GFP-positive (arrows). Most OHCs do not express detectable EGFP_L10a levels (arrowheads). IHCs (asterisks) and SGNs (not shown) are GFP-negative. *IHC* inner hair cell, *o/C* organ of Corti, *OHC* outer hair cell, *OSL* outer spiral lamina, *SGN* spiral ganglion neuron, *TM* tectorial membrane

4.4.3 IMMUNOHISTOLOGICAL DESCRIPTION OF OTHER TRAP MICE

Four TRAP mouse strains generated by the GENSAT venture were tested for GFP expression in the inner ear (Fig. 34): *DLX1*-, *NEUROD1-, SNAP25*- and *VGLUT3*-EGFP_L10a mice. The promoter of *Dlx1* directs GFP expression exclusively to satellite cells in the spiral ganglion (Fig. 34A). No staining is observed in the organ of Corti. Co-expression with B-FABP suggests that *Dlx1* is active in satellite cells surrounding type I (arrowheads) and type III SGNs (arrows). A serial section of one neuron-glia-couple shows the perinuclear staining pattern typical for ribosome-associated EGFP of TRAP mice (Fig. 34B).

No expression of EGFP was detected in the organs of Corti of *NEUROD1-, SNAP25*- and *VGLUT3*-EGFP_L10a mice (Fig. 34C, D, E). *NeuroD1* drives GFP expression only in the SGNs of the apical turns. Scattered expression is present in middle turns while basal turns are devoid of GFP-ir (Fig. 34C, arrows). *SNAP25*-EGFP_L10a mice show EGFP_L10a expression in all SGNs of all turns (Fig. 34D). This mouse line shows the highest signal strength of all TRAP mouse lines under scrutiny in this work.

VGLUT3-EGFP_L10a mice show no GFP-ir in inner and outer hair cells. However, vestibular hair cells exhibit very intense GFP-ir. Also, spiral ganglion neurons are GFP-positive – although much weaker than SGNs of *NEUROD1*- or *SNAP25*-TRAP mice (Fig. 34E). Different founder lines were checked for their GFP expression strength and specificity in vestibular end organs (Fig. 34F): Among the three lines tested line 1887 shows the highest percentage of GFP-positive vestibular hair cells in maculae and cristae. Expression in hair cells of younger animals is higher than in adult animals but never adds up to 100% (compare sections of P14 and P56 mice of founder line 1890).

In conclusion, this work describes the successful generation of two TRAP mouse lines. In total five TRAP lines were characterised for the expression of EGFP-tagged ribosomal protein L10a in the inner ear. Notably, *SNAP25*- and *VGLUT3*-TRAP mice display high and specific expression of the fusion protein. Both mouse models will be very useful for gene profiling studies of spiral ganglion neurons and vestibular hair cells, respectively.

FIG. 34: TRAP MOUSE LINES EXPRESS THE FUSION PROTEIN EGFP_L10a IN INNER EAR CELL TYPES
Several mouse lines carrying BACs with integrated *EGFP_L10a*-containing SVs were tested for GFP expression in inner ear cell types. EGFP_L10a is expressed under the control of the promoters of the genes *Dlx1* (A, B), *NeuroD1* (C), *SNAP25* (D), and *VGluT3* (E, F). Counterstaining with aPGP9.5 and aB-FABP ab is shown in A. The secondary antibody used for most aGFP stainings is coupled to Cy3 (A-E). Cy2 is used in F.

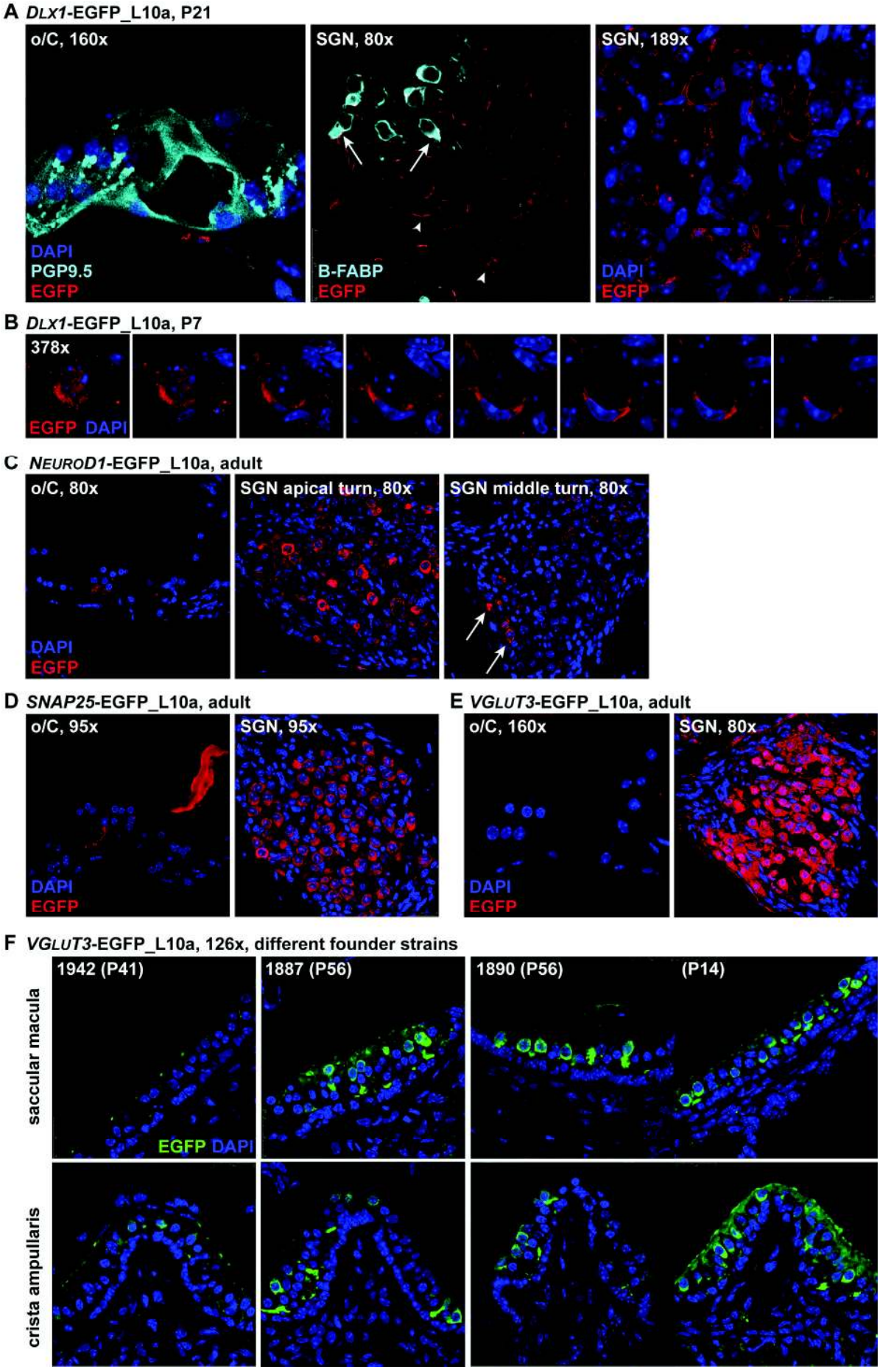
A DLX1-EGFP_L10a, P21
o/C, 160x
DAPI
PGP9.5
EGFP
SGN, 80x
B-FABP
EGFP
SGN, 189x
DAPI
EGFP
B DLX1-EGFP_L10a, P7
378x
EGFP DAPI
C NEUROD1-EGFP_L10a, adult
o/C, 80x
DAPI
EGFP
SGN apical turn, 80x
SGN middle turn, 80x
D SNAP25-EGFP_L10a, adult
o/C, 95x
DAPI
EGFP
SGN, 95x
E VGLUT3-EGFP_L10a, adult
o/C, 160x
DAPI
EGFP
SGN, 80x
F VGLUT3-EGFP_L10a, 126x, different founder strains
saccular macula
crista ampullaris
1942 (P41)
EGFP DAPI
1887 (P56)
1890 (P56)
(P14)

V. DISCUSSION

5.1 Targeting the neurotoxin GID to SGNs to silence specifically α7 nAChRs

A novel approach of conditionally silencing ion channels was pursued to find out the contribution of ACh to the LOC efferent system. This approach is based on a peptide toxin that blocks a specific target ion channel. Hereby toxin expression is directed to the cell type(s) of interest by BAC transgenesis[240]. To achieve successful silencing this approach needs careful choice of (1) the driver sequences on a chosen BAC which should promote and enhance the expression of the tethered toxin in the desired cell type (SGN) to a level where it efficiently blocks its target channel (α7 nAChR) and (2) the channel-specific toxin which should maintain its potency when expressed in mice in its tethered form. Preliminary data suggested that *Trpp2* might be a specific driver: GENSAT data of adult *TRPP2*-GFP mice show no signal in the brain – with the exception of SGN axons in the cochlear nucleus*. GFP-stainings in the cochlea of E15.5 *TRPP2*-GFP mice confirm that the cell bodies of prospective SGNs are heavily labelled†. Additionally, a recent study finds Trpp2 in SGNs of 8-week-old mice[214]. In the following paragraph *in vitro* data about different toxins blocking α7 nAChRs are summarised. Then the hearing ability of mice that successfully express the chosen toxin in spiral ganglion neurons is discussed. In the last part of this section the results of this study are reviewed in the light of recent data about the LOC efferent system.

5.1.1 tGID$_S$ EFFICIENTLY BLOCKS nAChRs *IN VITRO*

An appropriate toxin was selected by testing the abilities of different candidate toxins to block α7 *in vitro*. Due to its high efficiency in protein expression, the absence of endogenous nAChR subunits and its suitability for electrophysiological measurements the *Xenopus* oocyte expression system was employed. Studies on rat α7 subunits heterologously expressed in frog oocytes and natively produced in brain slices revealed similar potencies for an antagonist in both systems. This suggests that the blocking properties of the analysed toxins can be conveyed from frog to mouse[343,344]. For the α7 homomeric receptors reported on here it is known that their expression in *Xenopus* oocytes is fairly robust[345]. In other non-mammalian cells they are more difficult to express[346]. It seems that the efficient assembly of α7 AChRs is influenced by several regions of the large cytoplasmic domain and requires yet unknown factors[347]. This separates α7 from other nAChR subunits that in general do not exhibit receptor assembly

* http://www.gensat.org/imagenavigator.jsp?imageID=10963
† http://www.gensat.org/imagenavigator.jsp?imageID=11892

problems upon heterologous expression and may be a reason why maximum current amplitudes varied in our experiments within an order of magnitude (Fig. 9). The process of receptor assembly thus might me more susceptible to oocyte health varying from experiment to experiment. Because of the varying interexperimental maximum amplitudes (0.13 to 1.6 µA) of homomeric α7 nAChRs data obtained from different oocyte batches could not be pooled, although at least two experiments for each designated toxin-channel combination were performed independently and exhibited equivalent blocking percentages (not shown).

The snake toxins α- and κ-bungarotoxin were used as positive controls (Fig. 9). Both are promiscuous in their blocking behaviour so that applicability of their tethered forms *in vivo* seems not feasible. Among the more specific conotoxins MII was a promising candidate, but it failed to block nicotine-induced α7 nAChR currents when being expressed with a short linker (both, GPI-anchor and TM-domain versions). Also GPI-anchored PnIB only blocks about 90% of the current that is not as potent as GID – the last toxin that was employed in the study. For GID the short linker GPI-version consistently yielded the best block – rivalling even αBgtx. Longer linkers seem to hinder GID from blocking α7 effectively.

The receptor specificity of GID^{233} only slightly changes when being heterologously expressed with a short tether. $tGID_S$ continuingly blocks α7 nAChRs (>99%) and α3β2 nAChRs (>85%), but loses its vigour to block α4β2. Furthermore it modulates the desensitisation kinetics of α9α10 (Fig. 10). Hence, $tGID_S$ is even more specific when compared to the soluble toxin. The substitution of the non-proteinogenic amino acid γ-carboxyglutamic acid with glutamic acid (γ4E) could account for the selective loss of activity on α4β2 nAChRs. This hypothesis is supported by the finding that the deletion of four N-terminal residues of GID (GIDΔ1–4) leads to a ~4 fold decrease in activity at the α4β2 receptor, without affecting the functionality at α3β2 and α7 nAChRs. This new selectivity of $tGID_S$ opens the possibility for future studies using $tGID_S$ as an α7 / α3β2 nAChR-inhibitor to dissect the function of these channels and investigate their contribution in neuronal circuits without affecting also α4β2 nAChRs. The importance of the altered desensitisation of α9α10 receptors cannot be evaluated, as no data about soluble GID on α9α10 nAChRs are available.

Taken together, oocyte experiments encourage the notion that $tGID_S$ might be a potent inhibitor of α7 nAChR function also *in vivo*. Therefore the BAC-transgenic mouse generated in here will contain the genetic information for $tGID_S$.

5.1.2 The role of α7 nAChRs IN EFFERENT LOC SIGNALLING

So far the contribution of single LOC fibre neurotransmitters to the dynamic excitatory/inhibitory up- and downregulation of auditory nerve activity has not been addressed extensively. As the majority of LOC fibres (80-90%) sequester a mixture of transmitters,

experiments ablating entire cells do not yield meaningful results. The excitatory transmitter CGRP is implicated in MOC and LOC signalling, so both systems were tested audiometrically in CGRP null mice[294]. These mice do not show any signs of OHC dysfunction but display a mild reduction of sound-evoked activity in SGNs (ABR) that complies with both, the net excitatory and net inhibitory models of SGN modulation. As the systemic abrogation of the transmitters GABA or acetylcholine leads to more severe phenotypes than the loss of CGRP, other ways of elucidating their contributions in LOC signalling are needed. To explore if the function of the main transmitter in inner spiral bundle (ISB) terminals, acetylcholine, is inhibitory or excitatory, this study tries to silence cholinergic transmission without disturbing the release of e.g. GABA or enkephalins. In particular, the postsynaptic nicotinic receptor is targeted because altering acetylcholine synthesis or release pathways in LOC efferents is difficult without also affecting MOC efferents and the outer-hair-cell-system. The main nicotinic receptors of postsynaptic SGNs are α7 homomeric nAChRs. The usefulness of targeting nAChRs to study cholinergic neurotransmission has been proven by the successful analysis of $\alpha9^{-/-}$, α9 overexpressing and $\alpha10^{-/-}$ mice[53,55,60]. Like in CGRB knockout mice a change in the compound action potential (CAP) of auditory brainstem response (ABR) wave I is expected in mice with interrupted ISB cholinergic signalling.

At the time of study design no data from *Chrna7* knockout mice were available, so that the results would not only add proof that transgenically expressed tethered toxins can modify mammalian channels *in vivo*, but they would also give insights into the yet poorly understood LOC fibre system. In this work the successful generation of mice transgenically expressing the conotoxin GID is reported. Moreover, these *TRPP2*-$tGID_S$ mice express the toxin transcript in the desired cell type of interest, the spiral ganglion neurons. However, no curtailing of auditory function – including the expected change in the amplitude of ABR wave I – was measured (Fig. 14). Only after having generated the *TRPP2*-$tGID_S$ mouse strain, Maison and Liberman reported their auditory tests on mice with a targeted deletion of *Chrna7* (personal communication, 2008). They show that DPOAEs in unchallenged and noise-exposed ears are unchanged. This is not surprising as α7 nAChRs are not implied in OHC or MOC function. But interestingly, in the routine ABR they find neither an increase nor a decrease of the amplitude of the compound action potential of wave I. Also a possible threshold elevation as seen after destruction of a subset of LOC neurons in the high frequency range[71] is not observed in these mice. Unaltered thresholds over the complete frequency range thus also insinuate that α7 does not play a crucial role in the modulation of glutamatergic signalling by changes in gene expression in SGN terminals at the ISB.

It is known by Felix and Ehrenberger that ACh itself can induce SGN activity when injected beneath IHC[29]. Either α7-containing nAChRs have a different function, which is not assessed by

the auditory tests performed by in this study and by Maison and Liberman, or the released ACh binds to other receptors. As mentioned in the introduction also transcripts of α6 and β2 are present in type I SGNs[58]. They could constitute a yet undescribed nicotinic ACh receptor – possibly together with α7 or an unknown α or β subunit. Cholinergic neurotransmission is also mediated by another class of ACh receptors: G protein-coupled muscarinic (m)AChRs, which act through second-messenger systems[348,349]. Several studies detect muscarinic ACh receptors in the developing SGN[350-353]. Therefore mAChRs could also be potential targets of LOC-fibre-released ACh. Then however, the above mentioned observation by Felix and Ehrenberger has to be questioned, as signalling via muscarinic receptors cannot account for the observed fast increase in SGN activity. G_i-coupled mAChRs (M2 and M4) are expressed postsynaptically in SGNs where they mediate the slow excitatory effects of lateral olivocochlear activation[353]. The phenotype of $M2^{-/-}$ and $M4^{-/-}$mice (CAP depression) is similar to that seen in CGRP null mutant mice[294]. Taken together this suggests that (1) ACh likely acts as an excitatory transmitter in the ISB, and (2) it is likely that the cholinergic effect of LOC fibres does not involve nAChRs.

5.1.3 CONCLUSIONS AND OUTLOOK

As discussed in the previous chapter the role of α7 nAChRs in spiral ganglion neurons remains unclear. Due to the complete auditory testing of mice with a targeted deletion of *Chrna7* by Maison and Liberman the analysis of *TRPP2*-$tGID_S$ mice was not continued. Several follow-up experiments are needed to sufficiently characterise *TRPP2*-$tGID_S$ mice. Among them are stainings against the flag-epitope to prove toxin localisation at the membrane and electrophysiological recordings from single-unit auditory nerve fibres to show effective receptor blocking by the toxin also *in vivo.*

Additionally the promoter sequences of *Trpp2* are probably not ideal for directing toxin expression to adult SGNs. Contrary to aforementioned GENSAT data, expression levels of GFP in *TRPP2*-GFP mice drop sharply around P10 (see next chapter). ISH data confirm this notion as the age of highest detection of GID-transcripts in toxin mice matches the age of strongest GFP-signal in *TRPP2*-GFP mice (around P6). Possibly Trpp2 (and therefore GID) expression is low or maybe even completely absent in audiometrically tested mice (age: 8 weeks). However, Takumida and Anniko detect Trpp2 in SGNs of adult mice[214] so that in summary data about the presence of Trpp2 in adult SGNs are inconclusive. Nevertheless this does not rule out an effect of $tGID_S$ in development: LOC efferents expressing cholinergic markers (VAChT, ChT1) innervate the organ of Corti after MOC efferents[354] but still within the window of strong Trpp2 expression[355]. A blocking effect of GID on α7 nAChRs in the first postnatal week is conceivable because also α7 is expressed in SGNs before the onset of hearing. However, if α7 had an indispensable role in

establishing the LOC efferent fibre system the prospective resulting auditory phenotype would have been detected by Maison and Liberman.

In summary, the application of the tethered toxin strategy to a nicotinic acetylcholine receptor *in vivo* was partially successful. The role of acetylcholine in LOC fibre signalling remains unclear. However, this is not due to the employed tethered toxin approach. Recent data suggest that not the targeted nicotinic receptors but rather muscarinic receptors are involved in LOC signalling. The generation of a BAC-transgenic mouse strain that specifically expresses the tethered conotoxin GID in spiral ganglion neurons is accomplished. Furthermore *in vitro* experiments show that (1) tethered GID is an effective inhibitor of α7 homomeric nAChRs, (2) toxins with short linkers inhibit α7 nAChRs most effectively and (3) fluorescent markers coupled to a transmembrane domain do not hinder effective inhibition of α7 nAChRs by GID.

5.2 TRPP2 expression in the mouse cochlea

5.2.1 SUITABILITY OF BAC-GFP REPORTER MICE TO DISCOVER PREVIOUSLY UNKNOWN SITES OF GENE EXPRESSION

First evidence for the presence of *Trpp2* in the brain comes from Northern blot analyses in humans and mice[144,356]. No protein expression was found in the rat brain by antibody staining in a study scrutinising several rat tissues[306]. Explaining this discrepancy the authors think on species differences, lack of sensitivity of the immunofluorescence protocol, and/or posttranscriptional regulation of *Trpp2* expression in those organs. Obermüller et al. use a C-terminus-directed antibody (YCC2 by S. Somlo) and fail to detect expression. The antibody used by Foggensteiner et al.[139] (Pkd2-NP) is recognising a 12 amino acid epitope on the N-terminus. Unfortunately the authors did not report about any experiments done on brain slices. Another study on human foetuses[315] – which produced conflicting results of TRPP2 expression in the kidney when compared with the major body of publications – detects moderate expression of the protein in neuronal cell bodies in the cerebral cortex from week 33 onwards. However, this finding cannot be considered trustworthy as the authors only show difficult-to-interpret cut-outs. In this study Trpp2 protein could not be detected in neuronal tissues of mice by immunohistochemistry (not shown). Among the aTrpp2 ab tested in immunohistochemistry and Western blot experiments were the above mentioned YCC2 by S. Somlo, AB9088 by Millipore and sc-10376 by Santa Cruz (see 3.1.6). None of them targets epitopes on the N-terminus of the protein as the aPkd2-NP ab does. Possibly, the targeted epitopes are altered during the complex preparation (decalcification for immunohistochemistry and protein exposure for Western blot) of inner ear tissues so that they cease to be recognised by the tested antibodies.

Fortunately, the *TRPP2*-GFP reporter mouse strain shows a GFP expression pattern that matches existing antibody-derived data (see results in 4.2.1): The expression of GFP in the kidney of *TRPP2*-GFP mice (Fig. 15, Fig. 16Bii, E, G) highly follows the described expression of TRPP2 in kidney cells of rat, mouse and human. Also the presence of GFPs in bones and testes equates to known functions of Trpp2 in these organs (Fig. 16). Conversely, no GFP could be detected in cardiac septum, liver and pancreas where Trpp2 has been shown to fulfil vital functions[316]. Pc-1 is a known interaction partner of Trpp2. Hence a *PKD1*-GFP reporter line was analysed, too. Although some fluorescence is seen in the kidney, the overall levels in gene expression are lower than expected. Also the difference in the number of Pc-1-immunoreactive and GFP-ir structures is far more pronounced than in *TRPP2*-GFP mice. This high number of false negative tissues suggests that possibly vital promoter elements are missing on this BAC. However, the adult brain of *PKD1*-GFP mice shows bright fluorescence (Fig. 17A). Staining with functional aGFP abs on tissue sections of reporter mice could still reveal low-level expression of Pc-1 and Trpp2 in apparently non-fluorescing tissues. In summary, we reason that GFP-occurrence in BAC-GFP mice is a reliable reporter of protein-presence in all parts of the body. However, not all possible sites of Trpp2 and Pc-1 expression are disclosed by GFP fluorescence in these mouse strains.

5.2.2 PC-1 AND TRPP2 IN THE MOUSE INNER EAR

(I) TRANSCRIPTS

The results of this study show that *Pkd1* and *Trpp2* get transcribed in the cochlea (Fig. 18, Fig. 29). In the meantime the presence of these and other polycystin cDNAs in the inner ear has also been described by other authors: Cuajungco et al. detect PKD1, TRPP2, TRPP3 and PKDREJ cDNAs, but not the ones for other PKD1-like proteins and TRPP5[193]. Microarray data suggest that also PKD1L3 might be present[215]. Together with TRPP3 PKD1L3 is thought to have a function in the acquisition of sensory transduction in OHC. This becomes even more probable after the discovery that TRPP3 – as TRPP2 – can bind α-actinin[357]. *Trpp3* and *Pkd1L3* show a similar developmental expression pattern with a slow increase in transcript number until P4 to P6 (turn-dependent) and a sharp decrease afterwards[194]. That study, being basically an array of RT-PCR experiments on a cDNA bank obtained from differently aged organs of Corti (o/C), Reissner's membranes and striae vasculares, detected even all known polycystins. For *Pkd1L2* no specific expression pattern could be assigned, but *Pkd1* shows a constant increase over the time observed (E17 to P8). This finding is in line with the ISH data of the present study. Additionally, the specific *Pkd1*-positive cell type is revealed: At P2 and P4 no signal is seen in the entire cochlea. Around P6 transcripts can be detected in spiral and vestibular ganglion neurons, but not in other cells of the cochlea. At P8 the signal is strikingly clear (Fig. 18F).

Asai et al. found that the two transcripts for *Trpp2* (different splicing in the 3' UTR) showed opposing temporal expression gradients with *Trpp2_1* decreasing and *Trpp2_2* increasing over time[194]. With their probes they cannot distinguish between the consensus transcript and the suggested brain splice variant[136]. The antisense probes for *in situ* hybridisations in this work (see 3.6) are designed in a way to detect all of these three possible splice variants. Both probes show the most pronounced signal at around P2 (Fig. 18E). In contrast to *Pkd1 Trpp2* expression is getting reduced until P12 when no signal is detectable anymore (not shown). This suggests that *Trpp2_1* is possibly physiologically more relevant than *Trpp2_2*. As Asai et al. only examine tissues up to 8 days after birth, it is possible that the increase of *Trpp2_2* expression is only transient and is shut down until P12, too.

(II) PROTEINS

So far no protein expression data for PKD1-like proteins in the inner ear have been published. For TRPP2-like proteins one immunohistochemistry study has been conducted by Takumida and Anniko on adult mice[214]. Trpp2 is present in the outer lining of the lateral cochlear wall. Stria vascularis, spiral prominence, and spiral ligament show only faint Trpp2-ir. In the o/C immunoreactivity is evident in some supporting cells – but not in hair cells. A strong signal is observed in SGNs where cell bodies and nuclei are Trpp2-positive. In line with the proposed function for Trpp3 in OHC a weak signal is detected in both hair cell types. Strong Trpp3-ir is found in the stria vascularis and in SGN cell bodies. Contrary to Trpp2, Trpp3 is not present in SGN nuclei. Trpp5 expression is only detected weakly in spiral ganglia and not at all in the o/C. This study employs an aTrpp2 ab (Pierce Antibodies) which targets the '4th cytoplasmic loop' of Trpp2 which has to be put in question as Trpp2 only has 2 cytoplasmatic loops (Fig. 5). Apart from that this antibody seems to detect neuronal Trpp2 and could be useful for ongoing studies.

(III) DATA FROM BAC-GFP REPORTER MICE

Already well before Takumida and Anniko we noticed that spiral ganglion neurons are probably Trpp2-positive: SGNs of *TRPP2*-GFP mice are fluorescing brightly (Fig. 17C). First the specificity of this signal was confirmed by comparing *Pkd1*- and *Trpp2*-transcript occurrence with the presence of *GFP* transcripts and GF proteins (Fig. 18). The expression patterns on midmodiolar cochlea mouse sections are completely overlapping. The only cell type positive for Trpp2 is the spiral ganglion neuron whose cell body and neurites are filled with GFP. This is also the only cell type that exhibits a convincing staining in the study conducted by Takumida and Anniko[214]. Contrasting their findings the results of this study indicate that the faint GFP signals in stria vascularis, spiral prominence, spiral ligament, some supporting cells in the o/C and the outer lining of the cochlear wall are due to unspecific antibody uptake by (bone) tissue. Compared to the signals in the early postnatal SG fluorescence in these tissues is negligible. ISH does not

reveal *Trpp2* transcripts in any cell type except spiral ganglion neurons at P6 and P8 (Fig. 18E). Sections are devoid of any ISH signal at P12. Therefore it is considered unlikely, but not impossible, that Trpp2 expression is gaining momentum in these tissues until week 8, the mouse age Takumida and Anniko were examining.

Interestingly, the most dramatic difference between present data and data by Takumida and Anniko is found in the vestibular ganglion: Their antibody stains all adult vestibular ganglion neurons while in this work no GFP, *GFP* and *Trpp2* transcript signals are detected there in P2 (Fig. 18A), P6, P10, P12, P15 and P24 mice. Only at P0 GFP signals are obvious in VGNs. Signal strength is similar to the one in SGNs on the same slide (not shown). While Trpp2 expression in most SGNs is maintained at least until hearing onset, in VGNs expression drops sharply after birth. Again, expression levels could increase after P24 so that in week 8 Takumida and Anniko can detect Trpp2 anew. In the vestibular end organs, VHCs in the crista ampullaris and in utricular and saccular maculae show Trpp2-ir when stained with aTrpp2 ab[214]. Utricular maculae of P0 to P24 *TRPP2*-GFP mice exhibit no GFP expression (not shown).

5.2.3 TRPP2 IS EXPRESSED IN MOST SGNs IN THE FIRST POSTNATAL WEEK

GFP/Trpp2 expression in SGNs of *TRPP2*-GFP mice is developmentally regulated (Fig. 19). Similar to the decrease in transcript levels (see above) GFP signal diminishes in most SGNs from around P10 onwards. Around P12 no *Trpp2* transcript is found anymore, but still GF protein can be detected with antibodies. Even at P24, when the majority of SGNs are bare of green fluorescence, single neurons have persisting GFP expression (Fig. 19, arrow). Interestingly, this is not reflected by a detection of *Trpp2* mRNA in single SGNs of older mice so that the physiological importance of this finding is difficult to judge. The staining shown by Takumida and Anniko also shows a rather patchy and far from uniform labelling of neurons. Unfortunately they do not present a double labelling with a pan-neuronal marker that could unveil the subset of SGNs being Trpp2-positive. Nevertheless their image portends that in adults Trpp2 might be present in more SGNs than in 24-day-old mice as determined in this study. Of course, there is also a fair chance that Trpp2 expression is taken up again by more and more SGNs from week three to week eight. The development of the auditory sensory system is not finished until P13 when mice start to hear. In the first postnatal week cells differentiate and mature, synaptic contacts are made but also withdrawn (Fig. 35). It is thus reasoned that Trpp2 could have a function in setting up the correct innervation of spiral ganglion neurons, thus possibly influencing neurite outgrowth, retraction, or synapse formation.

5.2.4 POSSIBLE INTERACTION OF Pc-1 AND Trpp2 IN SGNS

Although TRPP2 is not passing currents when expressed alone, together with other interaction partners it produces cation currents (non-selective, calcium-permeable). When PC-1 is present as a partner[137] it brings TRPP2 from intracellular compartments to the plasma membrane[140]. PC-1/TRPP2 complexes may form mechanosensors in primary cilia and are involved in the development of a variety of organs, especially in tubulus formation. Without PC-1 TRPP2 probably acts as a channel in the membranes of intracellular organelles. *Pkd1*-driven and *Trpp2*-driven GFP expression as shown in this study are not completely congruent but exhibit a window where a joint physiological function is possible: While Trpp2-levels in SGNs stay stable from E15.5 to P6 and decline in most SGNs to undetectable levels around P15, Pc-1 is not found at E15.5* as well as at early postnatal ages. Pc-1 expression rises continuously until a strong signal is detected in P8 cochleae (Fig. 18, second column). Although *Pkd1*-driven GFP expression was not studied beyond P10, the two proteins can only be interaction partners between P6 (Pkd1-levels rise above detection limit) and P12 (Trpp2-levels decline in most SGNs).

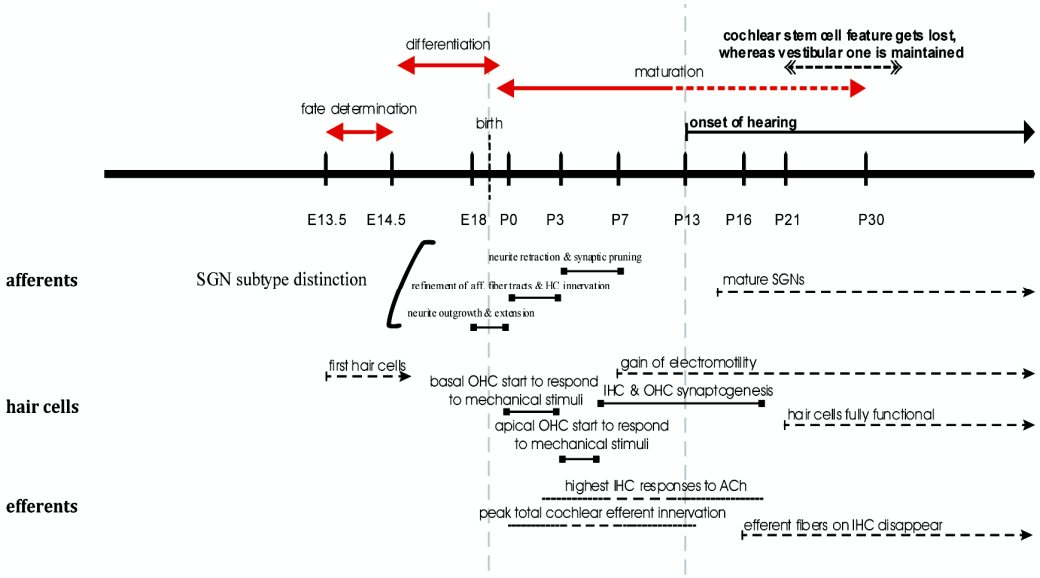

FIG. 35: SCHEMATIC SUMMARY OF DEVELOPMENTAL PROCESSES IN THE MOUSE COCHLEA

The employed ISH probe does not distinguish between the full *Trpp2* transcript and its brain splice variant *Trpp2Δ7*[136]. As Trpp2Δ7 is not interacting with PC-1 it needs to be determined which splicing form is present in SGNs to evaluate if the partial overlap of GFP expression in the ears of *PKD1*-GFP and *TRPP2*-GFP mice hints on a concerted function. This is important not only in the context of compartment localisation of the proteins but also in terms of signal cascade activation as at least one of the two described cleavages of PC-1 into biologically active fragments is TRPP2-dependent[358,359]. In adult SGNs Trpp2-ir is found throughout the soma,

* http://www.gensat.org/imagenavigator.jsp?imageID=12561

including the nucleus[214]. Neurites in the SG and dendrites in the o/C are not labelled[214]. The PM is not specifically stained so that Trpp2 likely exerts functions in intracellular membranes in SGNs of 8-week-old mice. The compartment localisation and thus function of Trpp2 might be different between P6 and P12 when Pc-1 is expressed, but this needs to be addressed in detail by antibody stainings. Triptolide, a drug that facilitates Ca^{2+} release through a TRPP2-dependent pathway[187], does not activate P6 SGNs of acutely isolated cochlea slices as assessed by Ca^{2+} imaging experiments (Laqua, unpublished). This also indicates an intracellular localisation of Trpp2.

5.2.5 RADIAL GLIA CELLS SURROUND SPIRAL GANGLION NEURONS

Radial glial cells are important in the development of the central nervous system. In particular, they are involved in neuronal migration and neurogenesis. They arise early in development from neuroepithelial cells and vanish in most parts of the brain when the adult cell patterns are established. Radial glial cells in the cerebellum ('Bergmann glia') and in the retina ('Müller glia') are known to persist into adulthood. A common protein marker for this cell type is B-FABP[332]. Although B-FABP has been described in the spiral ganglion recently[333], it is suggested here for the first time that the cells stained positively for B-FABP are cochlear radial glia cells (Fig. 20B, E and Fig. 24C). Until birth the majority of satellite cells are B-FABP-positive (Fig. 25C). Then expression is downregulated in most cells, so that at P10 only a subpopulation of satellite cells stains for B-FABP (Fig. 25I). Also in adults some satellite cells remain B-FABP-ir (Fig. 20B, E). Stainings against other radial glia markers like vimentin or astrocyte-specific glutamate transporter (GLAST) should confirm the identity of these cells. This finding would have implications on sensory neuronal hearing loss (SHL) research. Radial glia are thought to be the stem cells of glia and neurons, so stimulating proliferation and differentiation of these cells could prevent SGN loss in hearing-impaired patients.

5.2.6 TRPP2 IS POSSIBLY A MARKER FOR A NEW SGN CELL TYPE

In development *Trpp2*-driven GFP expression is present in the majority of SGNs (type I). At P10 some Peripherin-positive cells cease to express GFP and constitute another subclass of spiral ganglion neurons (type II). The existence of a new class of SGNs (type III) is proposed here for the first time in mice. Type III SGNs are characterised by typical type I SGN features like big cell size, random distribution over the entire ganglion area and satellite cell attachment, as well as by a typical type II SGN feature: expression of Peripherin. They are also presumably Trpp2-positive. However, these GFP-positive cells could also display a delayed loss of GFP when compared to the majority of SGNs (Table 15, middle panel). Future stainings on mice older than P24 will help to clarify this. Also, extensive *in situ* hybridisations should be conducted to substantiate conclusively if *Trpp2* transcripts are present in single SGNs of mice older than P10.

In adult mice type II SGNs are not only characterised by Peripherin-ir, but also by enhanced PGP9.5-ir and the entourage of B-FABP-positive satellite cells. Type III cells also exhibit these immunoreactivities. Additionally, they remain the only neurons that retain GFP fluorescence after GFP expression is gone in type I SGNs. Hence, at P24 Trpp2 becomes the only marker apart from their type I morphology that distinguishes type III SGNs from type II cells (Fig. 24; Table 15, lower panel).

In our study aNF-200 ab is the earliest marker for type II SGNs. At P0 it specifically labels the small subpopulation of SGNs that is not Trpp2-positive (Fig. 25A). As SGNs of P6 and P10 mice exhibit complete colocalisation of NF-200- and GFP-ir we assume that type II SGNs lose their NF-200-ir after P0 while type I and type III neurons obtain NF-200-ir. At P6 type II SGNs do not stain for any employed antibody, but at P10 Peripherin-ir indicates future type II neurons (Fig. 23). As type II cells do not show any reactivity to aGFP ab during development it is consequential to define Trpp2-negative and NF-200-positive neurons at P0 as type II SGNs.

The existence of more than two SGN subtypes has already been suggested in humans. Rask-Andersen distinguishes (1) large, (2) small spherical and (3) small spindle-shaped ganglion cells[14]. Liberman classified auditory-nerve units of cats according to their spontaneous rate into three distinct populations[360]. Also in guinea pigs the SGN population is more diverse than the morphology might suggest. In an expression study the proportions of SGNs positive for 4 given Ca^{2+}-binding proteins vary from 25% to 100% but do never coincide with the morphologically assumed 90-95% (type I) or 5-10% (type II) populations[361]. Nevertheless immunohistochemical stainings with functional antibodies directed against Trpp2 proper need to be done to confirm the identity of this new class of SGN. As Peripherin has been shown to label reliably afferent fibres coming from OHCs, we assume that Peripherin-positive type III fibres also do so. The separation of the already small subset of SGNs contacting OHC into type II and type III classes makes the physiological investigation of these neurons even more cumbersome. However, if intrinsic green fluorescence of type III SGNs is sufficiently glaring, the *TRPP2*-GFP strain could become useful for whole-mount and cell culture electrophysiological recordings of spiral ganglion neurons. The immanent GFP fluorescence in also the dendrites of *TRPP2*-GFP mice can possibly be used to investigate if type II and type III neurons exhibit different innervation patterns in the organ of Corti.

5.3 Tissue-specific knockouts of Trpp2 using the Cre-loxP-system

As the reliability of the obtained *Trpp2*flox mouse line has not been demonstrated before we first tested successfully that the flox allele of these mice is functional (Fig. 27). Hence the

deletion of exons 3 and 4 leads to a phenotype indistinguishable from the phenotype of null mutant mice. In the meantime a mouse line carrying loxP sites right before and after *Trpp2* exon 3 has been created[148]. These mice were crossed to mouse lines that express Cre recombinase specifically in kidney and pancreas. Subsequently, they show that offsprings are viable, but have kidney or pancreas cysts. Hence, the excision of exon 3 seems to be sufficient to create a true null allele.

5.3.1 ANALYSIS OF PROGENY OF *ISL1-CRE*::*Trpp2*flox BREEDINGS

ABRs and DPOAEs of six F1 hybrids of an *ISL1-Cre*::*Trpp2*flox breeding were measured. Half of them had severely elevated hearing thresholds (increase of 20 – 60 dB SPL). Unfortunately this was not due to the conditional inactivation of *Trpp2* as some *ISL1-Cre*$^{+}$ *Trpp2*$^{wt/wt}$ mice were affected as well. On the contrary, also two *ISL1-Cre*$^{+}$ *Trpp2*$^{flox/flox}$ mice showed normal hearing. Inappropriate handling of mice or malfunction of the experimental setup can be excluded as a cause as parallel hearing tests on another strain (see 4.3.3) produced meaningful results. Both, *ISL1-Cre* mice and *Trpp2*flox mice have a 129 background and have been crossed several times into a C57Bl/6 background before they were mated. Due to strain effects F1 hybrids in principle could exhibit phenotype differences but (1) threshold shifts are too dramatic that strain differences could possibly be the underlying cause and (2) all involved strains show similar hearing abilities in a variety of audiometry tests*. In our set of mice no correlation of coat colour and hearing deficit is observed. Still, a remote chance remains that unfavourably shuffled DNA sequences account for the observed hearing deficits in F1 hybrids. Auditory tests should be repeated with inbred mice to investigate this in more detail.

Isl1 is expressed in a number of non-neuronal tissues like retina and heart. Hence, phenotypes could also arise in other tissues of *ISL1-Cre*$^{+}$ *Trpp2*$^{flox/flox}$ offspring. Pancreas defects/cysts are possible as both, *Isl1* (hence the name) and *Trpp2*[315], are expressed there. *Isl1* is possibly also expressed in the kidney where *Trpp2* exerts its most intensively studied function in the primary cilia of epithelial cells[362]. However, kidneys and pancreases of *ISL1-Cre*$^{+}$ *Trpp2*$^{flox/flox}$ mice are not cystic, which suggests that *Isl1* is not a strong promoter in these tissues. Interestingly, kidney agenesis is found in 3 out of 20 mice (no side preference, all *ISL1-Cre*$^{+}$ *Trpp2*$^{eq/eq}$). The *ISL1-Cre* mouse is a knock-in strain. As both parents of agenesis mice were *Cre*$^{+}$ it is conceivable that the missing kidney is due to a lack of Isl1 (no *Trpp2* involvement). On the other hand *ISL1-Cre*$^{+/+}$ mice should be devoid of any Isl1 protein which reportedly leads to perinatal death.

Due to the cornucopia of queer phenotypes we refrain from further essential experiments with these mice. If a solid correlation between genotype and auditory phenotype can be established

* http://phenome.jax.org/db/q?rtn=projects/details&sym=Johnson1

in inbred mice e.g. the change of neuronal *Trpp2* transcript levels should be documented in Cre$^+$ flox/flox, Cre$^-$ flox/flox and Cre$^+$ wt/wt mice by RT-PCR or *in situ* hybridisation.

5.3.2 PROGENY OF *NES-CRE* AND *TRPP2*FLOX MICE DISPLAYS AN AUDITORY PHENOTYPE

The second Cre-expressing mouse strain employed in this study is *NES-Cre*. In this strain Cre recombinase expression is under the control of promoter elements of the gene *Nestin*. During development the gene is expressed transiently by many cell types but in adult tissues it is a marker for neural stem and progenitor cells (impressively demonstrated in *NES-GFP* reporter mice[363]). So far three mouse lines expressing Cre recombinase under the control of *Nestin* promoter elements have been created. However, the two lines made in the laboratory of N. Rajewsky display mosaic expression. To test stringency and tissue-specificity of Cre expression the *NES-Cre* mice made by R. Klein had been crossed with a reporter mouse strain. Resulting offspring shows that the reporter protein (β-galactosidase, β-gal) is present in all neurons and glia cells at E15.5*. Also modiolus and spiral ganglia of P0 mice exhibit strong expression of β-gal† so that the desired excision of floxed *Trpp2* exons 3 and 4 is likely to occur in SGNs of *NES-Cre*$^+$(R. Klein) *Trpp2*$^{flox/flox}$ mice. Additionally, this *NES-Cre* strain has been successfully employed to generate a targeted knockout of *Pkd1*[309].

(I) RENAL CYSTS – BUT NO HYDROCEPHALY

In *NES-Cre*$^+$ mice Cre recombinase is also active in non-neuronal tissues like in isolated kidney and heart cells. This finding is corroborated by the observation that Cre-positive *Trpp2*$^{flox/flox}$ offsprings of *NES-Cre*::*Trpp2*flox breedings have renal cysts (Fig. 28). Cystic kidneys exclusively occur in mice with truncated *Trpp2*. An influence on the auditory phenotype can be excluded as renal failure downgrades hearing (prolonged latencies, high frequency hearing loss) instead of increasing the amplitude of auditory brainstem responses[364,365]. Renal cysts also develop after crossing this *NES-Cre* strain with *Pkd1*$^{flox/\Delta}$ mice[309]. The superior importance of Pc-1 over Trpp2 in cyst development is demonstrated by the fact that these mice die because of kidney failure already at P12 whereas *NES-Cre*$^+$*Trpp2*$^{flox/flox}$ mice survive the first year.

Cre recombinase can cause decreased growth, cytopathic effects, and chromosomal aberrations[366]. High levels of Cre recombinase expression in nuclei of neuronal progenitors can even compromise normal brain development and lead to hydrocephalus[367]. This development of hydrocephali is demonstrated in mouse lines where Cre expression is driven by the *Nestin* promoter. Although Forni et al. investigate *NES-Cre* strains different from the one used in this study, disorders in brain development also in our strain do not seem unlikely. However, brains

* http://cre.jax.org/Nes/Nes_E15head_Images.html
† http://cre.jax.org/Nes/Nes_P0head_Images.html

of mice homozygous for *NES-Cre* do not show enlarged ventricles so that Cre levels in the mouse model employed in this study are probably below the toxic threshold. Additionally, this also indicates that Trpp2 does not hold an important function in ciliated ependymal and choroid plexus cells, as knocking-out *Pkd1* in these cells with the same approach and the very same Cre line leads to mild hydrocephalus[309].

(II) *Trpp2* TRANSCRIPTS IN THE COCHLEA

Analysis of RNA pools of different tissues demonstrates that the truncated, non-protein-coding *Trpp2* allele is only present in *NES-Cre*$^{+}$ *Trpp2*$^{flox/flox}$ mice (Fig. 29). The two exons are successfully excised in all tissues which have been reported as Nestin-positive (kidney, brainstem) – but not in Nestin-negative muscle-tissue. More importantly, the truncated *Trpp2* transcript is also present in the cochlea sample. In the cochlea – as already shown earlier in this work – *Trpp2* is only expressed by spiral ganglion neurons so that only these cells can account for the presence of *Trpp2* transcripts. However, in the same sample also intact transcripts are detected. Cochlea microdissection is a facile task so that contamination of the sample with other *Trpp2*-expressing tissues can be ruled out. Therefore the *Nestin* promoter is considered too weak to drive recombination between the two loxP sites on both alleles of all SGNs.

Alternatively, *Nestin* might not be transcribed in all Trpp2-expressing neurons. However, as *Nestin* is active in the majority of SGNs – as determined in the β-gal-reporter mouse (see above) – only a small subset of SGNs can possibly be Nestin-negative. Type III neurons could constitute this subset as they also show GFP(Trpp2)-ir. As pointed out in section 5.2 type III neurons maintain GFP expression at least until P24. The presence of intact – and the absence of truncated – transcripts would be expected in cDNA pools derived from P24 cochleae of *NES-Cre*$^{+}$ *Trpp2*$^{flox/flox}$ mice if Cre recombinase was not active in type III neurons. However, as *in situ* hybridisations with anti *Trpp2* probes on cochlear tissues of P12 mice do not give signals in prospective type III cells, the amount of *Trpp2* transcripts might not be sufficiently high to allow detection also by RT-PCR. Taken together the explanation of the presence of intact *Trpp2* in the cochlea is challenging. The complete absence of any intact *Trpp2* in the brainstem sample renders it unlikely that the *Nestin* promoter is not active (or only weakly active) in SGNs.

In any case the presence of intact *Trpp2* in the cochlea of P6 mice can explain both the lack of a morphological phenotype as well as the unchanged amplitude of ABR wave I. This wave is thought to be generated by cells with somata peripheral to the cochlear nucleus (CN) because even the most serious cell loss in the CN after inducing lesions with kainic acid does not change wave I. Also, surgical cutting of the auditory nerve leaves wave I unaffected[368]. Therefore remaining full-length Trpp2 might be sufficient to satisfy all – yet to be determined - physiological functions in SGNs. Arguably, *Trpp2* transcripts might be completely gone in *NES-*

Cre+ *Trpp2*$^{flox/\Delta}$ mice. If this is the case a detailed analysis of the pruning processes in these mice could be worth studying. In addition, these mice should also be tested audiometrically.

(III) *Trpp2* TRANSCRIPTS IN THE BRAINSTEM

In the light of leftover intact *Trpp2* transcripts in the cochlea it is particularly surprising that in the brainstem sample only truncated transcripts are detected. This suggests (1) that all cell-types in the brainstem are – or have been – Nes-positive and (2) that the *Nestin* promoter is potent enough to drive Cre recombinase expression to such high levels that recombination takes place in flox alleles of both chromosomes of all cells. Although the presence of *Trpp2* transcripts in the brain has been reported so far nothing is known about its expression pattern. This study provides first evidence that several cells in the cochlear nucleus likely express Trpp2 (Fig. 31). These cells are scattered over the anterior ventral cochlear nucleus (AVCN) and parts of the posterior VCN (PVCN) but are not found in the dorsal cochlear nucleus. GFP-positive fibres are present in the MNTB – and not in the lateral (LSO) or medial superior olive (MSO) – and form calyx-like presynapses. The synapses in the MNTB (medial nucleus of the trapezoid body) and the eccentric nuclei of the cells suggest that these CN neurons are globular bushy cells (GBC). GBCs make conspicuous synapses with MNTB principal cells ('Calyces of Held'), and are found in the AVCN and the PVCN. However, the total amount of GBCs far exceeds the number of GFP(Trpp2)-positive cells found in the CN, so that only a fraction of GBCs possibly expresses Trpp2. Based on morphological data (Nissl, Golgi stainings et al.) observers classify CN neurons into 9 to 55 distinct subgroups[369]. Additionally, physiologists define different CN cell types after analysing the response of single neurons stimulated at their characteristic frequency. Single GBCs respond in one out of three possible ways to these tones. Further morphological and electrophysiological analysis will surely help to define the nature of these Trpp2-positive neurons.

(IV) THE ABR PEAK N3 OF *Nes*-CRE+ *Trpp2*$^{flox/flox}$ MICE IS SIGNIFICANTLY ALTERED

'Calyx of Held' synapses are excitatory; however, all presynapses made by MNTB principal cells (with targets in the ipsilateral MSO and LSO, as well as on other MNTB principal cells) are inhibitory. Missing Trpp2 in GBCs could influence firing at the 'Calyx of Held' leading to a reduced activation of MNTB principal cells. Ultimately, the missing inhibitory input of MNTB principal cells could explain the increase in ABR amplitudes in mice expressing truncated *Trpp2* transcripts. This is especially important in respect to the most significant change in the ABR amplitude graph: The negative part of wave III (N3) becomes more negative in successfully targeted mice. Lesion experiments indicate that cells of the posterior AVCN and anterior PVCN are the only CN cells involved in the generation of N3, but known latencies of those cells suggest that they rather produce P2. As discussed in the previous chapter GBCs are most likely the cells of the posterior AVCN and anterior PVCN that express Trpp2. Hence the target cells of GBCs

might be responsible for N3 generation. Surprisingly, MNTB principal cells are not important for the generation of N3 as lesions in the superior olivary complex (SOC) do not influence N3 at all. The only known cells of the auditory pathway innervated by GBCs and located outside the SOC constitute the nuclei of the lateral lemniscus (NLL). The most extensive lesion study published so far does not explicitly exclude these nuclei as potential N3 generators[368]. SOC lesioning does not change NLL-generated N3 because of parallel loss of both inhibitory (MNTB principal cells) and excitatory SOC-input (MSO cells). In *NES-Cre*$^{+}$ *Trpp2*$^{flox/flox}$ mice the missing inhibitory effect of GBCs via MNTB principal cells is more important than the direct excitation of NLL neurons by GBCs – thus possibly explaining the increase in N3 amplitude.

Similar to the situation in the inner ear expression of Trpp2 in the brainstem is transient. The different performances in hearing tests were recorded on ±P23 mice. At this age no GFP fluorescence is detected in the MNTB of *TRPP2-GFP* mice anymore so that only permanent changes of innervation, synaptic strength, cell type distribution, – or cell numbers in the auditory system of *NES-Cre*$^{+}$ *Trpp2*$^{flox/flox}$ mice can conciliate these findings.

(V) *NES*-CRE^{+} *Trpp2*$^{flox/flox}$ MICE DISPLAY INCREASED OVERALL ABR AMPLITUDES

This study provides evidence that Trpp2 is transiently but robustly expressed by murine SGNs and cells in the CN. Partial loss of Trpp2 transcripts in the developing cochlea leads to a significant increase of the combined amplitudes of all ABR waves in hearing mice roughly two weeks later (Fig. 30B). The most robust change (in N3) has been discussed in the previous chapter but also increases of P1 and P2 in *NES-Cre*$^{+}$ *Trpp2*$^{flox/flox}$ mice are significant at certain volumes (Fig. 30C). Two scenarios might explain this observation. First, missing Trpp2 in type III SGNs of audiometrically tested mice could have a direct effect on the ABR. Type III SGNs constitute a part of the afferents of OHCs and as a part of a feedback loop they influence the response of type I SGNs. Altered signalling in Trpp2$^{\Delta/\Delta}$ type III SGNs might lead to a loss of type I SGN inhibition at the level of the cochlea (intraganglionic synapses; accounting for the increase in P1), but also to a loss of inhibition at the level of the brainstem (accounting e.g. for the increase of P2). In the second scenario the missing Trpp2 in the majority of SGNs leads to a structural or morphological aberration in the development of SGNs that becomes manifest. Thus increased ABR amplitudes can be recorded even two weeks after Trpp2 downregulation. Ganglion morphology and the innervation of hair cells by SGNs of *NES-Cre*$^{+}$ *Trpp2*$^{flox/flox}$ mice are unchanged when compared to their wt/wt littermates. Nevertheless subtle structural changes, which were not examined in detail, could account for increased ABR amplitudes (e.g. increase of type I SGN-IHC synapse number).

The interpretation of the amplitude-increase of the ABR of *NES-Cre*$^{+}$ *Trpp2*$^{flox/flox}$ is challenging. The bulk of data investigating which relay stations of the auditory pathway account for certain

positivities and negativities stems from chemical or mechanical lesion studies[370-373,368]. Depending on the lesioned structure extrema of one (or more) wave(s) converge to base level. However, in *NES-Cre*+ *Trpp2*flox/flox mice all extremes diverge away from the base level to more positive and, respectively, more negative compound action potentials (CAP). An increased (decreased) excitability of neurons – as seen in Kv1.1 / KCNA1 knockout mice – shifts the whole ABR graph to more positive (negative) CAPs[374] and therefore cannot explain the auditory phenotype. Spiral ganglion cells are generally accounted as generators of P1 and N1. SGNs bifurcate in the CN to innervate the dorsal and ventral parts. There the two axons branch even more to innervate nearly all different cell types in the CN. The remaining waves of the ABR result mainly from generators following one of two pathways, the globular cell pathway (starting from GBC in the posterior AVCN) and the spherical cell pathway (starting from spherical BC in the anterior AVCN). Within these above mentioned parallel brainstem pathways the other potential generating cell populations are arranged serially. Hence the generation of P4, N4 and P5 (SBC pathway) does not require inputs from the generators of P2 (GBC pathway) even though P2 precedes P4 to P5 in the ABR graph. The generators are arranged in parallel, not in series[19]. The amplitudes of N4 and P5 do not significantly differ between *NES-Cre*+ *Trpp2*flox/flox mice and their wildtype littermates at all volumes tested. It is therefore suggested that Trpp2 has its major physiological role in the GBC pathway.

(VI) SUMMARY

In summary we hypothesise that Trpp2 loss in SGNs and/or cells in the CN leads to a reduction of information which is particularly necessary for the globular (bushy) cell pathway. GBCs make excitatory synapses with MNTB principal cells that are the main inhibitory cells in the SOC. Reduced activation of MNTB principal cells therefore lessens their inhibitory output to various targets, which ultimately accounts for the increase of amplitude in the corresponding ABR waves. In particular MNTB principal cells inhibit cells in the NLL which likely account for N3. As the results of this study demand at least a transient change of synaptic transmission or synaptic plasticity in targeted mice (Trpp2 expression until hearing onset, auditory phenotype recorded 1-2 weeks later), hearing tests with several-week-old mice could proof a permanent change of hearing abilities. Following that, the histological and electrophysiological analysis of NLL neurons and MNTB principal cells of *NES-Cre*+ *Trpp2*flox/flox mice is suggested to clarify the underlying mechanisms of increased ABR amplitudes of those mice in more detail.

5.3.3 CONCLUSIONS AND OUTLOOK

The observed change of the amplitude of the recorded compound action potential of *NES-Cre*+ *Trpp2*flox/flox mice has to be regarded as an exceptional finding as conditional knockouts of *Trpp2* rarely yield phenotypes outside the kidney (Somlo, 2008, personal communication). In fact, this

is the first report about the *Trpp2*flox mouse line generated by the laboratory of S. Somlo. Herewith the functionality of this floxed allele is assured by (1) the reproduction of the knockout phenotype after crossing the *Trpp2*flox mouse to a (CMV)-*Cre* mouse strain and (2) the descriptiontion of known (kidney) and previously unknown (audition) phenotypes after crossing it to *NES-Cre* mice. Future studies on Trpp2 may take advantage of this *Trpp2*flox mouse strain because it does not display any functional disadvantage over the *Trpp2*flox mouse generated by the Wu laboratory[148].

5.4 Inner-ear-specific TRAP mouse strains

5.4.1 MOUSE STRAINS EXPRESSING EGFP_L10a IN INNER EAR HAIR CELLS

In this work the successful generation of *PRESTIN-EGFP_L10a* mice is reported. Prestin is a member of the SLC26A/SulP transporter family. It is specifically expressed in outer hair cells (OHCs) of the cochlea and is essential for auditory processing. The suitability of the promoter of this gene for BAC-transgenesis is confirmed by the obtained results: The fusion protein EGFP-L10a, which is required for the enrichment of polysome-bound mRNA, is exclusively expressed by outer hair cells. These mice therefore could become a useful tool for the study of the translatome of OHCs. However, the percentage of GFP-positive OHCs stays well behind expectations. It remains to be determined if the purification of polysome-bound OHC-transcripts is feasible when only ±5% of all OHCs express EGFP_L10a.

The generation of *CHRNA9-EGFP_L10a* and *CALB2-EGFP_L10a* mice failed at different stages. In the case of the former one this study shows the successful generation of the altered BAC ('co-integrate') and the recipience of several founder lines. However, immunohistochemistry shows that no GFP is expressed in both targeted cell types (IHCs, OHCs) of three independent founder lines. This is an unexpected finding as Zuo et al. have shown bright GFP-expression by all hair cells at P8, P13 and in adult cochleae of *CHRNA9*-GFP mice[375]. The BAC clone employed in this study is 92 kb bigger than the one used by Zuo. Missing promoter or enhancer elements therefore cannot account for the discrepancy.

Vesicular glutamate transporters (VGluT) mediate the uptake of glutamate into synaptic vesicles at presynaptic nerve terminals of excitatory neurons The three known VGluT isoforms exhibit a mutually exclusive distribution in the adult brain, suggesting a distinct role for each protein. VGluT1 and -2 are the predominant isoforms. They are associated with all classical glutamatergic neurons. VGluT3 (SLC17A8, DFNA25) is expressed by neuronal populations that are usually associated with the release of a transmitter other than glutamate, (e.g. serotonin, ACh, GABA) and is implicated in a variety of non-classical functions (e.g. retrograde synaptic release). In the organ of Corti, however, it functions as a classical transporter of glutamate into synaptic

vesicles at IHC presynapses. Genetic defects lead to a lack of glutamate release and subsequently to nonsyndromic deafness[201,376,377]. Immunohistochemical stainings confirmed that VGluT3 is expressed by IHCs but not by OHCs (unchanged OHC function of VGluT3$^{-/-}$ mice)[377]. In the vestibular apparatus VGluT3-ir was detected in a large number of sensory cells[378] but *VGluT3* knockout mice show normal righting reflexes and rotarod performances, suggesting normal motor and vestibular function[377]. As VGluT1 is expressed in VHCs[379] – but not in IHCs and OHCs – it could take over VGluT3 functions in maculae and cristae of knockout mice. In the present study *VGluT3* promoter elements direct EGFP_L10a expression to a subset of VHCs in *VGLUT3*-EGFP_L10a mice. The number of GFP-positive VHCs depends on the founder line but never adds up to all VGluT3-positive VHCs as determined by Zhang[379]. This proves that the fusion protein EGFP_L10a can be expressed outside the central nervous system. The detection of GFP in VHCs indicates that the targeting approach is feasible, and that the actual generation of BAC-transgenic mice was successful. However, no EGFP_L10a is detected in IHCs. Experiments in zebrafish suggest that VGluT3 has a similar function in the vestibular and the cochlear system[380]. Regulatory mechanisms driving *VGluT1* expression in VHCs could also enhance the expression of EGFP_L10a on the *VGLUT3*-BAC. These regulators might be missing in IHCs because of the absence of VGluT1 in these cells. Hence, VGluT3-positive IHCs are EGFP_L10a-negative. OHCs do not express any VGluT and are therefore GFP-negative on all section of all founder lines.

5.4.2 MOUSE STRAINS EXPRESSING EGFP_L10a IN SPIRAL GANGLIA

Spiral ganglion neurons (SGNs) of *VGLUT3*-EGFP_L10a mice exhibit a low but specific level of GFP-ir. So far expression of VGluT3 in SGNs has not been described. VGluT1 is likely the major glutamate transporter in SGNs[381] and stainings with an aVGluT3 ab in the organ of Corti of mice do not show labelled fibres in the intraganglionic spiral bundle[377].

SNAP25-EGFP_L10a mice exhibit high GFP-ir in SGNs and low GFP-ir in the o/C. SNAP25 is a member of the SNARE (soluble N-ethylmaleimide-sensitive factor attachment protein receptors) protein complex that mediates membrane docking and fusion of synaptic vesicles. The SNARE complexes of hair cells have a different composition than the ones of the CNS. Common to both is the presence of syntaxin-1, synaptobrevin (VAMP1) and the synaptic membrane synaptosome-associated protein (SNAP)25[382]. Thus it is surprising that no *SNAP25*-driven GFP expression is found in auditory hair cells (AHC) of *SNAP25*-EGFP_L10a mice. However, the extremely bright staining of SGNs could make this strain interesting for researchers interested in SGN physiology. In combination with data obtained from *NEUROD1*-EGFP_L10a mice these mice could furthermore help establishing differences in protein expression between apical and basal SGNs. *NeuroD1* encodes a member of the NeuroD family of basic helix-loop-helix (bHLH) transcription factors. In *NEUROD1*-EGFP_L10a cochleae it promotes expression of the fusion protein only in

SGNs of apical to midapical turns. Comparing the isolated translatomes of all (*SNAP25*) and apical SGNs (*NEUROD1*) will also indirectly tell which mRNAs are translated in basal turn SGNs.

5.4.3 CONCLUSIONS AND OUTLOOK

The analysis of *PRESTIN-EGFP_L10a* (Fig. 33B) and *VGLUT3-EGFP_L10a* (Fig. 34F) mice reveals a variability of GFP expression between different founder lines. In the seminal paper by Doyle et al. only little variation between independent founder lines was observed (comparable to variation between replicate samples isolated from the same line)[286]. Thus, they reason that the location of transgene insertion into the genome has little impact on GFP expression. Contrary to that, the two constructs of this work where several founder lines could be compared show varying GFP expression: *PRESTIN*-mouse/2751 exhibits patches of GFP-positive OHC of all three rows whereas in the other lines only single positive cells are found throughout the cochlea. The difference is even more pronounced in *VGLUT3*-mice as expression is seen in single positive (/1942) or up to ±50% positive VHCs (/1890). Differences in the procedure of BAC-transgenic mouse generation can be excluded as all examined *VGLUT3*-mice have been generated in the laboratory of J. Doyle. A conceivable possibility is that transcription or translation of *EGFP_L10a* in hair cells is more troublesome than in the brain. This, however, remains to be clarified.

None of the TRAP mouse lines under scrutiny showed EGFP_L10a expression in inner hair cells. Hitherto existing data suggest that IHCs of *CHRNA9*-EGFP_L10a, *VGLUT3*-EGFP_L10a and *SNAP25*-EGFP_L10a mice should be GFP-positive. The reasons for this phenomenon remain unclear but seem to be related to the TRAP methodology as other BAC-transgenic (reporter) mice exhibit fluorescence in IHCs (e.g. *CHRNA9*-GFP mice). Fortunately, EGFP_L10a was detected in OHCs and VHCs of some TRAP lines.

For the analysis of actively translated, hair-cell-specific mRNAs the *VGLUT3*-EGFP_L10a mouse strain is recommended. Due to the absence of GFP-tagged polysomes in the inner hair cells the isolated cochlear RNA (cDNA) sample will consist of VHC-derived transcripts. As the expression of this fusion protein in SGNs cannot be excluded it is recommended to separate mechanically the modiolus from the sensory-cell-containing epithelia. VHC physiology is not as thoroughly understood as AHC physiology. However, because of their similar function in the inner ear (converting mechanical into electrochemical signals) newly described VHC-transcripts (and -proteins) are likely expressed also by AHC – proteins of the elusive mechano-electrical transducer (MET) complex included. In concert with other, yet to be generated TRAP mice that express EGFP_L10a in IHCs and/or OHCs (possible promoters: *Otoferlin*, *Bassoon*) *VGLUT3*-EGFP_L10a mice might become a valuable tool for defining the difference of the translatome, and proteome, of vestibular and auditory hair cells.

Summary

Investigating the Contributions of α7 nAChR and TRPP2 to Mouse Auditory Function
Utilising Various Genetic Approaches

The tethered toxin (t-toxin) strategy for the recombinant expression of membrane-bound snake and snail toxins was developed based on the structure of mammalian prototoxins. It successfully has been used to modulate voltage-gated sodium and calcium channels in mice. The work here expands its usefulness to ligand-gated ion channels. It is shown that the tethered form of the conotoxin GID (tGID) completely blocks acetylcholine-induced α7 nicotinic acetylcholine receptor (nAChR) currents *in vitro*. Furthermore, for the first time the transgenic expression of *tGID* in mice is demonstrated. Hereby the expression is successfully restricted to one cochlear cell type (spiral ganglion neurons, SGNs). SGN nAChRs are thought to be involved in lateral olivocochlear (LOC) signalling. The assumed blocking of α7 nAChRs by tGID has no influence on the LOC system, though. However, this is not due to the t-toxin approach as recent data suggest that not the targeted nAChRs but rather muscarinic receptors are involved in LOC signalling.

TRP channels are important for mechanosensation in several animal models and physiological systems. This work presents data from reporter mice that suggest a function for Trpp2 and Pc-1 proteins in the auditory system. In particular it is shown that Trpp2 is expressed specifically from birth until hearing onset by few neurons in the cochlear nucleus and by the majority of SGNs. Few SGNs presumably remain Trpp2-positive even beyond hearing onset and are tentatively classified as type III SGNs. The presence of a third SGN subtype is also suggested by additional (immuno)histological findings at P24. For the first time this study describes a TRPP2-dependent phenotype in mammals outside the kidney. The accomplished neuron-specific knockout of *Trpp2* results in reduced levels of *Trpp2* in SGNs and a complete absence of *Trpp2* in the brainstem. This leads to a change of the amplitude of the compound action potential in auditory brainstem response recordings. It is hypothesised that the loss of Trpp2 in SGNs or cochlear nucleus cells influences the globular (bushy) cell pathway in a way that overall network activity in the lower auditory brainstem is increased.

Lastly, this report characterises transgenic mouse lines that specifically express the fusion protein EGFP_L10a in different inner ear cell types. Following the TRAP methodology these BAC-transgenic mice have been shown to be valuable tools for the identification of yet unknown proteins. Notably, *VGLUT3*-EGFP_L10a and *SNAP25*-EGFP_L10a mice will be useful for ribosome profiling of hair cells and spiral ganglion neurons, respectively. Ultimately, these mice could help to identify low-level transcripts of proteins that are part of the mechano-electrical transducer (MET) apparatus.

In conclusion this work presents evidence for the general applicability of two novel genetic methodologies in the inner ear (t-toxins, TRAP). Using a well-established method (Cre-loxP-system) it could additionally be shown that the ion channel TRPP2 fulfils a substantial role in auditory processing.

Zusammenfassung

Untersuchung der Beiträge von α7 nAChR und TRPP2 zu Hörprozessen in der Maus
durch verschiedene genetische Ansätze

Basierend auf der Struktur von in Säugetieren nachgewiesenen Prototoxinen wurde eine Methode zur rekombinanten Expression von membrangebundenen Schnecken- und Schlangentoxinen entwickelt: die Methode der angehefteten Toxine (tethered toxins). Diese Technologie wurde bereits erfolgreich zur Regulierung von spannungsabhängigen Natrium- und Kalziumkanälen in Mäusen angewandt. Die vorliegende Arbeit erweitert den Anwendungsbereich auf ligandenabhängige Ionenkanäle. Es wird gezeigt, dass das angeheftete Konotoxin GID (tGID) den nikotinischen Azetylcholinrezeptor α7 *in vitro* vollständig inhibiert. Darüber hinaus konnte zum ersten Mal die transgene Expression von *tGID* in Mäusen gezeigt werden. Die Expression wurde hierbei erfolgreich auf einen einzigen Zelltyp der Cochlea, das Spiralganglienneuron (SGN), beschränkt. Die nAChR der SGN werden mit dem lateralen olivocochleären (LOC) Signalweg in Verbindung gebracht. Allerdings hat die angenommene Inhibierung der α7 Rezeptoren durch tGID keinen messbaren Einfluss auf den LOC Signalweg. Dies ist jedoch nicht auf die Methode der angehefteten Toxine zurückzuführen. Vielmehr wurde kürzlich gezeigt, dass muskarinische – und nicht die in dieser Studie anvisierten nikotinischen – Rezeptoren an der cholinergen Erregungsübertragung des LOC Signalweges beteiligt sind.

TRP Ionenkanäle sind wichtig für Sinnesempfindungen, die durch mechanische Reize hervorgerufen werden. Die mithilfe von Reportermauslinien erlangten Ergebnisse dieser Arbeit weisen auf eine Beteiligung von Trpp2 und Pc-1 an Prozessen im Hörsystem hin. Insbesondere wird gezeigt, dass Trpp2 von der Geburt bis zum Hörbeginn von einigen Cochleariskernneuronen und der Mehrzahl der SGN exprimiert wird. Einige SGN bleiben vermutlich darüber hinaus Trpp2-positiv und werden vorläufig als SGN des Typs III klassifiziert. Die Existenz eines dritten Subtyps von SGN wird durch weitere, an P24 Mäusen gewonnene (immun)histologische Erkenntnisse dieser Untersuchung gestützt. Darüber hinaus wird in dieser Arbeit zum ersten Mal ein TRPP2-abhängiger Phänotyp in Säugetieren beschrieben, der nicht mit Nierenfunktionen assoziiert ist. Das spezifische Ausschalten von *Trpp2* in Neuronen der Maus führt zu einer Verringerung von *Trpp2*-Transkripten in der Cochlea und zu einem vollständigen Verlust dieser im Hirnstamm. Audiometriemessungen zeigen eine Amplitudenänderung des summierten Aktionspotenzials. Dieses Ergebnis stützt die Annahme, dass in den getesteten Mäusen der Verlust von funktionalem Trpp2 in SGN oder den Cochleariskernen den Signalweg der runden Krauszellen derart beeinflusst, dass die gesamte Netzwerkaktivität des auditorischen Hirnstamms erhöht wird.

Schließlich wurden im Rahmen dieser Studie transgene Mauslinien charakterisiert, die das Fusionsprotein EGFP_L10a in verschiedenen Zelltypen des Innenohres exprimieren. Diese Linien bilden die Voraussetzung für die Anwendung der TRAP-Technologie zur Bestimmung unbekannter Proteine. Es wurde dargelegt, dass insbesondere die Linien *VGLUT3*-EGFP_L10a und *SNAP25*-EGFP_L10a für die Ermittlung des Translatoms von Haarzellen beziehungsweise SGN wertvoll werden könnten. Letztendlich

wird dies auch die Identifizierung von seltenen Proteintranskripten des mechanoelektrischen Signalumwandlerkomplexes (MET) voranbringen.

Die Ergebnisse dieser Arbeit belegen die allgemeine Eignung zweier neuer, biotechnologischer Methoden (angeheftete Toxine, TRAP) zu weitergehenden Untersuchungen von Innenohrprozessen. Mit Hilfe der konditionellen Transgenese konnte zusätzlich gezeigt werden, dass der Ionenkanal TRPP2 eine wesentliche Aufgabe bei der Verarbeitung auditorischer Reize erfüllt.

APPENDIX

Index of figures

Index of tables

Abbreviations

ab(s)	antibody(-ies)
ABR / BERA	auditory brainstem response / brainstem evoked response audiometry
ACh	acetylcholine
AChE	acetylcholine esterase
AHC	auditory hair cell
AVCN	anterior ventral cochlear nucleus
BAC	bacterial artificial chromosome
BCIP	5-Bromo-4-Chloro-Chlor-3-indolylphosphate
BoC	border cells
BöC	cells of Böttcher
BSA	bovine serum albumin
CAP	compound action potential
CC	cells of Claudius
CD	collecting duct
cDNA	complementary DNA
CGRP	calcitonin gene-related peptide
ChAT	choline acetyltransferase
ChT1	high-affinity choline transporter 1
CN	cochlear nucleus / nuclei

CNS	central nervous system
DAS	dorsal acoustic stria
DCN	dorsal cochlear nucleus
DCT	distal convoluted tubule
DIG	dioxygenin
DMEM	Dulbecco's modified Eagle's medium
DMSO	dimethyl sulfoxide
DNA	deoxyribonucleic acid
dNTP	deoxynucleotidetriphosphate
DPOAE	distortion product otoacoustic emission
DRG	dorsal root ganglion
DTT	dithiothreitol
EDTA	ethylenediaminetetraacetic acid
EGFP	enhanced green fluorescent protein
FCS	fetal calf serum
GABA	γ-aminobutyric acid
GENSAT	gene expression atlas of the central nervous system
GID	first (**I**) α-conotoxin isolated from *Conus **g**eographus* (variant **D)**
GPI	glycosylphosphatidylinositol
HCl	hydrochloric acid
HeC	Hensen's cell
IC	inferior colliculus / colliculi
IGSB	intraganglionic spiral bundle
ihc	immunohistochemistry
IHC	inner hair cell
IPC	inner pillar cell (rod)
IPhC	inner phalangeal cells
ir	immunoreactivity
ISB	inner spiral bundle
ISH	*in situ* hybridisation
KO	knockout
LOC	lateral olivocochlear (fibre / tract / bundle)
MilliQ / MQ	ultrafiltrated water (from MilliQ-Plus water system, Millipore)
MOC	medial olivocochlear (fibre / tract / bundle)
mRNA	messenger ribonucleic acid
nAChR	nicotinic acetylcholine receptor
NaCl	sodium chloride
NaOH	sodium hydroxide
NBT	nitro blue tetrazolium chloride
OD	optical density
OHC	outer hair cell
OPC	outer pillar cell (rod)
OPhC	outer phanlangeal cells (Deiters' cells)
OSL	osseous spiral lamina
o/C	organ of Corti
o/n	over night
PDGF	platelet-derived growth factor
PBS	phosphate buffered saline
PBT	PBS-Tween-20
PC	fusion protein of the PDGF TM-domain and mCherry
PCR	polymerase chain reaction
PE	fusion protein of the PDGF TM-domain and EGFP
PFA	paraformaldehyde
pH	potentium hydrogenii
PKD1	polycystin-1 (gene product of polycystic kidney disease 1)
PM	plasma membrane
PNS	peripheral nervous system
PVCN	posterior ventral cochlear nucleus
RNase	ribonuclease
rpm	revolutions per minute

RT	room temperature
SDS	sodium dodecyl sulphate
SG(N)	spiral ganglion (neuron / cell)
SH	Southern hybridisation
SOC	superior olivary complex
SSC	sodiumchloride-sodiumcitrate
TAE	Tris-acetate EDTA
TAL	thick ascending loops of Henle
TE	Tris-EDTA
TM	transmembrane domain
TMJ	temporomandibular joint
TMRD	tetramethylrhodamine-conjugated dextran
Tris	Tris-(hydroxymethyl-) aminoethane
t-RNA	transfer ribonucleic acid
TRP	transient receptor potential (ion channel)
TRPP2	TRP channel polycystin-2
VAChT	vesicular acetylcholine transporter
VAS	ventral acoustic stria
VGSC	voltage-gated sodium channel
VNTB	ventral nucleus of the trapezoid body

REFERENCES

1. Fuchs, P.A., Glowatzki, E. & Moser, T. The afferent synapse of cochlear hair cells. *Curr. Opin. Neurobiol* **13**, 452-458 (2003).
2. Hawkins, R.D. & Lovett, M. The developmental genetics of auditory hair cells. *Hum. Mol. Genet* **13 Spec No 2**, R289-296 (2004).
3. Gillespie, P.G. & Müller, U. Mechanotransduction by hair cells: models, molecules, and mechanisms. *Cell* **139**, 33-44 (2009).
4. Spoendlin, H. Anatomy of cochlear innervation. *Am J Otolaryngol* **6**, 453-467 (1985).
5. Rubel, E.W. & Fritzsch, B. Auditory system development: primary auditory neurons and their targets. *Annu. Rev. Neurosci* **25**, 51-101 (2002).
6. Guinan, J.J. Olivocochlear efferents: anatomy, physiology, function, and the measurement of efferent effects in humans. *Ear Hear* **27**, 589-607 (2006).
7. Grant, L. & Fuchs, P.A. Auditory transduction in the mouse. *Pflugers Arch* **454**, 793-804 (2007).
8. Rusznák, Z. & Szucs, G. Spiral ganglion neurones: an overview of morphology, firing behaviour, ionic channels and function. *Pflugers Arch* **457**, 1303-25 (2009).
9. Fritzsch, B., Beisel, K.W. & Bermingham, N.A. Developmental evolutionary biology of the vertebrate ear: conserving mechanoelectric transduction and developmental pathways in diverging morphologies. *Neuroreport* **11**, R35-44 (2000).
10. Fritzsch, B. & Beisel, K.W. Keeping sensory cells and evolving neurons to connect them to the brain: molecular conservation and novelties in vertebrate ear development. *Brain Behav. Evol* **64**, 182-197 (2004).
11. Felix, H. Anatomical differences in the peripheral auditory system of mammals and man. A mini review. *Adv. Otorhinolaryngol* **59**, 1-10 (2002).
12. Pujol, R. & Puel, J.L. Excitotoxicity, synaptic repair, and functional recovery in the mammalian cochlea: a review of recent findings. *Ann. N. Y. Acad. Sci* **884**, 249-254 (1999).
13. Thiers, F.A., Nadol, J.B. & Liberman, M.C. Reciprocal synapses between outer hair cells and their afferent terminals: evidence for a local neural network in the mammalian cochlea. *J. Assoc. Res. Otolaryngol* **9**, 477-489 (2008).
14. Rask-Andersen, H., Tylstedt, S., Kinnefors, A. & Illing, R. Synapses on human spiral ganglion cells: a transmission electron microscopy and immunohistochemical study. *Hear. Res* **141**, 1-11 (2000).
15. Berglund, A.M. & Ryugo, D.K. Hair cell innervation by spiral ganglion neurons in the mouse. *J. Comp. Neurol* **255**, 560-570 (1987).
16. Jagger, D.J. & Housley, G.D. Membrane properties of type II spiral ganglion neurones identified in a neonatal rat cochlear slice. *J Physiol* **552**, 525-33 (2003).
17. Hackney, C.M., Osen, K.K. & Kolston, J. Anatomy of the cochlear nuclear complex of guinea pig. *Anat. Embryol* **182**, 123-149 (1990).
18. Cant, N.B. & Benson, C.G. Parallel auditory pathways: projection patterns of the different neuronal populations in the dorsal and ventral cochlear nuclei. *Brain Res. Bull* **60**, 457-474 (2003).
19. Melcher, J.R. & Kiang, N.Y. Generators of the brainstem auditory evoked potential in cat. III: Identified cell populations. *Hear. Res* **93**, 52-71 (1996).
20. Masterton, R.B. Role of the central auditory system in hearing: the new direction. *Trends Neurosci* **15**, 280-285 (1992).
21. Oliver, D.L. Ascending efferent projections of the superior olivary complex. *Microsc.*

Res. Tech **51**, 355-363 (2000).
22. Reuss, S. Introduction to the superior olivary complex. *Microsc. Res. Tech* **51**, 303-306 (2000).
23. Thompson, A.M. & Schofield, B.R. Afferent projections of the superior olivary complex. *Microsc. Res. Tech* **51**, 330-354 (2000).
24. Pollak, G.D., Burger, R.M. & Klug, A. Dissecting the circuitry of the auditory system. *Trends Neurosci* **26**, 33-39 (2003).
25. Katz, E. et al. Developmental regulation of nicotinic synapses on cochlear inner hair cells. *J Neurosci* **24**, 7814-20 (2004).
26. Morley, B.J. Nicotinic cholinergic intercellular communication: implications for the developing auditory system. *Hear Res* **206**, 74-88 (2005).
27. Elgoyhen, A.B., Johnson, D.S., Boulter, J., Vetter, D.E. & Heinemann, S. Alpha 9: an acetylcholine receptor with novel pharmacological properties expressed in rat cochlear hair cells. *Cell* **79**, 705-715 (1994).
28. Elgoyhen, A.B. et al. alpha10: a determinant of nicotinic cholinergic receptor function in mammalian vestibular and cochlear mechanosensory hair cells. *Proc. Natl. Acad. Sci. U.S.A* **98**, 3501-3506 (2001).
29. Felix, D. & Ehrenberger, K. The efferent modulation of mammalian inner hair cell afferents. *Hear. Res* **64**, 1-5 (1992).
30. Grando, S.A. Biological functions of keratinocyte cholinergic receptors. *J. Investig. Dermatol. Symp. Proc* **2**, 41-48 (1997).
31. Wessler, I., Kirkpatrick, C.J. & Racké, K. Non-neuronal acetylcholine, a locally acting molecule, widely distributed in biological systems: expression and function in humans. *Pharmacol. Ther* **77**, 59-79 (1998).
32. Gahring, L.C., Persiyanov, K. & Rogers, S.W. Neuronal and astrocyte expression of nicotinic receptor subunit beta4 in the adult mouse brain. *J. Comp. Neurol* **468**, 322-333 (2004).
33. Wang, H. et al. Nicotinic acetylcholine receptor alpha7 subunit is an essential regulator of inflammation. *Nature* **421**, 384-388 (2003).
34. Peng, H. et al. Characterization of the human nicotinic acetylcholine receptor subunit alpha (alpha) 9 (CHRNA9) and alpha (alpha) 10 (CHRNA10) in lymphocytes. *Life Sci* **76**, 263-280 (2004).
35. Skok, M., Grailhe, R. & Changeux, J. Nicotinic receptors regulate B lymphocyte activation and immune response. *Eur. J. Pharmacol* **517**, 246-251 (2005).
36. Macklin, K.D., Maus, A.D., Pereira, E.F., Albuquerque, E.X. & Conti-Fine, B.M. Human vascular endothelial cells express functional nicotinic acetylcholine receptors. *J. Pharmacol. Exp. Ther* **287**, 435-439 (1998).
37. Nguyen, V.T., Ndoye, A. & Grando, S.A. Novel human alpha9 acetylcholine receptor regulating keratinocyte adhesion is targeted by Pemphigus vulgaris autoimmunity. *Am. J. Pathol* **157**, 1377-1391 (2000).
38. Arredondo, J. et al. Central role of alpha7 nicotinic receptor in differentiation of the stratified squamous epithelium. *J. Cell Biol* **159**, 325-336 (2002).
39. Contant, C., Umbriaco, D., Garcia, S., Watkins, K.C. & Descarries, L. Ultrastructural characterization of the acetylcholine innervation in adult rat neostriatum. *Neuroscience* **71**, 937-947 (1996).
40. Descarries, L. The hypothesis of an ambient level of acetylcholine in the central nervous system. *J. Physiol. Paris* **92**, 215-220 (1998).
41. Le Novère, N. & Changeux, J.P. Molecular evolution of the nicotinic acetylcholine receptor: an example of multigene family in excitable cells. *J. Mol. Evol* **40**, 155-172 (1995).
42. Leonard, S. & Bertrand, D. Neuronal nicotinic receptors: from structure to function.

Nicotine Tob. Res **3**, 203-223 (2001).
43. Lustig, L.R. Nicotinic acetylcholine receptor structure and function in the efferent auditory system. *Anat Rec A Discov Mol Cell Evol Biol* **288**, 424-434 (2006).
44. Geerts, H., Finkel, L., Carr, R. & Spiros, A. Nicotinic receptor modulation: advantages for successful Alzheimer's disease therapy. *J. Neural Transm. Suppl* 203-216 (2002).
45. O'Neill, M.J., Murray, T.K., Lakics, V., Visanji, N.P. & Duty, S. The role of neuronal nicotinic acetylcholine receptors in acute and chronic neurodegeneration. *Curr Drug Targets CNS Neurol Disord* **1**, 399-411 (2002).
46. Fucile, S. Ca2+ permeability of nicotinic AChRs. *Cell Calcium* **35**, 1-8 (2004).
47. Eybalin, M. Neurotransmitters and neuromodulators of the mammalian cochlea. *Physiol. Rev* **73**, 309-373 (1993).
48. Maison, S.F., Adams, J.C. & Liberman, M.C. Olivocochlear innervation in the mouse: immunocytochemical maps, crossed versus uncrossed contributions, and transmitter colocalization. *J. Comp. Neurol* **455**, 406-416 (2003).
49. Vetter, D.E., Adams, J.C. & Mugnaini, E. Chemically distinct rat olivocochlear neurons. *Synapse* **7**, 21-43 (1991).
50. Dezaki, K., Kimura, I., Tsuneki, H. & Kimura, M. Enhancement by calcitonin gene-related peptide of non-contractile Ca2(+)-induced nicotinic receptor desensitization at the mouse neuromuscular junction. *Br. J. Pharmacol* **118**, 1971-1976 (1996).
51. Shigemoto, T. & Ohmori, H. Muscarinic agonists and ATP increase the intracellular Ca2+ concentration in chick cochlear hair cells. *J. Physiol. (Lond.)* **420**, 127-148 (1990).
52. Murugasu, E. & Russell, I.J. The effect of efferent stimulation on basilar membrane displacement in the basal turn of the guinea pig cochlea. *J. Neurosci* **16**, 325-332 (1996).
53. Vetter, D.E. et al. Role of alpha9 nicotinic ACh receptor subunits in the development and function of cochlear efferent innervation. *Neuron* **23**, 93-103 (1999).
54. Luebke, A.E. & Foster, P.K. Variation in inter-animal susceptibility to noise damage is associated with alpha 9 acetylcholine receptor subunit expression level. *J. Neurosci* **22**, 4241-4247 (2002).
55. Maison, S.F., Luebke, A.E., Liberman, M.C. & Zuo, J. Efferent protection from acoustic injury is mediated via alpha9 nicotinic acetylcholine receptors on outer hair cells. *J Neurosci* **22**, 10838-46 (2002).
56. Glowatzki, E. & Fuchs, P.A. Cholinergic synaptic inhibition of inner hair cells in the neonatal mammalian cochlea. *Science* **288**, 2366-2368 (2000).
57. Morley, B.J. & Simmons, D.D. Developmental mRNA expression of the alpha10 nicotinic acetylcholine receptor subunit in the rat cochlea. *Brain Res. Dev. Brain Res* **139**, 87-96 (2002).
58. Morley, B.J., Li, H.S., Hiel, H., Drescher, D.G. & Elgoyhen, A.B. Identification of the subunits of the nicotinic cholinergic receptors in the rat cochlea using RT-PCR and in situ hybridization. *Brain Res Mol Brain Res* **53**, 78-87 (1998).
59. Simmons, D.D. Development of the inner ear efferent system across vertebrate species. *J. Neurobiol* **53**, 228-250 (2002).
60. Vetter, D.E. et al. The alpha10 nicotinic acetylcholine receptor subunit is required for normal synaptic function and integrity of the olivocochlear system. *Proc Natl Acad Sci U S A* **104**, 20594-9 (2007).
61. Gómez-Casati, M.E. et al. Electrical properties and functional expression of ionic channels in cochlear inner hair cells of mice lacking the alpha10 nicotinic cholinergic receptor subunit. *J. Assoc. Res. Otolaryngol* **10**, 221-232 (2009).
62. Murthy, V. et al. SK2 channels are required for function and long-term survival of efferent synapses on mammalian outer hair cells. *Mol. Cell. Neurosci* **40**, 39-49 (2009).
63. Johnson, S.L., Adelman, J.P. & Marcotti, W. Genetic deletion of SK2 channels in mouse inner hair cells prevents the developmental linearization in the Ca2+ dependence of

exocytosis. *J. Physiol. (Lond.)* **583**, 631-646 (2007).
64. Kong, J., Adelman, J.P. & Fuchs, P.A. Expression of the SK2 calcium-activated potassium channel is required for cholinergic function in mouse cochlear hair cells. *J. Physiol. (Lond.)* **586**, 5471-5485 (2008).
65. Satake, M. & Liberman, M.C. Morphological subclasses of lateral olivocochlear terminals? Ultrastructural analysis of inner spiral bundle in cat and guinea pig. *J. Comp. Neurol* **371**, 621-632 (1996).
66. Safieddine, S., Prior, A.M. & Eybalin, M. Choline acetyltransferase, glutamate decarboxylase, tyrosine hydroxylase, calcitonin gene-related peptide and opioid peptides coexist in lateral efferent neurons of rat and guinea-pig. *Eur. J. Neurosci* **9**, 356-367 (1997).
67. Darrow, K.N., Simons, E.J., Dodds, L. & Liberman, M.C. Dopaminergic innervation of the mouse inner ear: evidence for a separate cytochemical group of cochlear efferent fibers. *J. Comp. Neurol* **498**, 403-414 (2006).
68. Warr, W.B., Boche, J.B. & Neely, S.T. Efferent innervation of the inner hair cell region: origins and terminations of two lateral olivocochlear systems. *Hear. Res* **108**, 89-111 (1997).
69. Le Prell, C.G., Shore, S.E., Hughes, L.F. & Bledsoe, S.C. Disruption of lateral efferent pathways: functional changes in auditory evoked responses. *J. Assoc. Res. Otolaryngol* **4**, 276-290 (2003).
70. Groff, J.A. & Liberman, M.C. Modulation of cochlear afferent response by the lateral olivocochlear system: activation via electrical stimulation of the inferior colliculus. *J. Neurophysiol* **90**, 3178-3200 (2003).
71. Le Prell, C.G., Halsey, K., Hughes, L.F., Dolan, D.F. & Bledsoe, S.C. Disruption of lateral olivocochlear neurons via a dopaminergic neurotoxin depresses sound-evoked auditory nerve activity. *J. Assoc. Res. Otolaryngol* **6**, 48-62 (2005).
72. Liberman, M.C. Effects of chronic cochlear de-efferentation on auditory-nerve response. *Hear. Res* **49**, 209-223 (1990).
73. Darrow, K.N., Maison, S.F. & Liberman, M.C. Cochlear efferent feedback balances interaural sensitivity. *Nat. Neurosci* **9**, 1474-1476 (2006).
74. Le Prell, C.G. Role for the lateral olivocochlear neurons in auditory function. Focus on "Selective removal of lateral olivocochlear efferents increases vulnerability to acute acoustic injury". *J. Neurophysiol* **97**, 963-965 (2007).
75. Darrow, K.N., Maison, S.F. & Liberman, M.C. Selective removal of lateral olivocochlear efferents increases vulnerability to acute acoustic injury. *J. Neurophysiol* **97**, 1775-1785 (2007).
76. Bozzi, Y. & Borrelli, E. Dopamine in neurotoxicity and neuroprotection: what do D2 receptors have to do with it? *Trends Neurosci* **29**, 167-174 (2006).
77. Mudo, G., Belluardo, N. & Fuxe, K. Nicotinic receptor agonists as neuroprotective/neurotrophic drugs. Progress in molecular mechanisms. *J Neural Transm* **114**, 135-147 (2007).
78. Liberman, M.C., Dodds, L.W. & Pierce, S. Afferent and efferent innervation of the cat cochlea: quantitative analysis with light and electron microscopy. *J. Comp. Neurol* **301**, 443-460 (1990).
79. Herber, D.L., Severance, E.G., Cuevas, J., Morgan, D. & Gordon, M.N. Biochemical and histochemical evidence of nonspecific binding of alpha7nAChR antibodies to mouse brain tissue. *J. Histochem. Cytochem* **52**, 1367-1376 (2004).
80. Moser, N. et al. Evaluating the suitability of nicotinic acetylcholine receptor antibodies for standard immunodetection procedures. *J. Neurochem* **102**, 479-492 (2007).
81. Bao, J. et al. Requirement of nicotinic acetylcholine receptor subunit beta2 in the maintenance of spiral ganglion neurons during aging. *J Neurosci* **25**, 3041-5 (2005).

82. Drescher, D.G. et al. Analysis of nicotinic acetylcholine receptor subunits in the cochlea of the mouse. *Comp. Biochem. Physiol. C, Pharmacol. Toxicol. Endocrinol* **112**, 267-273 (1995).
83. Flores, C.M., DeCamp, R.M., Kilo, S., Rogers, S.W. & Hargreaves, K.M. Neuronal nicotinic receptor expression in sensory neurons of the rat trigeminal ganglion: demonstration of alpha3beta4, a novel subtype in the mammalian nervous system. *J. Neurosci* **16**, 7892-7901 (1996).
84. Yeh, J.J. et al. Neuronal nicotinic acetylcholine receptor alpha3 subunit protein in rat brain and sympathetic ganglion measured using a subunit-specific antibody: regional and ontogenic expression. *J. Neurochem* **77**, 336-346 (2001).
85. Rau, K.K., Johnson, R.D. & Cooper, B.Y. Nicotinic AChR in subclassified capsaicin-sensitive and -insensitive nociceptors of the rat DRG. *J. Neurophysiol* **93**, 1358-1371 (2005).
86. Gerzanich, V., Kuryatov, A., Anand, R. & Lindstrom, J. "Orphan" alpha6 nicotinic AChR subunit can form a functional heteromeric acetylcholine receptor. *Mol. Pharmacol* **51**, 320-327 (1997).
87. Léna, C. et al. Diversity and distribution of nicotinic acetylcholine receptors in the locus ceruleus neurons. *Proc. Natl. Acad. Sci. U.S.A* **96**, 12126-12131 (1999).
88. Khiroug, S.S. et al. Rat nicotinic ACh receptor alpha7 and beta2 subunits co-assemble to form functional heteromeric nicotinic receptor channels. *J. Physiol. (Lond.)* **540**, 425-434 (2002).
89. Berg, D.K. & Conroy, W.G. Nicotinic alpha 7 receptors: synaptic options and downstream signaling in neurons. *J. Neurobiol* **53**, 512-523 (2002).
90. Tohgi, H., Utsugisawa, K. & Nagane, Y. Protective effect of nicotine through nicotinic acetylcholine receptor alpha 7 on hypoxia-induced membrane disintegration and DNA fragmentation of cultured PC12 cells. *Neurosci. Lett* **285**, 91-94 (2000).
91. Dajas-Bailador, F. & Wonnacott, S. Nicotinic acetylcholine receptors and the regulation of neuronal signalling. *Trends Pharmacol. Sci* **25**, 317-324 (2004).
92. López, M.G. et al. Unmasking the functions of the chromaffin cell alpha7 nicotinic receptor by using short pulses of acetylcholine and selective blockers. *Proc. Natl. Acad. Sci. U.S.A* **95**, 14184-14189 (1998).
93. Zbarsky, V., Thomas, J. & Greenfield, S. Bioactivity of a peptide derived from acetylcholinesterase: involvement of an ivermectin-sensitive site on the alpha 7 nicotinic receptor. *Neurobiol. Dis* **16**, 283-289 (2004).
94. Greenfield, S.A., Day, T., Mann, E.O. & Bermudez, I. A novel peptide modulates alpha7 nicotinic receptor responses: implications for a possible trophic-toxic mechanism within the brain. *J. Neurochem* **90**, 325-331 (2004).
95. Bond, C.E., Zimmermann, M. & Greenfield, S.A. Upregulation of alpha7 Nicotinic Receptors by Acetylcholinesterase C-Terminal Peptides. *PLoS ONE* **4**, e4846 (2009).
96. Morley, B.J. The embryonic and post-natal expression of the nicotinic receptor alpha 3-subunit in rat lower brainstem. *Brain Res. Mol. Brain Res* **48**, 407-412 (1997).
97. Winzer-Serhan, U.H. & Leslie, F.M. Codistribution of nicotinic acetylcholine receptor subunit alpha3 and beta4 mRNAs during rat brain development. *J. Comp. Neurol* **386**, 540-554 (1997).
98. Hanson, M.G. & Landmesser, L.T. Characterization of the circuits that generate spontaneous episodes of activity in the early embryonic mouse spinal cord. *J. Neurosci* **23**, 587-600 (2003).
99. Bansal, A. et al. Mice lacking specific nicotinic acetylcholine receptor subunits exhibit dramatically altered spontaneous activity patterns and reveal a limited role for retinal waves in forming ON and OFF circuits in the inner retina. *J. Neurosci* **20**, 7672-7681 (2000).

100. Maggi, L., Le Magueresse, C., Changeux, J. & Cherubini, E. Nicotine activates immature "silent" connections in the developing hippocampus. *Proc. Natl. Acad. Sci. U.S.A* **100**, 2059-2064 (2003).
101. Ene, F.A., Kullmann, P.H.M., Gillespie, D.C. & Kandler, K. Glutamatergic calcium responses in the developing lateral superior olive: receptor types and their specific activation by synaptic activity patterns. *J. Neurophysiol* **90**, 2581-2591 (2003).
102. Montell, C. The TRP superfamily of cation channels. *Sci. STKE* **2005**, re3 (2005).
103. Nilius, B. & Voets, T. TRP channels: a TR(I)P through a world of multifunctional cation channels. *Pflugers Arch* **451**, 1-10 (2005).
104. Damann, N., Voets, T. & Nilius, B. TRPs in our senses. *Curr. Biol* **18**, R880-889 (2008).
105. Cosens, D.J. & Manning, A. Abnormal electroretinogram from a Drosophila mutant. *Nature* **224**, 285-287 (1969).
106. Montell, C. & Rubin, G.M. Molecular characterization of the Drosophila trp locus: a putative integral membrane protein required for phototransduction. *Neuron* **2**, 1313-1323 (1989).
107. Lin, S. & Corey, D.P. TRP channels in mechanosensation. *Curr. Opin. Neurobiol* **15**, 350-357 (2005).
108. Ramsey, I.S., Delling, M. & Clapham, D.E. An introduction to TRP channels. *Annu. Rev. Physiol* **68**, 619-647 (2006).
109. Dong, X., Wang, X. & Xu, H. TRP channels of intracellular membranes. *J. Neurochem* **113**, 313-328 (2010).
110. Nilius, B., Owsianik, G., Voets, T. & Peters, J.A. Transient receptor potential cation channels in disease. *Physiol. Rev* **87**, 165-217 (2007).
111. Delmas, P. Polycystins: polymodal receptor/ion-channel cellular sensors. *Pflugers Arch* **451**, 264-276 (2005).
112. Delmas, P. Polycystins: from mechanosensation to gene regulation. *Cell* **118**, 145-148 (2004).
113. Nomura, H. et al. Identification of PKDL, a novel polycystic kidney disease 2-like gene whose murine homologue is deleted in mice with kidney and retinal defects. *J. Biol. Chem* **273**, 25967-25973 (1998).
114. Chen, X.Z. et al. Polycystin-L is a calcium-regulated cation channel permeable to calcium ions. *Nature* **401**, 383-386 (1999).
115. Shimizu, T., Janssens, A., Voets, T. & Nilius, B. Regulation of the murine TRPP3 channel by voltage, pH, and changes in cell volume. *Pflugers Arch* **457**, 795-807 (2009).
116. Lopez-Jimenez, N.D. et al. Two members of the TRPP family of ion channels, Pkd1l3 and Pkd2l1, are co-expressed in a subset of taste receptor cells. *J. Neurochem* **98**, 68-77 (2006).
117. Ishimaru, Y. et al. Transient receptor potential family members PKD1L3 and PKD2L1 form a candidate sour taste receptor. *Proc. Natl. Acad. Sci. U.S.A* **103**, 12569-12574 (2006).
118. Huang, A.L. et al. The cells and logic for mammalian sour taste detection. *Nature* **442**, 934-8 (2006).
119. Chang, R.B., Waters, H. & Liman, E.R. A proton current drives action potentials in genetically identified sour taste cells. *Proc Natl Acad Sci U S A* (2010).doi:10.1073/pnas.1013664107
120. Hughes, J., Ward, C.J., Aspinwall, R., Butler, R. & Harris, P.C. Identification of a human homologue of the sea urchin receptor for egg jelly: a polycystic kidney disease-like protein. *Hum. Mol. Genet* **8**, 543-549 (1999).
121. Sutton, K., Jungnickel, M., Ward, C., Harris, P. & Florman, H. Functional characterization of PKDREJ, a male germ cell-restricted polycystin. *JOURNAL OF CELLULAR PHYSIOLOGY* **209**, 493-500 (2006).

122. Koulen, P. et al. Polycystin-2 is an intracellular calcium release channel. *Nat. Cell Biol* **4**, 191-7 (2002).
123. Pritchard, L. et al. A human PKD1 transgene generates functional polycystin-1 in mice and is associated with a cystic phenotype. *Hum. Mol. Genet* **9**, 2617-2627 (2000).
124. Geng, L. et al. Syntaxin 5 regulates the endoplasmic reticulum channel-release properties of polycystin-2. *Proc. Natl. Acad. Sci. U.S.A* **105**, 15920-15925 (2008).
125. Tsiokas, L. Function and regulation of TRPP2 at the plasma membrane. *Am. J. Physiol. Renal Physiol* **297**, F1-9 (2009).
126. Cantiello, H.F. Regulation of calcium signaling by polycystin-2. *Am J Physiol Renal Physiol* **286**, F1012-29 (2004).
127. Giamarchi, A. et al. The versatile nature of the calcium-permeable cation channel TRPP2. *EMBO Rep* **7**, 787-93 (2006).
128. Tsiokas, L., Kim, S. & Ong, E. Cell biology of polycystin-2. *Cell. Signal* **19**, 444-453 (2007).
129. Köttgen, M. TRPP2 and autosomal dominant polycystic kidney disease. *Biochim Biophys Acta* **1772**, 836-50 (2007).
130. McGrath, J., Somlo, S., Makova, S., Tian, X. & Brueckner, M. Two populations of node monocilia initiate left-right asymmetry in the mouse. *Cell* **114**, 61-73 (2003).
131. Pennekamp, P. et al. The ion channel polycystin-2 is required for left-right axis determination in mice. *Curr. Biol* **12**, 938-943 (2002).
132. Tsiokas, L. et al. Specific association of the gene product of PKD2 with the TRPC1 channel. *Proc Natl Acad Sci U S A* **96**, 3934-9 (1999).
133. Zhang, P. et al. The multimeric structure of polycystin-2 (TRPP2): structural-functional correlates of homo- and hetero-multimers with TRPC1. *Hum. Mol. Genet* **18**, 1238-1251 (2009).
134. Bai, C. et al. Formation of a new receptor-operated channel by heteromeric assembly of TRPP2 and TRPC1 subunits. *EMBO Rep* (2008).at <353>
135. Köttgen, M. et al. TRPP2 and TRPV4 form a polymodal sensory channel complex. *J Cell Biol* **182**, 437-47 (2008).
136. Hackmann, K. et al. A splice form of polycystin-2, lacking exon 7, does not interact with polycystin-1. *Hum. Mol. Genet* **14**, 3249-3262 (2005).
137. Qian, F. et al. PKD1 interacts with PKD2 through a probable coiled-coil domain. *Nat. Genet* **16**, 179-183 (1997).
138. Tsiokas, L., Kim, E., Arnould, T., Sukhatme, V.P. & Walz, G. Homo- and heterodimeric interactions between the gene products of PKD1 and PKD2. *Proc. Natl. Acad. Sci. U.S.A* **94**, 6965-6970 (1997).
139. Foggensteiner, L. et al. Cellular and subcellular distribution of polycystin-2, the protein product of the PKD2 gene. *J. Am. Soc. Nephrol* **11**, 814-827 (2000).
140. Hanaoka, K. et al. Co-assembly of polycystin-1 and -2 produces unique cation-permeable currents. *Nature* **408**, 990-994 (2000).
141. Nauli, S.M. et al. Polycystins 1 and 2 mediate mechanosensation in the primary cilium of kidney cells. *Nat. Genet* **33**, 129-137 (2003).
142. Delmas, P. et al. Gating of the polycystin ion channel signaling complex in neurons and kidney cells. *FASEB J* **18**, 740-742 (2004).
143. Delmas, P. et al. Constitutive activation of G-proteins by polycystin-1 is antagonized by polycystin-2. *J. Biol. Chem* **277**, 11276-11283 (2002).
144. Mochizuki, T. et al. PKD2, a gene for polycystic kidney disease that encodes an integral membrane protein. *Science* **272**, 1339-1342 (1996).
145. Zerres, K. et al. Prenatal diagnosis of autosomal recessive polycystic kidney disease (ARPKD): molecular genetics, clinical experience, and fetal morphology. *Am. J. Med. Genet* **76**, 137-144 (1998).

146. Zhang, M. et al. PKHD1 protein encoded by the gene for autosomal recessive polycystic kidney disease associates with basal bodies and primary cilia in renal epithelial cells. *Proc. Natl. Acad. Sci. U.S.A* **101**, 2311-2316 (2004).
147. Kim, I. et al. Fibrocystin/polyductin modulates renal tubular formation by regulating polycystin-2 expression and function. *J. Am. Soc. Nephrol* **19**, 455-468 (2008).
148. Kim, I. et al. Conditional mutation of Pkd2 causes cystogenesis and upregulates beta-catenin. *J. Am. Soc. Nephrol* **20**, 2556-2569 (2009).
149. Wu, G. & Somlo, S. Molecular genetics and mechanism of autosomal dominant polycystic kidney disease. *Mol. Genet. Metab* **69**, 1-15 (2000).
150. Sutters, M. & Germino, G.G. Autosomal dominant polycystic kidney disease: molecular genetics and pathophysiology. *J. Lab. Clin. Med* **141**, 91-101 (2003).
151. Wang, K. et al. Evidence for pathogenicity of atypical splice mutations in autosomal dominant polycystic kidney disease. *Clin J Am Soc Nephrol* **4**, 442-449 (2009).
152. Somlo, S. & Markowitz, G.S. The pathogenesis of autosomal dominant polycystic kidney disease: an update. *Curr. Opin. Nephrol. Hypertens* **9**, 385-394 (2000).
153. Bhunia, A.K. et al. PKD1 induces p21(waf1) and regulation of the cell cycle via direct activation of the JAK-STAT signaling pathway in a process requiring PKD2. *Cell* **109**, 157-168 (2002).
154. Li, X. et al. Polycystin-1 and polycystin-2 regulate the cell cycle through the helix-loop-helix inhibitor Id2. *Nat. Cell Biol* **7**, 1202-1212 (2005).
155. Sohara, E. et al. Nek8 regulates the expression and localization of polycystin-1 and polycystin-2. *J. Am. Soc. Nephrol* **19**, 469-476 (2008).
156. Wodarczyk, C. et al. Nephrocystin-1 forms a complex with polycystin-1 via a polyproline motif/SH3 domain interaction and regulates the apoptotic response in mammals. *PLoS ONE* **5**, e12719 (2010).
157. Koupepidou, P. et al. Cyst formation in the PKD2 (1-703) transgenic rat precedes deregulation of proliferation-related pathways. *BMC Nephrol* **11**, 23 (2010).
158. Christensen, A.P. & Corey, D.P. TRP channels in mechanosensation: direct or indirect activation? *Nat. Rev. Neurosci* **8**, 510-521 (2007).
159. Jurczyk, A. et al. Pericentrin forms a complex with intraflagellar transport proteins and polycystin-2 and is required for primary cilia assembly. *J. Cell Biol* **166**, 637-643 (2004).
160. Yoder, B.K., Hou, X. & Guay-Woodford, L.M. The polycystic kidney disease proteins, polycystin-1, polycystin-2, polaris, and cystin, are co-localized in renal cilia. *J. Am. Soc. Nephrol* **13**, 2508-2516 (2002).
161. Praetorius, H.A. & Spring, K.R. Bending the MDCK cell primary cilium increases intracellular calcium. *J. Membr. Biol* **184**, 71-79 (2001).
162. Montalbetti, N., Li, Q., Wu, Y., Chen, X. & Cantiello, H.F. Polycystin-2 cation channel function in the human syncytiotrophoblast is regulated by microtubular structures. *J. Physiol. (Lond.)* **579**, 717-728 (2007).
163. Li, Q. et al. Polycystin-2 cation channel function is under the control of microtubular structures in primary cilia of renal epithelial cells. *J. Biol. Chem* **281**, 37566-37575 (2006).
164. Wu, Y. et al. Kinesin-2 mediates physical and functional interactions between polycystin-2 and fibrocystin. *Hum. Mol. Genet* **15**, 3280-3292 (2006).
165. Montalbetti, N. et al. Cytoskeletal regulation of calcium-permeable cation channels in the human syncytiotrophoblast: role of gelsolin. *J. Physiol. (Lond.)* **566**, 309-325 (2005).
166. Li, Q. et al. Alpha-actinin associates with polycystin-2 and regulates its channel activity. *Hum. Mol. Genet* **14**, 1587-1603 (2005).
167. Li, Q. et al. Polycystin-2 associates with tropomyosin-1, an actin microfilament component. *J. Mol. Biol* **325**, 949-962 (2003).

168. Li, Q., Shen, P.Y., Wu, G. & Chen, X. Polycystin-2 interacts with troponin I, an angiogenesis inhibitor. *Biochemistry* **42**, 450-457 (2003).
169. Gallagher, A.R., Cedzich, A., Gretz, N., Somlo, S. & Witzgall, R. The polycystic kidney disease protein PKD2 interacts with Hax-1, a protein associated with the actin cytoskeleton. *Proc. Natl. Acad. Sci. U.S.A* **97**, 4017-4022 (2000).
170. Montalbetti, N. et al. Effect of hydro-osmotic pressure on polycystin-2 channel function in the human syncytiotrophoblast. *Pflugers Arch* **451**, 294-303 (2005).
171. González-Perrett, S. et al. Polycystin-2, the protein mutated in autosomal dominant polycystic kidney disease (ADPKD), is a Ca2+-permeable nonselective cation channel. *Proc. Natl. Acad. Sci. U.S.A* **98**, 1182-1187 (2001).
172. Chen, X. et al. Submembraneous microtubule cytoskeleton: interaction of TRPP2 with the cell cytoskeleton. *FEBS J* **275**, 4675-4683 (2008).
173. Rundle, D.R., Gorbsky, G. & Tsiokas, L. PKD2 interacts and co-localizes with mDia1 to mitotic spindles of dividing cells: role of mDia1 IN PKD2 localization to mitotic spindles. *J. Biol. Chem* **279**, 29728-29739 (2004).
174. Bai, C. et al. Activation of TRPP2 through mDia1-dependent voltage gating. *EMBO J* **27**, 1345-56 (2008).
175. Ma, R. et al. PKD2 functions as an epidermal growth factor-activated plasma membrane channel. *Mol. Cell. Biol* **25**, 8285-8298 (2005).
176. Köttgen, M. et al. Trafficking of TRPP2 by PACS proteins represents a novel mechanism of ion channel regulation. *EMBO J* **24**, 705-16 (2005).
177. Liang, G. et al. Polycystin-2 down-regulates cell proliferation via promoting PERK-dependent phosphorylation of eIF2alpha. *Hum. Mol. Genet* **17**, 3254-3262 (2008).
178. Liang, G. et al. Polycystin-2 is regulated by endoplasmic reticulum-associated degradation. *Hum. Mol. Genet* **17**, 1109-1119 (2008).
179. Hidaka, S., Könecke, V., Osten, L. & Witzgall, R. PIGEA-14, a novel coiled-coil protein affecting the intracellular distribution of polycystin-2. *J. Biol. Chem* **279**, 35009-35016 (2004).
180. Streets, A.J., Moon, D.J., Kane, M.E., Obara, T. & Ong, A.C.M. Identification of an N-terminal glycogen synthase kinase 3 phosphorylation site which regulates the functional localization of polycystin-2 in vivo and in vitro. *Hum Mol Genet* **15**, 1465-73 (2006).
181. Wegierski, T. et al. TRPP2 channels regulate apoptosis through the Ca2+ concentration in the endoplasmic reticulum. *EMBO J* **28**, 490-499 (2009).
182. Li, Y., Wright, J.M., Qian, F., Germino, G.G. & Guggino, W.B. Polycystin 2 interacts with type I inositol 1,4,5-trisphosphate receptor to modulate intracellular Ca2+ signaling. *J. Biol. Chem* **280**, 41298-41306 (2005).
183. Weber, K.H. et al. Heterologous expression of polycystin-1 inhibits endoplasmic reticulum calcium leak in stably transfected MDCK cells. *Am. J. Physiol. Renal Physiol* **294**, F1279-1286 (2008).
184. Sutters, M. The pathogenesis of autosomal dominant polycystic kidney disease. *Nephron Exp. Nephrol* **103**, e149-155 (2006).
185. Grantham, J.J. The etiology, pathogenesis, and treatment of autosomal dominant polycystic kidney disease: recent advances. *Am. J. Kidney Dis* **28**, 788-803 (1996).
186. Patel, V., Chowdhury, R. & Igarashi, P. Advances in the pathogenesis and treatment of polycystic kidney disease. *Curr. Opin. Nephrol. Hypertens* **18**, 99-106 (2009).
187. Leuenroth, S.J. & Crews, C.M. Studies on calcium dependence reveal multiple modes of action for triptolide. *Chem Biol* **12**, 1259-68 (2005).
188. Leuenroth, S.J. et al. Triptolide is a traditional Chinese medicine-derived inhibitor of polycystic kidney disease. *Proc. Natl. Acad. Sci. U.S.A* **104**, 4389-94 (2007).
189. Leuenroth, S.J., Bencivenga, N., Igarashi, P., Somlo, S. & Crews, C.M. Triptolide reduces cystogenesis in a model of ADPKD. *J Am Soc Nephrol* **19**, 1659-62 (2008).

190. Géléoc, G.S., Lennan, G.W., Richardson, G.P. & Kros, C.J. A quantitative comparison of mechanoelectrical transduction in vestibular and auditory hair cells of neonatal mice. *Proc. Biol. Sci* **264**, 611-621 (1997).
191. Farris, H.E., LeBlanc, C.L., Goswami, J. & Ricci, A.J. Probing the pore of the auditory hair cell mechanotransducer channel in turtle. *J. Physiol. (Lond.)* **558**, 769-792 (2004).
192. Coste, B. et al. Piezo1 and Piezo2 are essential components of distinct mechanically activated cation channels. *Science* **330**, 55-60 (2010).
193. Cuajungco, M.P., Grimm, C. & Heller, S. TRP channels as candidates for hearing and balance abnormalities in vertebrates. *Biochim. Biophys. Acta* **1772**, 1022-1027 (2007).
194. Asai, Y., Holt, J.R. & Géléoc, G.S.G. A quantitative analysis of the spatiotemporal pattern of transient receptor potential gene expression in the developing mouse cochlea. *J. Assoc. Res. Otolaryngol* **11**, 27-37 (2010).
195. Peters, L.M. et al. Signatures from tissue-specific MPSS libraries identify transcripts preferentially expressed in the mouse inner ear. *Genomics* **89**, 197-206 (2007).
196. Corey, D.P. et al. TRPA1 is a candidate for the mechanosensitive transduction channel of vertebrate hair cells. *Nature* **432**, 723-730 (2004).
197. Bautista, D.M. et al. TRPA1 mediates the inflammatory actions of environmental irritants and proalgesic agents. *Cell* **124**, 1269-1282 (2006).
198. Kwan, K.Y. et al. TRPA1 contributes to cold, mechanical, and chemical nociception but is not essential for hair-cell transduction. *Neuron* **50**, 277-289 (2006).
199. Zheng, J. et al. Vanilloid receptors in hearing: altered cochlear sensitivity by vanilloids and expression of TRPV1 in the organ of corti. *J. Neurophysiol* **90**, 444-455 (2003).
200. Salas, M.M., Hargreaves, K.M. & Akopian, A.N. TRPA1-mediated responses in trigeminal sensory neurons: interaction between TRPA1 and TRPV1. *Eur. J. Neurosci* **29**, 1568-1578 (2009).
201. Greene, C.C. et al. DFNA25, a novel locus for dominant nonsyndromic hereditary hearing impairment, maps to 12q21-24. *Am. J. Hum. Genet* **68**, 254-260 (2001).
202. Liedtke, W. et al. Vanilloid receptor-related osmotically activated channel (VR-OAC), a candidate vertebrate osmoreceptor. *Cell* **103**, 525-535 (2000).
203. Vriens, J. et al. Cell swelling, heat, and chemical agonists use distinct pathways for the activation of the cation channel TRPV4. *Proc. Natl. Acad. Sci. U.S.A* **101**, 396-401 (2004).
204. Nilius, B., Vriens, J., Prenen, J., Droogmans, G. & Voets, T. TRPV4 calcium entry channel: a paradigm for gating diversity. *Am. J. Physiol., Cell Physiol* **286**, C195-205 (2004).
205. Tabuchi, K., Suzuki, M., Mizuno, A. & Hara, A. Hearing impairment in TRPV4 knockout mice. *Neurosci. Lett* **382**, 304-308 (2005).
206. Nakaya, K. et al. Lack of pendrin HCO3- transport elevates vestibular endolymphatic [Ca2+] by inhibition of acid-sensitive TRPV5 and TRPV6 channels. *Am. J. Physiol. Renal Physiol* **292**, F1314-1321 (2007).
207. Balaban, C.D., Zhou, J. & Li, H. Type 1 vanilloid receptor expression by mammalian inner ear ganglion cells. *Hear. Res* **175**, 165-170 (2003).
208. Kitahara, T., Li, H. & Balaban, C.D. Changes in transient receptor potential cation channel superfamily V (TRPV) mRNA expression in the mouse inner ear ganglia after kanamycin challenge. *Hear. Res* **201**, 132-144 (2005).
209. Bauer, C.A., Brozoski, T.J. & Myers, K.S. Acoustic injury and TRPV1 expression in the cochlear spiral ganglion. *Int Tinnitus J* **13**, 21-28 (2007).
210. Ishibashi, T., Takumida, M., Akagi, N., Hirakawa, K. & Anniko, M. Expression of transient receptor potential vanilloid (TRPV) 1, 2, 3, and 4 in mouse inner ear. *Acta Otolaryngol* **128**, 1286-1293 (2008).
211. Shen, J. et al. Functional expression of transient receptor potential vanilloid 4 in the

mouse cochlea. *Neuroreport* **17**, 135-139 (2006).
212. Takumida, M., Ishibashi, T., Hamamoto, T., Hirakawa, K. & Anniko, M. Age-dependent changes in the expression of klotho protein, TRPV5 and TRPV6 in mouse inner ear. *Acta Otolaryngol* **129**, 1340-1350 (2009).
213. Atiba-Davies, M. & Noben-Trauth, K. TRPML3 and hearing loss in the varitint-waddler mouse. *Biochim. Biophys. Acta* **1772**, 1028-1031 (2007).
214. Takumida, M. & Anniko, M. Expression of transient receptor potential channel mucolipin (TRPML) and polycystine (TRPP) in the mouse inner ear. *Acta Otolaryngol* 1-8 (2009).doi:10.1080/00016480903013593
215. Gabashvili, I.S., Sokolowski, B.H.A., Morton, C.C. & Giersch, A.B.S. Ion channel gene expression in the inner ear. *J Assoc Res Otolaryngol* **8**, 305-28 (2007).
216. Raybould, N.P. et al. TRPC-like conductance mediates restoration of intracellular Ca2+ in cochlear outer hair cells in the guinea pig and rat. *J. Physiol. (Lond.)* **579**, 101-113 (2007).
217. Phan, P.A.B., Tadros, S.F., Kim, Y., Birnbaumer, L. & Housley, G.D. Developmental regulation of TRPC3 ion channel expression in the mouse cochlea. *Histochem. Cell Biol* **133**, 437-448 (2010).
218. Tadros, S.F., Kim, Y., Phan, P.A.B., Birnbaumer, L. & Housley, G.D. TRPC3 ion channel subunit immunolocalization in the cochlea. *Histochem. Cell Biol* **133**, 137-147 (2010).
219. Takumida, M. & Anniko, M. Expression of canonical transient receptor potential channel (TRPC) 1-7 in the mouse inner ear. *Acta Otolaryngol* **129**, 1351-1358 (2009).
220. Twede, V.D., Miljanich, G., Olivera, B.M. & Bulaj, G. Neuroprotective and cardioprotective conopeptides: an emerging class of drug leads. *Curr Opin Drug Discov Devel* **12**, 231-239 (2009).
221. Terlau, H. & Olivera, B.M. Conus venoms: a rich source of novel ion channel-targeted peptides. *Physiol. Rev* **84**, 41-68 (2004).
222. Lewis, R.J. & Garcia, M.L. Therapeutic potential of venom peptides. *Nat Rev Drug Discov* **2**, 790-802 (2003).
223. Nicke, A., Wonnacott, S. & Lewis, R.J. Alpha-conotoxins as tools for the elucidation of structure and function of neuronal nicotinic acetylcholine receptor subtypes. *Eur. J. Biochem* **271**, 2305-2319 (2004).
224. Azam, L. & McIntosh, J.M. Alpha-conotoxins as pharmacological probes of nicotinic acetylcholine receptors. *Acta Pharmacol. Sin* **30**, 771-783 (2009).
225. McIntosh, J.M., Santos, A.D. & Olivera, B.M. Conus peptides targeted to specific nicotinic acetylcholine receptor subtypes. *Annu. Rev. Biochem* **68**, 59-88 (1999).
226. McIntosh, J.M. et al. A nicotinic acetylcholine receptor ligand of unique specificity, alpha-conotoxin ImI. *J. Biol. Chem* **269**, 16733-16739 (1994).
227. Luo, S. et al. Single-residue alteration in alpha-conotoxin PnIA switches its nAChR subtype selectivity. *Biochemistry* **38**, 14542-14548 (1999).
228. Quiram, P.A., McIntosh, J.M. & Sine, S.M. Pairwise interactions between neuronal alpha(7) acetylcholine receptors and alpha-conotoxin PnIB. *J. Biol. Chem* **275**, 4889-4896 (2000).
229. Ellison, M., McIntosh, J.M. & Olivera, B.M. Alpha-conotoxins ImI and ImII. Similar alpha 7 nicotinic receptor antagonists act at different sites. *J. Biol. Chem* **278**, 757-764 (2003).
230. Loughnan, M.L. et al. Chemical and functional identification and characterization of novel sulfated alpha-conotoxins from the cone snail Conus anemone. *J. Med. Chem* **47**, 1234-1241 (2004).
231. Ullian, E.M., McIntosh, J.M. & Sargent, P.B. Rapid synaptic transmission in the avian ciliary ganglion is mediated by two distinct classes of nicotinic receptors. *J. Neurosci* **17**,

7210-7219 (1997).
232. Kaiser, S.A., Soliakov, L., Harvey, S.C., Luetje, C.W. & Wonnacott, S. Differential inhibition by alpha-conotoxin-MII of the nicotinic stimulation of [3H]dopamine release from rat striatal synaptosomes and slices. *J. Neurochem* **70**, 1069-1076 (1998).
233. Nicke, A. et al. Isolation, structure, and activity of GID, a novel alpha 4/7-conotoxin with an extended N-terminal sequence. *J. Biol. Chem* **278**, 3137-3144 (2003).
234. Millard, E.L. et al. Inhibition of neuronal nicotinic acetylcholine receptor subtypes by alpha-Conotoxin GID and analogues. *J. Biol. Chem* **284**, 4944-4951 (2009).
235. Forss-Petter, S. et al. Transgenic mice expressing beta-galactosidase in mature neurons under neuron-specific enolase promoter control. *Neuron* **5**, 187-197 (1990).
236. Akopian, A.N. et al. The tetrodotoxin-resistant sodium channel SNS has a specialized function in pain pathways. *Nat. Neurosci* **2**, 541-548 (1999).
237. Inchauspe, C.G., Martini, F.J., Forsythe, I.D. & Uchitel, O.D. Functional compensation of P/Q by N-type channels blocks short-term plasticity at the calyx of held presynaptic terminal. *J. Neurosci* **24**, 10379-10383 (2004).
238. Abel, T. et al. Genetic demonstration of a role for PKA in the late phase of LTP and in hippocampus-based long-term memory. *Cell* **88**, 615-626 (1997).
239. Auer, S. et al. Silencing neurotransmission with membrane-tethered toxins. *Nat. Methods* **7**, 229-236 (2010).
240. Stürzebecher, A.S. et al. An in vivo tethered toxin approach for the cell-autonomous inactivation of voltage-gated sodium channel currents in nociceptors. *J. Physiol. (Lond.)* **588**, 1695-1707 (2010).
241. Lechner, H.A.E., Lein, E.S. & Callaway, E.M. A genetic method for selective and quickly reversible silencing of Mammalian neurons. *J. Neurosci* **22**, 5287-5290 (2002).
242. Lerchner, W. et al. Reversible silencing of neuronal excitability in behaving mice by a genetically targeted, ivermectin-gated Cl- channel. *Neuron* **54**, 35-49 (2007).
243. Ibañez-Tallon, I. et al. Tethering naturally occurring peptide toxins for cell-autonomous modulation of ion channels and receptors in vivo. *Neuron* **43**, 305-311 (2004).
244. Miwa, J.M. et al. lynx1, an endogenous toxin-like modulator of nicotinic acetylcholine receptors in the mammalian CNS. *Neuron* **23**, 105-114 (1999).
245. Hruska, M. & Nishi, R. Cell-autonomous inhibition of alpha 7-containing nicotinic acetylcholine receptors prevents death of parasympathetic neurons during development. *J. Neurosci* **27**, 11501-11509 (2007).
246. Wu, Y., Cao, G., Pavlicek, B., Luo, X. & Nitabach, M.N. Phase coupling of a circadian neuropeptide with rest/activity rhythms detected using a membrane-tethered spider toxin. *PLoS Biol* **6**, e273 (2008).
247. Théveniau, M., Durbec, P., Gennarini, G., Wood, J.N. & Rougon, G. Expression and release of phosphatidylinositol anchored cell surface molecules by a cell line derived from sensory neurons. *J. Cell. Biochem* **48**, 61-72 (1992).
248. Holford, M., Auer, S., Laqua, M. & Ibañez-Tallon, I. Manipulating neuronal circuits with endogenous and recombinant cell-surface tethered modulators. *Front Mol Neurosci* **2**, 21 (2009).
249. Gong, S. et al. A gene expression atlas of the central nervous system based on bacterial artificial chromosomes. *Nature* **425**, 917-925 (2003).
250. Gong, S., Yang, X.W., Li, C. & Heintz, N. Highly efficient modification of bacterial artificial chromosomes (BACs) using novel shuttle vectors containing the R6Kgamma origin of replication. *Genome Res* **12**, 1992-1998 (2002).
251. Heintz, N. BAC to the future: the use of bac transgenic mice for neuroscience research. *Nat. Rev. Neurosci* **2**, 861-870 (2001).
252. Gong, S. et al. Targeting Cre recombinase to specific neuron populations with bacterial artificial chromosome constructs. *J. Neurosci* **27**, 9817-9823 (2007).

253. Sternberg, N. & Hamilton, D. Bacteriophage P1 site-specific recombination. I. Recombination between loxP sites. *J. Mol. Biol* **150**, 467-486 (1981).
254. Sauer, B. & Henderson, N. Site-specific DNA recombination in mammalian cells by the Cre recombinase of bacteriophage P1. *Proc. Natl. Acad. Sci. U.S.A* **85**, 5166-5170 (1988).
255. Jamesdaniel, S., Salvi, R. & Coling, D. Auditory proteomics: methods, accomplishments and challenges. *Brain Res* **1277**, 24-36 (2009).
256. Zheng, Q.Y., Rozanas, C.R., Thalmann, I., Chance, M.R. & Alagramam, K.N. Inner ear proteomics of mouse models for deafness, a discovery strategy. *Brain Res* **1091**, 113-121 (2006).
257. Selbach, M. et al. Widespread changes in protein synthesis induced by microRNAs. *Nature* **455**, 58-63 (2008).
258. Touriol, C. et al. Generation of protein isoform diversity by alternative initiation of translation at non-AUG codons. *Biol. Cell* **95**, 169-178 (2003).
259. Namy, O., Rousset, J., Napthine, S. & Brierley, I. Reprogrammed genetic decoding in cellular gene expression. *Mol. Cell* **13**, 157-168 (2004).
260. Arava, Y. et al. Genome-wide analysis of mRNA translation profiles in Saccharomyces cerevisiae. *Proc. Natl. Acad. Sci. U.S.A* **100**, 3889-3894 (2003).
261. Baek, D. et al. The impact of microRNAs on protein output. *Nature* **455**, 64-71 (2008).
262. Kathiresan, T., Harvey, M., Orchard, S., Sakai, Y. & Sokolowski, B. A protein interaction network for the large conductance Ca(2+)-activated K(+) channel in the mouse cochlea. *Mol. Cell Proteomics* **8**, 1972-1987 (2009).
263. Zheng, J., Anderson, C.T., Miller, K.K., Cheatham, M. & Dallos, P. Identifying components of the hair-cell interactome involved in cochlear amplification. *BMC Genomics* **10**, 127 (2009).
264. Fettiplace, R. Defining features of the hair cell mechanoelectrical transducer channel. *Pflugers Arch* **458**, 1115-1123 (2009).
265. Pompeia, C. et al. Gene expression profile of the mouse organ of Corti at the onset of hearing. *Genomics* **83**, 1000-1011 (2004).
266. Abe, S., Koyama, K., Usami, S. & Nakamura, Y. Construction and characterization of a vestibular-specific cDNA library using T7-based RNA amplification. *J. Hum. Genet* **48**, 142-149 (2003).
267. Resendes, B.L. et al. Gene discovery in the auditory system: characterization of additional cochlear-expressed sequences. *J. Assoc. Res. Otolaryngol* **3**, 45-53 (2002).
268. Maubaret, C., Delettre, C., Sola, S. & Hamel, C.P. Identification of preferentially expressed mRNAs in retina and cochlea. *DNA Cell Biol* **21**, 781-791 (2002).
269. Luijendijk, M.W.J. et al. Cloning, characterization, and mRNA expression analysis of novel human fetal cochlear cDNAs. *Genomics* **82**, 480-490 (2003).
270. Morris, K.A. et al. Differential expression of genes within the cochlea as defined by a custom mouse inner ear microarray. *J. Assoc. Res. Otolaryngol* **6**, 75-89 (2005).
271. Okazaki, Y. et al. Analysis of the mouse transcriptome based on functional annotation of 60,770 full-length cDNAs. *Nature* **420**, 563-573 (2002).
272. Beisel, K.W. et al. Identification of unique transcripts from a mouse full-length, subtracted inner ear cDNA library. *Genomics* **83**, 1012-1023 (2004).
273. Cho, Y., Gong, T.L., Stöver, T., Lomax, M.I. & Altschuler, R.A. Gene expression profiles of the rat cochlea, cochlear nucleus, and inferior colliculus. *J. Assoc. Res. Otolaryngol* **3**, 54-67 (2002).
274. Chen, Z. & Corey, D.P. An inner ear gene expression database. *J. Assoc. Res. Otolaryngol* **3**, 140-148 (2002).
275. Sajan, S.A., Warchol, M.E. & Lovett, M. Toward a systems biology of mouse inner ear organogenesis: gene expression pathways, patterns and network analysis. *Genetics* **177**,

631-653 (2007).
276. Hildebrand, M.S. et al. Gene expression profiling analysis of the inner ear. *Hear Res* **225**, 1-10 (2007).
277. Zhang, L. et al. Gene expression profiles in normal and cancer cells. *Science* **276**, 1268-1272 (1997).
278. McDermott, B.M., Baucom, J.M. & Hudspeth, A.J. Analysis and functional evaluation of the hair-cell transcriptome. *Proceedings of the National Academy of Sciences* **104**, 11820-11825 (2007).
279. He, D.Z., Zheng, J., Edge, R. & Dallos, P. Isolation of cochlear inner hair cells. *Hear. Res* **145**, 156-160 (2000).
280. Anderson, C.T. & Zheng, J. Isolation of outer hair cells from the cochlear sensory epithelium in whole-mount preparation using laser capture microdissection. *J. Neurosci. Methods* **162**, 229-236 (2007).
281. Pagedar, N.A. et al. Gene expression analysis of distinct populations of cells isolated from mouse and human inner ear FFPE tissue using laser capture microdissection--a technical report based on preliminary findings. *Brain Res* **1091**, 289-299 (2006).
282. Zheng, J. et al. Prestin is the motor protein of cochlear outer hair cells. *Nature* **405**, 149-155 (2000).
283. Heiman, M. et al. A translational profiling approach for the molecular characterization of CNS cell types. *Cell* **135**, 738-748 (2008).
284. Sanz, E. et al. Cell-type-specific isolation of ribosome-associated mRNA from complex tissues. *Proc. Natl. Acad. Sci. U.S.A* **106**, 13939-13944 (2009).
285. Ingolia, N.T., Ghaemmaghami, S., Newman, J.R.S. & Weissman, J.S. Genome-wide analysis in vivo of translation with nucleotide resolution using ribosome profiling. *Science* **324**, 218-223 (2009).
286. Doyle, J.P. et al. Application of a translational profiling approach for the comparative analysis of CNS cell types. *Cell* **135**, 749-762 (2008).
287. Costa, V., Angelini, C., De Feis, I. & Ciccodicola, A. Uncovering the complexity of transcriptomes with RNA-Seq. *J. Biomed. Biotechnol* **2010**, 853916 (2010).
288. Wang, E.T. et al. Alternative isoform regulation in human tissue transcriptomes. *Nature* **456**, 470-6 (2008).
289. Hardiman, G. Ultra-high-throughput sequencing, microarray-based genomic selection and pharmacogenomics. *Pharmacogenomics* **9**, 5-9 (2008).
290. Mustroph, A. et al. Profiling translatomes of discrete cell populations resolves altered cellular priorities during hypoxia in Arabidopsis. *Proc. Natl. Acad. Sci. U.S.A* **106**, 18843-18848 (2009).
291. Halbeisen, R.E. & Gerber, A.P. Stress-Dependent Coordination of Transcriptome and Translatome in Yeast. *PLoS Biol* **7**, e105 (2009).
292. McGehee, D.S., Heath, M.J., Gelber, S., Devay, P. & Role, L.W. Nicotine enhancement of fast excitatory synaptic transmission in CNS by presynaptic receptors. *Science* **269**, 1692-1696 (1995).
293. Luebke, A.E. Molecular characterization of novel acetylcholine receptors in the guinea pig cochlea. *http://www.aro.org/archives/1995/772.html* (1995).at <948>
294. Maison, S.F., Emeson, R.B., Adams, J.C., Luebke, A.E. & Liberman, M.C. Loss of alpha CGRP reduces sound-evoked activity in the cochlear nerve. *J. Neurophysiol* **90**, 2941-2949 (2003).
295. Wu, G. et al. Somatic inactivation of Pkd2 results in polycystic kidney disease. *Cell* **93**, 177-188 (1998).
296. Garcia-Gonzalez, M.A. et al. Pkd1 and Pkd2 are required for normal placental development. *PLoS ONE* **5**, (2010).
297. Kim, I. et al. Polycystin-2 expression is regulated by a PC2-binding domain in the

intracellular portion of fibrocystin. *J. Biol. Chem* **283**, 31559-31566 (2008).
298. Ermakov, A. et al. Mouse mutagenesis identifies novel roles for left-right patterning genes in pulmonary, craniofacial, ocular, and limb development. *Dev. Dyn* **238**, 581-594 (2009).
299. Gong, S., Yang, X.W., Li, C. & Heintz, N. Highly efficient modification of bacterial artificial chromosomes (BACs) using novel shuttle vectors containing the R6Kgamma origin of replication. *Genome Res* **12**, 1992-1998 (2002).
300. Witkin, E.M. Ultraviolet mutagenesis and inducible DNA repair in Escherichia coli. *Bacteriol Rev* **40**, 869-907 (1976).
301. Keithley, E.M., Canto, C., Zheng, Q.Y., Fischel-Ghodsian, N. & Johnson, K.R. Age-related hearing loss and the ahl locus in mice. *Hear. Res* **188**, 21-28 (2004).
302. Hall, J. *III. Handbook of Auditory Evoked Responses.* (Allyn and Bacon Publishers: 1992).at <980>
303. Glattke, T. & Robinette, M. *Otoacoustic Emissions, Clinical Applications.* (Thieme Publishers: 2002).at <979>
304. Azam, L. et al. Alpha-conotoxin BuIA, a novel peptide from Conus bullatus, distinguishes among neuronal nicotinic acetylcholine receptors. *J. Biol. Chem* **280**, 80-87 (2005).
305. Markowitz, G.S. et al. Polycystin-2 expression is developmentally regulated. *Am J Physiol* **277**, F17-25 (1999).
306. Obermüller, N. et al. The rat pkd2 protein assumes distinct subcellular distributions in different organs. *Am. J. Physiol* **277**, F914-925 (1999).
307. Geng, L. et al. Identification and localization of polycystin, the PKD1 gene product. *J. Clin. Invest* **98**, 2674-2682 (1996).
308. Ibraghimov-Beskrovnaya, O. et al. Polycystin: in vitro synthesis, in vivo tissue expression, and subcellular localization identifies a large membrane-associated protein. *Proc. Natl. Acad. Sci. U.S.A* **94**, 6397-6402 (1997).
309. Wodarczyk, C. et al. A novel mouse model reveals that polycystin-1 deficiency in ependyma and choroid plexus results in dysfunctional cilia and hydrocephalus. *PLoS ONE* **4**, e7137 (2009).
310. Xiao, Z. et al. Cilia-like structures and polycystin-1 in osteoblasts/osteocytes and associated abnormalities in skeletogenesis and Runx2 expression. *J. Biol. Chem* **281**, 30884-30895 (2006).
311. Xiao, Z., Zhang, S., Magenheimer, B.S., Luo, J. & Quarles, L.D. Polycystin-1 regulates skeletogenesis through stimulation of the osteoblast-specific transcription factor RUNX2-II. *J. Biol. Chem* **283**, 12624-12634 (2008).
312. Xiao, Z.S. & Quarles, L.D. Role of the polycytin-primary cilia complex in bone development and mechanosensing. *Ann. N. Y. Acad. Sci* **1192**, 410-421 (2010).
313. Purcell, P. et al. Temporomandibular joint formation requires two distinct hedgehog-dependent steps. *Proc. Natl. Acad. Sci. U.S.A* **106**, 18297-18302 (2009).
314. Ioi, H. et al. Capsaicin receptor expression in the rat temporomandibular joint. *Cell Tissue Res* **325**, 47-54 (2006).
315. Ong, A.C. et al. Coordinate expression of the autosomal dominant polycystic kidney disease proteins, polycystin-2 and polycystin-1, in normal and cystic tissue. *Am. J. Pathol* **154**, 1721-1729 (1999).
316. Wu, G. et al. Cardiac defects and renal failure in mice with targeted mutations in Pkd2. *Nat. Genet* **24**, 75-78 (2000).
317. Chen, Y. et al. Expression of Pkd2l2 in testis is implicated in spermatogenesis. *Biol. Pharm. Bull* **31**, 1496-1500 (2008).
318. Barr, M.M. & Sternberg, P.W. A polycystic kidney-disease gene homologue required for male mating behaviour in C. elegans. *Nature* **401**, 386-389 (1999).

319. Gao, Z., Ruden, D.M. & Lu, X. PKD2 cation channel is required for directional sperm movement and male fertility. *Curr. Biol* **13**, 2175-2178 (2003).
320. Watnick, T.J., Jin, Y., Matunis, E., Kernan, M.J. & Montell, C. A flagellar polycystin-2 homolog required for male fertility in Drosophila. *Curr. Biol* **13**, 2179-2184 (2003).
321. Kierszenbaum, A.L. Polycystins: what polycystic kidney disease tells us about sperm. *Mol. Reprod. Dev* **67**, 385-388 (2004).
322. Buzzell, G.R. The Harderian gland: perspectives. *Microsc. Res. Tech* **34**, 2-5 (1996).
323. Huang, L., Thorne, P.R., Housley, G.D. & Montgomery, J.M. Spatiotemporal definition of neurite outgrowth, refinement and retraction in the developing mouse cochlea. *Development* **134**, 2925-33 (2007).
324. Lee, M.K., Tuttle, J.B., Rebhun, L.I., Cleveland, D.W. & Frankfurter, A. The expression and posttranslational modification of a neuron-specific beta-tubulin isotype during chick embryogenesis. *Cell Motil. Cytoskeleton* **17**, 118-132 (1990).
325. Lallemend, F. et al. Activation of protein kinase CbetaI constitutes a new neurotrophic pathway for deafferented spiral ganglion neurons. *J Cell Sci* **118**, 4511-25 (2005).
326. Lallemend, F. et al. New insights into peripherin expression in cochlear neurons. *Neuroscience* **150**, 212-22 (2007).
327. Hafidi, A. Peripherin-like immunoreactivity in type II spiral ganglion cell body and projections. *Brain Res* **805**, 181-190 (1998).
328. Berglund, A.M. & Ryugo, D.K. Neurofilament antibodies and spiral ganglion neurons of the mammalian cochlea. *J. Comp. Neurol* **306**, 393-408 (1991).
329. Reid, M.A., Flores-Otero, J. & Davis, R.L. Firing patterns of type II spiral ganglion neurons in vitro. *J. Neurosci* **24**, 733-742 (2004).
330. Fechner, F.P., Nadol JB, J.R., Burgess, B.J. & Brown, M.C. Innervation of supporting cells in the apical turns of the guinea pig cochlea is from type II afferent fibers. *J. Comp. Neurol* **429**, 289-298 (2001).
331. Belecky-Adams, T. et al. An intact intermediate filament network is required for collateral sprouting of small diameter nerve fibers. *J. Neurosci* **23**, 9312-9319 (2003).
332. Mita, R. et al. B-FABP-expressing radial glial cells: the malignant glioma cell of origin? *Neoplasia* **9**, 734-744 (2007).
333. Saino-Saito, S. et al. Localization of fatty acid binding proteins (FABPs) in the cochlea of mice. *Ann. Anat* **192**, 210-214 (2010).
334. Barclay, M., Julien, J., Ryan, A.F. & Housley, G.D. Type III intermediate filament peripherin inhibits neuritogenesis in type II spiral ganglion neurons in vitro. *Neurosci. Lett* **478**, 51-55 (2010).
335. Liu, W., Kinnefors, A., Boström, M. & Rask-Andersen, H. Expression of peripherin in human cochlea. *Cell Tissue Res* (2010).doi:10.1007/s00441-010-1081-6
336. Lu, W. et al. Perinatal lethality with kidney and pancreas defects in mice with a targetted Pkd1 mutation. *Nat. Genet* **17**, 179-181 (1997).
337. Hol, E.M. et al. Regulation of the LIM-type homeobox gene islet-1 during neuronal regeneration. *Neuroscience* **88**, 917-925 (1999).
338. Adam, J. et al. Cell fate choices and the expression of Notch, Delta and Serrate homologues in the chick inner ear: parallels with Drosophila sense-organ development. *Development* **125**, 4645-4654 (1998).
339. Li, H. et al. Islet-1 expression in the developing chicken inner ear. *J Comp Neurol* **477**, 1-10 (2004).
340. Camarero, G. et al. Delayed inner ear maturation and neuronal loss in postnatal Igf-1-deficient mice. *J. Neurosci* **21**, 7630-7641 (2001).
341. Oshima, K., Teo, D.T.W., Senn, P., Starlinger, V. & Heller, S. LIF promotes neurogenesis and maintains neural precursors in cell populations derived from spiral ganglion stem cells. *BMC Dev. Biol* **7**, 112 (2007).

342. Oshima, K. et al. Differential Distribution of Stem Cells in the Auditory and Vestibular Organs of the Inner Ear. *J Assoc Res Otolaryngol.* **8**, 18–31 (2007).
343. Pereira, E.F., Alkondon, M., McIntosh, J.M. & Albuquerque, E.X. Alpha-conotoxin-ImI: a competitive antagonist at alpha-bungarotoxin-sensitive neuronal nicotinic receptors in hippocampal neurons. *J. Pharmacol. Exp. Ther* **278**, 1472-1483 (1996).
344. Kaiser, S. & Wonnacott, S. alpha-bungarotoxin-sensitive nicotinic receptors indirectly modulate [(3)H]dopamine release in rat striatal slices via glutamate release. *Mol. Pharmacol* **58**, 312-318 (2000).
345. Couturier, S. et al. A neuronal nicotinic acetylcholine receptor subunit (alpha 7) is developmentally regulated and forms a homo-oligomeric channel blocked by alpha-BTX. *Neuron* **5**, 847-856 (1990).
346. Cooper, S.T. & Millar, N.S. Host cell-specific folding and assembly of the neuronal nicotinic acetylcholine receptor alpha7 subunit. *J. Neurochem* **68**, 2140-2151 (1997).
347. Mukherjee, J., Kuryatov, A., Moss, S.J., Lindstrom, J.M. & Anand, R. Mutations of cytosolic loop residues impair assembly and maturation of alpha7 nicotinic acetylcholine receptors. *J. Neurochem* **110**, 1885-1894 (2009).
348. Caulfield, M.P. Muscarinic receptors--characterization, coupling and function. *Pharmacol. Ther* **58**, 319-379 (1993).
349. Wess, J. Molecular biology of muscarinic acetylcholine receptors. *Crit Rev Neurobiol* **10**, 69-99 (1996).
350. Safieddine, S., Bartolami, S., Wenthold, R.J. & Eybalin, M. Pre- and postsynaptic M3 muscarinic receptor mRNAs in the rodent peripheral auditory system. *Brain Res. Mol. Brain Res* **40**, 127-135 (1996).
351. Rome, C., Luo, D. & Dulon, D. Muscarinic receptor-mediated calcium signaling in spiral ganglion neurons of the mammalian cochlea. *Brain Res* **846**, 196-203 (1999).
352. Khan, K.M., Drescher, M.J., Hatfield, J.S., Khan, A. & Drescher, D.G. Muscarinic receptor subtypes are differentially distributed in the rat cochlea. *Neuroscience* **111**, 291-302 (2002).
353. Maison, S.F. et al. Muscarinic signaling in the cochlea: presynaptic and postsynaptic effects on efferent feedback and afferent excitability. *J. Neurosci* **30**, 6751-6762 (2010).
354. Simmons, D.D., Moulding, H.D. & Zee, D. Olivocochlear innervation of inner and outer hair cells during postnatal maturation: an immunocytochemical study. *Brain Res. Dev. Brain Res* **95**, 213-226 (1996).
355. Bergeron, A.L., Schrader, A., Yang, D., Osman, A.A. & Simmons, D.D. The final stage of cholinergic differentiation occurs below inner hair cells during development of the rodent cochlea. *J. Assoc. Res. Otolaryngol* **6**, 401-415 (2005).
356. Wu, G. et al. Molecular cloning, cDNA sequence analysis, and chromosomal localization of mouse Pkd2. *Genomics* **45**, 220-223 (1997).
357. Li, Q. et al. Direct binding of alpha-actinin enhances TRPP3 channel activity. *J. Neurochem* **103**, 2391-2400 (2007).
358. Qian, F. et al. Cleavage of polycystin-1 requires the receptor for egg jelly domain and is disrupted by human autosomal-dominant polycystic kidney disease 1-associated mutations. *Proc. Natl. Acad. Sci. U.S.A* **99**, 16981-16986 (2002).
359. Bertuccio, C.A. et al. Polycystin-1 C-terminal cleavage is modulated by polycystin-2 expression. *J. Biol. Chem* **284**, 21011-21026 (2009).
360. Liberman, M.C. Auditory-nerve response from cats raised in a low-noise chamber. *J. Acoust. Soc. Am* **63**, 442-455 (1978).
361. Imamura, S. & Adams, J.C. Immunolocalization of peptide 19 and other calcium-binding proteins in the guinea pig cochlea. *Anat. Embryol* **194**, 407-418 (1996).
362. Dong, J., Asa, S.L. & Drucker, D.J. Islet cell and extrapancreatic expression of the LIM domain homeobox gene isl-1. *Mol. Endocrinol* **5**, 1633-1641 (1991).

363. Mignone, J.L., Kukekov, V., Chiang, A., Steindler, D. & Enikolopov, G. Neural stem and progenitor cells in nestin-GFP transgenic mice. *J Comp Neurol* **469**, 311-24 (2004).
364. Thodi, C., Thodis, E., Danielides, V., Pasadakis, P. & Vargemezis, V. Hearing in renal failure. *Nephrol. Dial. Transplant* **21**, 3023-3030 (2006).
365. Aspris, A.K. et al. Auditory brainstem responses in patients under treatment of hemodialysis. *Ren Fail* **30**, 383-390 (2008).
366. Loonstra, A. et al. Growth inhibition and DNA damage induced by Cre recombinase in mammalian cells. *Proc. Natl. Acad. Sci. U.S.A* **98**, 9209-9214 (2001).
367. Forni, P.E. et al. High levels of Cre expression in neuronal progenitors cause defects in brain development leading to microencephaly and hydrocephaly. *J. Neurosci* **26**, 9593-9602 (2006).
368. Melcher, J.R., Guinan, J.J., Knudson, I.M. & Kiang, N.Y. Generators of the brainstem auditory evoked potential in cat. II. Correlating lesion sites with waveform changes. *Hear. Res* **93**, 28-51 (1996).
369. Rhode, W.S. Response patterns to sound associated with labeled globular/bushy cells in cat. *Neuroscience* **154**, 87-98 (2008).
370. Buchwald, J.S. & Huang, C. Far-field acoustic response: origins in the cat. *Science* **189**, 382-384 (1975).
371. Gardi, J.N. & Bledsoe, S.C. The use of kainic acid for studying the origins of scalp-recorded ABRs in the guinea pig. *Neurosci. Lett* **26**, 143-149 (1981).
372. Pratt, H., Zaaroor, M., Bleich, N. & Starr, A. Effects of myelin or cell body brainstem lesions on 3-channel Lissajous' trajectories of feline auditory brainstem evoked potentials. *Hear. Res* **53**, 237-252 (1991).
373. Zaaroor, M. & Starr, A. Auditory brain-stem evoked potentials in cat after kainic acid induced neuronal loss. I. Superior olivary complex. *Electroencephalogr Clin Neurophysiol* **80**, 422-435 (1991).
374. Ison, J., Allen, P., Walton, J., O'Neill, W. & Bowers, W. Latency and amplitude differences in ABR wave pattern of KCNA1 null-mutant and wild-type mice. *The Meeting of the Society for Neuroscience* (2002).at <979>
375. Zuo, J., Treadaway, J., Buckner, T.W. & Fritzsch, B. Visualization of alpha9 acetylcholine receptor expression in hair cells of transgenic mice containing a modified bacterial artificial chromosome. *Proc. Natl. Acad. Sci. U.S.A* **96**, 14100-14105 (1999).
376. Ruel, J. et al. Impairment of SLC17A8 encoding vesicular glutamate transporter-3, VGLUT3, underlies nonsyndromic deafness DFNA25 and inner hair cell dysfunction in null mice. *Am. J. Hum. Genet* **83**, 278-292 (2008).
377. Seal, R.P. et al. Sensorineural deafness and seizures in mice lacking vesicular glutamate transporter 3. *Neuron* **57**, 263-275 (2008).
378. Wang, Y. et al. Localization of vesicular glutamate transporters in the peripheral vestibular system of rat. *Neurosci Bull* **23**, 175-179 (2007).
379. Zhang, F.X. et al. Expression of vesicular glutamate transporters in peripheral vestibular structures and vestibular nuclear complex of rat. *Neuroscience* (2010).doi:10.1016/j.neuroscience.2010.11.013
380. Obholzer, N. et al. Vesicular glutamate transporter 3 is required for synaptic transmission in zebrafish hair cells. *J. Neurosci* **28**, 2110-2118 (2008).
381. Zhou, J., Nannapaneni, N. & Shore, S. Vessicular glutamate transporters 1 and 2 are differentially associated with auditory nerve and spinal trigeminal inputs to the cochlear nucleus. *J. Comp. Neurol* **500**, 777-787 (2007).
382. Safieddine, S. & Wenthold, R.J. SNARE complex at the ribbon synapses of cochlear hair cells: analysis of synaptic vesicle- and synaptic membrane-associated proteins. *Eur. J. Neurosci* **11**, 803-812 (1999).

ERKLÄRUNG

Hiermit versichere ich, dass ich die vorgelegte Dissertationsschrift mit dem Titel 'Investigating the Contributions of TRPP2 and α7 nAChR to Mouse Auditory Function Utilising Various Genetic Approaches' selbständig und ohne (unzulässige) Hilfe Dritter angefertigt habe. Ich habe keine anderen als die angegebenen Quellen und Hilfsmittel benutzt.

Ort, Datum

Unterschrift

CURRICULUM VITAE

For reasons of data protection,
the curriculum vitae is not included in the online version